Instrumental techniques for improving the measurements based on quartz crystal microbalances

ROBINSON ALBERTO TORRES VILLA

EDITORIAL
UNIVERSITAT POLITÈCNICA DE VALÈNCIA

UNIVERSIDAD
POLITÉCNICA
DE VALENCIA

DEPARTAMENTO DE INGENIERÍA
ELECTRÓNICA

TESIS DOCTORAL

"Instrumental techniques for improving the measurements based on Quartz Crystal Microbalances"

By: Róbinson Alberto Torres Villa
Adviser: Dr. Antonio Arnau Vives

This editorial is member of the UNE, which guarantees the diffusion and commercialization of its publications at national and international level.

ISBN: 978-84-9048-017-5 (printed version)
Ref. editorial: 5609

To my parents for all the experiences
and teachings they have transmitted to me.

To Santiago who gives me the opportunity
to discover and develop new aspects
in my life.

To my brothers who share with me
the great adventure to live for
something superior than us.

To the Antioquia School of Engineering, EIA,
and the Heatlh Sciences Institute, CES,
for their support for developing my doctoral degree.

To my adviser, Antonio for all his recommendations, appreciations and encouraged words; and because without his help it would not have been possible the development of this thesis work.

To Yolanda for her continuous support and permanent kind words.

To the members of the IDDD laboratory of the Polytechnic University of Valencia for their company during my stay and for their opportune advices in some stages of the project design.

To the members of the LISE laboratory of the CNRS in Paris for all their help during the experimental stage of the thesis.

It is the direction of our progress that matters
—not where we stand at present.

Sri Ram.

Acknowledgements

This work is developed thanks to PETRA II project in the frame of European Alfa project to establish cooperation networks between European Community and Latin American countries for technology and knowledge transfer.

In addition the author is very grateful with the Polytechnic University of Valencia, The Electrochemical Systems and Interfaces Laboratory (LISE) of the CNRS and the Pierre and Marie Curie University in France and the Biomedical Engineering program in agreement between The Antioquia School of Engineering (EIA) and the Health Sciences Institute (CES) in Colombia.

Resumen

La Electrogravimetría AC emplea una microbalanza de cuarzo electroquímica (EQCM) en régimen dinámico. En la EQCM uno de los electrodos de oro depositados sobre el cristal es recubierto con una fina película de un polímero electroactivo y es empleado como electrodo de trabajo (WE) dentro de una celda electroquímica. Las variaciones de la frecuencia de resonancia de la microbalanza de cuarzo (QCM) permiten obtener la respuesta masa asociada con la transferencia de carga que se da en la interfaz polímero-electrolito. La Electrogravimetría AC fue propuesta con el fin de caracterizar y separadamente identificar el movimiento de los iones y el solvente en la interfaz polímero-electrolito. En esta técnica se analiza en el domino de la frecuencia la respuesta de masa ante pequeñas perturbaciones de voltaje gracias al empleo de la microbalanza de cuarzo en régimen dinámico. Para este propósito se aplica una pequeña perturbación sinusoidal superpuesta a una tensión continua, entre el electrodo de referencia y el electrodo de trabajo de la celda. Posteriormente, se puede graficar la función de transferencia electrogravimétrica (EGTF), definida ésta como la razón ($\Delta m/\Delta E$) entre la amplitud de los cambios de masa inducidos (Δm) y la amplitud de la perturbación sinusoidal aplicada (ΔE). Esta función de transferencia se grafica en un plano complejo para cada una de las frecuencias de la señal de perturbación. Las distintas especies iónicas involucradas son identificadas en el plano complejo por medio de bucles característicos siempre y cuando dichos bucles no se superpongan.

Por medio de esta tesis doctoral se propone un novedoso sistema de conversión de frecuencia-tensión basado en un doble ajuste frecuencia implementado pon medio de un PLL mezclando elementos analógicos y digitales (A-D PLL). Los resultados encontrados tanto en la caracterización electrónica del dispositivo como en la fase experimental prueban la fiabilidad del sistema para las mediciones realizadas en la técnica de Electrogravimetría AC.

PALABRAS CLAVE: Electrogravimetría AC; microbalanza de cristal de cuarzo; bucles de enganche de fase; compromiso ancho de banda-resolución; ajuste grueso y fino.

Resum

L'Electrogravimetria AC empra una microbalança de quars electroquímica (EQCM) en règim dinàmic. En l'EQCM un dels elèctrodes d'or depositats sobre el cristall és recobert amb una fina pel·lícula d'un polímer electroactiv i és emprat com a elèctrode de treball (WE) dins d'una cel·la electroquímica. Les variacions de la freqüència de ressonància de la microbalança de quars (QCM) permeten obtindre la resposta massa associada amb la transferència de càrrega que es dóna en la interfície polímer-electròlit. L'Electrogravimetria AC va ser proposta a fi de caracteritzar i separadament identificar el moviment dels ions i el solvent en la interfície polímer-electròlit. En esta tècnica s'analitza en el domine de la freqüència la resposta de massa davant de xicotetes pertorbacions de voltatge gràcies a l'ocupació de la microbalança de quars en règim dinàmic. Per a este propòsit s'aplica una xicoteta pertorbació sinusoidal superposada a una tensió contínua, entre l'elèctrode de referència i l'elèctrode de treball de la cel·la. Posteriorment, es pot dibuixar la funció de transferència electrogravimètrica (EGTF), definida esta com la raó ($\Delta m/\Delta E$) entre l'amplitud dels canvis de massa induïts (Δm) i l'amplitud de la pertorbació sinusoïdal aplicada (ΔE). Esta funció de transferència se dibuixa en un pla complex per a cada una de les freqüències de la senyal de pertorbació. Les distintes espècies iònicas involucrades són identificades en el pla complex per mitjà de bucles característics sempre que els bucles no se superposen.

Per mitjà d'esta tesi doctoral es proposa un nou sistema de conversió de freqüència-tensió basat en un doble ajust de freqüència implementat amb un PLL mesclant elements analògics i digitals (*AD* PLL). Els resultats trobats tant en la caracterització electrònica del dispositiu com en la fase experimental proven la fiabilitat del sistema per als mesuraments realitzats en la tècnica d'Electrogravimetria AC.

PARAULES CLAU: Electrogravimetria AC; microbalança de cristall de quars; bucles d'enganxall de fase; compromís ample de banda-resolució; ajuste gros i fi.

Abstract

AC Electrogravimetry is based on an electrochemical quartz crystal microbalance (EQCM) used in dynamic regime. In EQCM one of the deposited gold electrodes of the quartz crystal resonator can be coated with an electroactive polymer film and be used as the working electrode (WE) following a classical electrochemical configuration. The frequency shift of the quartz crystal microbalance (QCM) allows obtaining the mass response associated with the charge transfer, which occurs at polymer/electrolyte interface. AC Electrogravimetry was proposed to characterise and separately identify ions and solvent motion at the film/electrolyte interface. In this technique the mass response to a small potential perturbation is analysed in the frequency domain thanks to a fast QCM used in dynamic regime; for that, a continuous voltage with a superimposed small potential sinusoidal perturbation is applied between the reference electrode and the WE of the electrochemical cell. Thus, the so-called Electrogravimetric Transfer Function (EGTF) defined as the ratio ($\Delta m/\Delta E$) between the amplitude of induced mass change (Δm) and the perturbation amplitude (ΔE) can be plotted in a complex plane for the entire range of perturbation frequencies. The various species involved are characterised by a loop in the complex plane and can be separately identified when the loops do not overlap.

A new frequency-voltage conversion system based on a double tuning analogue-digital phase locked loop (A-D PLL) is proposed. The reported electronic characterisation and experimental results prove its reliability for AC Electrogravimetry measurements.

Key words: AC Electrogravimetry; quartz crystal microbalance; phase locked loops; bandwidth-resolution trade-off; coarse and fine tuning, Nyquist response; polymer characterisation.

Contents

1 Introduction

1.1 Quartz Crystal as a Sensor

1.1.1 Brief Historical Review

The *quartz crystal resonator* was firstly used as a frequency reference element in oscillator applications, for stabilising the radio broadcasting's carriers. For an accurate control of the oscillator frequency, a very small mass was deposited on the crystal by means of a marker paintbrush until the frequency reached the desired one. This frequency tuning was based on the result obtained by Lord Rayleigh in 1945 [Rayleigh45], who demonstrated that a perturbation in the *resonance frequency* occurred when a small change in the inertia of a mechanical vibrating system is provoked. This was the first use of the quartz crystals as microbalance sensors.

The use of the quartz crystal as a microbalance sensor is one of its most antique applications. This use was consolidated by the Sauerbrey's works who demonstrated by experimental means that for thin films uniformly deposited on the quartz crystal the resonance frequency shift of the compound resonator was proportional to the added mass [Sauerbrey59]. *Sauerbrey* established a mathematical relationship between the frequency and surface mass changes, which is only valid when the layer deposited on the crystal surface is very thin and rigid. Under these conditions, the material deposited is coupled in a rigid way to the quartz' surface, suffering a negligible strain when the acoustic wave propagates through it; the consequence for this is the elastic material's properties do not affect the resonance frequency of the sensor and the variation in the resonant frequency of the compound resonator is due to a pure inertial effect [Martin91].

Subsequent studies demonstrated that the quartz's sensitivity allowed to measured mass from *50* to *100 pg* on a surface of $10mm^2$ [Stockbridge62]. This great sensitivity, one million higher than conventional microbalances systems, is due to the tremendous acceleration suffered by the particles rigidity joined to the quartz crystal's surface [Jimenez04, Mecea89].

In the quartz crystal resonator, the maximum displacement of the particles occurs on the crystal surfaces. The vibrating amplitude of the resonator's particles depends on the applied potential and its quality factor. This amplitude can be in the order of angstroms for applied potential in the range of volts. Despite the low vibrating amplitude, the acceleration at

which the film deposited on the quartz surface is submitted is very big; concretely, this acceleration increases with the square of the frequency [Arnau99, Mecea96] and is around $10^7 g$, for a 10MHz AT-cut quartz crystal, where g is the gravity. It means that a particle subjected to this acceleration would weigh 10^7 times more in a quartz microbalance than in a conventional balance [Jimenez04].

Thanks to the great sensitivity and good accuracy of mass-monitoring in the case of thin films deposited on the *AT-cut quartz resonator*, its use has been extended as thin-film thickness monitoring in vacuum metal deposition systems. The resonator's frequency shifts can be related to the added mass through the Sauerbrey equation.

In 1964, King created a selective gas detector; for this application he covered the crystal with some substrates sensitive to certain gasses. The gas' absorption in the substrate increases the surface mass density of the coating and produces a decrease of the quartz resonance frequency which can be calculated through the Sauerbrey's equation [King64]. This idea was used to detect organophosphate compounds and pesticides in the environment [Guilbault81, Guilbault83, Guilbault85]; explosives [Tomita79] and contaminant agents [Edmonds80].

When the mass of the deposited film is significant the presumption that the acoustic wave does not deform the material is less and less acceptable and Sauerbrey's equation becomes invalid. Actually, quartz crystal resonator is sensitive to the viscoelastic properties of the material under study and then its application as microbalance is very useful but limited. The limitation of making a purely inertial interpretation is evident when the viscoelastic effect is transferred into a resonance frequency shift that overcomes the mass effect. In these cases the physical model established by Sauerbrey is not appropriate for monitoring the mass changes and then it is essential to study in depth the sensor response and to extract the physical properties of the coating from the sensor electrical characterisation.

The limitation of the Sauerbrey lineal relationship, associated with the elastic behaviour of the coating, was established by Miller and Bolef [Miller68]. A useful formulation for this behaviour was presented by Lu and Lewis in 1972, which developed a compact expression for the frequency change including the film's elasticity, but not its losses [Lu72]. The difficulty of using this expression lies on the requirement to know the *acoustic impedance* of the media deposited on the sensor. Additionally, the contributions to the frequency shift caused by a *mass change* or a change in the *viscoelastic properties* can not be separated in a simple way by only measuring the frequency shifts. From now on it was clear that the term *microbalance* applied to quartz sensor is probably imprecise due to the fact

that the resonance frequency of the compound resonator is affected by different effects.

Several researchers considered the use of the resonator in liquid media; however, this idea was discarded on the basis that the addition of a liquid on one of sensor's surface would cause an excessive load which would produce the stop of crystal oscillation. Nevertheless, the amplitude of the shear wave transmitted into de liquid is exponentially reduced with the distance; therefore the finite penetration depth of this wave limits the effect of the load.

Konash and Bastiaans demonstrated in 1980 that it was possible to maintain the oscillator stability controlled by a quartz crystal when it was in contact with a liquid medium [Konash80]. This study would open the possibility to use the quartz crystal as a sensor in *liquid medium*. However it would be necessary a more detailed study of the physical phenomena which determined the resonant characteristics for AT-cut quartz crystal in contact with a liquid. It allowed to obtain a more precisely model that quantified the effect of the physical properties of the medium on the vibrating characteristics of the compound resonator. *Kanazawa* and Gordon obtained in 1985, starting from a physical model, the relationship between the resonance frequency shift and the physical properties of a *Newtonian fluid* (viscosity and density) in contact with the resonator [Kanazawa85-1, Kanazawa85-2].

The availability of electronic systems based on quartz resonators to operate in liquid media and the mathematical models developed for liquid environment in contact with the resonator, like the one introduced by Kanazawa and Gordon, opened the possibility of using the quartz crystal in detection process which had to take place in liquid media instead of in gas. One of the most interesting applications of the quartz crystal in liquid media is a *Biosensor* for the great expectative it has created.

A quartz crystal covered by a polymer or a biochemical modified surface constitutes a *biological interface* able to immobilise a biomolecular complex in aqueous solution (aq). The biosensors based on quartz systems are becoming an adequate tool for measuring biofluids in situ, particularly for detecting online immunological reactions [Hengerer99, Sakti00], and bioelectrochemical enzymes redox reactions [Buttry91].

The great and innovative amount of ideas about the use of this type of sensor made the necessity to develop more advanced electronic instrumentation equipment and at the same time new mathematical models capable of establishing appropriate relationships between electrical parameters given by the monitoring systems and the physical properties of the materials deposited on the sensor.

In that sense, Reed, Kanazawa and Kaufmann in 1990 [Reed90] made an important contribution with a *mathematical model* for electrical admittance of a resonant compound consisted of an AT-cut quartz crystal and a finite thickness viscoelastic layer deposited uniformly over the surface of one of the sensor's electrodes. From this work it becomes evident the fact of every event which modifies the properties of *sensitive interfaces*, i.e. the layer thickness affected by the acoustic wave generated in the quartz's surface, which is susceptible to be measured by the quartz sensor. In this sense, the only monitoring of the resonance frequency does not allow to discriminate between different effects which are involved. Researches increased the efforts in developing electronic circuits for monitoring other parameters additional to the resonance frequency in quartz crystal sensors, e.g. the *motional resistance* [Fruböse93, Auge94, Auge95, Arnau00-1, Arnau01-1, Aranu02].

Martin and Granstaff in 1991obtained an *equivalent electrical model* for the resonant quartz crystal based on the admittance equation of Reed and Kanazawa [Martin91]. These researches studied the resonant compound consisted of a *quartz crystal* in contact with a *thin rigid layer* contacting a *semi-infinite Newtonian liquid*[1]. As it will be shown the model obtained by Martin et al is an extension of the *Butterworth-van-Dyke (BVD) model*.

Starting from the physical model established by Reed and Kanazawa, the general theory for a compound consisted of different layers of several thicknesses and different characteristic impedances can be developed [Granstaff94]. It has been demonstrated that the contribution of load on the quartz crystal response can be modelled with a *Lumped Element Model, LEM,* in which a complex impedance is added to the *motional branch* in the BVD. This lumped element model can be used to characterise microbalance applications in which the relationship between the acoustic impedance of the coating and that of the quartz is smaller than 0.2 without meaningful error [Cernosek98]. After that, it has been demonstrated that this added complex impedance can be decomposed in an equivalent series RLC circuit of frequency independent parameters which constitute the *Extended Butterworth-Van Dyke model, EBVM* [Arnau01-2].

As mentioned it can be inferred that the a precise knowledge of interfacial phenomena is of paramount importance; in that sense studies on secondary effects, no considered before, were developed, e.g. vibrating amplitude distribution on the quartz surface [Mecea89], roughness [Daikhin96, Daikhin97, Daikhin02, Etchenique00] or slip of the layer deposited on the electrode [Ferrante94].

[1] This infinite consideration is regarding the very thin sensitive layer on the quartz surface and due the profundity of penetration of the acoustic wave is very low.

Nowadays, many of the materials studied by acoustic wave devices are not rigidly coupled to the electrode surface; instead they express viscoelastic behaviours that follow the admittance model proposed by Reed and Kanazawa or its variants. This is the case of polymers which are typically used in quartz crystal applications and where its physical and chemical properties are monitored. There are two reasons for the great use of this sensor for the study of *polymers* behaviour: a) for conducting their characterisation it is necessary a few quantity of material; this allows the study of the dynamic behaviour in thin layers for high frequencies; b) due to the low quantity of material a good control over temperature for all the sample can be established, which is an advantage, because temperature is one of the factors that most affects parameters like viscosity.

More recent applications of the quartz crystal which employ polymers use sensor arrays as electronics noses [DiNatale00]. Other extended applications use the quartz sensor for detecting viscoelastic properties in samples; this is the case of polymeric coatings which protect the coated objects. In these cases it is more important to know the rigidity of the layer instead of its thickness [Wolff00]. Other rising application for the quartz crystal as a sensor is the *electrochemical microbalance, EQCM*, in which one of the resonator's electrodes is employed as reference electrode into a three electrodes *electrochemical cell* [Kanazawa93, Oyama95, Hillman01, Calvo97, Varela00]. A particular application of the electrochemical microbalance is that one constituted by the *AC Electrogravimetry* which was proposed by Gabrielli et al. in 1988 [Bourkane88, Bourkane89]. In this application, as it will be shown below, the purpose is to study the different species which take part in an electrochemical *redox process* in an electrochemical cell. Since this technique was proposed, many different applications has been conducted [AlSana03, AlSana04, Benito02, Gabrielli99-1, Gabrielli99-2, Gabrielli00-1, Gabrielli00-2, Gabrielli01, Gabreilli02-1, Gabrielli02-2, García-Jareño00-1, García-Jareño00-2, García-Jareño03]. This quartz crystal sensor application will be treated in a separated section because it constitutes the bases of the whole realisation of the thesis work exposed here.

Other quartz sensor application has appeared recently which is related to particle gels. In this application the quartz sensor is introduced as an alternative method to study those gels [Buckin01]. Particle gels have a small strain region in which their viscoelastic parameters are constant; these materials can be easily broken with strong external strain. For this the measurements of their viscoelastic properties must be conducted whereas the material is subjected to small strains which are usually lower than the range covered by conventional meters. Displacements of the shear strains generated by this technique are extremely small, about Angstroms,

which correspond to the lowest limits for classical instruments that measure such properties [Buckin01]. For instance, for a 5 MHz quartz crystal the average displacement amplitudes on the crystal surface are on the order of 0.5 nm and the maximum amplitude is located in the crystal midpoint where the displacements produced are about 1nm. Technically, the excitation amplitude that can be obtained is on the order of 0.1nm, which corresponds to the atom size and the atomic groups of molecules and it is lower than the characteristic size of the molecular aggregates [Buckin01].

The new range of applications that is opened needs the optimisation of the sensor design in terms of sensitivity, reproducibility and accuracy in the measurements. In the same way, the development of new measurement principles requires a better understanding of the quartz crystal-based resonator's transduction mechanisms.

In this section has been shown that resonators based on quartz sensors are becoming into good alternative analysis method in numerous applications. In order to conduct an adequate interpretation for the results given by these methods is important to know their constitutive steps and take into account the possible error sources to avoid its propagation. The three most important steps included in the *sensor analysis* are the following:

1. Measurement of the adequate resonator's electrical parameters. This step includes the development of electronic instrumentation systems just as properly cells which support the sensor and deform as little as possible its vibrating behaviour.
2. Resonant compound modelling and extraction of the effective physical parameters of the materials deposited on the sensor, using the model of the selected resonator according to a specific application. Appropriate monitoring of the changes of the compound resonator impedance which is contributed by the physical properties of the contacting media; the relationship between impedance changes and the changes in the properties of the contacting media established by using adequate models. Extraction of the effective physical parameters is one of the most complicated tasks and includes the elaboration of mathematical algorithms which receive as inputs the results given by the electronic systems of the previous step.
3. Quantitative and qualitative interpretation of physical, chemical or biological phenomena which are responsible of the change in the equivalent effective parameters of the selected model. For this it is essential to systematically carry out experimental works and design tools which help to do such interpretation. In that sense it is important

the development of simulation environments which allow analysing the effect of certain phenomena like roughness or slip of the material deposited on the sensor on the effective physical parameters. Although final interpretation depends on the application it must be coherent with the changes in the effective physical properties of the coating which were used to define the sensor's physical model. Then it is required a previous interpretation of the changes in the physical properties associated with the changes in the measured experimental parameters. It is not possible to do a coherent realisation of physical, chemical or biological phenomena responsible of the changes in experimental data without correct interpretation of the changes in the properties which define the model.

In this *analytical model*, the error is a consequence of the error propagation which begins with uncertainty introduced in the measurement by the electronic system, follows with the accuracy of the mathematical model used to describe the physical behaviour of the resonant compound employed and ends with the real physical behaviour of the deposited layer.

This thesis work presents a contribution to first and third steps of the analytical model described, because it proposes a novel *electronic instrumentation system* for a specific *quartz crystal microbalance application* which will be described later on. In addition, the results given by the system proposed allow conducting an effective quantitative and qualitative interpretation that enhances the characterisation of the polymers studied by this application.

In order to design an electronic instrumentation system that uses an *EQCM* for *polymers characterisation*, it is of paramount importance a depth knowledge of the physical models used to explain the sensor's behaviour as a continuous electromechanical system. This model allows establishing properly electrical analogies which at the same time allow the introduction of the sensor in the electronic instrumentation system designed.

1.1.2 Quartz Crystal Sensor Fundamentals: Models

Fig. 1.1 shows a section of an *AT-cut quartz crystal* of thickness h_q in contact with a *finite viscoelastic layer* of thickness h_1, contacting a *semi-infinite viscoelastic medium*. This configuration can be considered quite general in sensor applications.

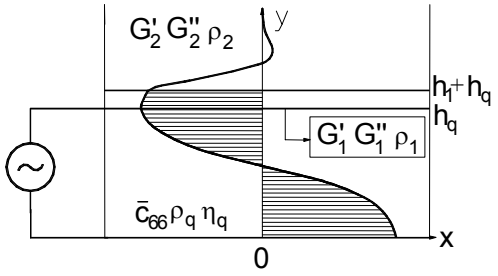

Fig. 1.1. Cross section of a Thickness Shear Mode (TSM) quartz-resonator loaded with a first finite viscoelastic layer and a second semi-infinite viscoelastic layer.

The quartz crystal piezoelectric properties are included in $\bar{c}_{66}$ constant and crystal losses in η_q. For both media on the quartz their viscous and elastic properties are considered and represented by $G_i^{'}$, *shear storage modulus*, and $G_i^{"}$, *shear loss modulus*, where *i=1* and *2* are, respectively, for the first and the second layer.

A *shear strain* is induced in the quartz when an alternating-current (AC) voltage is applied across the crystal through opposite electrodes deposited on its surfaces. It generates a *transversal acoustic wave* propagating through the quartz to the contacting media. The mechanical interaction between the resonator and the contacting media influences the electrical response of the device. This makes possible the use of the resonator as sensor device to detect changes in the physical properties of the contacting media.

In order to treat the sensor as a component included in electronic circuits and to be able of analysing its performance in relation to the external circuitry, an *electrical model* appropriately representing its impedance would be very useful.

The most comprehensive, *one dimensional model* derived, either from the Transmission Line Representation, [Cernosek98, Lucklum97-2, Rosenbaum88] or from a continuous electromechanical model [Arnau99] describes the complex electrical input impedance, *Z*, between the terminals of a loaded QCR as:

$$Z = \frac{1}{j\omega C_0}\left(1 - \frac{\bar{\bar{K}}^2}{\bar{\bar{\alpha}}_q}\frac{2\tan\frac{\bar{\bar{\alpha}}_q}{2} - j\Lambda}{1 - j\Lambda\cot\bar{\bar{\alpha}}_q}\right) \tag{1.1}$$

where $\overline{\overline{K}}$ is the complex electromechanical coupling factor for lossy quartz, $\overline{\overline{\alpha}}_q$ is the complex acoustic wave phase across the lossy quartz, ω is the angular oscillating frequency, C_o is the static capacitance, and $\Lambda = Z_L / Z_q$, where Z_L is the surface load mechanical impedance and $Z_q = (\overline{\overline{c}}_{66}\,\rho_q)^{1/2}$ is the quartz characteristic impedance with ρ_q the quartz density and $\overline{\overline{c}}_{66} = c_{66} + \left(e_{26}^2 / \varepsilon_{22}\right) + j\,\omega\,\eta_q$, the complex effective shear modulus of quartz, c_{66} is the shear stiffness constant, e_{26} is the piezoelectric constant, ε_{22} is the permittivity, and η_q the effective viscosity of quartz (see Table1.1 for *quartz parameters*).

Table 1.1. Properties of typical 10MHz AT-cut quartz

Quartz Parameter	Value	Description
ε_{22}	3.982×10^{-11} A^2 s^4 Kg^{-1} m^{-3}	Permittivity
η_q	9.27×10^{-3} Pa s	Effective viscosity
$\bar{c}_{66}$	2.947×10^{10} N m^{-2}	Piezoelectrically stiffened shear modulus
e_{26}	9.657×10^{-2} A s m^{-2}	Piezoelectric constant
ρ_q	2651 Kg m^{-3}	Density
A_S	2.92×10^{-5} m^2	Effective electrode surface area
h_q	166.18×10^{-6} m	Thickness

The *electrical impedance*, Z, can be transformed into a parallel circuit consisting of a *static capacitance*, C_o, and the so-called *motional impedance*, Z_m, arising from mechanical resonance:

$$Z = \frac{1}{j\,\omega\,C_o} \,//\, Z_m = \frac{Z_m}{1 + j\,\omega\,C_o\,Z_m} \tag{1.2}$$

Where:

$$Z_m = R_m + jX_m = \frac{1}{j\omega C_0}\left(\frac{1 - j\Lambda\cot\overline{\overline{\alpha}}_q}{\frac{\overline{\overline{K}}^2}{\overline{\overline{\alpha}}_q}\left(2\tan\frac{\overline{\overline{\alpha}}_q}{2} - j\Lambda\right)} - 1\right) \tag{1.3}$$

Equation (1.3) can be split into two parts, the first one representing the motional impedance of the unperturbed quartz, Z_m^q, which only depends on

the sensor's parameters and the second one representing the contribution to the global motional impedance created by the surface load, Z_m^L.

$$Z_m = \frac{1}{j\omega C_0}\left(\frac{\bar{\bar{\alpha}}_q}{\bar{\bar{K}}^2} - 1\right) + \frac{1}{\omega C_0}\frac{\bar{\bar{\alpha}}_q}{4\bar{\bar{K}}^2}\frac{\Lambda}{1 - j\dfrac{\Lambda}{2\tan\dfrac{\bar{\bar{\alpha}}_q}{2}}} = Z_m^q + Z_m^L \tag{1.4}$$

Usually the input *electrical admittance*, *Y*, of a quartz sensor rather than its impedance is computed and analysed. From Eqs.(1.2) and (1.3), the admittance is given by:

$$Y = \frac{1}{Z} = j\,\omega\, C_o^* + \frac{1}{Z_m^q + Z_m^L} = G + j\,B \tag{1.5}$$

where $C_o^* = C_o + C_p$ with C_p an added external capacitance parallel to C_o accounting for packaging, connection, etc., *G* is the conductance and *B* the susceptance.

The additive character of the motional quartz impedance and the motional contribution created by the surface load is exact within one-dimensional models and Eq.(1.4) can be applied without restrictions to the load on the quartz crystal [Lucklum97-2].

Equations presented correspond to a generic case where certain extreme cases corresponding to different kinds of load can be studied. Actually, even in these cases the equation that represents the impedance of the resonant compound is still Eq. (1.1); and then Z_L is the only changing parameter in accordance with the load. A complete deduction of the relationship between Z_L and mechanical and geometrical parameters for several kinds of loads are shown elsewhere [Jimenez04].

Both the general model and the simple cases according to load are valid for any frequency and this is the reason why these models are named *Broadband Models* being the so-called *Transmission Line Model*, *TLM*, the most general case deduced; its name comes from the analogy with transmission line impedance equations used in electromagnetic waves propagation.

The motional impedance associated to an unperturbed resonator, Z_m^q, can be simplified, at frequencies near the mechanical resonance into a series of lumped elements (*Lumped Element Model*, *LEM*,) [Martin91, Cady64, Bottom82, Nwankwo98, Arnau01-1, Arnau01-2, Sogorb03] as it is shown in Fig. 1.2 c).

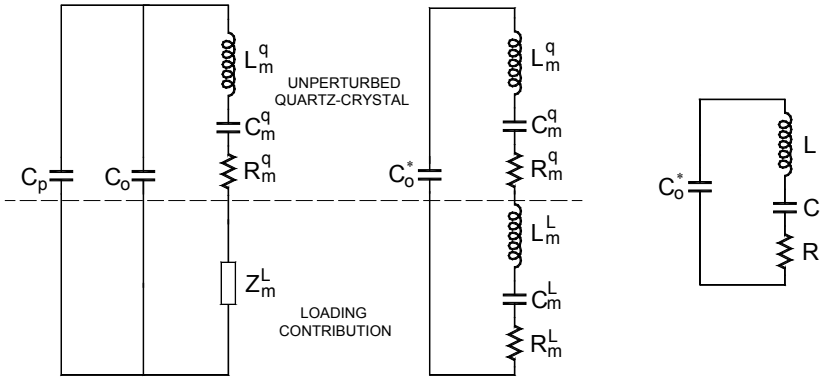

a) b) c)

Fig. 1.2 Equivalent circuit models for load QCR vibrating in TSM: a) LEM Model, b) Extended BVD Model and c) BVD Model.

Z_m^q is given from Eq. (1.4) by:

$$Z_m^q = \frac{1}{j\omega C_0}\left(\frac{\frac{\bar{\bar{\alpha}}_q}{\bar{\bar{K}}^2}}{2\tan\frac{\bar{\bar{\alpha}}_q}{2}} - 1\right) = R_m^q + j\omega L_m^q + \frac{1}{j\omega C_m^q} \tag{1.6}$$

Last member in the former expression describes the motional impedance for the Butterworth-Van Dyke (BVD) equivalent circuit of an unperturbed resonator (Fig. 1.2 a). The circuit elements for the BVD model are [Martin91, Cernosek98]:

$$\begin{aligned} C_o &= \frac{\varepsilon_{22} A_s}{h_q} \\ R_m^q &= \frac{(n\pi)^2 \eta_q}{8 K^2 C_o \bar{c}_{66}} \\ C_m^q &= \frac{8 K^2 C_o}{(n\pi)^2} \\ L_m^q &= \frac{1}{\omega_s^2 C_m^q} \end{aligned} \tag{1.7}$$

where $\bar{c}_{66} = c_{66} + e_{26}^2 / \varepsilon_{22}$ is the quartz effective shear modulus, A_s is the effective area of the electrodes on the crystal, K is the lossless effective electromechanical coupling factor, n (n = 1, 3, 5,..) is the harmonic resonance of quartz, and $\omega_s=2\pi f_s$ is the series resonant angular frequency for the lumped-element approximation given by [Cernosek98, Rossebaum88]:

$$\omega_s \approx \frac{1}{h_q}\sqrt{\frac{\bar{c}_{66}}{\rho_q}}\sqrt{(n\pi)^2 - 8K^2} \tag{1.8}$$

In terms of electrical elements in Fig. 1.2 c), the resonance frequency of the series branch, i.e. the motional series resonance frequency is given by:

$$f_s = \frac{1}{2\pi\sqrt{L \cdot C}} \tag{1.9}$$

From Eq.(1.4) the impedance element associated to the loading interaction, Z_m^L, is given by:

$$Z_m^L = \frac{1}{\omega C_0}\frac{\bar{\bar{\alpha}}_q}{4\bar{\bar{K}}^2}\frac{\Lambda}{1 - j\dfrac{\Lambda}{2\tan\dfrac{\bar{\bar{\alpha}}_q}{2}}} \tag{1.10}$$

Under *small surface load* conditions $Z_L << Z_q$, $(\Lambda << 1)$ and when frequency is near the *motional series resonance frequency, MSRF*, the phase shift experienced by wave crossing the quartz, α_q, is approximately π, then $\tan(\alpha_q/2) \to \infty$ and the term $\Lambda/2\tan(\alpha_q/2)$ in Eq.(1.10) is very lower than one. Under these conditions and assuming $\eta_q \approx 0$, the load motional impedance can be reduced to: [Granstaff94, Cernosek98]

$$Z_m^L = \frac{n\pi}{4K^2\omega_s C_0}\frac{Z_L}{Z_q} \tag{1.11}$$

which corresponds to the expression of Z_m^L in the lumped element model (LEM) in Fig. 1.2 a).

In the LEM Model an electrical impedance is added to the motional branch which represents the loading effects and is expressed by Eq. (1.11). This new model constitutes a simplification of the *Transmission Line Model*, TLM and is used in many cases when viscoelastic layers are employed [Bandey97, Cernosek98]. However, under certain conditions, e.g., near coating resonance, Z_L suffers a meaningful increment so $\Lambda << 1$ is not true anymore; at the same time, the

compound resonance frequency moves further away from unperturbed crystal frequency, and then $\tan(\alpha_q/2) \to \infty$ becomes invalid. Consequently, it can not be assumed $\Lambda/2\tan(\alpha_q/2)$ much smaller than one and the LEM is not longer valid [Cernosek98]. This LEM Model is the starting point for determining the extended Butterworth Van-Dyke Model, Extended-BVD.

It can be proved that the impedance Z_m^L can be split into three elements associated to a resistance $R_m{}^L$, an inductance $L_m{}^L$ and a capacitance $C_m{}^L$. It is not necessary to know, for this thesis purposes, the expressions relating $R_m{}^L$, $L_m{}^L$ and $C_m{}^L$ to the physical and geometrical properties of the quartz and load and they can be found elsewhere [Arnau01-2]. The most important fact is that the loaded quartz can be appropriately described by an *extended BVD equivalent circuit* Fig. 1.2 b) which is composed by parallel capacitor $C_0{}^*$ and the motional branch ($R_m{}^q$, $L_m{}^q$, $C_m{}^q$, $R_m{}^L$, $L_m{}^L$ and $C_m{}^L$) [Martin91]. The response of the unperturbed crystal is determined by $C_0{}^*$, $R_m{}^q$, $L_m{}^q$ and $C_m{}^q$; whereas load contributions are associated to $R_m{}^L$, $L_m{}^L$ and $C_m{}^L$.

When the sensor works in direct contact with a *thin rigid layer* contacting a *semi-infinite fluid*, an especial case appears in which the resonance frequency shift due to the global contribution of the media can be expressed as the additive contribution of the frequency shifts due to each medium separately. This special approach follows the well-known Martin equation and the corresponding extended BVD model includes an inductance representing the contribution of the thin rigid layer as a pure inertial mass contribution on the impedance response of the sensor [Martin91]. Under these circumstances the MSRF is given by:

$$f_s = \frac{1}{2\pi\sqrt{(L_m^q + L_m^L)\cdot C_m^q}} \tag{1.12}$$

When a thin rigid layer is assume to be deposited on the quartz sensor, i.e., when the Sauerbrey behaviour of the coat has been validated, a decrease or increase in resonant frequency shift regarding MSRF, from the unperturbed state, are associated respectively with an increase or a decrease in the surface mass density [Arnau04]. The Sauerbrey's equation expresses this relationship and is given by [Sauerbrey59]:

$$\Delta f_s = \frac{-2f_0^2}{A_s\sqrt{\mu_q\rho_q}}\cdot\Delta m = -K_s\cdot\Delta m' \tag{1.13}$$

Where Δf_s is the resonance frequency shift, $\Delta m'$ is the surface mass density variation in the deposited layer, A_s is the effective piezoelectric area, μ_q is

the quartz shear modulus, ρ_q is the quartz crystal density and f_0 is the fundamental or resonance frequency of the crystal.

As indicated above Eq. (1.13) is valid assuming rigid film behaviour or negligible phase shift of the acoustic wave across the deposited layer. In these conditions the contribution of the viscoelastic properties of the medium in the sensor response is negligible and only inertial contribution is expected [Edwards94]. In a following section it will be shown that the Sauerbrey's equation represents the fundamental relationship for the simplest QCM and EQCM techniques. The mass sensitivity given by the linear relationship between the resonance frequency shift of the quartz sensor and the mass change given by Eq. (1.13) is approximately 40 pg/mm^2 for a 10MHz AT-cut quartz when a resolution of 1Hz is assumed. This extreme sensitivity allows the detection of atomic interactions close to the quartz sensor and establishes the base for the use of quartz microbalance techniques for electrochemical analyse purposes.

In general, the frequency shift associated with the contribution of the media in contact with the sensor does not follow a simple expression [Arnau04]; therefore, it must be understood that the special cases described before have been included with the purpose of explaining in a simple way the basics of the QCM and EQCM techniques. However, it is important to make clear that when the viscoelastic behaviour of the sensitive layer in contact with the quartz sensor can not be neglected in the sensor response, the data interpretation can not be longer made in terms of mass effect. Moreover, the only measurement of motional series resonant frequency and motional resistance shifts are not enough for extracting the sensitive layer properties, and for making any physical or chemical interpretation of what is happening if at least some of the layer properties are assumed to be known. Furthermore, the frequency and resistance shifts provided by typical oscillators are not always related to the motional series resonant frequency and resistance shifts, which are normally taken as the maximum conductance frequency shift and as the difference of the reciprocal of the conductance peaks, respectively. In general, a complete monitoring of the admittance spectrum of the sensor around resonance by means of an *impedance analyser* gives more precise information. However the specific characteristics of the AC Electrogravimetry (this is the application directly related to this thesis work), make impossible the use of the impedance analyser for an appropriate monitoring of the interesting parameters as it will be explained next. For more information about the impedance analyser and other techniques for monitoring the parameters of a QCM see the appendix I.

1.2 AC Electrogravimetry Technique Fundamentals

When Quartz Crystal Microbalances began to be used in situ, in electrochemical systems, they became to be known as *Electrochemical Quartz Crystal Microbalances, EQCM* [Varela00], in these systems one of the quartz crystal electrodes is used as the working electrode in an electrochemical cell. This fact has allowed getting relevant information for understanding charge transport processes at molecular level. This schema provides important information related to electron, ion and solvent activities and mass transfer associated with different electrochemical studies [Bourkane89, Varela00, Bruckenstein85, Melroy86, Lu84]. EQCM systems could be catalogued as potentiostatic or galvanostatic. In the first type the potential of the specific electrode (cathode or anode) is controlled while in the second type the current through the working electrode is controlled.

Figure Fig. 1.3 shows a typical experimental set-up for a potentiostatic EQCM system [Varela00]. The system is composed by an electrochemical cell with three electrodes: working electrode WE, reference electrode RE, and counter electrode CE; additionally, according to the structure of a potentiostatic system [Skoog94, Skoog97]), a potentiostat, a frequency meter, a power source, a controlled quartz sensor oscillator, and a computer are present.

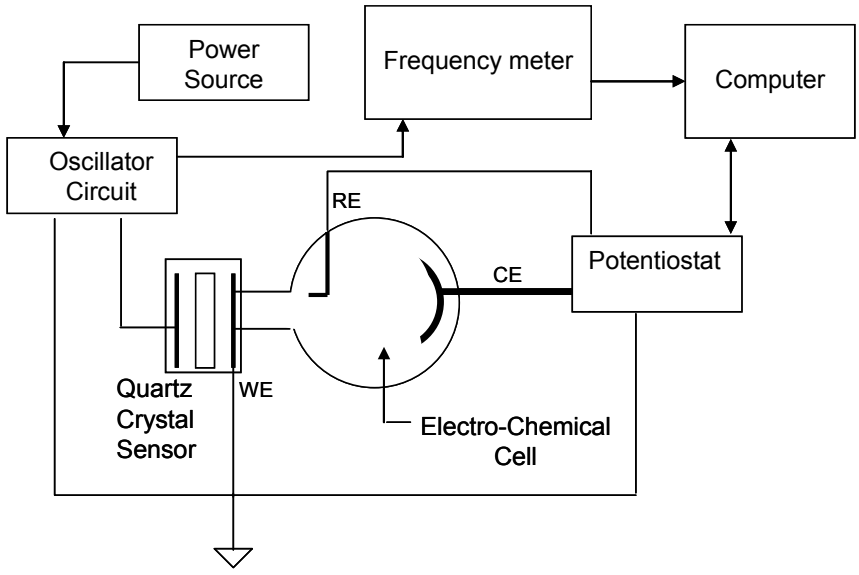

Fig. 1.3. Typical experimental distribution with EQCM, adapted from [Varela00].

It can be noticed that one of the sensor electrodes in the QCM is in contact with the electrolyte inside the electrochemical cell, operating as a working electrode which is interface to a conducting solution containing electroactive species. For instance, metal cations may be dissolved in an acidic solution. By applying a negative potential to the working electrode, the cations can be deposited onto the electrode as metal atoms. The deposited mass is sensed using the QCM. Moreover, the current during the deposition is also monitored and by integration, the charge per unit area can be measured. If it is known from the chemistry that all of the charge is used for the deposition, the charge-to-mass ratio can then be determined. Or if some of the current goes into other reactions (for example the creation of hydrogen molecules), then the fraction of the current used to deposit the metal atoms (the Faradaic efficiency) can be measured [Arnau04]. In electrical terms, the working electrode is normally grounded to ensure the complete separation of the electrochemical electric fields from the radio frequency electric fields.

An oxidation-reduction reaction (*redox*) produced by the application of an electrochemical perturbation, i.e., by the application of a potential difference between the working and reference electrodes, will produce a mass variation in the material layer (conducting polymer for instance) in contact with one face of the QCM. This mass variation, according to Eq. (1.13), will produce a resonance frequency shift of the sensor and then in the oscillating frequency of the QCM controlled sensor oscillator.

This frequency is monitored in the frequency meter and registered in a central computer and then the linear relationship described by Eq. (1.13) can be used to calculate the amount of mass transfer in the experiment.

The potentiostat is concerned to provide the potential difference between working and reference electrodes to produce the electrolysis, to measure the potential difference between working and reference electrodes, during the process, and finally to measure the current of the electrochemical cell.

All these variables must be monitored and can be used to obtain some specific transfer functions important in several electrochemical studies [Bourkane88, Gabrielli99, Gabrielli00, García-Jareño00, Gabrielli02, Benito02, AlSana03, AlSana04].

1.2.1 General Electrogravimetry

In general, *Electrogravimetry* is a measurement or experimentation in analytical chemistry in which electrolysis in a electrochemical cell is conducted for long periods of time in order to assure that a measured or

analysed substance, called *analyte*, immerse in a solution or *electrolyte*, becomes completely oxidised or reduced to a known composition product. This product of the electrolysis process is deposited on one of the electrodes of the electrochemical cell, the working electrode, and then subsequently is weighted [Skoog97]. The process by means a material is deposited, generally a metal, is known as electrolytic precipitation.

Some electrogravimetry measurement techniques are based on *electrochemical cell working principle* [Skoog94], which are composed by two electrodes immerse each one in an adequate electrolyte solution and connected by a dissolution called salt bridge which allows the ions flow between the two dissolutions where electrodes are immerse.

When an electric voltage is applied between the two electrodes in this electrochemical cell, current flows between them whose value depends on both the cell specific characteristics and the deposited material properties on the working electrode after electrolysis has been achieved.

Electrogravimetry is a moderately sensitive and quick technique and is ones of the most precise and accurate techniques in chemistry nowadays [Skoog97].

There are traditionally two types of electrogravimetric methods. In the first one the voltage on the working electrode is not controlled and the voltage applied to the electrochemical cell is maintained in an approximately constant value to produce the flow of a current large enough to fulfil the electrolysis in a reasonable time. This method is used when it is desired a separation of an easily reducible cation, i.e., to separate substances which different separation voltages easily discernible [Skoog97]. This is the galvanostatic method introduced above.

When substances or metals with near separation voltages are required to be separated, the second method called *potentiostatic method* or cathode or anode controlled method, is used. In this method there are three electrodes: a working electrode, WE, a reference electrode, RE (for instance, standard SCE calomel electrode [Skoog97] with 0.244 V reference voltage at 25ºC) and a counter electrode, CE, or additional electrode. Al three electrodes are organised in such a way they build two independent circuits.

The first circuit is a reference or control circuit and it is composed by the reference electrode, a voltage meter and the working electrode. Another circuit is the electrolysis circuit, which is composed by the working electrode, the counter electrode, a voltage power supply, a current meter and a voltage divider. Voltage divider circuit allows a continuous variation in the voltage applied between the working electrode and the counter electrode to avoid co-deposition of metals with similar separation voltage.

The purpose of the reference circuit is a continuous measurement of the voltage applied between the working electrode and the reference electrode.

When this voltage reaches certain level in which the substances or metals *co-deposition* is close to be produced, an order is sent to the voltage divider circuit, by mean of the feedback signal, to decrease the voltage applied between working electrode and counter electrode avoiding this way co-depositions. This task is constantly performed during whole *electrolysis process.*

The system involved for both measuring currents and voltages and controlling the voltage difference between counter electrode and working electrode is called potentiostat.

Methods shown above specifically look for extracting a material, generally a metal, present into a solution, which is separated from the solution and is deposited by precipitation over the working electrode; then the mass quantity of this material, is required to be measured. It is important to note the material deposited over the working electrode generally has very low weight

In addition it is pretended to study the behaviour of certain *conductive polymers* deposited over the working electrode by electrogravimetry, in order to kwon their performance and provided interesting data for many industrial applications [Varela00].

Electrogravimetry is classified as an *interface dynamic method* [Skoog97] in the electroanalytical chemistry because it studies about phenomena that take part in electode-electolyte interface or electrode-polymer deposited interface or polymer deposited-electrolyte interface; in addition, it is a dynamic method due to the presence of electrical current.

The work developed in this thesis project is mainly concerned to AC Electrogravimetry which is a special variation of the most general electrogravimetry subject just explained above. Next section is involved in the explanation of the fundamentals of AC Electrogravimetry in order to show the basis of this technique for better understanding of the specific problem this thesis work deals with and then to establish the objectives to solve that problem.

1.2.2 AC Electrogravimetry

1.2.2.1 Overview

The mechanism by which the charge transfer is produced in a conductive sensitive layer in contact with an electrode or an electrolyte has been a

topic of study by several authors, due to its important applications in industrial, environmental and biological process such as: metal electrodepositing [Bruckenstein85], corrosion sensors [Hager86], electrochemical process characterisation which govern alkaline batteries [Varela00], study of polymers behaviour in presence of antibodies [AlSana03] or for making devices that emulate certain corporal senses function like smell [Beeley04], among others.

The *redox* mechanism has been studied using several techniques, but these do not give all the information needed in order to discriminate with certainty the activity or kinetic of each particle involved in the process over the conductive polymer, i.e., anions, cations and solvent or electrolyte [Gabrielli99-1].

A technique called "*AC Electrogravimetry*", firstly proposed by Gabrielli et al [Bourkane88], at LISE (Laboratory of electrochemical systems and interfaces), can be used to discriminate the activity of the different species involved in the charge transfer during an electrochemical process, including the case in which a conductive polymer is used as a substrate. This technique can be combined with Electrochemical Impedance Spectroscopy, EIS [Gabrielli99] (which is used to monitor the impedance of the electrochemical cell during electrolysis) to obtain additional useful information in different applications.

The AC Electrogravimetry's operation principle can be explained by means of Fig. 1.4 and Fig. 1.5.

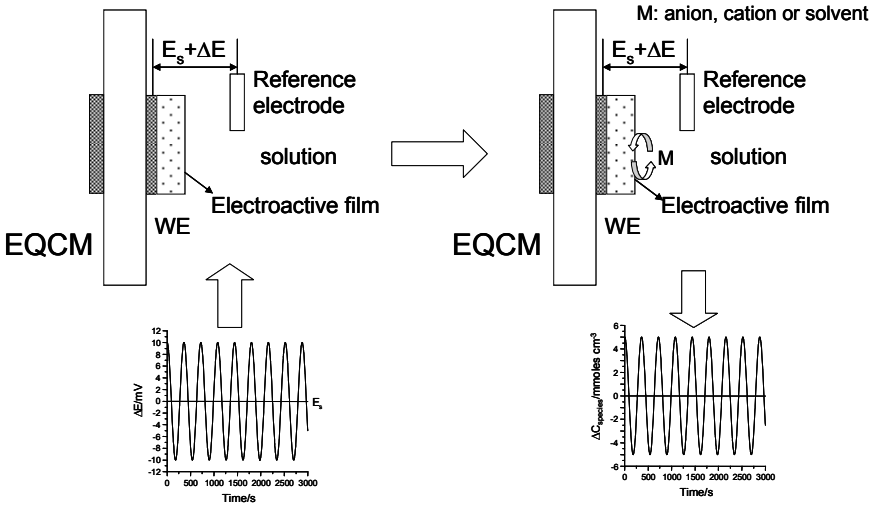

Fig. 1.4. AC Electrogravimetry operation principle. Voltage difference applied to EQCM.

Fig. 1.4 represents the QCM immerse in a solution with the conductive polymer (electroactive film) to be analysed deposited on the electrode of the QCM which acts as the WE of the electrochemical cell, i.e., it is acting as an EQCM. A low voltage sinusoidal wave is superimposed to a continuous voltage (E_s+ΔE) and applied between the reference electrode and the working electrode. This sinusoidal wave will produce a *charge transfer* (*mass variation*) in the polymer due to *redox processes* in the presence of both ions and solvent (M) in the solution.

Fig. 1.5 shows how this mass transfer, produced by the incoming and outgoing of ions and solvent in the polymer, produces a density change and then a resonance frequency shift in the working crystal. This resonance frequency shift of the crystal is related to the mass change in the working electrode under dynamic regime, i.e., following constrains imposed by Sauerbrey equation and explained above, Eq. (1.13).

Finally, the so-called *Electrogravimetric Transfer Function*, *EGTF*, is obtained by combining the *voltage change* provided by the potentiostat to the QCM in the electrochemical cell and the *mass transfer* monitored by the EQCM as Δm/ΔE.

This transfer function is calculated for each frequency of the superimposed sinusoidal wave (modulating signal) by means of a frequency analyser. EGTF and Electrochemical Impedance, ΔE/ΔI, data are registered in a computer which provides the graphic analysis for all electrochemical study that is conducted. For the purposes of this thesis is only required the information regarding EGTF, so the most information related here will be about it.

It is important to make clear that the AC Electrogravimetry technique allows both finding relevant results regarding to the kinetic of the ions involved in the process and discriminating the different species participating in the electrochemical process [Bourkane88, Bourkane89, Gabrielli99, Gabrielli00, García-Jareño00, García-Jareño01, Gabrielli01-Gabrielli02, Benito02, García-Jareño03, AlSana03, AlSana04]. This is possible thanks to the different reacting response of the different species involved in the electrochemical process as a function of the frequency of the superimposed modulating signal.

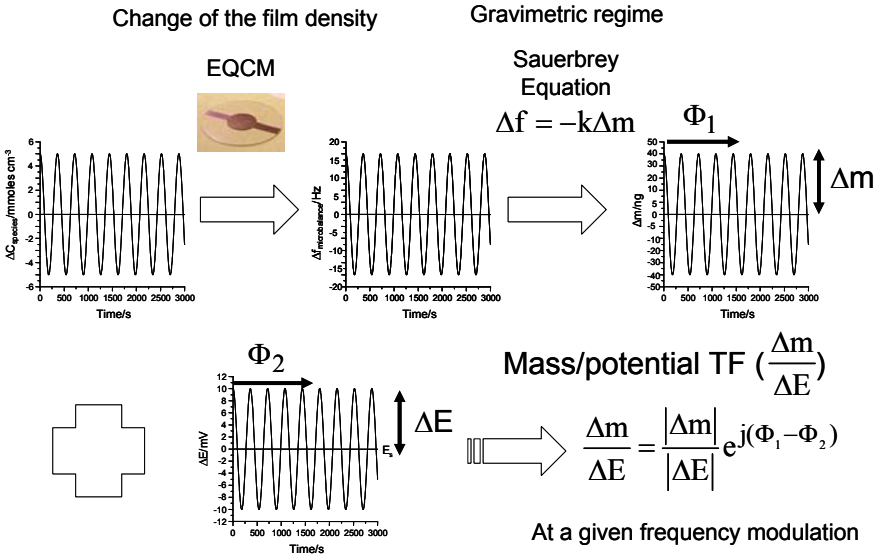

Fig. 1.5. AC Electrogravimetry operation principle. Process to obtain the Electrogravimetry Transfer Function, EGTF.

Before showing the typical responses obtained from the AC Electrogravimetry technique it is important to introduce a theoretical modelling [Gabrielli02] for the electrode-film and film-electrolyte interfaces and mass transport associated to an EQCM in the AC Electrogravimetry.

1.2.2.2 Charge Transfer and Mass Transfer Modelling

Fig. 1.6 shows a schematic representation of an electrode modified by a conductive polymer (EQCM) of thickness *d.* This modified electrode, immerse in an electrolyte, defines two interfaces: metal-polymer at *x=0* and polymer-electrolyte at *x=d*. The first interface is an ion blocking interface and second is an electron blocking interface. For this one-dimensional model the metal-polymer interface is located at *x=0* and the polymer-electrolyte interface is located at *x=d.*

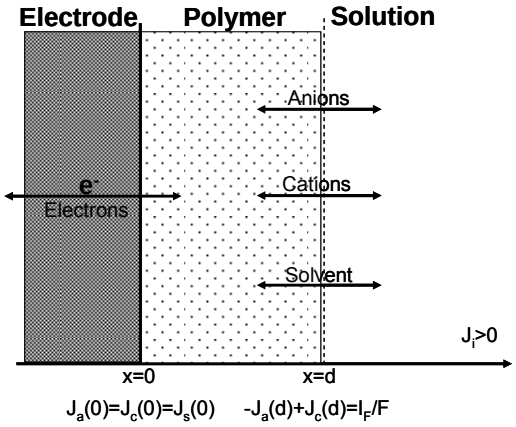

Fig. 1.6. Schematic representation for the interfaces of a EQCM in contact with solution.

The hypotheses of the simplified model presented are the following:

Anions (a), cations (c) and solvent (s) are supposed to be transported through the polymer only by diffusion; so the diffusion equations are defined as [Gabrielli00-3]:

$$J_i = -D_i \frac{\partial C_i}{\partial x}$$

and

$$\frac{\partial C_i}{\partial t} = -\frac{\partial J_i}{\partial x} \tag{1.14}$$

where C_i is the concentration of a, c or s, D_i and J_i are the diffusion coefficient and flux of species i respectively.

The solution considered is an electrolytic medium where cations, anions and solvent can move through the solution-polymer interface to neutralise the charges created by the *redox* reaction of the electroactive polymer. By definition fluxes of species i (i= c, a or s), J_i, are positive for outgoing ions, i.e.:

$$J_i > 0 \quad for \quad x > 0 \qquad i = a, c, s \tag{1.15}$$

The following boundary conditions are applied:
At metal-polymer interface:

$$x = 0 \quad J_a(0) = J_c(0) = J_s(0) = 0 \tag{1.16}$$

Electroneutrality imposes the condition that charges, which cross the polymer-electrolyte interface balance the electrons which enter or leave the

electrode at electrode-polymer interface and leads to the Faraday current density, I_F:

$$x = d \quad -J_a(d) + J_c(d) = \frac{I_F}{F} \tag{1.17}$$

where F is the Faraday constant and I_F is the Faraday current density.

When cations (c), anions (a) and solvent (s) are involved in the reaction, the associated mass change and the electric charge passed through the electrode-polymer interface, per surface unit, are given by:

$$\Delta q = -F\Delta\xi_c + F\Delta\xi_a \tag{1.18}$$

$$\Delta m = m_c\Delta\xi_c + m_a\Delta\xi_a + m_s\Delta\xi_s \tag{1.19}$$

where m_c, m_a, and m_s are the molar masses of cation, anion an solvent respectively, and $\Delta\xi_c$, $\Delta\xi_a$ and $\Delta\xi_s$ are the number of moles exchanged for cationic species, anionic species and solvent per surface unit respectively.

In a simple way, the doping mechanism of an electroactive polymer can be described by

$$< P > + e^- + M^+ \underset{k_c'}{\overset{k_c}{\Longleftrightarrow}} < P, M > \tag{1.20}$$

and

$$< P > + A^- \underset{k_a'}{\overset{k_a}{\Longleftrightarrow}} < P, A^- > + e^-$$

where <*P*>is the host electroactive polymer and <*P,M*> and <*P,A*$^-$> are the species (cations, c and anions, a) inserted in the electroactive film (polymer). Therefore, the net instantaneous molar flux of species *i* (c, a or s) is $J_i = d\xi_i/dt$ in mol cm^{-2} s^{-1}; this can be expressed in terms of concentrations as $C_i = \xi_i/d$, where d is the polymer thickness as it is shown in Fig. 1.6.

According to a formalism introduce elsewhere [Gabrielli00-3] and by applying the classical kinetic law for heterogeneous reactions, the time derivative of the concentration for each species C_i is given by

$$J_i(d) = -\frac{d\xi_i}{dt} = -d\frac{dC_i}{dt} = k_i(C_i - C_{i\min}) - k_i'(C_{i\max} - C_i)C_{isol} \tag{1.21}$$

where $dC_i/dt > 0$ for species inserted in the polymer, C_{imax} is the maximum concentration of sites available for insertion, C_{imin} is the minimum concentration of sited occupied the species in the host film

(polymer), C_{isol} is the concentrations of the species i in the solution, and k_i and k_i' are the kinetics rate constants of transfer, which are potential dependent, $k_i = k_{i0}\exp(b_i(E-E_i^0))$ and $k_i^{'} = k_{i0}^{'}\exp(b_i^{'}(E-E_i^0))$, where E is the voltage and E_i^0 is the normal potential and $b_i = \alpha_i nF/RT$ are the Tafel coefficients whose values depends on the particles involved in reaction [Gabrielli99-1, Arnau04].

This formulation for the modified electrode can be analysed under two circumstances: *steady state* and *dynamic behaviour*.

At *steady state* the global flux of species is zero, $J_i(x)=0$; therefore, concentrations C_i and voltage E are constants throughout the polymer.

From Eq.(1.21) it can be obtained:

$$\frac{C_i - C_{i\min}}{C_{i\max} - C_i} = C_{isol}\frac{k_i^{'}}{k_i} = C_{isol}\frac{k_{i0}^{'}}{k_{i0}}e^{(b_i^{'}-b_i)(E-E_i^0)} = e^{(b_i^{'}-b_i)(E-E_i^0-E_i)} \tag{1.22}$$

where E_i is such that $C_{isol}k_{io}^{'}/k_{io} = e^{-(b_i^{'}-b_i)E_i}$.

Operating Eq. (1.22) it is obtained:

$$C_i(E) = \frac{C_{i\max}e^{(b_i^{'}-b_i)(E-E_i^0-E_i)} + C_{i\min}}{1+e^{(b_i^{'}-b_i)(E-E_i^0-E_i)}} \tag{1.23}$$

Thus, the derivative of the concentration of species i regarding to the voltage, i.e., the derivative of the insertion-expulsion law is equal to:

$$\frac{dC_i(E)}{dE} = \frac{b_i - b_i^{'}}{4}\frac{C_{i\max} - C_{i\min}}{\cosh^2\left[\dfrac{(b_i^{'}-b_i)(E-E_i^0-E_i)}{2}\right]} \tag{1.24}$$

In the *dynamic regime* when a small sine wave potential change, ΔE, is superimposed onto the polarisation potential difference across electrode-polymer-electrolyte interfaces, low-amplitude sine wave concentrations, ΔC, and fluxes, ΔJ, are observed, from Eq. (1.14):

$$\begin{aligned}\Delta J_i &= -D_i\frac{\partial \Delta C_i}{\partial x}\\ j\omega\Delta C_i &= -\frac{\partial \Delta J_i}{\partial x}\end{aligned} \tag{1.25}$$

where $\omega=2\pi f$ is the angular frequency and f is the sine wave linear frequency. At $x=d$, Eq. (1.17) becomes:

$$-\Delta J_a(d) + \Delta J_c(d) = \frac{\Delta I_F}{F} \tag{1.26}$$

Applying the total differential[2] to Eq. (1.21) is obtained the following expression:

$$\Delta J_i(d) = \left[\frac{\partial\left[k_i(C_i - C_{i\min}) - k_i^{'}(C_{i\max} - C_i)C_{isol}\right]}{\partial E}\right]\Delta E + \left[\frac{\partial\left[k_i(C_i - C_{i\min}) - k_i^{'}(C_{i\max} - C_i)C_{isol}\right]}{\partial C_i}\right]\Delta C_i \quad (1.27)$$

and using the expressions for k_i and $k_i^{'}$ introduced above and their derivatives respect E:

$$\partial k_i / \partial E = b_i k_{i0} \exp(b_i(E - E_i^0))$$
$$\partial k_i^{'} / \partial E = b_i^{'} k_{i0} \exp(b_i^{'}(E - E_i^0))$$

the previous expression leads to:

$$\Delta J_i(d) = \left[b_i k_i(C_i - C_{i\min}) - b_i^{'}k_i^{'}(C_{i\max} - C_i)C_{isol}\right]\Delta E + \left[k_i - k_i^{'}C_{isol}\right]\Delta C_i \quad (1.28)$$

Finally using Eq. (1.25) the previous expression can be written as:

$$\Delta J_i(d) = -j\omega d\Delta C_i = K_i\Delta C_i(d) + G_i\Delta E \quad with\ i = c,a,s \quad (1.29)$$

where

$$G_i = [b_i k_i(C_i - C_{i\min}) - b_i^{'}k_i^{'}(C_{i\max} - C_i)C_{isol}] \quad (1.30)$$

and

$$K_i = k_i + k_i^{'}C_{isol} \quad (1.31)$$

In Eq. (1.30) $G_i<0$ for inserting species and $G_i>0$ for expelling species.

The relationship between the species concentration in the polymer, ΔC_i, and voltage variation induced, ΔE, according to Eq. (1.29) is given by:

$$\frac{\Delta C_i}{\Delta E}(\omega) = \frac{-G_i}{j\omega d + K_i} \quad (1.32)$$

The previous expressions allows to the electrochemical impedance, $(\Delta E/\Delta I)(\omega)$ and the Electrogravimetry Transfer Function, EGTF,

[2] Total differential for a variable $z(x,y)$ is $\Delta z=(\partial z/\partial x)\Delta x+(\partial z/\partial y)\Delta y$.

(Δm/ΔE)(ω) to be calculated as follows in the AC Electrogravimetry experimental technique.

Faraday current density change, ΔI_F is related to the charge change, Δq, by $\Delta I_F = j\omega \Delta q$ and dividing Eq. (1.18) ΔE and by using $C_i = \xi_i / d$, the electrochemical impedance becomes:

$$\frac{\Delta E}{\Delta I}(\omega) = \frac{1}{j\omega dF\left[-\frac{\Delta C_c}{\Delta E}(\omega) + \frac{\Delta C_a}{\Delta E}(\omega)\right]} \tag{1.33}$$

and considering the polymer-solution interface as a capacitance (electrolyte resistance has been neglected [Gabrielli02]) in series to this impedance, previous expression leads to:

$$\frac{\Delta E}{\Delta I}(\omega) = \frac{1}{j\omega C_{\text{int}erface} + j\omega dF\left[-\frac{\Delta C_c}{\Delta E}(\omega) + \frac{\Delta C_a}{\Delta E}(\omega)\right]} \tag{1.34}$$

In the same way, using expression cited above the EGTF can be established as:

$$\frac{\Delta m}{\Delta E}(\omega) = d\left[m_c \frac{\Delta C_c}{\Delta E}(\omega) + m_a \frac{\Delta C_a}{\Delta E}(\omega) + m_s \frac{\Delta C_s}{\Delta E}(\omega)\right] \tag{1.35}$$

By using Eq.(1.32) it is obtained:

$$\frac{\Delta E}{\Delta I}(\omega) = \frac{1}{j\omega C_{\text{int}erface} + j\omega dF\left[\frac{G_c}{j\omega d + K_c} - \frac{G_a}{j\omega d + K_a}\right]} \tag{1.36}$$

and

$$\frac{\Delta m}{\Delta E}(\omega) = -d\left[m_c \frac{G_c}{j\omega d + K_c} + m_a \frac{G_a}{j\omega d + K_a} + m_s \frac{G_s}{j\omega d + K_s}\right] \tag{1.37}$$

As it can be noticed in Eq. (1.36) only charged species, anions and cations, are implied in the electrochemical impedance whereas the EGTF, Eq.(1.37), depends on cations, anions and solvent all together.

Two other important expressions related to EGFT that can be obtained to discriminate the influence of the various species: the *electric charge-potential transfer function*, $(\Delta q/\Delta E)(\omega)$, and the *mass-electric charge transfer function*, $(\Delta m/\Delta q)(\omega)$. First one can be calculated using $\Delta I_F = j\omega \Delta q$ and from Eq.(1.36) as follows:

$$\frac{\Delta q}{\Delta E}(\omega) = \frac{1}{j\omega}\frac{\Delta I_F}{\Delta E}(\omega) = dF\left(\frac{G_c}{j\omega d + K_c} - \frac{G_a}{j\omega d + K_a}\right) \tag{1.38}$$

In a similar way for $(\Delta m/\Delta q)(\omega)$ becomes:

$$\frac{\Delta m}{\Delta q}(\omega) = j\omega\frac{\Delta E}{\Delta I_F}(\omega)\frac{\Delta m}{\Delta E}(\omega) =$$

$$= \frac{-\left(m_c\frac{G_c}{j\omega d + K_c} + m_a\frac{G_a}{j\omega d + K_a} + m_s\frac{G_s}{j\omega d + K_s}\right)}{F\left(\frac{G_c}{j\omega d + K_c} - \frac{G_a}{j\omega d + K_a}\right)} \tag{1.39}$$

It can be noticed when only one species, a or c, is involved in the charge exchange, $(\Delta m/\Delta q)(\omega)$ is independent about frequency and equals to m_i/F.

For the purposes of this project the most important quantities to be used are the calculated based on EGTF.

In order to explain the basic concepts of this approach about the transfer function obtained; for simple systems EGTF is calculated from Eq.(1.37) for one interfering ion, which can be inserted in the polymer or expulses from it. In this case EGTF response found for one species is given by:

$$\frac{\Delta m(\omega)}{\Delta E(\omega)} = -d\left(m_i\frac{G_i}{j\omega d + K_i}\right) \quad with\, i = c, a\ or\ s \tag{1.40}$$

1.2.2.3 Typical Graphical Responses

After the introduction of the model for the AC Electrogravimetry Technique, some typical graphical responses are introduced.

According to Eq.(1.40), Fig. 1.7 shows a schematic diagram of a typical EGTF response plotted in a complex plane. This kind of figure is well-known as Nyquist plot and its purpose is to show the behaviour of a magnitude or variable both in amplitude and phase as the frequency changes.

It can be noticed that when only one species is involved in the experiment the plot is characterised by one loop. The location of the loop depends on the charge of the ion, so it is placed in the first quadrant if the experiment deals with an anion insertion and in the third quadrant if it is a cation expulsion. The arrows in the figure indicate the direction of the modulating signal frequency increase.

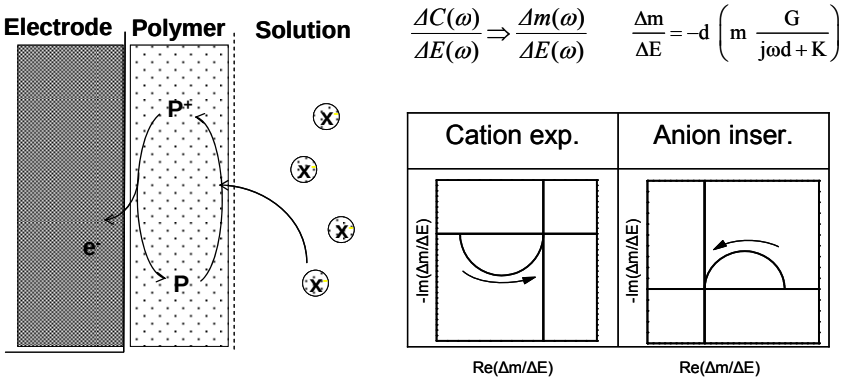

Fig. 1.7. Nyquist response of EGTF for one species analysed. Adapted from [Gabrielli02-1].

The reason for the presence of the plot in the first or third quadrant depends on the sign provided by the constant *G* (minus for anion insertion and plus for cation expulsion).

For the electrochemical behaviour of the polymer there is an explanation about the location of the loops according to Eq.(1.40) as follows: when the polymer is *oxidise* ($\Delta E > 0$), positive sites are created in the polymer and if the cation expulsion is considered ($\Delta m < 0$) during the charge compensation the low-frequency limit of the EGTF becomes negative ($(\Delta m/\Delta E)(\omega \rightarrow 0) < 0$) and equals to $-dm_iG_i/K_i$ (Considering the sign provided by the constant *G* as it was mentioned) as it is illustrated in the previous figure. If the charge compensation is due to an anion insertion, an increase in mass of the polymer is induced ($\Delta m > 0$) and, therefore, $(\Delta m/\Delta E)(\omega \rightarrow 0)$ tends to the positive value dm_iG_i/K_i. In addition, the diameter of the Nyquist response for the EGTF depends on the mass of the involved ionic species, m_i, since $(\Delta m/\Delta E)(\omega \rightarrow 0) = -dm_iG_i/K_i$.

The mass-electric charge transfer function in Eq.(1.39), multiplied by the Faraday constant, *F*, gives directly the atomic mass of the ion with a negative value for the cation and a positive value for the anion. Moreover, the ratio mass-charge is independent of frequency, *f*, when only one ionic species is involved in the *redox* process as it was mentioned above.
Summarising if *EGTF* and *mass-charge transfer* functions are obtained it is possible to determinate some data regarding kinetics and mass of the ion involved in the *redox* process.

When three species are involved in the process the model is a little bit more complicated [Gabrielli02-2] due to the contribution of the different species; in this case the expression which models the EGTF follows the Eq.(1.37) and is expressed in a compact way as:

$$\frac{\Delta m(\omega)}{\Delta E(\omega)} = -d\left(m_i \sum_{i=1}^{3} \frac{G_i}{j\omega d + K_i} \right) \tag{1.41}$$

where *i* can be a, c or s. In this case a typical Nyquist response is depicted in Fig. 1.8.

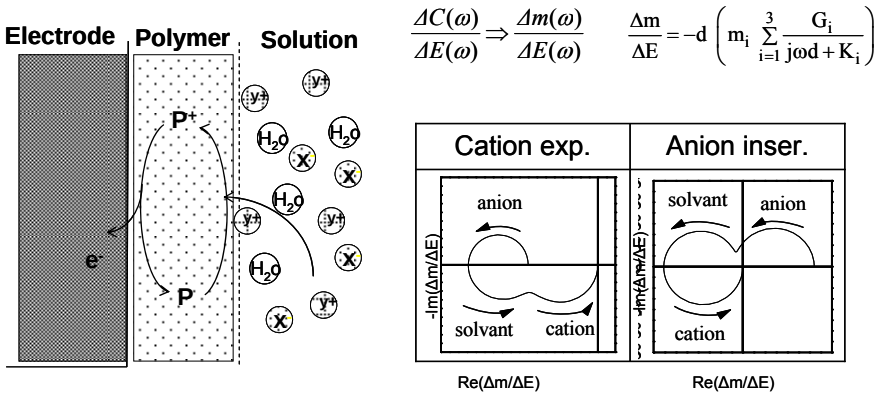

Fig. 1.8. Nyquist response of EGTF for three species analysed. Adapted from [Gabrielli02-2].

Fig. 1.8 shows the schematic description for two typical situations: a) cations and solvent expelled and anion inserted and b) cation expelled and anion and solvent inserted. Again the arrows indicate the direction of increasing frequency.

Electrogravimetry Transfer Function, EGTF, in this case takes into account all of the species involved in the *redox* reaction, in Fig. 1.8 three species: cations for highest frequencies and anions for the lowest frequencies, Therefore, the kinetics of cations is faster than that of the anions. For several species involved the low frequency limit for Eq.(1.41), $(\Delta m/\Delta E)(\omega \rightarrow 0)$, depends on all species that take part in the redox reaction. Concerning the *mass-electric charge transfer function*, $(\Delta m/\Delta q)(\omega)F$, it is frequency dependent and produces some loops in its Nyquist response [Gabrielli02-2].

Generally, loops found in responses in Fig. 1.8 are not prior identified for each frequency range, so it is necessary to design a strategy to determine which part of the found loops is concerning to each species that takes part in the redox process. Because three quantities are unknown, the cation, anion and solvent responses to ΔE and only two quantities, $(\Delta E/\Delta I)(\omega)$ and $(\Delta m/\Delta E)(\omega)$ are measured in the experimental setup. It is not possible to separately calculate the three unknown quantities [Gabrielli02-1].

However it is possible to eliminate the contribution of one species from the EGTF.

If the response of the anion "a" is eliminated from the EGTF, the *Partial Electrogravimetric Transfer Function* left is calculated as follows:

As it was shown above when only one species is involved in the charge exchange, ($\Delta m/\Delta q$)(ω) equals to m_i/F, in the case of anions it will be:

$$\frac{\Delta m}{\Delta q}(\omega) = \frac{m_a}{F} \tag{1.42}$$

and from Eq. (1.39):

$$\frac{\Delta m_a}{\Delta E}(\omega) = \frac{\Delta m}{\Delta q}(\omega)\frac{\Delta I_F}{j\omega\Delta E}(\omega) \tag{1.43}$$

by substituting $\Delta I_F = j\omega\Delta q$ and Eq.(1.42) the previous expression becomes:

$$\frac{\Delta m_a}{\Delta E}(\omega) = \frac{m_a}{F}\frac{\Delta q}{\Delta E}(\omega) \tag{1.44}$$

now if the anion response is eliminated from the EGTF, the Partial Electrogravimetric Transfer Functions due to cations and solvent, $PEGFT_{cs}$ are given by:

$$\frac{\Delta m_{cs}}{\Delta E}(\omega) = \frac{\Delta m}{\Delta E}(\omega) - \frac{\Delta m_a}{\Delta E}(\omega) \tag{1.45}$$

and substituting Eq.(1.44) the $PEGFT_{cs}$ becomes [Gabrielli99-2]:

$$\frac{\Delta m_{cs}}{\Delta E}(\omega) = \frac{\Delta m}{\Delta E}(\omega) - \frac{m_a}{F}\frac{\Delta q}{\Delta E}(\omega) \tag{1.46}$$

by using Eq.(1.37) and (1.38) the previous expression leads to:

$$\frac{\Delta m_{cs}}{\Delta E}(\omega) = -d\left[(m_c + m_a)\frac{G_c}{j\omega d + K_c} + m_s\frac{G_s}{j\omega d + K_s}\right] \tag{1.47}$$

Similarly if the cation contribution is eliminated in the Electrogravimetric Transfer Function, the resulting $PEGTF_{as}$ is equal to [Gabrielli99-2]:

$$\frac{\Delta m_{as}}{\Delta E}(\omega) = \frac{\Delta m}{\Delta E}(\omega) + \frac{m_c}{F}\frac{\Delta q}{\Delta E}(\omega) \tag{1.48}$$

and substituting Eq.(1.37) and (1.38) previous expression leads to:

$$\frac{\Delta m_{as}}{\Delta E}(\omega) = -d\left[(m_a + m_c)\frac{G_a}{j\omega d + K_a} + m_s \frac{G_s}{j\omega d + K_s}\right] \tag{1.49}$$

From the plot of the Partial Electrogravimetric Transfer Functions the discrimination and evaluation of the number of species taking part in the redox process in the AC Electrogravimetry Technique, can be established [Gabrielli02] as it is illustrated in Fig. 1.9.

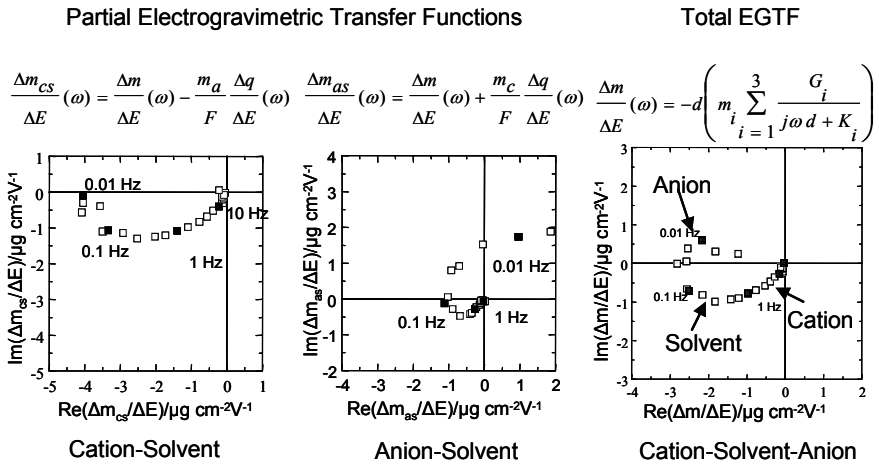

Fig. 1.9. Partial Electrogravimetric Transfer Functions to discriminate the presence of each species involved in the redox process [Gabrielli02].

In the previous figure it can be noticed how the response for partial transfer function corresponding to Cation-Solvent present a decreasing tendency in the third quadrant and has a minimum around -2 μgcm^{-2} V^{-1} for the Real axis. This tendency is absent for the response of the partial transfer function corresponding to Anion-Cation; therefore, in the complete transfer function response this tendency is due to the Cation's behaviour as it is indicated in the figure.

In a similar way, the response for Anion-Solvent partial transfer function has a loop in the second quadrant and it is absent in the Cation-Solvent partial response; therefore, it can be concluded that this portion of the curve in the complete EGTF corresponds to the Anion's behaviour. The remaining part in the complete EGTF is due to the Solvent's behaviour.

This is the way how different species involved in the *redox* process for a polymer under study can be discriminated in the AC Electrogravimetric Technique.

Finally, according to the mass of the involved ionic species, the diameter of the Nyquist response has different sizes as it was mentioned above. Fig. 1.10 shows an experimental response [Gabrielli00-3] of the EGTF measured on polyaniline polymer in three different electrolytes: $HClO_4$, HCl and HNO_3.

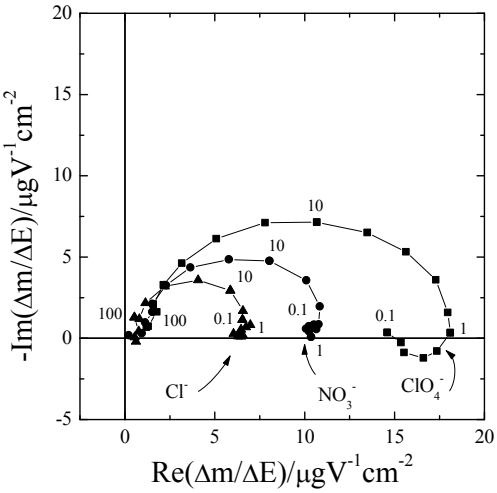

Fig. 1.10. Electrogravimetry Transfer Function measured on polyaniline polymer immersed in various media [Gabrielli00-3].

As it can be noticed the radius of the response obtained depends on the mass of the tested anion (Cl^-, NO_3^- and ClO_4^- in this case). These responses have a loop in the first quadrant as it was indicated for anions insertion in Fig. 1.7. Other experimental expression can be calculated from the EGTF according to some parameters that are desired to find [Gabrielli00, Gabrielli02].

All figures, expressions and data obtained from the AC Electrogravimetric technique are based in part on the Electrogravimetric Transfer function, $(\Delta m/\Delta E)(\omega)$ and they are consequently based on the variation of the mass in the polymer on the Crystal's surface. This measurement as it was indicated above is made by an indirect way using the variation in the resonance frequency of the oscillator in which the QCM is inserted and using the Sauerbrey expression (Eq.(1.13)). So it is important to perform an accurate measurement of the frequency of the oscillator in order to obtain a good measurement of the change in the mass density of the polymer.

For this reason before explaining the experimental setups in the AC Electrogravimetry Technique it is important to know about the methods of

measuring frequency. Therefore, in the next section some classical methods for frequency measurement are described.

1.3 Frequency Measurement Techniques

There are several techniques, modes or strategies to measure frequency in electronic instrumentation application. These techniques go from simple basic counter until more sophisticated tracking frequency, particularly in QCM applications.

Next a brief review of some of these methods or techniques for measuring frequency will be introduced.

1.3.1 Frequency Counters

Electronic counter or *universal counter* is maybe the simplest way to measure the frequency in any system, because in general terms this instrument offers high precision and analysis for researching and developing applications, low cost and portability [Coombs00].

Electronic counter can offer more than just a frequency measurement. It can measure the period, time intervals, and delays among others operational modes [Jones91, Agilent97]; under these conditions the universal counter is called *multifunction counter*.

In the simplest mode of operation the ***basic universal counter*** counts the input pulses during a certain pre-established time. The control of time is achieved by applying a rectangular pulse of known duration using a very stable clock reference. This technique is named as "gating the counter". Several gate times can be established from the clock source as it can be shown in the block diagram of Fig. 1.11.

According to the signal to be measure the selector of the gate is localised in one of the points shown in the figure; it determines the time in which the gate is "open" to measure the frequency.

The frequency of the input signal is calculated as:

$$f = \frac{N}{t} \tag{1.50}$$

where f is the frequency of the input signal, N is the number of pulses counted and t is the duration of the gate.

One important point about this mode of operation is to calculate the error made by the electronic counter when any frequency is desired to be measured.

When a measurement is made with a basic universal counter a ±1 count ambiguity can exists in the Least Significant Digit (LSD). The error caused by this ambiguity is in absolute terms ± 1 count for the total accumulated count; therefore, as the total accumulated count increases, the percentage of error attributable to ±1 count error decreases.

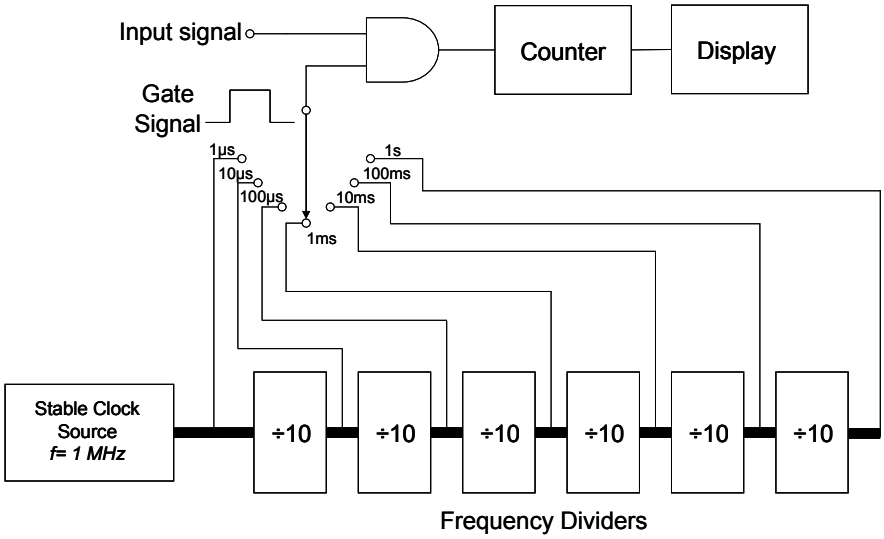

Fig. 1.11. Block diagram of the frequency mode for a basic universal counter. Adapted from [Jones91].

An example is illustrated in Fig. 1.12. In the figure an input signal of 10 MHz is desired to be measure and a time gate of 1ms is selected.

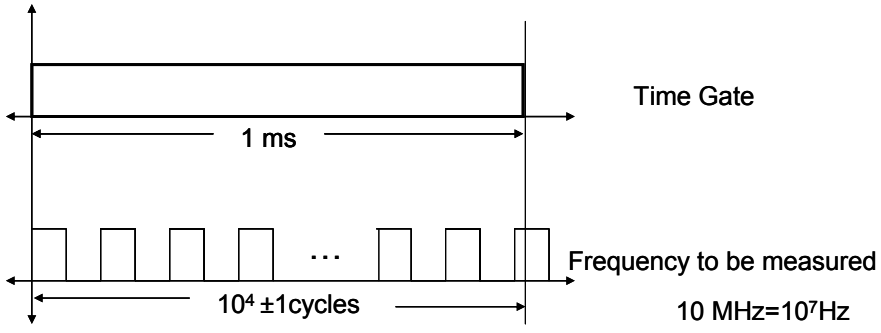

Fig. 1.12. Example of frequency measurement using 1ms time gate.

For these conditions exposed, from Eq.(1.50) there are 10^4 counts plus ±1 count in error is considered. As a result the possible error over total count in the measurement is equal to:

$$Error = \frac{\pm 1 count}{10^4} \Rightarrow \frac{10^3}{10^7} \Rightarrow 10^3 \frac{ciclos}{1s} \Rightarrow 1KHz \tag{1.51}$$

If the time gate is increased this error is minimised. A typical gate for measuring signals in the mega hertz range is 1s so the error calculated using Eq.(1.51) is around 1Hz which is accurately enough for a simple mega hertz frequency measurement, but the accuracy is limited for low frequencies.

When the basic electronic counter is working in its *period measurement* mode a signal of unknown period is measured counting pulses of a reference high frequency signal, i.e., the input signal works as a gate for the high frequency signal. Then the period of the signal is the time taken for the signal to complete one period. If the time is measured over several input cycles, then the average period of the repetitive signal is determined. This schema is referred as *multiple period averaging*.

Fig. 1.13 shows the basic block diagram for the universal counter is its period mode. As it can be noticed the time in which the gate is opened depends on the period of the input signal rather than on the time base signal. The counter counts the pulses from the time base signal for a period of the input signal; in this ways the unknown period of the input signal is calculated according to the pulses of the known time base signal.

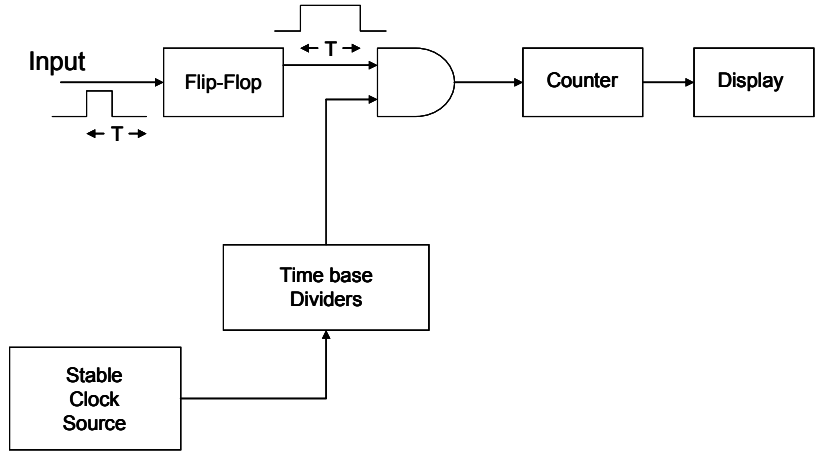

Fig. 1.13. Block diagram of the period mode for a basic universal counter. Adapted from [Agilent97].

Period measurement allows an improvement in the implicit low accuracy for determining low frequencies in the basic counter because of increased resolution. For example, a frequency measurement of 60 Hz signal on a basic counter with 10 MHz time base and a 1-second gate time in the frequency mode will be displayed as 60.00000 Hz, but if the frequency is 60.00001 Hz the answer of the basic counter is still 60 Hz because the event counter would count only 60 events, but in the period mode the time measured is 16.6666 ms then the frequency will be 60.00002 Hz which is more accurate regarding the basic counter. Therefore, the resolution is notably improved by using the period mode.

As it can be inferred the error committed in the period mode depends on the reference signal counts measured, then if the frequency of this signal is increased the error will be minimised.

Some most modern architectures use a different structure for measuring frequency in order to avoid the disadvantages of the universal basic counter. This new schema is known as ***reciprocal counters*** [Coombs00, Agilent97].

As it was shown above the basic universal counter is restricted to decade gate times because using these decades the division in Eq.(1.50) was easily performed for the incipient digital devices, but modern digital architectures becomes common and effective to do some mathematical operation as division, so in principle the limitation of decades becomes vanished. With these modern structures the reciprocal counters becomes a good solution for the limitations in the basic counters.

The reciprocal counters always make a period measurement on the input signal. The frequency information is obtained taking the reciprocal of this period measurement. The reciprocal technique has popularity due two major features:

- The ±1 count error is independent of the frequency of the input signal frequency, then the resolution in the measurement is independent of the input signal, i.e., it does not decrease when the input frequency decrease as it happened with basic universal counters.
- The period mode characteristic of the reciprocal technique provides control capability of the main gate in real time.

In addition to these advantages, the time gate could be synchronised to the input signal and then the resolution of the measurement can be tied to the time base and not to the input frequency. This characteristic allows to a faster measurement of low frequency signals. Because resolution is

determined by the ability to measure time, it can be improved using a higher frequency time base.

Nevertheless these improvements achieved with reciprocal counters or even increasing the time base frequency fall when the frequency of the signal is changing rapidly or abruptly and when a very accurate, fast and continuous frequency tracking is required.

In applications where the frequency is continuously changing and has to be accurately measured, some other strategies need to be planned in order to accomplish this task. One of them is the use of a phase locked loop as it will shown next.

1.3.2 Phase Locked Loop, PLL

A Phase Locked Loop, PLL, is a feedback system which provides a signal which is continuously tracking an input signal taken as reference. The output signal is provided by a voltage control oscillator system which thanks to the feedback maintains the same frequency as that of the input signal and, in some cases, the same phase [Arnau00-3, Best05, Wolaver91]. This way it is said that the feedback signal is locked with the reference one.

In addition to this locking characteristic, if the input signal is a frequency modulated signal, the PLL provides information regarding to the modulating signal; in fact the inherent behaviour of the PLL is to perform a continuous tracking of the input signal in order to extract the information related to the modulating signal. Then if the reference signal is a frequency modulated signal the PLL performs a continuous tracking of this voltage and provides a signal which maintains the same frequency and phase as the modulating signal in a specific frequency range.

A PLL can be built in an analogical way or mixing analogical and digital subsystems [Best05, Wolaver91]. In the following figure a summarised block diagram for a PLL is presented.

This basic schema of the PLL is composed by a Phase-Frequency Detector, a Low Pass Filter and a Voltage Controlled Oscillator (VCO).

The voltage at the output of the low pass filter is involved in controlling the oscillation of the VCO and it is the so-called demodulated signal which continuously tracks the modulating signal, in other words, this control voltage is a direct measurement of the frequency provided by the VCO.

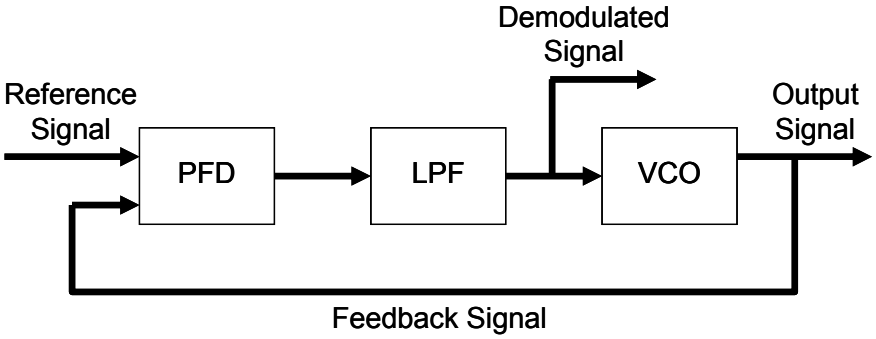

Fig. 1.14. Summarised block diagram of a PLL adapted from [Arnau00-3]

As it will be shown later on, this PLL schema is ideal for performing the fast and continuous frequency tracking in the AC Electrogravimetry experimental technique and a more detailed explanation will be conducted in the third chapter.

After this basic introduction to the methods for frequency measurement the current experimental setups for obtaining the Electrogravimetric Transfer Function in the AC Electrogravimetry technique will be presented in order to clarify the facts to promote the development of the present doctoral thesis project.

1.4 Current AC Electrogravimetry experimental setups

Once the principles involved in the AC Electrogravimetry and the techniques for measuring frequency has been explained, some current experimental setups used to obtain the Electrogravimetry Transfer Function, EGTF, will be presented as an introduction to define the specific problems and the subsequent goals which motivate the development of this thesis project.

1.4.1 Problem outline

In order to determine the EGTF, one stage is required for an appropriate continuous measuring of the resonance frequency shift of the Quartz Crystal Microbalance, QCM, for instance the frequency shift of a quartz crystal sensor controlled oscillator. Moreover, the determination of the EGTF requires a voltage signal accurately related to the resonance frequency shift of the EQCM, both in phase and magnitude.

As it was mentioned, the resonance frequency shift is, taking into account some restrictions [Edwards94], proportionally related to the mass variation of the conductive polymer under study, which has been thin-film deposited on the working electrode of the electrochemical cell [Bourkane89]. These mass variations are induced by a variable-frequency sinusoidal low potential superimposed to a constant polarisation voltage applied between working and reference electrodes of the electrochemical cell. It can be understood that the QCM output signal is related to a frequency modulation process, where the carrier signal is provided by the sensor controlled local oscillator and the modulating signal is the superimposed sine wave applied to the electrochemical cell. It is important to notice that the carrier's frequency is in the MHz range (6 MHz-10 MHz) meanwhile the modulating one is in the Hz range (few mHz until 1000 Hz). The modulating signal induces mass variations in the conductive polymer and then in the mass deposited on the working electrode as it was shown in Fig. 1.4 and Fig. 1.5, i.e., on the QCM sensor, due to oxidation-reduction (*redox)* process in the polymer.

Nowadays, at the Laboratory of electrochemical systems and interfaces, LISE, some transfer function equipment is used for a real-time obtaining of the EGTF. For this equipment two input voltages are needed, one is the superimposed sine wave applied to the electrochemical cell and the other one is a voltage proportional to the induced frequency change in the EQCM. As it can be understood an accurate frequency measurement and then a high accurate frequency–voltage conversion is necessary to avoid any distortion of the EGTF.

Two different approaches are currently used for the frequency measurements which are based on two framework frequency-voltage converters [Gabrielli07].

The first framework is based on a frequency-voltage converter composed by a multivibrator that provides a pulse of appropriate constant width at the output at each zero crossing of the input signal. The average value of this output signal is obtained with an appropriate average-value filter and directly related to the frequency shift of the input signal that comes from the EQCM [Gabrielli99-1].

Another schema is formed by a Phase Locked Loop, PLL, which is a feedback system composed by an analogue mixer working as a phase-detector, a low pass filter, an amplifier and a voltage controlled oscillator or synthesizer [Gabrielli01].

These systems present problems both for obtaining an appropriate resolution in the frequency-voltage conversion and for a proper continuous frequency-voltage tracking.

1.4.2 Specific problems associated with the AC experimental setups

Since the AC Electrogravimetry technique was proposed, the two mentioned electronic systems have been used to get the data necessary for the calculation of the EGTF. One of those experimental setups is depicted in the following figure.

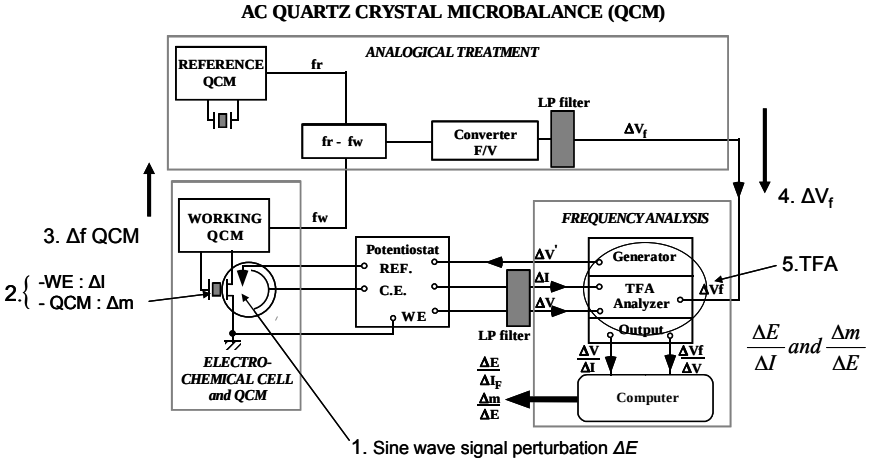

Fig. 1.15. First experimental setup for obtaining the EGTF in the AC Electrogravimetry technique. Adapted from [Gabrielli99-1, Torres06-1]

The experimental setup in Fig. 1.15 shows an electrochemical cell, in which the WE is one of the electrodes of the quartz sensor and it is ground connected; the QCM, in this case working as a EQCM as it was presented above, is controlling an oscillator whose output frequency is named as f_W, and an analogical subsystem composed by several electronic devices to get a voltage variation related to the frequency shift produce by mass variation; a Transfer Function Analyser and a computer to process the data obtained.

In the AC Electrogravimetry technique the frequency of the superimposed sinusoidal difference voltage, ΔE, applied in stage number 1 between the reference electrode and the working electrode WE, is ranged between a few mHz and 1KHz, i.e. its speed of variation goes from 1 KHz when the experiment starts and progressively decreases until few mHz when the experiments is almost finished. This voltage difference produces a current variation, ΔI, in the cell and then a mass variation, Δm, in the

EQCM in stage 2. Subsequently this mass variation is transferred into frequency variations of the QCM resonance frequency Δf_{QCM} in stage 3. It is clear to understand the system like a frequency modulator system in which the carrier signal is provided by the quartz sensor controlled oscillator and the modulating signal is the superimposed sinusoidal voltage applied to the electrochemical cell. It is important to emphasise that the oscillators' frequencies are in the megahertz range meanwhile the sine wave applied has a maximum frequency of 1 KHz. Experimental frequency shifts (from the frequency of the carrier signal, i.e. the frequency deviation) in the range of 10 to 50 Hz are found when the sinusoidal voltage is applied to the electrochemical cell; this means that it is necessary to measure the frequency shifts around a central frequency of about 10MHz with high resolution, 0.1Hz, and very quickly, in less than 0.1ms (due to the fact that the maximum speed of the modulating signal is 1KHz). In other words it is necessary to follow frequency shifts of around 10-50Hz or less, over a carrier of 10MHz, very quickly and with high resolution; additionally these frequency changes have to be converted in voltage changes to be used at the input of the EGTF system. This is not an easy task whose problems will be analysed in detail next.

As an example it can be supposed that a high frequency signal, for instance 10MHz, is required to be measured. There are several methods for performing this task as it was presented in the previous section. One of these is an extension of the *basic universal counter* in which a very high frequency signal is used as a reference, to count up pulses or cycles of this signal during certain time and at the same time count up the pulses or cycles of the signal whose frequency must be measured; then a simple operation provides the frequency measured. The principle is illustrated in Fig. 1.16.

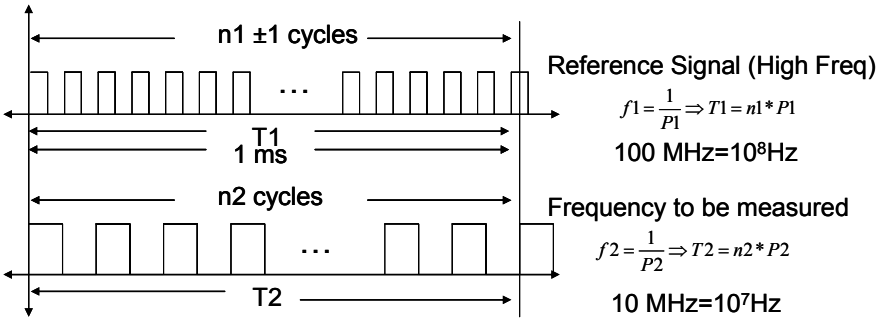

Fig. 1.16. Frequency measurement using a high frequency reference signal. Adapted from [Torres05].

The figure shows a 100 MHz reference signal used to measure the 10 MHz frequency signal. As it can be noticed, during 1ms *n1±1* cycles are counted, *T1* is the time analysed, *f1* is the frequency and *P1* is the period of the reference signal, meanwhile *n2* cycles are counted, *T2* is the time analysed, *f2* is the frequency and *P2* is the period of the signal whose frequency must be measured.

The error in the measurement is given by:

$$\Delta f = \frac{2n2}{n1^2 - 1} f1 \approx \frac{2n2}{n1^2} f1 \tag{1.52}$$

Replacing data from Fig. 1.16 ($n1 = 10^5$ and $n2 = 10^4$) in Eq. (1.52) it is obtained an error of 200 Hz.

This result is useful to show that, unless the frequency of the reference signal is as higher as 10GHz, any system that uses this method to measure a 10MHz frequency commit an error which is not negligible for an AC Electrogravimetry system as the one described above, where the deviation is in the range of 50Hz maximum.

Two solutions could be developed to improve both the system's accuracy and the resolution: the first one is to increase the temporal window in which cycles from both signal are counted up, and the second one is to increase the frequency of the reference signal. But these two solutions arise with more additional problems that do not allow solving the problem.

In the first case if the temporal window is increased the resolution is improved even until 0.1 Hz or more; however, the problem is that it causes a very slow response of the system, which is not a problem for a "static" signal, but in the case of measuring a quickly changing frequency signal (1KHz, for instance in AC Electrogravimetry set-up) the system is unable to measure the frequency evolution, and only the average frequency during the temporal window is measured.

In the second case when the reference frequency is increased some additional problems related to stability and noisy of the high frequency signal appear and the measurement becomes more complicated.

As it was mentioned above, at LISE, the transfer function equipment used for obtaining the EGTF in the stage 5 of the Fig. 1.15 requires two input voltages, one is the superimposed sine wave applied to the electrochemical cell and the other one is a voltage proportional to the frequency change measured in the EQCM. As it can be noticed, in addition to a good resolution frequency measurement method an accurate frequency-voltage converter is necessary to avoid any distortion of the EGTF. This aspect supposes an additional challenge to any electronic system that presumes to recover the voltage proportional to the frequency change.

The first approach currently implemented for the frequency-voltage converter at LISE, stage 4 in Fig. 1.15 uses a similar frequency measurement method described above. This system is composed by a multivibrator that provides a pulse of appropriate constant width at its output according to the frequency measured. The average value of this output signal is obtained with an appropriate average-value filter and directly related to the measurement of the frequency shift of the input signal that comes from the EQCM.

This system has to cover all the frequency range variation of the modulating signal (from few Hz until 1 KHz) with good resolution and accurately, but when the pulse width is large ("low" frequency) the system tends to saturation, so a calibration to the dynamic range is required in order to avoid this saturation; however, this calibration reduces the dynamic range of the system and then the resolution as well, mainly when the pulse width is short ("high" frequency). To solve the paradox a trade-off must be established between dynamic range and resolution.

Another schema is shown in Fig. 1.17. The circuit is formed by a PLL, composed by an analogue mixer working as a phase-detector, a low pass filter, an amplifier and a voltage controlled oscillator or synthesizer, as it was mentioned.

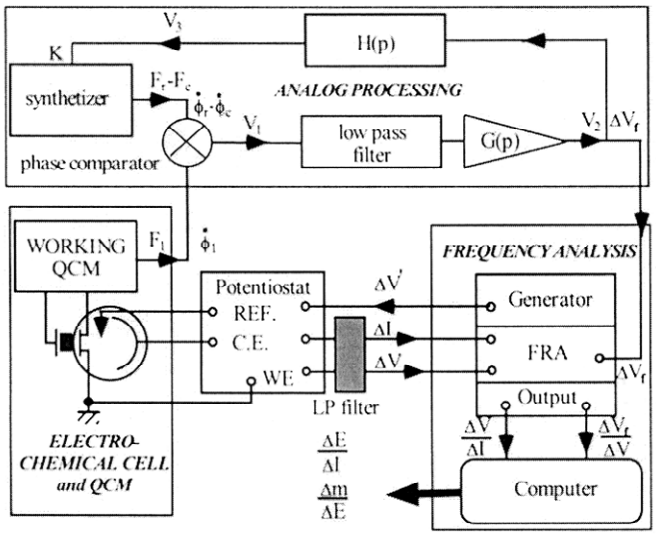

Fig. 1.17. Second experimental setup for obtaining the EGTF in the AC Electrogravimetry technique. Adapted from [Gabrielli01].

This system execute a down-conversion of the sensor controlled oscillator output signal by mixing with the signal coming from a synthesiser and provides a low frequency modulating signal (a few KHz carrier signal) at the input of the phase-detector; therefore, in order to extract the modulating signal, a low pass and slow response filter must be implemented. This low pass filter is not an inconvenient to the modulation deviation (50 Hz as a maximum), but it is a real inconvenient for the speed of the modulation (1KHz. maximum), and then the conflict between resolution and bandwidth appears again.

Nevertheless, although the experimental set-ups provide good results regarding the polymer characterisation it can be noted that these systems present problems both for obtaining an appropriate resolution in the frequency-voltage conversion and for a proper continuous and fast frequency-voltage tracking. These problems are associated with their inherent performance and produce certain inaccuracy inconveniences which are transferred as a distortion in the transfer function [Gabrielli99-2, Gabrielli01].

1.5 Summary

A detailed study regarding to Quartz Crystal Microbalances principles and its inherent sensor applications has been conducted as an introduction to formulate a specific experimental challenge presented in the AC Electrogravimetry technique. This study was performed in order to establish the main characteristic and specifications to improve the accuracy, resolution and bandwidth requirements of the current AC Electrogravimetry set-ups at LISE (Laboratoire Interfaces et Systemes Electrochemiques) in the CNRS (Centre National de la Recherche Scientifique) in Paris.

In order to solve the inconveniences in the measurement of the frequency shift of the modulating signal in the AC Electrogravimetry experimental set-ups is necessary to design a system which has to be able to establish an optimum trade-off between both resolution and bandwidth, and in addition an accurate, fast and continuous frequency-voltage tracking.

The PLL framework is ideal for tracking the frequency of the modulating signal, because this is its inherent behaviour [Best05, Wolaver91]. The problem of slow responses in case of using a low frequency PLL described before could be improved by using a high-

frequency PLL. In this case we have to deal with the problem of low resolution or low level of sensitivity in the frequency-voltage conversion. This problem could be avoided by using a voltage controlled crystal oscillator (VCXO) instead a simple VCO in the loop. This configuration will improve the sensitivity while reducing the dynamic range and the PLL lock range; this implies a new problem since it is not known “a priori” the central frequency of the sensor controlled oscillator and then the PLL could not track this signal.

All these problems motivate the development of the present thesis project an as it will be explained in the subsequent chapters the solution presented contributed to improve the performance of the actual experimental setups in the AC Electrogravimetry technique and then an improvement in the data obtained for polymer characterisation is achieved.

The system solution proposed in the thesis mainly deals with the method to improve the system’s performance in two ways: Obtaining good resolution, in the measurement of the frequency deviation of the carrier frequency signal, i.e., the amplitude for the modulating signal related to mass transfer and enlarge the bandwidth to be able to follow fast changes in this modulating signal (until 1 KHz). In addition an improving in the accuracy of these measurements is achieved.

2 Objectives

2.1 General Objective

The main objective of this thesis is to provide a monitoring system based on analogue and digital electronic devices for improving the experimentation techniques involved in electrochemical quartz crystal microbalance applications through the improvement in resolution and accuracy of the experimental data acquired.

2.2 Specific Objectives

In order to achieve the main objective proposed is required to accomplish some stages or specific goals. These specific aims are listed below:

1. To analyse the specific problems involved in the distortion of the measurement of the relevant parameters of the Quartz Crystal Microbalance sensor employed in the AC Electrogravimetry Technique.
2. To propose, design and develop an electronic system that improves the polymer characterisation in the AC Electrogravimetry experimental setup and the experimental accuracy data obtained with it.
3. To conduct experimental characterisation of the electronic system designed to evaluate its behaviour in typical studies in the AC Electrogravimetry Technique.
4. To compare the behaviour of the system proposed with another current system employed in the AC Electrogravimetric technique to test the enhancement obtained with the new system regards the current one.
5. To conduct an experimental validation of the theoretical model for the Electrogravimetry Transfer Function, EGTF, using the proposed system and the current one and establish a comparison between the results obtained with them in order to test the usefulness of the new system.

3 Contributions

Once the requirements of the AC Electrogravimetry experimental setup are known and the objectives of this doctoral thesis are stated some contributions to improve the experimental technique will be described in the following sections.

3.1 Contribution I: First Approach by using an Analog/Digital Phase Locked Loop.

3.1.1 General Block Diagram

The system proposed as a first approach to get the main objective is shown in Fig. 3.1.

As it can be noticed the system is composed by eight different subsystems:

1. The electrochemical cell signal represents the signal provided by the electrochemical quartz crystal microbalance (EQCM) controlled oscillator. This signal is called as *reference signal*.
2. A first signal conditioning subsystem that takes the reference signal and the signal coming from a *numerically controlled oscillator, NCO*, which is named as *feedback signal*. The objective of this *conditioning subsystem* is to provide the adequate voltage level to the input signal of the *phase-frequency detector*.
3. The phase-frequency detector is involved in providing a voltage related to the phase difference between the reference and feedback signals.

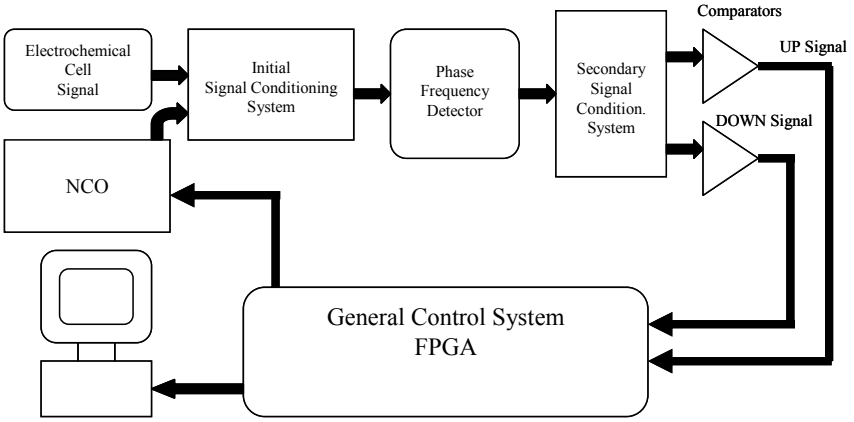

Fig. 3.1. Analog/Digital phase locked loop where the feedback branch is implemented in the FPGA system.

4. A secondary conditioning signal subsystem which is an analogical subsystem and is involved in taking the output of the phase-frequency detector and provide a voltage range to excite the comparators.
5. Two comparators which give the control signal to a *Field Programmable Gate Array, FPGA*.
6. A *digital control subsystem* which was implemented in a FPGA. This subsystem controls the operation of the NCO and the general system.
7. A digital controlled oscillator which is implemented by the NCO. This subsystem provides a suitable signal according to the measurement and control established by the FPGA.
8. An output stage that takes collects the data from the FPGA and transmits the data to a PC for its posterior analysis.

3.1.2 Description of the System Operation

The reference signal coming from the oscillator controlled by the electrochemical quartz crystal microbalance and the feedback signal from the numerically controlled oscillator are conducted as inputs to the frequency phase-detector which takes the difference between the phases of the input signals and provides an appropriated signal related to this difference. After some conditioning two comparison levels are established in order to point out whether the reference signal is *leading* the feedback one or the contrary, i.e., the reference signal is *lagging* the feedback one.

When the reference signal is leading the feedback one the *upper comparator* in Fig. 3.1 puts a high logic level, '1' (*UP signal*) in its output and the *lower comparator* puts a low logic level, '0'; it means the feedback signal needs to be increased to lock the system. On the other hand, when the reference signal is lagging the feedback ones the upper comparator puts a low logic level and the lower one puts a high logic level (*DOWN signal*) which means the feedback signal needs to be decreased.

If both upper and lower comparator put high logic level or low logic level at the same time the control system in the FPGA does not produce any action.

The UP and DOWN signals are transferred into the FPGA with a previous conditioning. In the FPGA a *control algorithm* has been implemented to do the frequency correction to allow the system is locked all time. In addition to the control task, the FPGA is involved in programming the NCO to put the appropriated frequency ate the phase-frequency comparator input.

When the FPGA receives an UP signal starts a process to look for the reference frequency, this searching is conducted to above the current frequency value until the UP signal is off. During the process the NCO is programmed several times and after each one a new frequency measurement is made. All the process stops when the feedback phase signal is almost similar to the reference one, i.e., when the system is locked.

Similarly when a DOWN signal is perceived the searching process is started, but in the opposite direction.

As it was mentioned if the FPGA receive UP and DOWN signal at the same time it does not perform any frequency correction because some error is present and if no one signal is high logic it means the system is locked.

The output of the FPGA is a forty bit word control to programme the NCO. In this word, as it will be explained is this chapter, some bits for control, phase and frequency data are included. Another possible output of the FPGA is the data for the processing in the PC which is concerned to the shifts in the reference frequency measured.

The loop in the Fig. 3.1 is closed by the NCO whose output frequency is conducted to the phase-frequency detector.

The Fig. 3.2 is a photo of the system designed.

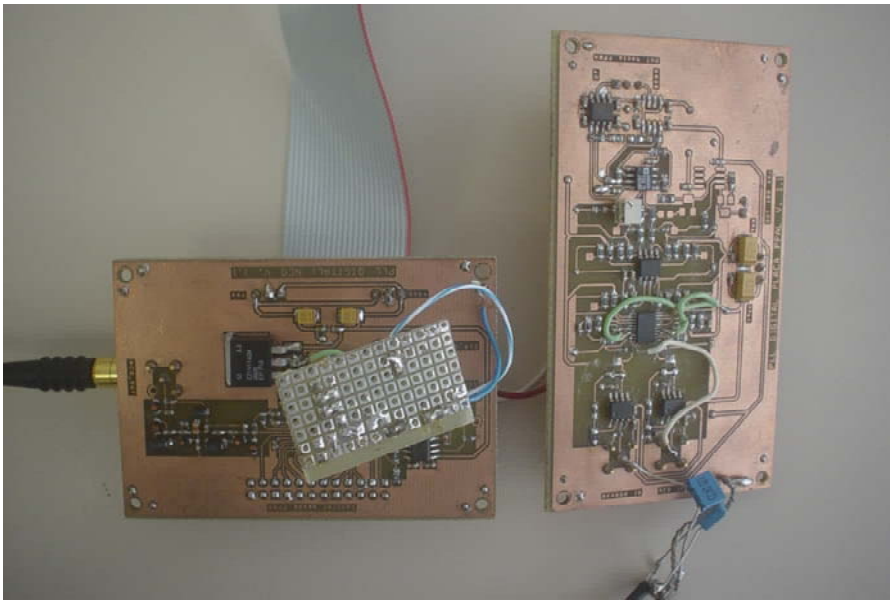

Fig. 3.2. Digital high frequency PLL designed.

3.1.3 Drawbacks associated to the first contribution

After some preliminary experiments the first system designed present irregularities in its behaviour. Some of the characteristics and irregularities observed are listed bellow:

1. Under controlled situations, i.e., introducing step changes in the UP and DOWN signal by a *manual procedure*, the system's behaviour is acceptable because it follows the reference signal frequency and the locked condition is achieved, as it was anticipated by the design.
2. Nevertheless the good results under manual procedure were not reproduced for frequency modulated signals. In these cases the system presented an erratic behaviour putting alternatively UP and DOWN signal avoiding a real locked condition. The signals observed at the output of comparators were noisy and the locked condition was not achieved.

Due to these inconveniences the whole system was redefined in order to avoid this tracking troubles and noisy signals. After some attempts the final proposal implemented will be shown in the next section.

3.2 Contribution II: Analogue-Digital Phase Locked Loop (A-D PLL). Instrumentation system proposed for frequency monitoring in the AC Electrogravimetry experimental technique.

In chapter 1 a detailed study regarding to AC Electrogravimetry technique was performed in order to establish the main characteristics and specifications to improve the accuracy, resolution and bandwidth requirements of the actual AC Electrogravimetry setups at LISE (Laboratory of electrochemical systems and interfaces) in the CNRS (National Centre for Scientific Research) in Paris.

These requirements were tried to cover by the contribution explained in the previous section, but as mentioned, due to some inconveniences of the electronic system proposed, a good *trade-off* between resolution, accuracy and bandwidth was not possible to establish and then to solve the paradox existing in the actual set-ups. This section describes the final system proposed to solve the inconveniences and then providing good data and performing an improvement in the AC Electrogravimetry experimental technique.

3.2.1 Measuring strategy

The *electronic instrumentation system* which pretends to solve the inconveniences and challenges proposed by the AC Electrogravimetry technique mainly needs to deal with the method to improve the system's performance in two ways: First by *obtaining good resolution* in the measurement of the frequency deviation of the carrier frequency signal, i.e., the amplitude for the modulating signal related to mass transfer and second, by *broadening the locking frequency bandwidth* to follow the fast frequency changes in the modulating signal (until 1 KHz). Moreover, an *improvement of the accuracy* of these measurements is mandatory.

In order to cover these requirements the most reliable solution must be based in a Phase Locked Loop, due to its inherent *tracking frequency behaviour*, but taking into account the upper cut off frequency given by the 1 KHz modulating frequency and how to improve the resolution of the system.

To improve the resolution of the PLL it is necessary to modified one important element in the classic PLL schema shown in Fig.1.28. Instead of using a *voltage controlled oscillator, VCO*, a *voltage controlled crystal oscillator, VCXO* could be used to reduce the frequency range covered by

the VCO because the extremely narrow range frequency in typical VCXO's, then an increase in resolution is achieved.

But due to this narrow frequency range of the VCXO, a coarse frequency tuning is necessary in order to centre the operative frequency range of the PLL on the centre frequency of the EQCM to warrant the locking condition and then increasing the dynamic range. To do this coarse frequency tuning, it is necessary to include additional blocks in the classic PLL.

The strategy stated is to perform a *double tuning* in the system. A *fine tuning* to be made by a VCXO obtaining an improvement in resolution and a *coarse tuning* to be made by additional blocks to increase the operative frequency range of the system. This strategy will be explained in detail in the following sections.

3.2.2 General description of the system proposed

3.2.2.1 General block diagram

The general block diagram for the second contribution and the final system implemented is shown in Fig. 3.3.

As it can be noticed two different parts are distinguished: a *main loop* which is essentially an *analogue subsystem* and a *secondary loop* which is built by means of *digital and programmable circuits*.

The *main loop* is a *classic PLL* which is composed by an Electrochemical Quartz Crystal Microbalance, EQCM, i.e., an electrochemical cell in which the QCM is inserted; a mixer (*main mixer* in Fig. 3.3) working as a *phase detector*, a *low pass filter* followed by a *signal conditioning circuit* and a *voltage controlled crystal oscillator, VCXO*. The output of the VCXO is connected again to the phase detector through a *feedback path* formed by two filters and an additional mixer which acts as the interface with the secondary loop.

The *Secondary Loop* makes a *digitally controlled feed-forward correction* based on a *numerically controlled oscillator, NCO*, which is managed by a *purposed algorithm* implemented in a *Field Programmable Gate Array, FPGA*.

Finally from the main loop the appropriate signal to a *Transfer Function Analyser, TFA*is extracted, to be processed in order to obtain the *Electrogravimetry Transfer Function, EGTF*.

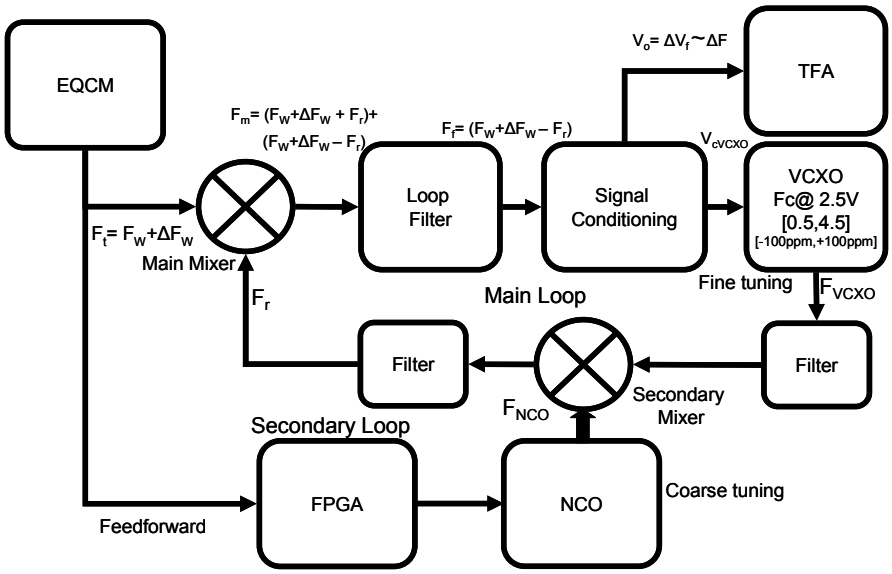

Fig. 3.3. Analogue-Digital phase locked loop implemented. Adapted from [Torres07-1].

A detailed explanation of each subsystem shown in Fig. 3.3 will be presented in the following sections.

3.2.2.2 Operating principle outline

As it was shown in Fig. 3.3 the system proposed is built in two loops. The main loop is involved in performing a *fine tuning* of the system, i.e., the main loop performs a *continuous tracking* of the small frequency shifts in the reference signal. These small changes are followed with good precision and resolution due to the presence of the VCXO, which performs a reduction in the frequency range in comparison with a typical VCO.

As it was mentioned there is a risk that the system becomes unlocked due to the extremely narrow frequency range covered by the VCXO, but the solution to this threat comes from the secondary loop which performs the *feed-forward correction* to centre the VXCO in the appropriated frequency range, in which it is capable to follow the small sine wave frequency changes in the reference signal. This feed-forward correction has been named *coarse tuning* in Fig. 3.3.

The general behaviour of the system is as follows [Torres07-1]: at power on, the FPGA performs a reset of the whole system and then the NCO is programmed with an initial frequency selected from the range 6 to

10 MHz and the system waits for the reference signal coming from the EQCM controlled oscillator to the main mixer input; afterwards, the algorithm programmed into the FPGA compares the previous frequency programmed with the new one measured and makes the corresponding adjustment to the NCO's frequency; this constitutes the *coarse tuning* mentioned before. After the coarse tuning, the small sine wave frequency changes introduced by AC Electrogravimetry can be followed by the VCXO, i.e., the *fine tuning* of the system. In this way the procedure warrants that the system is locked and the measurement process is accurate.

If at any moment the central frequency of the EQCM abruptly changes, the system responds in an effective way, due to the correction made by the secondary loop, i.e., the subsystem composed by the FPGA and the NCO. If there are not abrupt changes and frequency changes are only due to the small sine wave frequency changes the tracking of the frequency is performed only by the main loop.

3.2.3 Theoretical Model of the system designed

Before starting any detailed explanation about the design of each part of the system it is important to conduct a *theoretical modelling* of the whole system in order to investigate its behaviour in advance and design the system according to the requirements provide by the AC Electrogravimetry technique and the restrictions of the elements employed and simulated by the *theoretical model*.

The model present in the following lines is based in the classic theory of the phase locked loop, but introducing some changes in order to take into account the contribution of the secondary loop of the system.

Fig. 3.3 shows the reference signal (F_t), which can be considered as a frequency modulated signal whose carrier or central frequency is the high frequency signal of the oscillator (F_W), which is in the 6 to 10 MHz range according to any particular QCM employed during the experimentation. The modulating signal is the AC Electrogravimetric voltage applied on the EQCM which produces corresponding frequency shifts in the oscillator frequency (ΔF_W) [Torres06-1], given by:

$$\Delta F_W = \left|\Delta F_W\right| * \sin(\omega t + \varphi_W) \tag{3.1}$$

where $\left|\Delta F_W\right|$ is the peak in the frequency shift; $\omega=2\pi f$ is the angular frequency of the modulating signal and φ_W is the phase shift.

The reference signal is connected to the main mixer, the feedback signal whose frequency is F_r, is also applied to the mixer input.

As a result of the mixing the output of the mixer provides the following signal:

$$v_m = |v_m| * \cos\left[2\pi\left(F_W - F_r + \Delta F_W\right) * t + \phi_t - \phi_r\right] - |v_m| * \cos\left[2\pi\left(F_W + F_r + \Delta F_W\right) * t + \phi_t + \phi_r\right] \quad (3.2)$$

where $|v_m| = |A_t * A_r/2| \equiv K_m$. A_t and A_r are the amplitudes of the signals coming from the EQCM controlled oscillator (reference signal) and from the feedback path, respectively.

As it can be noticed in Eq. (3.2) v_m has two components: one corresponding to the high frequency component of the mixing and another corresponding to the low frequency part. The low frequency part is only required for locking purposes [Arnau00-3, Best05, Wolaver91], then by applying the low pass filter in Fig. 3.3 the low pass component can be extracted:

$$v_m = K_m \cos\left[2\pi\left(F_W - F_r + \Delta F_W\right) * t + \phi_t - \phi_r\right] \quad (3.3)$$

It can be noticed from Eq. (3.3) that, for two similar frequency and phase signals at the input of the main mixer, the low frequency component of the signal at the output of the mixer is only dependent on the carrier frequency shifts which are directly related to the amplitude of the modulating signal, i.e., the AC Electrogravimetric signal.

Defining the absolute phase error as:

$$\Phi_e(t) = (\Phi_t - \Phi_r) + \frac{\pi}{2} = [2\pi(F_W + \Delta F_W - F_r) * t + \phi_t - \phi_r] + \frac{\pi}{2} \quad (3.4)$$

where Φ_t and Φ_r are the absolute phases of the referent signal and feedback one respectively; the Eq. (3.3) can be expressed as:

$$v_m = K_m \cos\left[\Phi_e(t) - \frac{\pi}{2}\right] = K_m sen\Phi_e(t) \quad (3.5)$$

In the previous equation when the phase shift between the signals at the main mixer inputs is small around $\pi/2$, the following linear relationship can be established [Arnau00-3, Best05, Wolaver91]:

$$\frac{v_m}{\Phi_e} \approx K_m \quad (3.6)$$

According to Eq. (3.6) the transfer function of the main mixer acting as a phase detector is K_m whose value can be adjusted according to the expected behaviour of the system.

The transfer function of the low pass integrator filter implemented, located at the output of the main mixer is given by [Arnau00-3, Best05]:

$$F_F(s) = -\frac{1+\tau_2 s}{\tau_1 s} \tag{3.7}$$

where τ_1 and τ_2 are parameters to be adjusted for a specific design as it will be shown below.

The filtered signal goes through a conditioning circuit which is composed by two elements. The first one, built by means of an active low pass filter [Pertence94, Coughlin93], is used to provide a signal with an adequate amplitude level to be processed by the Transfer Function Analyser, TFA, in order to obtain the Electrogravimetry Transfer Function, EGTF. The second element in the signal conditioning block establishes the desired frequency range around the central frequency of the VCXO, which is 16.384.000 Hz for an input voltage of 2.5V. This second element also includes a voltage divider which introduces a constant K_a that needs to be considered for the calculation of the total system gain.

After the signal conditioning block, its output signal is connected to the VCXO which has a lineal relationship between its input voltage (control voltage) and the frequency shift of the signal at its output. This lineal relationship is given by:

$$\Delta F_{VCXO} = K_v \cdot \Delta V_{cVCXO} \tag{3.8}$$

where K_v is the *frequency-voltage gain conversion* of the VCXO which is constant, ΔV_{cVCXO} is the control voltage in mV relative to 2.5 V at the VCXO input and ΔF_{VCXO} is the frequency shift regarding the central frequency of the VCXO.

With this information and according to the behaviour of voltage controlled oscillators [Arnau00-3, Best05, Wolaver91] the transfer function for the VCXO is given by:

$$F_{VCXO}(s) = \frac{\Phi_{VCXO}(s)}{v_c(s)} = \frac{2\pi K_v}{s} \tag{3.9}$$

where Φ_{VCXO} is the relative phase at the VCXO output.

After this stage the VCXO output is band pass filtered by a fifth order elliptic filter [Williams95] with a pass bandwidth of 14 -18 MHz, which is designed to extract the fundamental frequency of the VCXO signal. Under this condition the band pass the filter can be considered as a linear element with constant gain.

At this step the model for the system is similar to a classic PLL, but in the feedback branch of the system proposed some additional elements appear and they need to be modelled in order to establish the complete model of the system.

The first element that appears in the feedback path is the secondary mixer according to the Fig. 3.3. As it happens in the main mixer this secondary mixer can be modelled as an element whose transfer function is constant, because it depends on the amplitudes of the input signals as it was expressed after Eq. (3.2), then the constant of the secondary mixer can be adjusted to 1.

Subsequently the output signal of the secondary mixer is band pass filtered selecting the low frequency bandwidth component of the mixing [5-12 MHz]. Similarly to the previous bandpass filter this second filter can be considered with constant gain in the pass bandwidth.

After these elements presented in the secondary loop and its corresponding filter the signal is finally fed back to the main mixer and the loop is closed.

When all the previous subsystems are interconnected the complete system obtained can be modelled by a transfer function, according to the classical PLL theory [Best05, Wolaver91]. It is important to notice that although this characterisation is just an approximation of the system's behaviour in real experimental conditions, the experimental results, which will be shown later on, will validate the theoretical analysis next introduced.

In general the transfer function of a PLL is given by:

$$H(s) = \frac{KF_F(s)}{s + KF_F(s)} \tag{3.10}$$

where $K = 2\pi K_m K_v K_a$ all constants given above, and $F_F(s)$ is the transfer function of the loop filter given by the Eq. (3.7).

Taking Eq. (3.7) into Eq. (3.10) it leads to:

$$H(s) = \frac{K\dfrac{1+\tau_2}{\tau_1 s}}{s + K\dfrac{1+\tau_2}{\tau_1 s}} \tag{3.11}$$

And after some operation the previous equation can be expressed as:

$$H(s) = \frac{2s\xi\omega_n + \omega_n^2}{s^2 + 2s\xi\omega_n + \omega_n^2} \tag{3.12}$$

where $\omega_n = (K/\tau_1)^{1/2}$ is the natural oscillating frequency for PLL and $\xi = \omega_n \tau_2 / 2$ is the damping factor.

As it can be noticed both natural frequency and damping factor depend strongly on the loop filter's characteristics which must be appropriately designed for a good static and dynamic performance of the PLL.

Before starting the design of the system, some simulations were conducted with the previous model presented both in Matlab® by a property script designed and by a simulating circuit implemented in ORCAD®. These simulation tools and their results will be shown in next chapters.

3.2.4 Detailed description of the system designed

After the introduction of the theoretical model a complete explanation of the procedures followed, the strategies taken and the circuits used for the implementation of the Analogue-Digital PLL will be presented.

3.2.4.1 Main Mixer

The *main mixer* performs the analogue mixing between the signal coming from the oscillator that contains the EQCM, and the signal coming from the PLL feedback path. After the analogue mixing of the signals, two components are obtained: a "high" frequency component and a "low" frequency one. The operating principle of the main mixer is presented in Fig. 3.4.

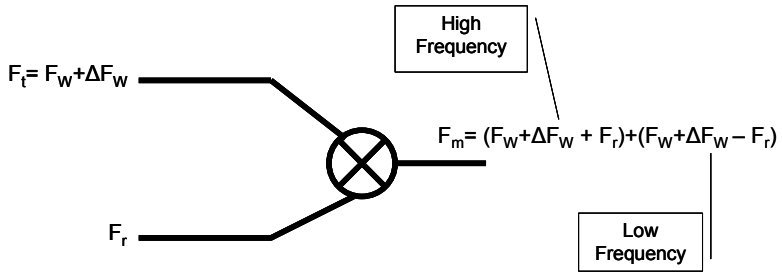

Fig. 3.4. Main mixer operating principle.

In this figure F_t is the frequency of the reference signal as it was mentioned before in the theoretical model, F_W is the central frequency of

the EQCM controlled oscillator which is in the range (6 to 10 MHz) and ΔF_W is given by Eq. (3.1). F_r is the frequency of the feedback signal. At the mixer output it can be shown the two frequency components that are presented due to the inherent behaviour of the mixer (multiplier).

The circuit implementation of the main mixer was performed by an integrated circuit (AD835) of Analog Devices® and its schematic diagram is shown.

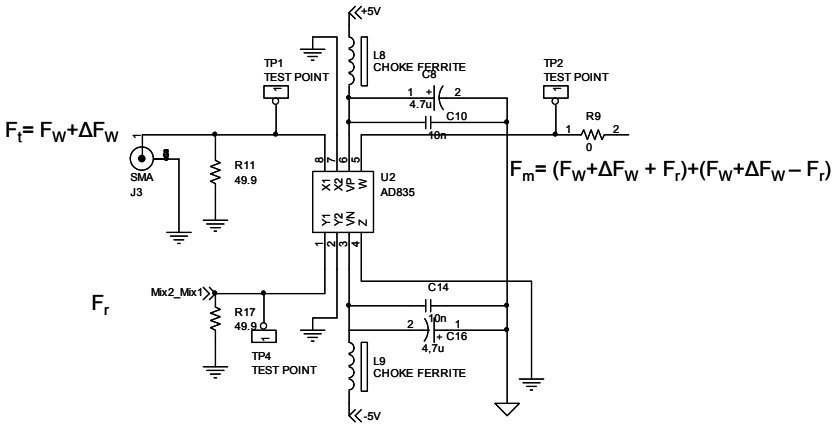

Fig. 3.5. Main mixer schematic diagram.

Two signal conditioning subsystems were put at the mixer inputs in order to adjust the amplitude of the input signals to acquire the desired value of K_m as it was indicated above; additionally these subsystems achieve a DC voltage level cancellation. The schematic diagram of these conditioning subsystems is shown in Fig. 3.6.

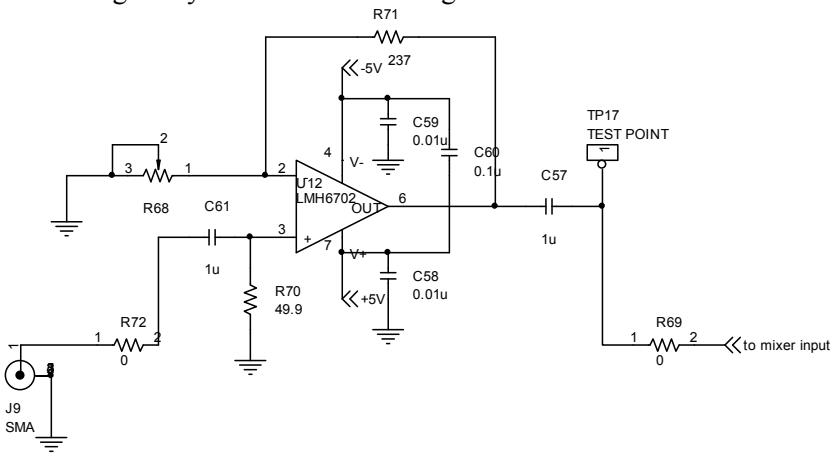

Fig. 3.6. Signal conditioning subsystem for mixer inputs.

3.2.4.2 Low pass integrator filter

Fig. 3.7 shows the frequency response of the *low pass integrator filter* according to Eq.(3.7).

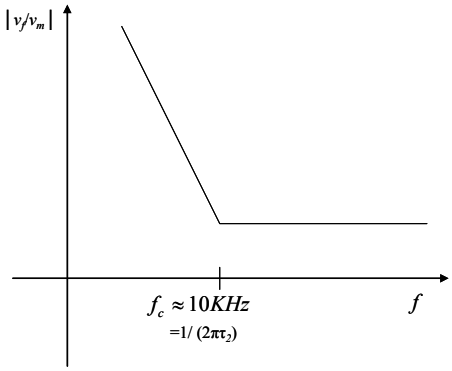

Fig. 3.7. Low pass integrator filter frequency response.

From Fig. 3.7, it can be noticed that frequency signals beyond 10 KHz will be considerably attenuated whereas low frequency signals will be amplified; then the high frequency component in Eq.(3.2) is highly attenuated whereas the low frequency component is kept according to Eq.(3.3). This signal, which is related to the AC Electrogravimetry voltage applied on the EQCM cell, will be applied to the input of the VCXO after appropriate conditioning explained below.

The schematic diagram of the low pass integrator filter is shown in Fig. 3.8.

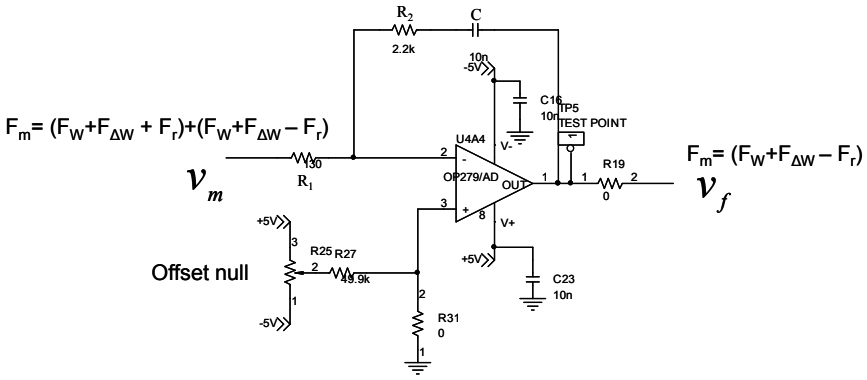

Fig. 3.8. Low pass integrator filter schematic diagram.

From this figure the parameters τ_1 and τ_2 of the Eq.(3.7) can be calculated. According to the values of R_1, R_2 and C the values of the time constants are $\tau_1 = 1.3 \times 10^{-6}$ s and $\tau_2 = 2.2 \times 10^{-5}$ s. Using these values the cut-off frequency of the system is calculated as $f_c \approx 10$ KHz. All these values will be used to calculate the main parameters of the A-D PLL according to the expected behaviour.

These values are only used to show the general loop filter behaviour, because the final setup values will be shown in the next chapter.

3.2.4.3 Signal conditioning subsystem

As it was mentioned the filtered signal conditioning circuit is composed by two elements. The first one, built by means of an active low pass filter, is used to provide a signal with an adequate amplitude level to be processed by the Transfer Function Analyser, TFA, in order to obtain the Electrogravimetry Transfer Function, EGTF. This first part is composed by a Butterworth active low pass filter [Pertence94, Coughlin94] with 1 KHz cut-off frequency; its schematic diagram is shown in Fig. 3.9.

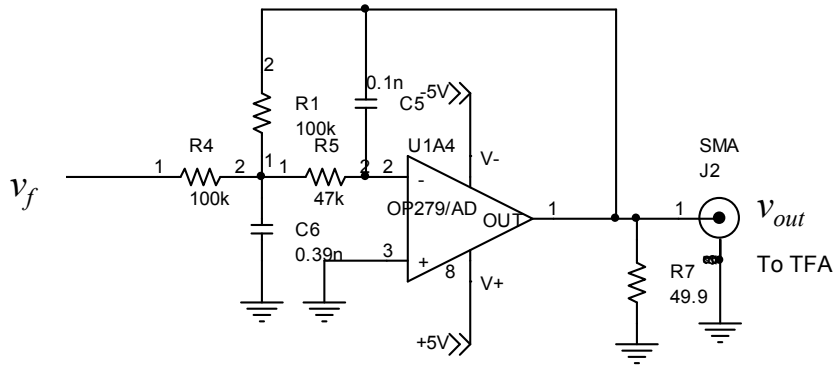

Fig. 3.9. Butterworth active low pass filter.

Because of the TFA only accepts non-DC voltage signals, a DC level canceller is required to be put at the output of the circuit in the Fig. 3.9, and in addition to this the canceller can amplify the output signal in case of great attenuation of the filter. The Fig. 3.10 shows the DC- voltage canceller implemented.

The circuit in the previous figure is composed by a follower that takes the output signal of the low pass filter, a DC level put by a potentiometer (*R37* in the figure) and finally an active adder. It can be noticed that the gain of the final active adder can be controlled by another potentiometer

(*R38* in the figure). This last potentiometer controls the final sensitivity (gain) of the whole system.

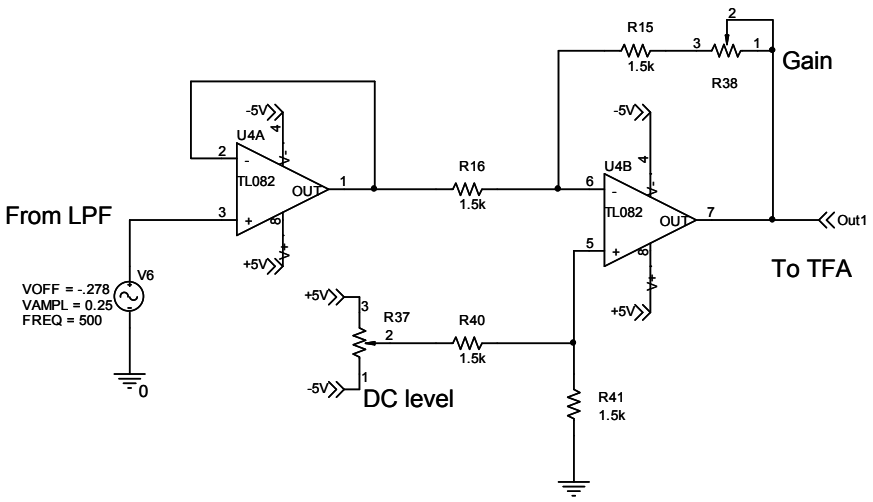

Fig. 3.10. DC level canceller circuit for conditioning the TFA's input signal.

The second element in the signal conditioning block establishes the desired frequency range around the central frequency of the VCXO, which is 16.384.000 Hz for an input voltage of 2.5V. For this purpose the second element is composed by a DC lever adder to set the voltage around 2.5 V at the VCXO input; a voltage divider which is involved in reducing the frequency range covered by the VCXO in order to increase the resolution of the system, this block introduces de constant K_a mentioned above.

The activity developed by the second element in the signal conditioning system is summarised in the Fig. 3.11.

In the figure the block A represents the output of the loop filter whose values alternate between –Vsat and +Vsat depending on the difference phase at the main mixer input. Block B is the DC level required to be added to the signal to put the VCXO input around 2.5V. Block C represents the voltage divider. Block D is the active adder and block E is the VCXO input whose central value is 2.5V for a frequency of 16.384 MHz as it was mentioned. It can be noticed that when the system is locked (90º of phase difference between reference and feedback signal [Arnau00-3, Best05, Wolaver91] the voltage at the VCXO input (V_{cVCXO}) is around Vdc=2.5V and its maximum and minimum values (Vmax and Vmin) depends on the K_a constant.

The schematic diagram of the second element in the signal conditioning system is shown in Fig. 3.12. The capital letters in this figure are in correspondence with those of the block diagram in Fig. 3.11.

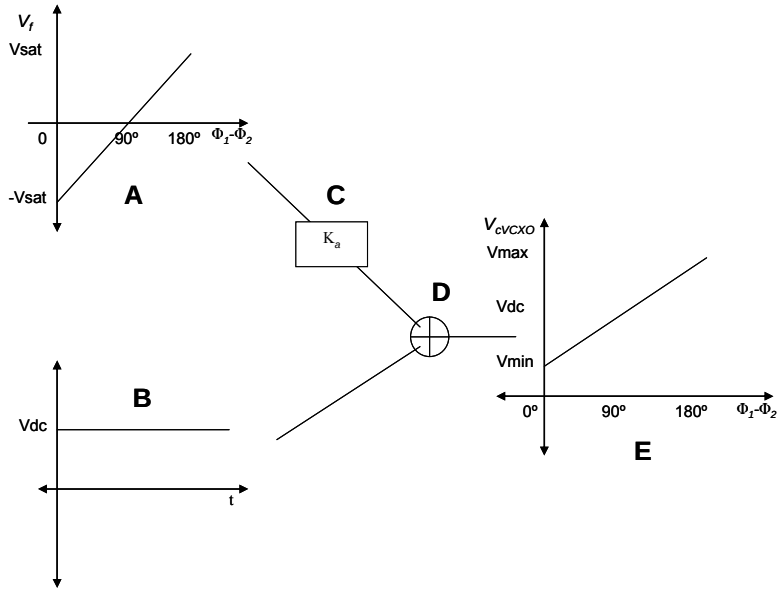

Fig. 3.11. Block diagram of the second element in the signal conditioning subsystem.

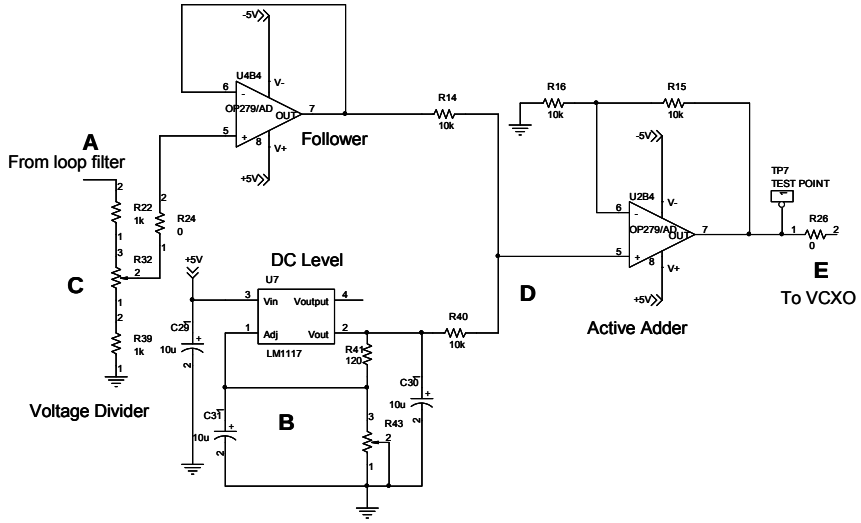

Fig. 3.12. Schematic diagram of the second element in the signal conditioning subsystem.

3.3.4.4 Voltage Controlled Crystal Oscillator, VCXO

A VCXO produced by C-MAC® is used to select a small frequency lock range about ±75 ppm around its central frequency for an input voltage excursion of ±1.5 V around 2.5 V. This range is established according to the value K_a fixed at the voltage divider. The frequency-voltage gain conversion of the VCXO used was K_v=0.8192 Hz/mV.

The high frequency-voltage gain conversion of the VCXO and its good linearity make easy to establish an accurate relationship between the EQCM frequency shifts and voltages shifts at the input of the VCXO as it was shown in Eq.(3.8).

The small frequency range achieved by the presence of the VCXO allows the *fine frequency tuning* performance and the increase in the resolution of the system since a large voltage excursion provides a small frequency sweep.

The schematic diagram of the VCXO and its correspondent filter at the output are shown in Fig. 3.13.

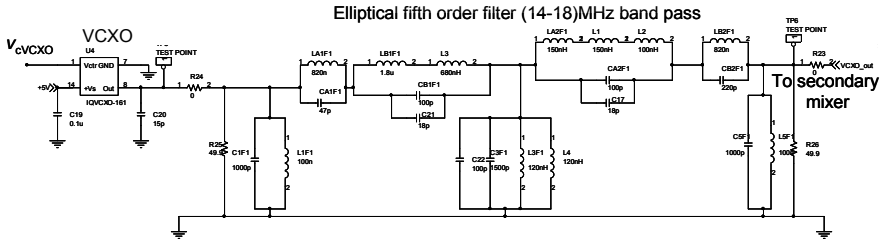

Fig. 3.13. Schematic diagram of the VCXO and the filter in its output.

3.2.4.5 Secondary mixer

The secondary mixer is the link between the main and the secondary loop. It is involved in taking the signal coming from the VCXO after filtered and the signal coming from the NCO and producing the appropriated feedback signal at the main mixer input in such a way the system is locked.

The output of the secondary mixer is also filtered by an elliptical fifth order filter [Williams95] with a band pass between 5 and 12 MHz because all quartz crystal microbalances employs are in this range.

Similarly to the main mixer for the circuit implementation was employed an AD835 integrated circuit of Analog Devices®. The schematic diagram of the secondary mixer and its filter are shown in the Fig. 3.14.

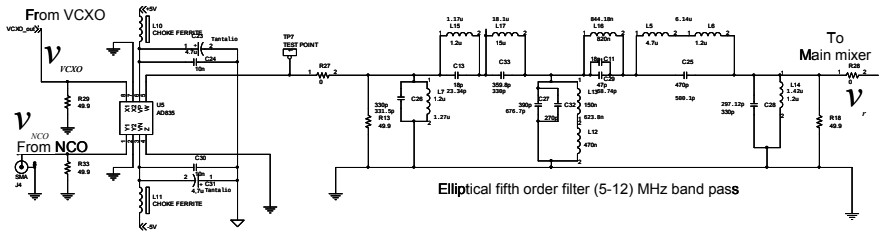

Fig. 3.14. Schematic diagram of the secondary mixer and its filter.

In the figure v_r is the feedback signal that after an appropriated conditioning is conducted to the main mixer to close the loop.

It is important to notify that similarly as the main mixer the inputs of the secondary mixer were conditioned in order to obtain a desired constant value in its transfer function. The circuit for conditioning these inputs is the same as in Fig. 3.6.

3.2.4.6 Numerically Controlled Oscillator, NCO

As it was shown above because of the extremely narrow frequency range of the VCXO, a *coarse frequency tuning* is necessary in order to centre the operative frequency range of the PLL near the centre frequency of the EQCM. This coarse tuning is performed by means of a numerically controlled oscillator, NCO, and the secondary mixer, once a rough frequency measurement of the EQCM output signal is made as it will be shown in the next section. This so-called *feed-forward* correction is performed by selecting the frequency of the NCO in such a way that the up-conversion of the EQCM frequency and the frequency of the NCO (F_{NCO}) falls in the frequency range covered by the VCXO; it is to say, (F_{EQCM} + F_{NCO}) $\in$ (16.384.000±$K_V \Delta V_{cVCXOmax}$). For this objective a bandpass filter selecting the low frequency bandwidth component [5-12 MHz] of the signal at the output of the mixer is included in the feedback path.

With this double frequency adjustment an optimum behaviour of the system is achieved. On one hand, a good resolution is obtained thanks to the narrow frequency range of the VCXO and, on the other hand, an extension of the dynamic range is guaranteed by the feed-forward correction; for this, a rough frequency measurement of the EQCM frequency is performed by means of a Field Programmable Gate Array, FPGA, which is also used to implement the complete control of the system.

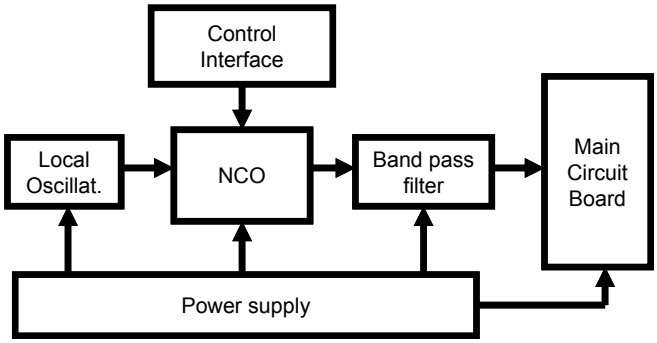

Fig. 3.15. Block diagram of the NCO's board.

Due to the NCO is an independent functional unit whose output signal can be led to the main circuit board by means of appropriated radio frequency connectors, an exclusive board composed by the NCO, a local oscillator, a band pass filter [5-12 MHz] was built to select the first harmonic for the NCO and the required interface connection to the main board containing the digital control and the radio frequency signal. Fig. 3.15 shows the block diagram of the NCO's board.

In order to implement the block diagram of the previous figure the NCO AD9851 produced by Analog Devices® was used, whose complete characteristics can be found elsewhere [Analog04]. The schematic diagram of the circuit implemented is shown in the Fig. 3.16 in which each subsystem is in correspondence with each part of the block diagram presented in the previous figure.

Once the circuit board in Fig. 3.16 was implemented the next step was the verification of this performance previously to be connected to the whole A-D PLL. In order to do the verification some tool from the Analog Devices® were used. These elements and the verification will be presented in the next chapter.

Finally in the Fig. 3.17 appears a photo of the NCO's circuit board implemented.

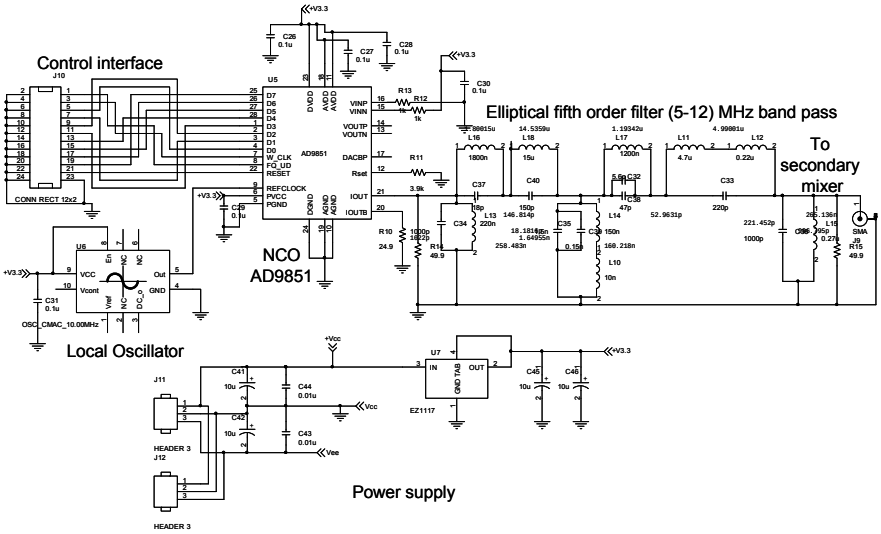

Fig. 3.16. Schematic diagram of the NCO's board.

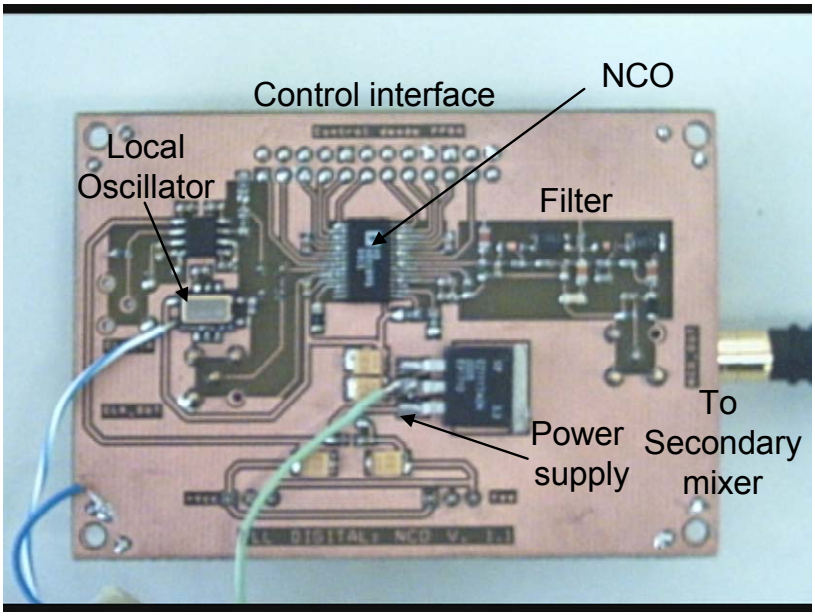

Fig. 3.17. Printed circuit of the NCO's board.

3.2.4.7 Field programmable gate array, FPGA

An *algorithm* implemented in the FPGA performs the control of the system and the *rough measurement* of the central frequency of the signal coming from the EQCM. With this schema a very fast and accurate monitoring of the frequency shifts can be achieved in a broad frequency bandwidth. A summarised *flow diagram* of the algorithm programmed in the FPGA is shown in Fig. 3.18.

In order to follow the instructions given by the flow diagram it is essential to design the *hardware architecture* according to the resources available in the FPGA selected (Spartan™ II-E produced by Xilinx®), this architecture is shown in Fig. 3.19. Once the architecture setup was achieved, the algorithm was modelled in *VHDL* for its subsequent implementation into the FPGA [Villar97].

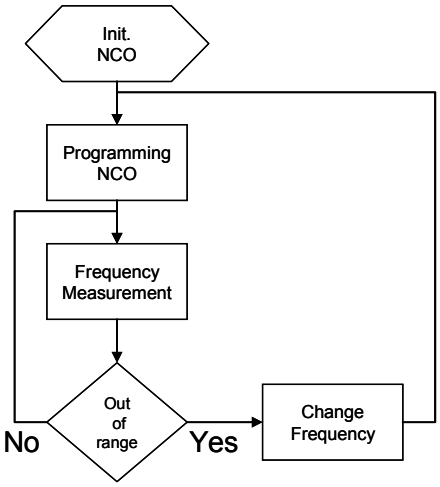

Fig. 3.18. Flow diagram of the general algorithm implemented in the FPGA.

The system in Fig. 3.19 includes three inputs: GENERAL RESET, which is connected to an external push button in the FPGA system development board; clock input (CLK) which is connected to the main clock of 50 MHz in the same board; and the reference input (REF) which is the input for the signal coming from the electrochemical cell which has been firstly pre-conditioned into a digital signal to be processed by the FPGA.

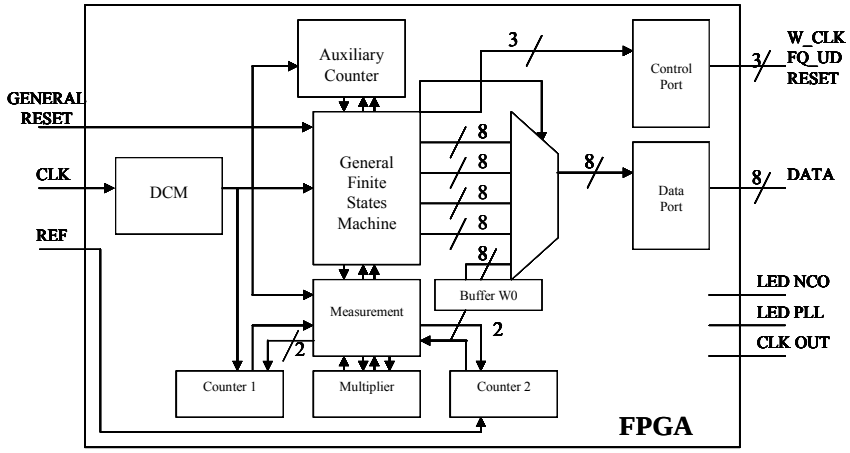

Fig. 3.19. General hardware architecture for implementing the algorithm into the FPGA.

Besides, the system has seven outputs: W_CLK, FQ_UD and RESET for programming the NCO; LED NCO indicates the programming state of the NCO; LED PLL indicates if the PLL is locked and CLK OUT is the mapping for the main clock inside the FPGA. This clock signal is conditioned internally in the FPGA by a digital clock manager, DCM.

A finite state machine, FSM, is the main part of the FPGA architecture and is involved in distributing the tasks according to Fig. 3.18 and Fig. 3.19. Furthermore, the FSM controls the programming of the NCO by using the additional elements in the diagram like the measurement block, counter 1 and counter 2. The Auxiliary Counter is used to control the steps in the FSM.

The programming process of the NCO inside the FSM has to follow a special protocol and general characteristics according to system requirements [Analog04]. These special conditions are summarised as follows:

1. The NCO has a frequency configuration word of 32 bits (named W1 to W4) which allows a maximum resolution of 0.04 Hz using a clock system of 180 MHz. The following expression can be used to calculate the resolution depending of any clock system employed:

$$R = \frac{F_{System}}{(2^{32} - 1)} \tag{3.13}$$

In this project the NCO's board works with a clock system of 60 MHz which is obtained employing an external clock of 10 MHz

plus and internal multiplication by six as it will be mentioned next. Under this condition using Eq. (3.13) the resolution in frequency of the NCO output will be 0.01397 Hz.

2. The NCO has an internal frequency multiplier by six (6X). Thus, with an external clock of 10 MHz an internal clock system of 60 MHz can be generated.
3. In addition to the 32 bits of frequency programming the NCO has 5 bits for programming the phase of the output signal, but in this project they are left in a low logic level indicating zero-phase.
4. The frequency, control and phase words are loaded into the NCO asynchronously by a serial or parallel interface. For this project was employed the parallel one.
5. For parallel loading the sequence followed is composed of five iterations with eight bits each one for a total of 40 bits. The first group (W0) controls: the phase (5 bits), the activation of the 6X multiplier (1 bit), the enable (1 bit, it must be in low logic level) and the power down control (to lead the system under sleep mode, 1 bit). The 32 bits left compose the frequency word to be programmed and put at the NCO's output.
6. The relationship between the output frequency, the system clock and the configuration word is given by:

$$F_{out} = \frac{\left(\Delta Phase * CLK_{System}\right)}{2^{32}} \tag{3.14}$$

where $\Delta Phase$ is the decimal value of the 32 bits configuration word. CLK_{System} is the internal clock of the system whose value depends on the external clock and whether the 6X multiplier is active or not. F_{out} is the output frequency of the NCO.

It is expected that the output frequency range of the NCO, F_{out}, is in the range of 6 - 10 MHz.

7. The external reference clock has to be 1 MHz as minimum when the 6X multiplier is off, and 5 MHz when the 6X multiplier is active.
8. It is possible to observe some noise in the phase of the signal at the output, mainly when the 6X multiplier is used. This phase noise is given by: $20 \log_{10}(F_{out}/F_{CLK})$.
9. It must be taken special attention to the bit number 1 of the control register (W0[1]), because if it is put in high logic level an industrial test option is enable for the circuit. For leaving this option, if it is accidentally enabled, a RESET to the system is enough.

10. There is a possibility to come into the industrial test if a FQ_UD pulse is sent after the system is power up and initial reset, because of the RESET does not clean the 40 bits configuration register whose previous value is unknown. For this reason it is more convenient to load again the 40 bits register after RESET and then to send the FQ_UD pulse.
11. In the parallel mode the 40 bits of data (W0 to W4) are loaded by means of an eight bits data bus. For the iterative loading five pulses are employed by means of the W_CLK input pin; with each one of these pulses an eight bits register is loaded.
12. After loading the 40 bits register in five stages it is necessary to put a pulse in the FQ_UD input pin in order to transfer the 40 bits data into an internal configuration register of the NCO. This FQ_UD pulse produces additionally a reset in the internal NCO process and it waits for the next configuration word starting at W0 register. If the FQ_UD or RESET pulse is not applied after the five pulses in W_CLK, these pulses will be ignored and the process starts again waiting for the first configuration data (W0).

In order to clarify the programming process of the NCO a time diagram included elsewhere [Analog04] is reproduce here in Fig. 3.20.

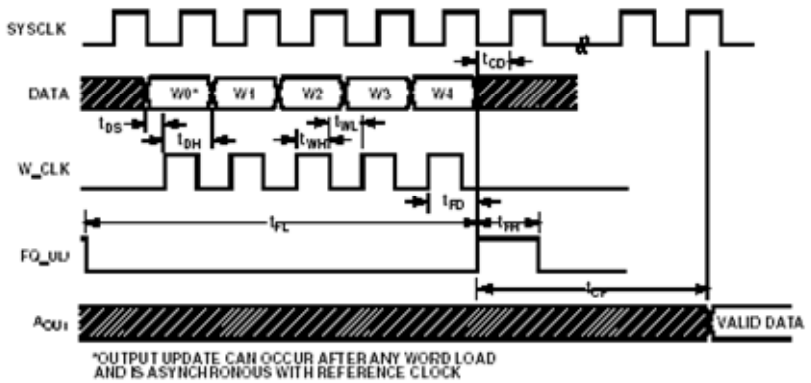

Fig. 3.20. Time diagram for programming the NCO. Adapted from [Analog04].

According to the previous figure the procedure to program the NCO is as follows: firstly the control word W0 is loaded in the data register which has eight bits, then after some time (t_{DS}) a pulse in W_CLK needs to be applied to take into account this initial data. Once some time has passed (t_{DH}) a new data W1 can be loaded and waits for the next W_CLK pulse. The process is repeated until the last configuration data W4 is load. From

the begin of the last W_CLK pulse given to load W4 it is necessary to wait some time (t_{FD}) to put the FQ_UD pulse in order to load the full 40 bits configuration word into the internal NCO register. Finally after t_{CF} time the new frequency is valid at the output of the NCO. If a new frequency is required to be programmed the process needs to be started again from the first step. The values of different times shown in the figure are given in [Analog04].

Another important time diagram to programme the NCO is presented in Fig. 3.21.

In this figure it is shown that the reset command sent to the NCO needs to be kept almost during t_{RS} = 5 sysclk cycles to be valid then the NCO has an additional latency time of t_{RR} = 2 sysclk cycles. For the system developed in the A-D PLL these times correspond to 0.1μs and 40ns respectively. These values are the minima according to the figure. In general the minimum reset output latency can be fixed at t_{OL} = 13 sysclk cycles.

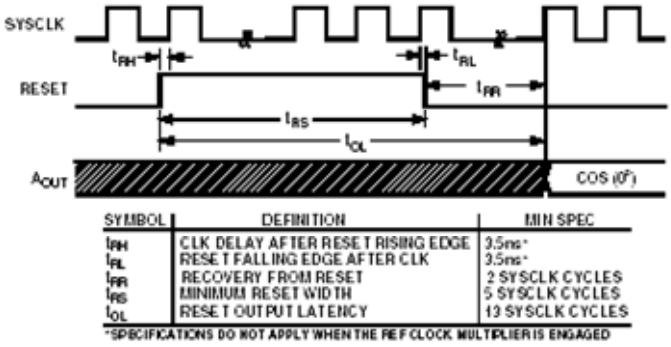

SYMBOL	DEFINITION	MIN SPEC
t_{RH}	CLK DELAY AFTER RESET RISING EDGE	3.5ns*
t_{RL}	RESET FALLING EDGE AFTER CLK	3.5ns*
t_{RR}	RECOVERY FROM RESET	2 SYSCLK CYCLES
t_{RS}	MINIMUM RESET WIDTH	5 SYSCLK CYCLES
t_{OL}	RESET OUTPUT LATENCY	13 SYSCLK CYCLES

*SPECIFICATIONS DO NOT APPLY WHEN THE REFCLOCK MULTIPLIER IS ENGAGED

Fig. 3.21**.** Reset time diagram for the NCO. Adapted from [Analog04].

Taking into account the information provided by Fig. 3.20 and Fig. 3.21 the general process of the block programming NCO in Fig. 3.18 is shown in the Fig. 3.22.

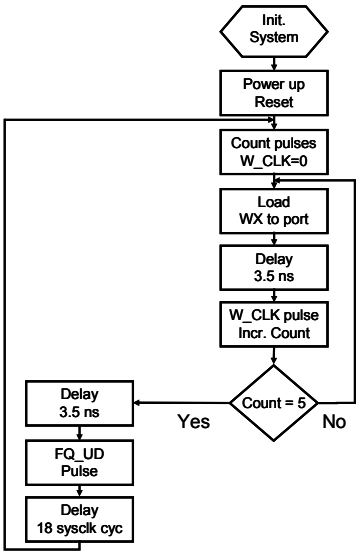

Fig. 3.22. Flow diagram for programming the NCO.

Another important element in Fig. 3.19 is the *measurement block* which is the implementation of a procedure to measure the central frequency of the reference signal coming from the EQCM controlled oscillator.

For this purpose the following blocks: counter 1, multiplier and counter 2 are employed. The algorithm implemented to perform the central frequency measurement, due to its requirements are not very critical, was developed using the extension of the *basic universal counter* strategy already mentioned in section 1.6.2 and summarized in Fig. 1.30. In this case the reference clock signal for the measurement was the system clock, i.e., 50 MHz.

The block in Fig. 3.19 is a small finite state machine, FSM, which is subordinated to the main FSM. This main FSM orders the measurement to the small FSM to operate according to the flow diagram in the Fig. 3.19.

In the Fig. 3.23 it is shown a photo of the development kit board of the Spartan™ II-E FPGA in which both the frequency measurement algorithm and the NCO control were programmed; additionally an input-output board to test the board's performance is also shown.

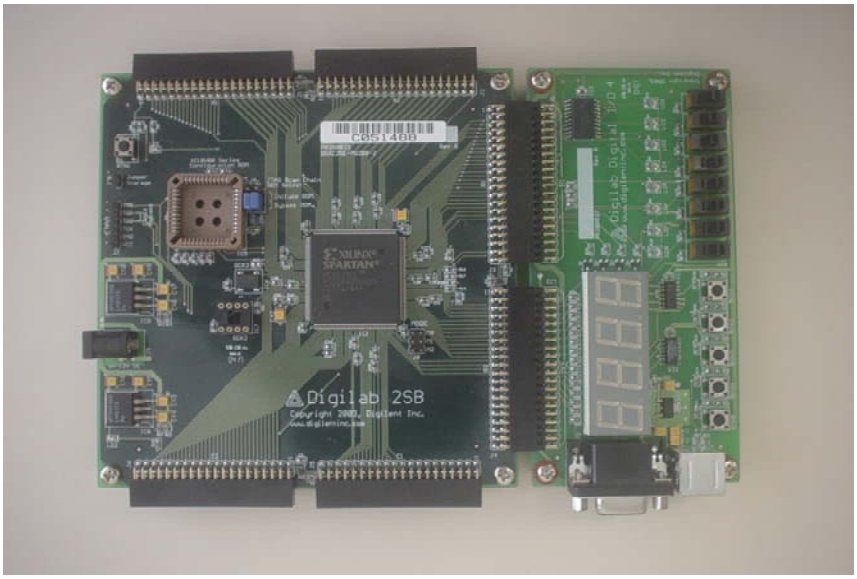

Fig. 3.23. FPGA development kit board employed in the A-D PLL algorithm implementation.

As it was mentioned, the reference oscillator signal was pre-conditioned into a digital signal to be processed by the FPGA. The schematic diagram of this pre-conditioning subsystem is shown in the Fig. 3.24.

The subsystem in the previous figure is built employing a high speed, low power comparator (MAX903) produce by MAXIM.

Finally, the complete algorithm modelled in VHDL and programmed into the FPGA is sown in the appendix II.

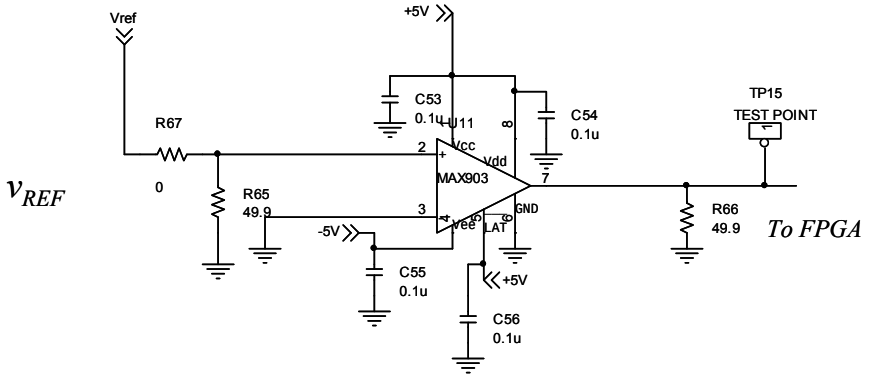

Fig. 3.24. FPGA pre-conditioning subsystem to transfer the reference analogue signal into a digital one.

Once all the subsystems of the A-D PLL have been put forward the next step is to present the whole system as a functional unit to extract the appropriated signal to obtain the Electrogravimetric Transfer Function, EGTF, in the AC Electrogravimetry experimental technique.

3.2.4.8 Complete system assembled

As it was presented above in the theoretical model, the whole system can be modelled by the Eq. (3.12) and its operating principle was outlined in section 3.2.2.2.

A photo of the whole system designed is shown in the following figure. In the next chapter the different materials and methods employed will be introduced, and both the design of A-D PLL and the performance simulation will be made under several conditions

Fig. 3.25. Photo of the A-d PLL complete system assembled.

4 Materials and Methods

This chapter describes the different *materials* and *methods* employed during each one of the stages of the development of the system: both in the design and simulation stages and in the experimentation once.

The first part of the chapter describes the design and simulation tools which include some hardware instruments and circuits and the software elements employed.

Subsequently, the chemical and electronics instrumentation employed during the experimentation stage are introduced; and finally, everything related to the experimentation stages, including the experimental setup, the experimental protocol and the experimental form will be introduced.

4.1 Design and simulation tools

4.1.2 A-D PLL simulation script

Before stating the hardware design of the system, the first stage during the development of the project was the testing of the theoretical model of the A-D PLL introduced in section 3.2.3. For conducting the simulation of the system a Matlab® *script* was developed in which all the parameters of the system considered in the model were introduced.

The script developed is shown in Fig. 4.1.

```
clear all;
close all;
% z=0.707;
% wn=20*pi*1e3;
% b=[2*z*wn wn^2];
% a=[1 2*z*wn wn^2];
% w=logspace(-1,6);
% % h=freqs(b,a,w);
% freqs(b,a,w);
% sys=tf(b,a);
% figure
% step(sys)
% kd=0.5;
%
% BEGINNING OF THE FIRST PART
km=0.5;     %Main mixer constant sensitivity
```

```
kv=819.2;   %VCXO constant sensitivity
% ka= 0.1493;   %Testing values for Ka
% ka= 0.2236;
% ka= 0.298;
% ka=0.366;
ka=1;
k=2*pi*km*kv*ka;    %PLL loop constant
% wnreal= 2*pi*10e3;
% zreal=0.707;
% t1=k/wnreal^2;
% t2=(2*zreal)/wnreal;
R1=680;     %Low pass filter resistors
R2=12000;
C=10e-9;    %Low pass filter capacitor
% R1=t1/C;
% R2=t2/C;
%
% END OF THE FIRST PART
%
% BEGINNING OF THE SECOND PART
t1=R1*C;    %Time constant 1
wnreal=sqrt(k/t1)  %Natural frequency
fnreal=wnreal/(2*pi)    %Linear frequency
t2=R2*C;    %Time constant 2
zreal=(wnreal*t2)/2   %Damping factor
breal=[2*zreal*wnreal wnreal^2];    %Factors of the Transfer Function
areal=[1 2*zreal*wnreal wnreal^2];
wreal=logspace(-1,6);
Ksens=1/(kv*ka) %System's sensitivity constant [V/Hz]
% figure
freqs(breal,areal,wreal);   %Frequency response output
sysreal=tf(breal,areal);
%
% END OF THE SECOND PART
%
% BEGINNING OF THE THIRD PART
figure
step(sysreal)
figure
% t = 0:.000001:2e-3;
% y = square(2*pi*1000*t);
[y,t]=gensig('square',1e-3,4e-3,1e-6);  %Pulse response
lsim(sysreal,y,t)
figure
yy =1*sin(2*pi*500*t);  %Steady state response
lsim(sysreal,yy,t)
figure
escalon =[zeros(size(t(1:100)));ones(size(t(101:end)))];    %Step response
lsim(sysreal,escalon,t)
% END OF THE THIRD PART
```

Fig. 4.1. Script for simulating the A-D PLL.

The figure shows that the *simulating script* is divided in three main steps. Firstly the parameters of the PLL are introduced, secondly, the time constants, natural frequency, damping factor and the transfer function of the whole system according to the theoretical model presented. Finally some responses, like step and frequency responses among others, are calculated employing this transfer function.

As it can be noticed for simulating purposes the values for the different parameters are as follows: the main mixer constant, K_m=0.5, the VCXO

constant, K_v=819.2 Hz/V, the voltage divider constant, K_a=1, the loop filters' resistors, *R1*=680 Ω, *R1*=12000 Ω and C=10 nf.

The configuration of the different responses is: frequency response between 0.1 Hz and 1 MHz to simulate the modulating signal. The "step response 1" is a built-in Matlab function which takes the transfer function input and performs the step responses until the output is stabilised. The "pulse response" is the response of the system when a square signal of 1 KHz is applied, the duration of the square signal is four cycles and the time sample is 1 μs. For a steady state response a sine wave of 500 Hz is applied. Finally a second step response, "step response 2", is a "home-made" signal applied to calculated the step response and for comparing the results with the first one.

The results of the simulation for this script will be presented in the following chapter.

4.1.2 A-D PLL circuit simulation

After the first simulation step made with the script a complete *circuit simulation* was performed in ORCAD®. The circuit for conducting this simulation is shown in the Fig. 4.2.

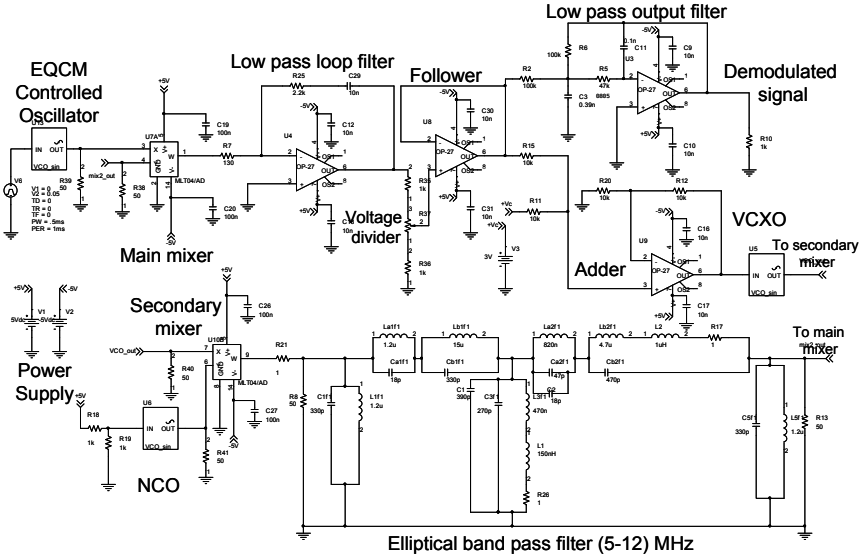

Fig. 4.2. Simulation circuit of the complete A-D PLL.

As it can be noticed all the elements considered in the theoretical model are included in the circuit for simulation purposes.

For the EQCM controlled oscillator simulation it was employed a VCO of the ORCAD's library. This VCO is excited by a sine wave signal, i.e., the variation in the central frequency of the VCO is modified by a sine wave signal, then the output of the VCO is a frequency modulated, FM, signal in which the carrier is the central frequency of the VCO and the modulating signal is the sine wave applied.

Similarly, the NCO and the VCXO are simulated by a VCO element, but in case of the NCO the control signal is constant, so the output frequency of the NCO is fixed, because the simulation is performed for a specific and fixed carrier frequency between 6 and 10 MHz, according to the characteristics of the QCM employed in the AC Electrogravimetry technique.

The mixer was simulated by an own ORCAD model too. The model is a common multiplier.

The rest of the components of the circuit are simulated almost identically as they were designed, i.e., without changing any element of the design previously shown in chapter 3.

For the simulation it was employed a carrier frequency of 10 MHz and a modulating sine wave signal of 50 mV and a frequency of 1 KHz. The simulation was conducted during 6 ms, i.e., taking 6 complete periods of the input modulating signal. The results of the simulation will be presented in the next chapter.

After the previous simulations work fine, the design process continued by the hardware or the printed circuit board, PCB design which is introduced in the following section.

4.1.3 PCB design

For developing the PCB it was employed ORCAD® *Layout*.

The system was designed employing four (4) *layers*: TOP, DOWN, GND plane and POWER (+ 5V) plane. The next figures show each one of the layers designed.

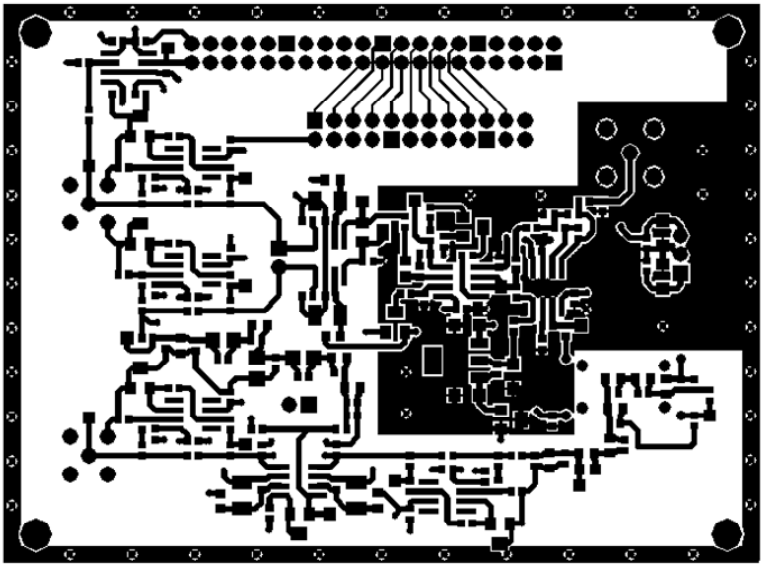

Fig. 4.3. Top layer of the A-D PLL PCB designed.

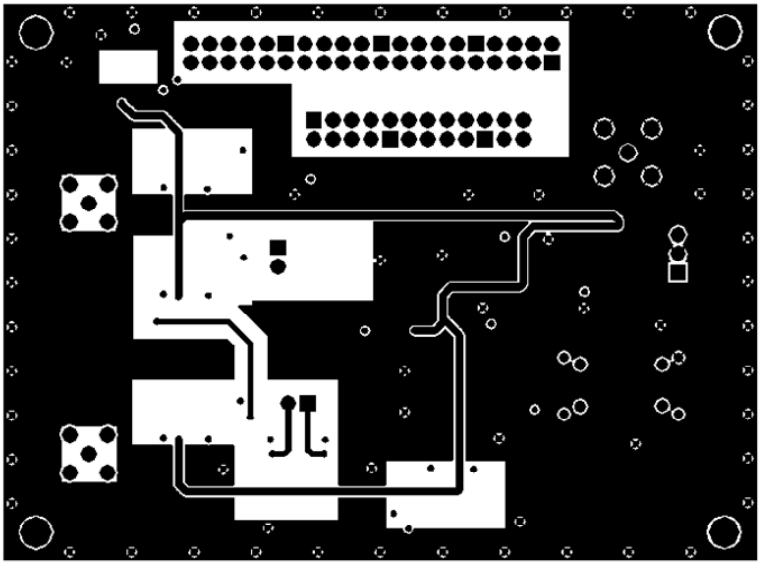

Fig. 4.4. Bottom layer of the A-D PLL PCB designed.

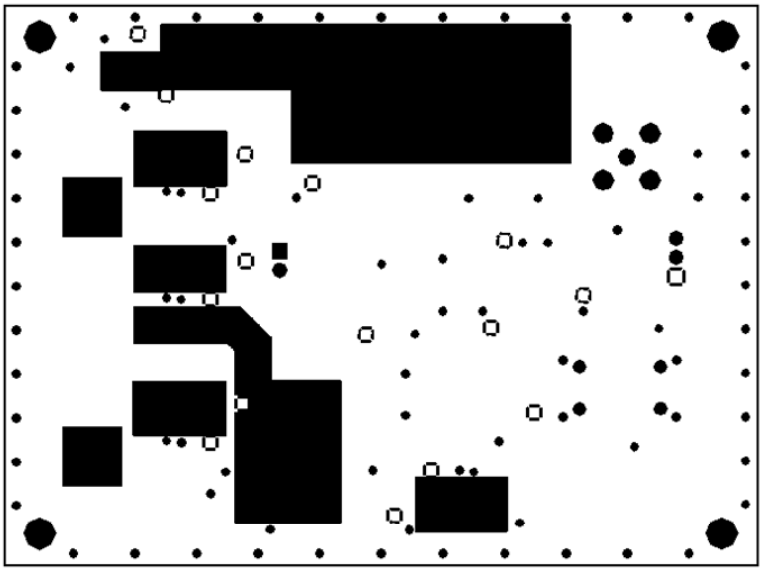

Fig. 4.5. Power layer of the A-D PLL PCB designed.

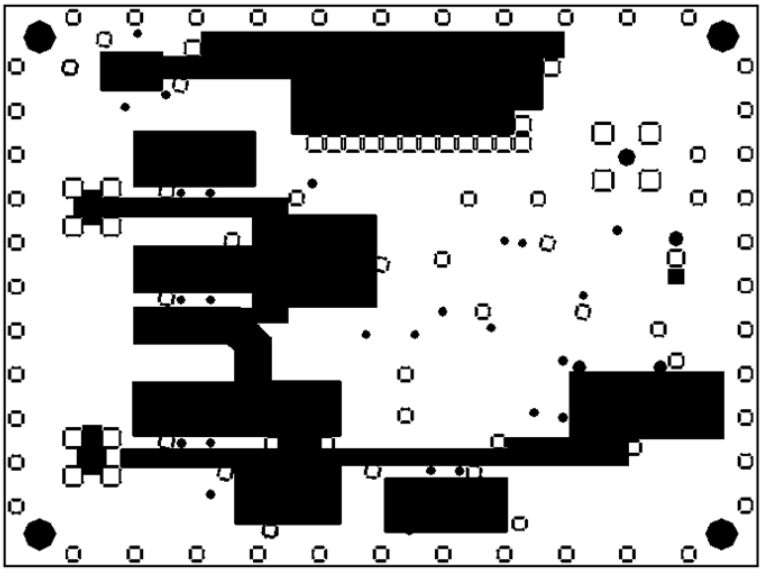

Fig. 4.6. Ground layer of the A-D PLL PCB designed.

4.1.4 NCO design and simulation tools

Once the main hardware of the A-D PLL is designed, some other additional subsystems both hardware and software must be designed to achieved a complete working unit. One of these is the NCO system whose previous testing procedure requires a *hardware and software simulation*.

The Fig. 4.7 shows the hardware interface for programming and testing the working conditions of the NCO once the NCO's PCB shown in Fig. 3.16 was implemented.

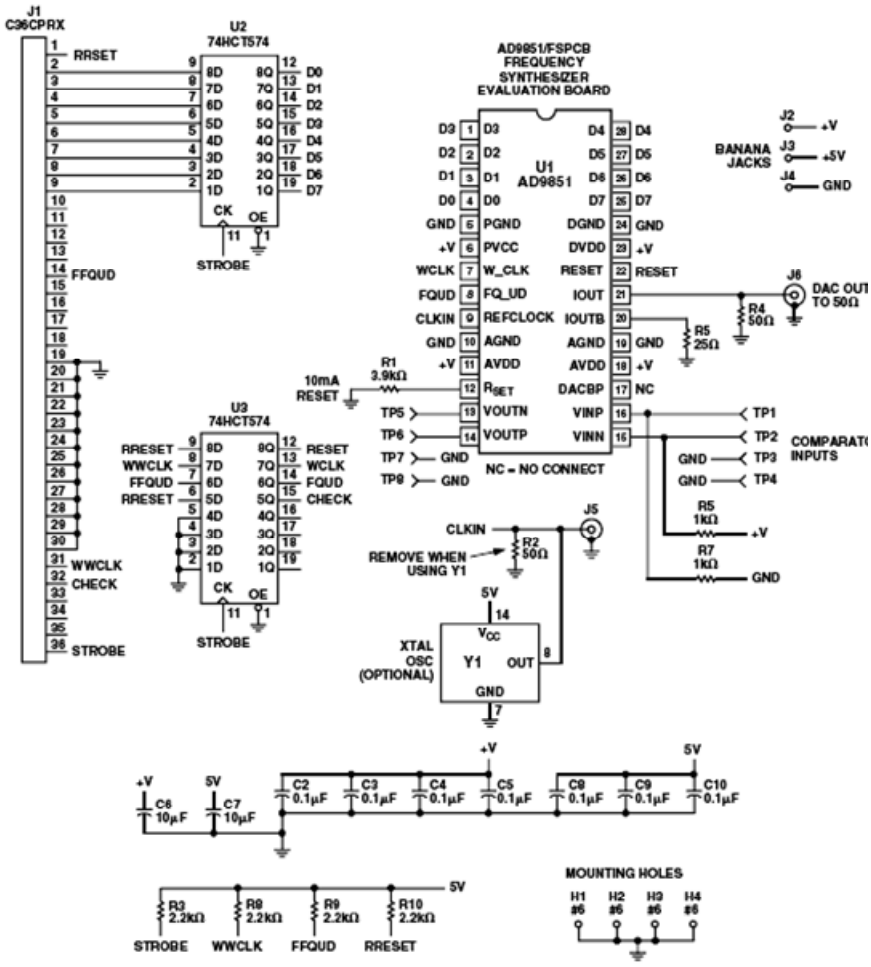

Fig. 4.7. NCO hardware programming and testing interface. Adapted from [Analog04].

The hardware interface is composed by a 36 pinout parallel port connector, two buffers, a power supply, connectors and the AD9851 synthesiser.

In conjunction with the system shown in the Fig. 4.7, a software interface must be used. The Fig. 4.8 shows this software interface.

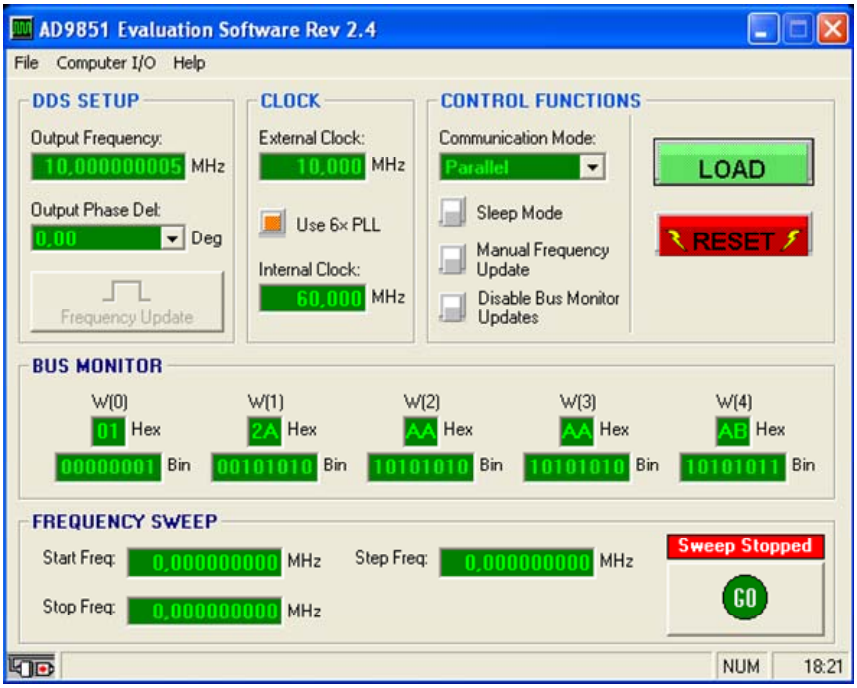

Fig. 4.8. NCO software programming and testing interface. Taken from Analog Devices® web site.

Using these two interfaces the main characteristics of the programming procedures and protocols to be implemented in the FPGA were established.

4.1.5 FPGA design and simulation tools

In order to programme the algorithm shown in the flow diagram of the Fig. 3.17 and its hardware architecture shown in the Fig. 3.18 it was employed a hardware interface *Digilab* 2SB by Digilent, Inc, cables and connectors; and a software development system composed by the ISE Foundation Software by Xilinx, Inc., a simulation subsystem by Modelsim® and a programming tool Adept by Digilent, Inc.
Fig. 4.9 shows the block diagram of the Digilab 2SB *development board*.

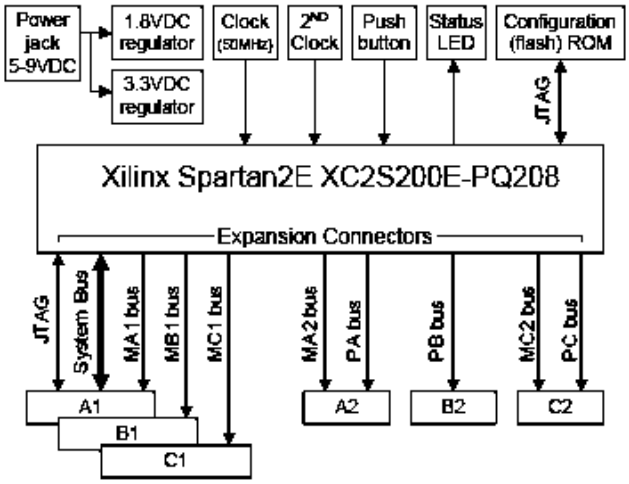

Fig. 4.9. Digilab 2SB development board block diagram. Adapted from [Digilent03].

The Digilab development board is composed by a Spartan™ II-E FPGA, a 50 MHz clock source, a power supply and some peripheral buses. The *JTAG bus* is employed to program the unit by means of the Adept programming tool.

4.1.6 System box design

The design of the distribution of the whole system in a *project box* was performed in Autocad® 2007. The diagrammatic schema of the distribution is shown in Fig. 4.10.

In this figure it can be observed the top view (**a**) of the system in which all the subsystems are recognised: the FPGA development board, NCO board and an *additional conditioning block* used to cancel the DC voltage level at the output of the system.

In the front view (**b**) different inputs or outputs are shown. The EQCM input is the reference signal that comes from the EQCM controlled oscillator, the JTAG interface is employed to programme the FPGA using the Adept tool seen in the previous section, the power supply input includes the inputs for a dual voltage source (± 5V), the Reset is a push button connected to the general FPGA reset and the output is the demodulated signal of the system, i.e., the voltage that is proportional to the frequency shifts regarding the central frequency in the reference signal.

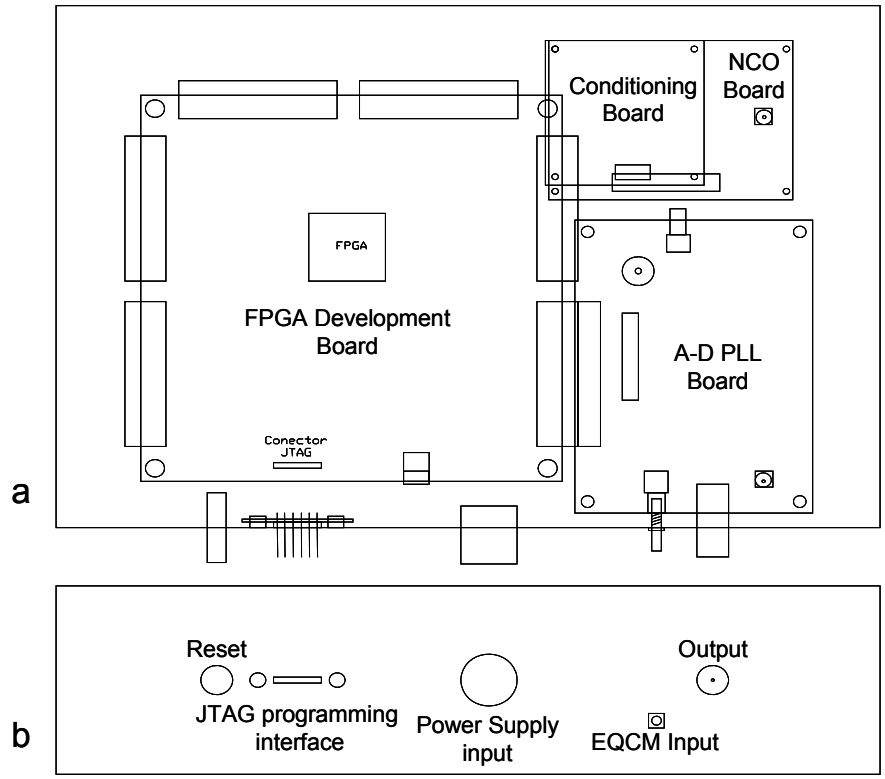

Fig. 4.10. Distribution schema of the complete system, **a.** top view, **b.** front view.

4.2 Chemical instrumentation associated

4.2.1 Electrochemical cell

As the *electrochemical cell* a beaker reaction of Pyrex glass was employed. This cell has an input hole to setup the *reference electrode*; the *counter electrode* and the *working electrode* were put inside the cell supported by a rubber top cover of the cell.
Fig. 4.11 shows the cell employed and Fig. 4.12 the complete cell assembled.

Fig. 4.11. Cell employed during experimentation stage.

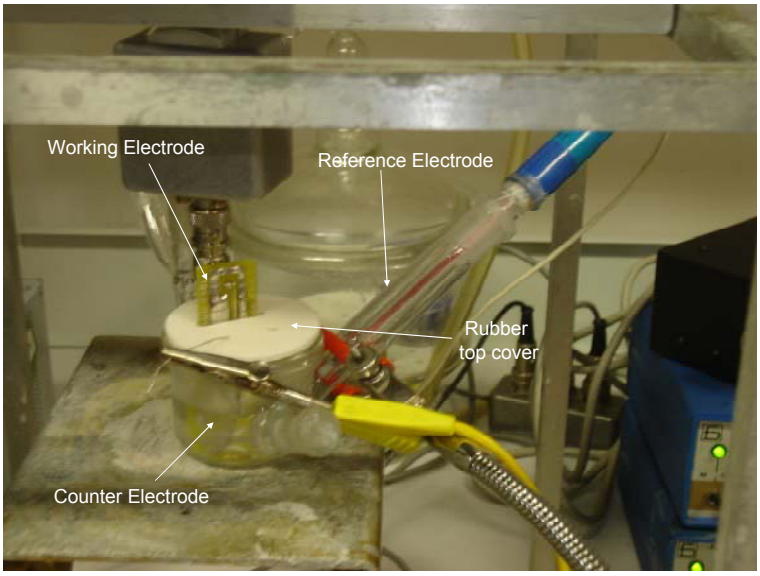

Fig. 4.12. Assembled electrochemical cell.

4.2.2 Potentiostat

The instrument employed to provide the voltage difference to conduct the Electrogravimetry was a *potentiostat/galvanostat* P.G-STAT.Z1 produced by Sotelem®. This equipment additionally measures the flow current in the electrochemical cell and controls the *polarization voltage* and the *electrochemical impedance*. Fig. 4.13 shows the *potentiostat* used in the experimentation.

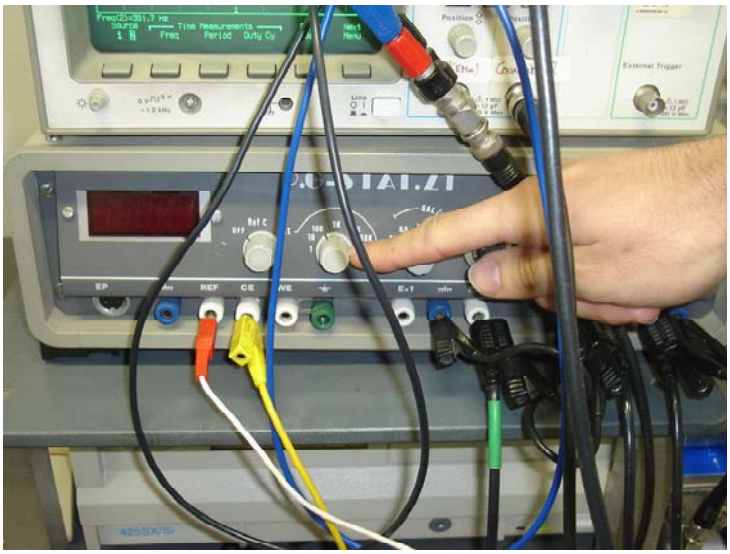

Fig. 4.13. Potentiostat P.G-STAT.Z1 used in the experimentation.

4.2.3 Quartz Crystal Microbalance Electrodes

The resonators of the microbalances were *AT-cut planar quartz crystal*, 14 mm in diameter with a 9 MHz *nominal resonance frequency* (Matel-Fordhal, France [Gabrielli07]) . Two identical *gold electrodes*, 2000 A° thick and 5 mm in diameter, were deposited by evaporation techniques on both sides of a quartz crystal; one of these electrodes is covered by any special polymer subjected to study during the experimentation process. The resonator was connected by a *silver conducting paste*, through a *printed circuit board* to a BNC adaptor. After the assembly the silver contacts are covered by *silicone* to avoid the electrolyte contacts them. Fig. 4.14 shows the arrangement for the EQCM.

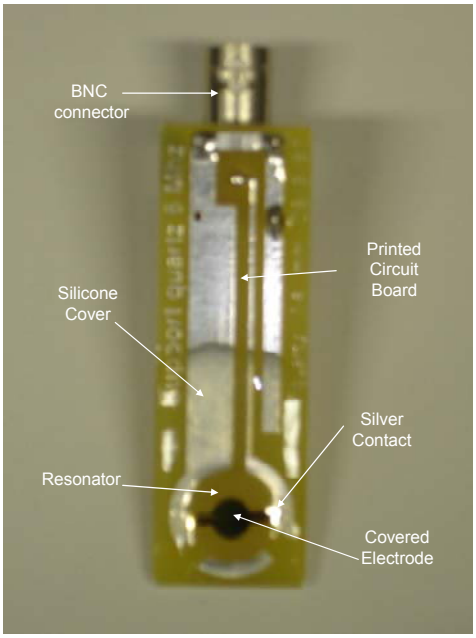

Fig. 4.14. EQCM employed in the AC Electrogravimetry experimentation.

4.2.4 Polymers and solutions

To conduct the AC Electrogravimetry experimentation three *polymers* were used: Prussian Blue, Polypyrrole and Polyaniline.

The *Prussian Blue*, PB, is called ferric ferrocyanide and its chemical formula is $Fe_7(CN)_{18}(H_2O)_x$ where $14 \leq x \leq 16$. Their use in electrochromic devices, rechargeable batteries, among others has increased their technological interest [García-Jareño00]. The PB was deposited at 10 uA during 150 s on the gold electrode and it was studied in KCl 1M.

The *Polypyrrole*, PPy, is also called polypyrrole black; it is a chemical compound formed by a number of connected pyrrole (C_4H_5N) ring structures. For example a tetrapyrrole is a compound with four pyrrole rings connected. Polypirrole is a conductive polymer used in multiples applications [Gabrielli02-2]. The PPy was deposited at 2 mA during 2 s on the gold electrode and it was studied in KCl 1M.

The *Polyaniline*, PANI [Gabrielli00-3] is the last conducting polymer employed during the AC Electrogravimetry experimentation. The PANI was deposited at 10 uA during 150 s on the gold electrode and it was studied in three different media: KCl 1M, $HClO_4$ 1 M and HNO_3 1 M.

The results for the experiments conducted with these polymers will be shown in the next chapter. Now, a description of the electronic instrumentation employed in the experimentation will be shown.

4.3 Electronic instrumentation associated

4.3.1 Transfer Function Analyser, TFA

One of the key elements in the AC Electrogravimetry experimentation is the *transfer function analyser* or *frequency response analyser, FRA* which calculates the *Electrogravimetry transfer function, EGTF*. In this project a four channel frequency analyser produced by Solartron® was employed for this purpose. One input channel is used for the current in the cell measurement and another is used to measure the voltage coming from the A-D PLL which is related to the frequency variation in the resonance frequency of the EQCM controlled oscillator and then the mass variation in the QCM. Moreover, the TFA has two outputs: the first one is a signal generator output and the second one is a communication interface which is connected to the computer to send the processed data and to receive the control commands.

The control instructions are introduced in a specific configuration file and they are related to the parameters of the signal provided by the signal generator and the characteristics of the experiment conducted.

Fig. 4.15 shows the TFA Solartron 1254 employed during the experimentation.

Fig. 4.15. Transfer Function Analyser Solartron 1254 used in the AC Electrogravimetry experimentation.

4.3.2 Specific instrumentation software

This subsystem is not properly and electronic instrument, but it is a measurement element that works in conjunction with the transfer function analyser to calculate the EGTF. The element is a private software application called *Measurer*. This software is programmed in the computer connected to the TFA and has as outputs the graphical representation both the *Bode* and the *Nyquist* plots of the EGTF and the impedance measured in the cell. The Fig. 4.16 shows a photo of the computer in which the Measurer software is included.

Fig. 4.16. Measurer software in the PC connected to the TFA.

4.3.3 Digital Scope

In order to continuously check the different signals obtained in each one of experimentation stages a digital scope Tektronix® TDS 3012B was employed. This scope has the possibility to save the data acquired into a floppy disc, it can calculate the FFT several measurement utilities. Fig. 4.17 shows a photo of the scope used.

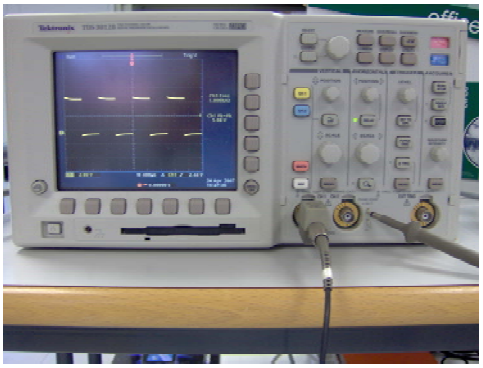

Fig. 4.17. Tektronix scope TDS 3012B employed in the experimentation.

4.3.4 Frequency meter

To follow the resonance frequency of the EQMC during the experimentation process a *frequency meter* HP 53181A was used. This instrument measures until 3 GHz and has high stability due the presence of an oven controlled oscillator. The Fig. 4.18 shows the frequency meter employed.

Fig. 4.18. Frequency meter HP 53181A employed in the experimentation.

4.3.5 Signal generators

In different stages of the development of the project both in the design process and the experimentation, *signal generators* were used. One of these is the Marconi® 2023 which is a radio frequency generator until 1.2 GHz of carrier frequency with some modulation and programmable utilities. The photo of the Marconi generator is shown in Fig. 4.19.

Fig. 4.19. Signal generator Marconi 2023 employed in the experimentation.

Another signal generator employed, mainly in the design and the simulation stages of the project, was the 20 MHz function/arbitrary waveform generator Agilent® 33220A. This generator has multiple modulation modes and a GPIB control bus among other characteristics. The Agilent generator employed is shown in the Fig. 4.20.

Fig. 4.20. Function generator Agilent 33220A.

4.3.6 Other instruments

Additionally to the instrumentation presented above, some other electronic instruments were used to complete the elements employed in the design, simulation or experimentation stages. Digital multimeters produced by Fluke®, dual power supplies by Tektronix® and *auxiliary generators* among others, were used to arrange the systems which will be introduced in the following sections.

4.4 Experimental methodology

Experimental validation of the system developed at the (Laboratoire Interfaces et Systemes Electrochemiques) in the CNRS (Centre National de la Recherche Scientifique) in Paris was performed in three stages: first, a *static characterisation* was performed to measure the sensitivity of the system designed and its operating frequency range; subsequently, a comparison between the current system AC Electrogravimetry experimental setup (named "current" from now on) (see Fig. 1.29) and the system proposed in this project thesis (named "new") in terms of system frequency performance, called *dynamic characterisation* was made; and finally, some *experimental analysis* with some polymers used at LISE were carried out.

A detailed description of these three experimental stages is introduced in the following sections.

4.4.1 Static characterisation

The *static characterisation* is referred to the test conducted to the system designed [Torres06-2] in which small frequency variation regarding the central frequency were provided by a signal synthesiser (Marconi 2023). By these means the EQCM controlled oscillator signal is simulated.

Using this static characterisation it is possible to draw a response plot whose slope will be the system sensitivity given in mV/Hz. Moreover, with this static characterisation it is possible to investigate the *lineal operating frequency range* of the system, i.e., the upper and lower interval of frequencies, regarding the central frequency of the synthesiser, in which the system's behaviour is linear.

For a comparison between the current AC Electrogravimetry experimental setup and the new system proposed, the experimental arrangement shown in Fig. 4.21 was used.

It can be noticed from the figure that for the characterisation of the current system an auxiliary synthesiser is required whose central frequency must have a difference of 400 Hz regarding the central frequency of the EQCM simulator synthesiser.

For the EQCM simulator is it was introduced 50 Hz shifts frequency between -1000 Hz and 1000 Hz approximately (regarding the central frequency of 9 MHz), for a total frequency range of 2000 Hz covered, then the sensitivity and linearity of both systems in this range can be tested.

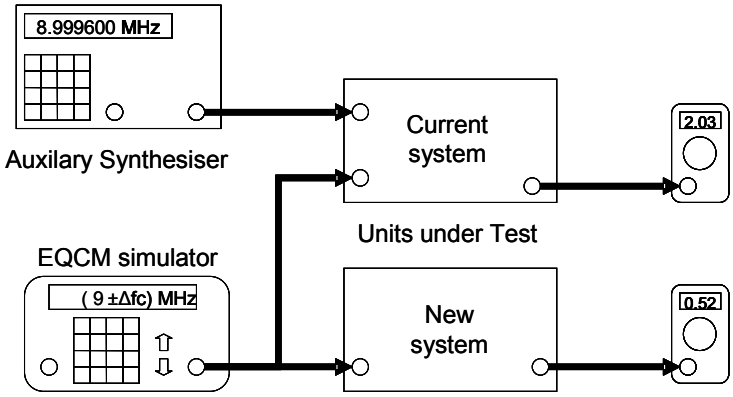

Fig. 4.21. Experimental setup for static characterisation.

The general configuration of the system in Fig. 4.21 is as follows:

- Auxiliary generator or synthesiser: RF generator HP 3325B whose output frequency is: $f_{aux}=f_c$ - 400 Hz, where f_c is the central frequency of the EQCM simulator.
- EQCM cell simulator: function generator Marconi 2023 with $f_{out}=f_c \pm \Delta f_c$ where Δf_c is given by the frequency steps inserted, and f_c= 9 MHz (f_c can be whatever frequency in the 6-10 MHz range).
- True RMS Digital Fluke® meters.
- Frequency range covered: [-1000,1000] Hz regarding f_c.
- Frequency shift steps inserted: ± 50 Hz.

The responses acquired of this static characterisation will be introduced in the following chapter.

4.4.2 Dynamic characterisation

The *dynamic characterisation* is just the *frequency response* of the system which is calculated in conjunction with the frequency and transfer function analyser, TFA (Solartron 1254) and a computer. A comparison between the current and the new systems was performed. Again, for simulating the electrochemical cell with the EQCM the synthesiser Marconi 2023 was used. Fig. 4.22 depicts a block diagram for the characterisation setup of the current system in frequency response.

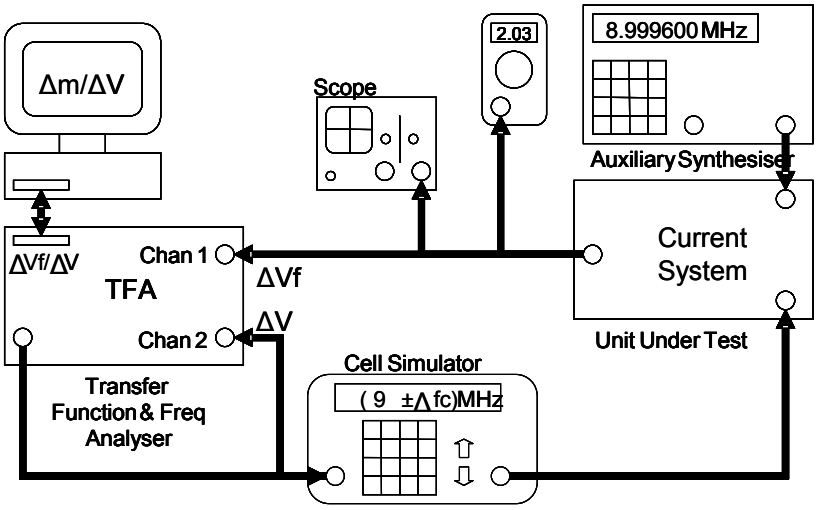

Fig. 4.22. Block diagram of the dynamic characterisation setup for the current system.

The configuration established for this system is as follows:

- Auxiliary synthesiser: RF generator HP33325B with $f_{aux}=f_c$ - 400 Hz.
- Cell Simulator: RF programmable generator Marconi with $f_{out}=f_c \pm \Delta f_c$, with several carrier frequencies (Between 6-10 MHz).
- Δf_c is provided by the generator present in the Transfer Function Analyser, TFA, Solartron 1254. It is a sine wave of 100 mV rms and variable frequency between 63 KHz and 1 mHz.
- True RMS Digital Fluke meter.

In Fig. 4.22 the sine wave signal, Δf_c, coming from the TFA is used to provide the modulation in the EQCM simulator, then the frequency modulated signal at the EQCM simulator (Marconi) output is connected to the unit under test, UTT, in this case the current system, and the output of the system is the voltage shift, ΔV_f related to the Δf_c introduced by the sine wave. In addition to the voltage variation inserted in the cell simulator, ΔV, this system's output is relayed to the TFA for obtaining the Electrogravimetric transfer function, EGTF. At the same time the system's output is monitored in the scope and the meter.

For the new system the characterisation setup is shown in Fig. 4.23.

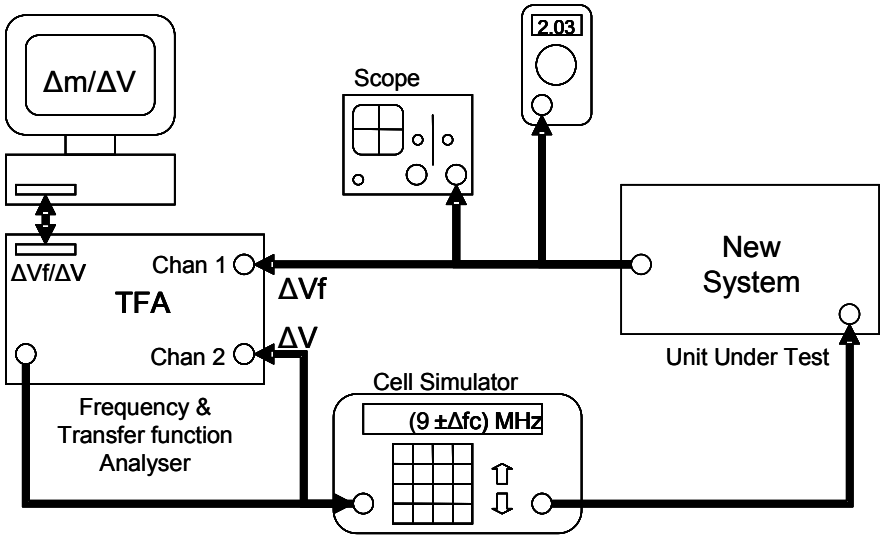

Fig. 4.23. Block diagram of the dynamic characterisation setup for the new system.

As it can be previously noticed, for the characterisation of the new system the auxiliary synthesiser is absent. The other components are the same as those in the Fig. 4.22.

The experimental results for the dynamic characterisation process will be shown in the following chapter.

4.4.3 Experimentation with polymers

In these *experimental analysis* three *polymers*, introduced in section 4.24, were taken and subject to a *redox process* during several minutes in the AC Electrogravimetry experimental setup. The experimental arrangements for the current and new systems are shown in the Fig. 4.24 and Fig. 4.25 respectively. Again, for the new system characterisation the auxiliary synthesiser is not necessary.

The configuration established for these systems during the polymers experimentation is as follows:

- Carrier frequency ≈ 9 MHz.
- Deviation voltage (at TFA): 50 mV rms.
- Modulator frequency sweep: (1 mHz- 63 KHz).

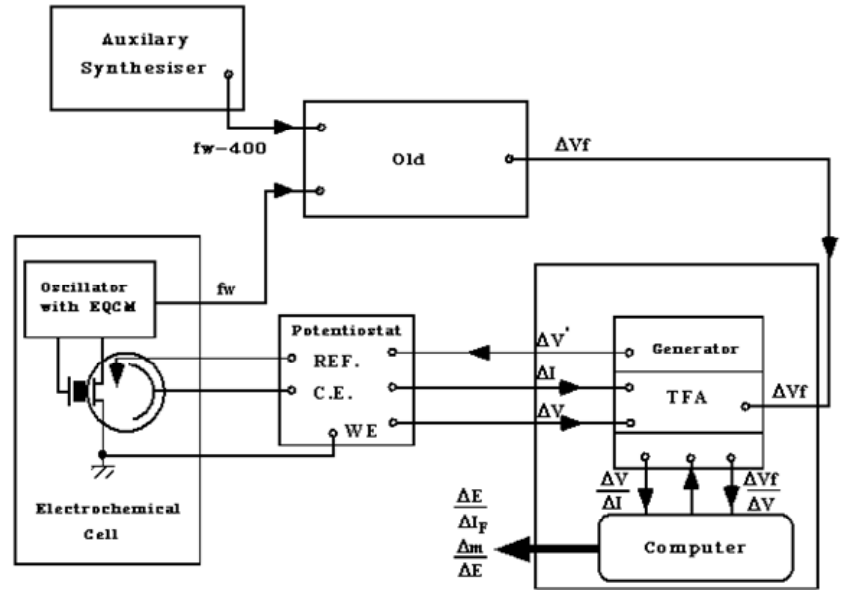

Fig. 4.24. Polymer characterisation setup for the current system.

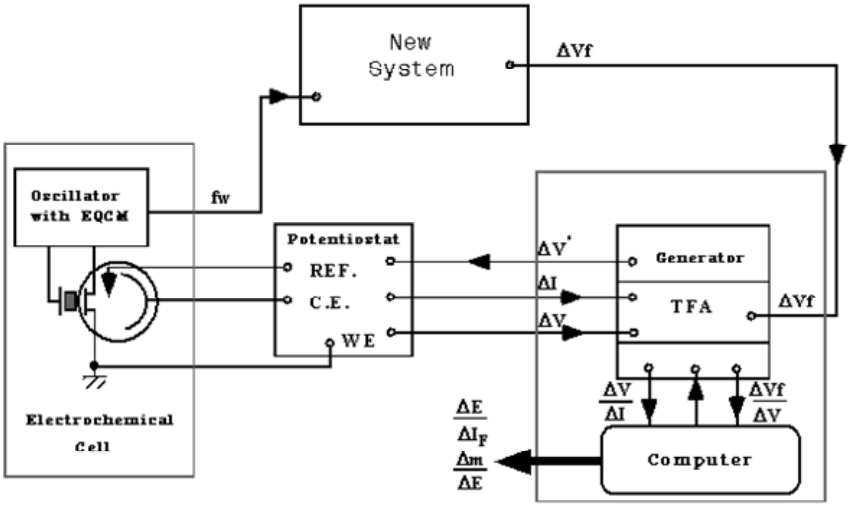

Fig. 4.25. Polymer characterisation setup for the new system.

- Polymer used: Prussian Blue, Polypirrole and Polyaniline deposited.

- Electrolytes used: KCl 0.1M, KCl 1M, $HClO_4$ 1 M and HNO_3 1 M.
- Potentiostat polarisation voltages: 0.000 V, +0.100 V, +0.200 V and +0.300 V depending of the experiment conducted.

It can be noticed in these two previous figures that the TFA receives information from the computer which consists in a *configuration file* containing the experimental parameters, i.e., the *frequency sweep* of the signal generator, the number of points by decade to be calculated, the amplitude of the modulating signal and the electrochemical impedance, among others.

It can also be seen that the TFA send the output signal generator to the potentiostat and receive from it the information about the current, ΔI, and voltage, ΔV, variations required to process the transfer functions.

The last input of the TFA is reserved to the voltage variation related to the frequency shift, ΔV_f, and then with the mass variation.

The TFA takes all the inputs: current and frequency variation, and calculates two *partial transfer functions* sending the data to the computer in order to calculate the *electrochemical impedance*, $(\Delta E/\Delta I)(\omega)$ and the *Electrogravimetry Transfer Function*, EGTF, $(\Delta m/\Delta E)(\omega)$[1] . These transfer functions are important in the AC Electrogravimetry technique as it was stated in section 1.4.

On the other hand the *potentiostat* establishes a continuous control of the voltage difference applied between the reference and working electrodes and measures the current that flows between the working and *counterelectrode*.

The reference signal provided by the EQCM controlled oscillator is carried on to the unit under test, UUT, to translate the frequency shifts into adequate voltage shifts to be processed by the TFA.

A comparison is established between the results obtained for the current and the new systems, under special conditions explained next:

- For Polypirrole, PPy, only one electrode was tested at different times in order to test the repeatability of the current and the new systems.
- For Prussian Blue, PB, three different electrodes where test at different polarisation voltages: +0.000 V, +0.200 V and +0.300 V. The electrolyte employed was KCl 1 M, the amplitude of the modulating signal at the TFA configuration file

[1] ΔE is related to ΔV whose value was measured before.

was 50 mV, and the impedance of the potentiostat was set in 100Ω. The purpose of this experiment was to see the influence of the polarisation voltage in the responses obtained both for the current and the new systems.

- For Polyaniline, PANI, the same electrode was tested for three different media, KCl 1M, $HClO_4$ 1 M and HNO_3 1 M in order to see the influence of the electrolyte in the responses obtained for both the current and the new systems.

All the results obtained for all the experiments introduced in this chapter will be presented and discussed in the following chapter.

5 Results and Discussion

Once the general structure of the system proposed in this project and the experimental methodologies have been introduced the next step is to show and discuss the results obtained with the system developed.

This chapter deals with the *experimental results* during the design, the characterisation and during the experimental stages. The results of the first stage presented correspond to the output of several *simulations* conducted during the system design. For the *characterisation stage* the results presented are those obtained during the static and dynamic characterisation and finally, for the *experimental section* the results obtained correspond to the different polymer experiments explained in the previous chapter.

In addition to the presentation of the data obtained, some explanations and *discussion* about them are conducted.

5.1 System Simulation Results

Regarding the simulation of the system, the results obtained correspond to the two simulations proposed in section 4.1, i.e., the results found for the *script simulation* presented in the Fig. 4.1 and the results for the *circuit simulation* in Fig. 4.2.

5.1.1 Results of the A-D PLL simulation script

The simulation of the system performed by the script presented in the Fig. 4.1 is conducted varying one parameter each time for evaluating the dependence of this parameter in the total system's response. The outputs of the system considered in the simulation are: the damping factor, ξ, the natural frequency of the PLL, ω_n or f_n and the total system' sensitivity $K_{sens}=1/(K_v*K_a)$ in Hz/mV. Moreover, some graphical responses are given by the script simulation.

Table 5.1 shows the responses obtained when the main mixer constant, K_m, is varied and the other parameters remain constant ($R1$=680 Ω, $R1$=12000 Ω and C=10 nf).

Table 5.1. Simulation script's output varying the multiplier constant.

K_m	K_a	K_v(Hz/mV)	ω_n(Krad/s)	f_n(KHz)	ξ	K_{sens}(mV/Hz)
0.1	1	0.819	8.7	1.38	0.5220	1.2
0.2	1	0.819	12.3	1.96	0.7382	1.2
0.5	1	0.819	19.45	3.09	1.1673	1.2
1	1	0.819	27.5	4.38	1.6508	1.2
1.5	1	0.819	33.7	5.36	2.02	1.2

As it can be noted the system's constant sensitivity does not change when the multiplier's constant is changed, the only parameters affected are the natural frequency and the damping factor, i.e., the locking characteristics of the PLL.

When the value of K_m is increased the system becomes overdamped which constitutes a problem for the A-D PLL concerning the Electrogravimetry transfer function, because the time that the system takes to be stable (the lock-up time) is increased [Arnau00-3, Best05, Philips88] and the system could not response in time to any fast change in the reference signal, in addition, the high frequency noise becomes considerably higher.

On the other hand, when the multiplier's constant in decreased the system becomes underdamped and the bandwidth of the PLL is diminished. This could be a problem because an excessive decrease in the bandwidth would make the tracking of "high" frequency (until 1 KHz) modulating signals difficult; i.e., the system would present the same drawbacks as the current electronics systems described in the section 1.6.2.

According to the data in the Table 5.1 the ideal value for K_m could be 0.2, because the system becomes almost critically damped and the bandwidth is enough for the modulating signal characteristics, but because of the mulplier's constant is directly related to the mixer output, this small value produces a signal at the main mixer output with a small amplitude which is difficult to process in the subsequent systems stages. One solution could be to put an amplifier subsystem at the main mixer output, but this

would complicate the design and would introduce an additional phase to the loop that needs to be considered. A better choice is to modify the parameter of the voltage divider, K_a to achieve a good trade-off between all the output parameters considered in the design.

Table 5.2 shows the script simulation results when the parameter K_a is changed. The rest of the parameters are kept constant.

Table 5.2. Simulation script's output varying the constant K_a.

K_m	K_a	K_v(Hz/mV)	ω_n(Krad/s)	f_n(KHz)	ξ	K_{sens}(mV/Hz)
0.5	1	0.819	19.45	3.09	1.1673	1.2
0.5	0.8	0.819	17.4	2.77	1.0440	1.5
0.5	0.6	0.819	15.1	2.4	0.9042	2.0
0.5	0.5	0.819	13.76	2.19	0.8254	2.4
0.5	1/3	0.819	11.2	1.79	0.6739	3.7
0.5	0.2	0.819	8.7	1.38	0.5220	6.1
0.5	0.1	0.819	6.5	0.98	0.3691	12.2

It is clear that the parameter K_a is the key element to control de system's sensitivity, but it is necessary to calibrate this value because it affects both the natural frequency and the damping factor.

When K_a has its maximum value the system is overdamped and the lock-up time is increased as it happens when the multiplier`s constant is increased with the inherent delay implied. This state is equivalent to put the total system without the voltage divider circuit.

As the K_a value is decreased the system's sensitivity is increased, but both the bandwidth and the damping factor are diminished and so the values for these parameters must be carefully chosen.

A good value that allows a good trade-off could be K_a=1/3 since the system is almost critically damped, the bandwidth is appropriated for

processing the reference signal in the AC Electrogravimetry technique and the achieved sensitivity is relatively high enough for post processing.

In Fig. 5.1 appears graphical responses obtained with the script simulation for K_a=1/3 and K_m=0.5.

As it can be noticed in Fig. 5.1 the system behaviour is like a critically damped second order system. The response in Fig. 5.1a. corresponds to the *Bode plot* of the system's frequency response; according to this the system has a flat response both in magnitude and phase until around 10 Krad/s as it was indicated in Table 5.2. This is an ideal condition for the AC Electrogravimetry experiments. Fig. 5.1b and c. show the *step response* on the system in which it can be noticed that the system takes almost $4x10^{-4}$s to have a stable output signal. Fig. 5.1d. shows the response for a *periodic pulse signal*; this response predicts a good behaviour of the system when some abrupt input reference signal is connected, indeed this kind of signal will not be present during the real experimentation, but this simulation is useful to see the good system's performance. Finally Fig. **5.1**e. shows the *steady state response* in which a good tracking is achieved when the modulating signal is a sine wave.

5.1.2 Results of the A-D PLL circuit simulation

The results obtained by the *circuit simulation* serve to corroborate the expected behaviour of the system under certain similar conditions to the real experimentation. As it was said in the previous chapter this simulation was conducted using some built-in ORCAD® models that are similar to the electronic components used in the design, but that are not exactly the same. Under these circumstances the results of the circuit simulations only acts as merely indicators of the general correspondence between the expected behaviour of the system and the real one.

As the input, i.e., the reference signal, a frequency modulated, FM, signal with 10 MHz as a carrier, a sine wave of 1 KHz and 50 mV of amplitude as a modulating signal and 1V of amplitude was used.

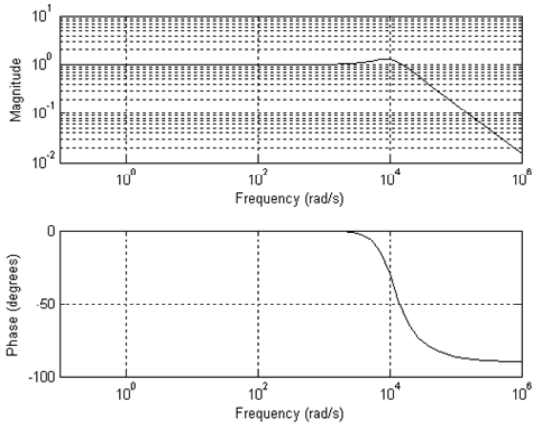

a

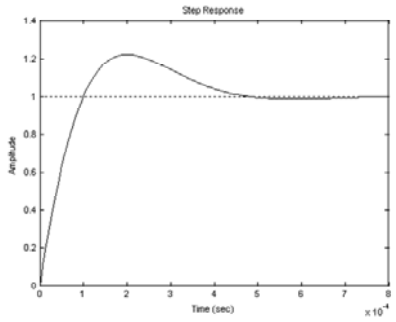

b

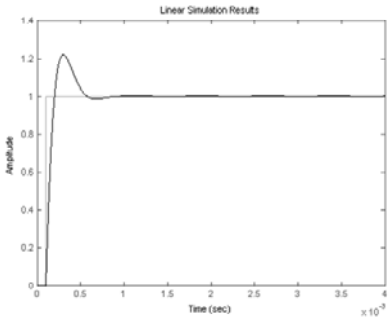

c

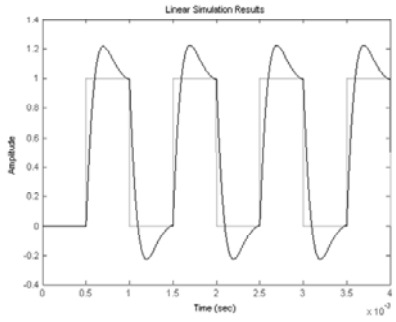

d

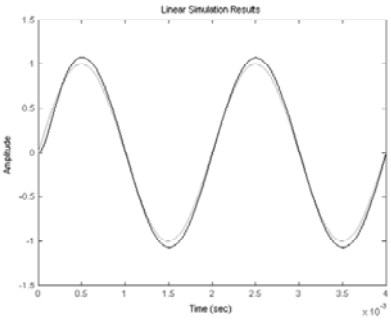

e

Fig. 5.1. Output responses of the script simulation for K_m=0.5 and K_a=1/3. **a.** Bode plots, **b.** Step response, **c.** Long-time step response, **d.** Pulse response and **e.** steady step response.

Fig. 5.2 shows the time response of the system when the FM is applied. Fig. 5.2a shows a complete response of the system until 12 ms, i.e., the response of the simulation for 12 cycles of the input modulating signal. Fig. 5.2b is the detailed response when reaching the stability. In the figure the light trace corresponds to the modulating input signal whereas the dark one corresponds to the system's output.

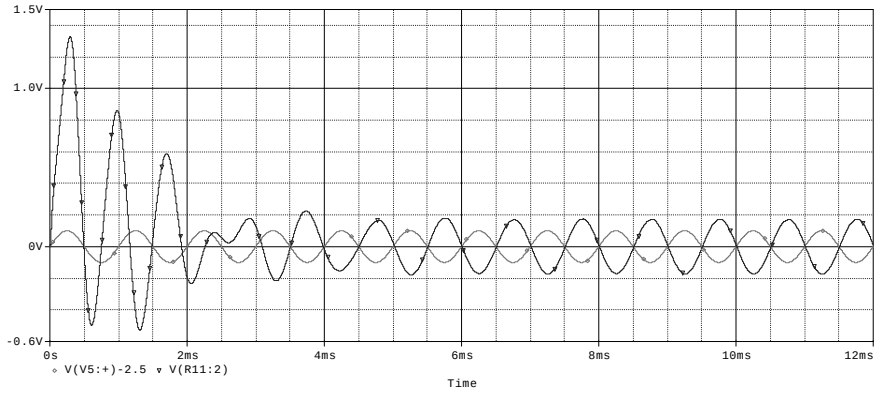

a

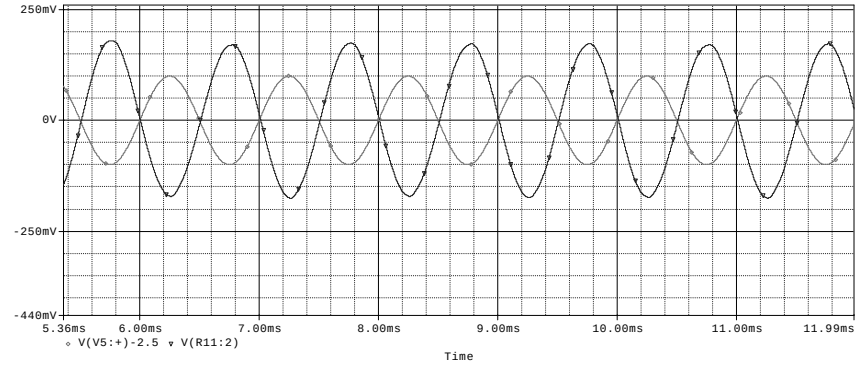

b

Fig. 5.2. Temporal response of the A-D PLL circuit simulation. **a.** Completed response. **b.** Detailed response.

As it can be noticed in the figure the system behaviour is appropriated and according to it was expected during the design stage. The system's output follows the variations imposed by the modulating input signal. Moreover, the amplification characteristic, due to the amplitude of the

output signal is higher than the input one. This allows seeing in advance the increase in the sensitivity of the measurement.

Another response obtained from the circuit simulation is the *Fourier component analysis* of the system under the simulation conditions stated above. Fig. 5.3 shows the magnitude response for both the input and the output signals. Again the light trace corresponds to the input signal and the dark one to the system's output.

It can be noticed that the input signal has only one frequency component at 1 KHz, whereas the output presents the same components plus some additional frequency components which could announce the necessity of good filtering for the system's output signal, but this is not completely accurate because these additional components can be due to the transient behaviour of the system and as the time elapses they can be vanished. A time-frequency joint analysis could be ideal to see if the previous statement is true, but it is not rigorous to conduct such analysis because the circuit simulation is only performed to have an idea of the general design performance.

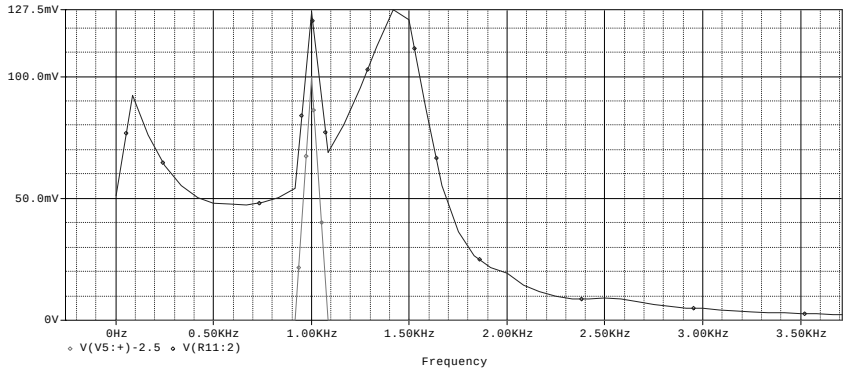

Fig. 5.3. Frequency response of the A-D PLL circuit simulation.

5.2 Characterisation Results

Once the A-D PLL was designed and implemented the next step was to perform a circuit characterisation by simulating the conditions under the real experimentation conditions. These results correspond to the two first experimentation processes explained in the section 4.4.

Previous to the static and dynamic characterisation responses a preliminary characterisation was conducted. The results obtained in the characterisation will be presented next.

5.2.1 Preliminary Characterisation

For the *preliminary characterisation* a frequency modulated signal was recreated using a sine wave generator (Agilent 33120A). The modulating frequency was changed in the range from 1 mHz to 1 KHz. The peak of the frequency shift $\left|\Delta F_W\right|$ in Eq. 3.1 was established in 50 Hz.

In a preliminary stage the system was designed with ω_n= 11.2Krad/s and ξ=0.6739 according to the data obtained in the Table 5.2. for K_a=1/3. These values provide the following time constants in Eq. (3.7): τ_1=6.8x10^{-6} s and τ_2=12x10^{-5} s.

Some preliminary results related to the proposed system were introduced elsewhere [Torres06-2] and are reproduced in Fig. 5.4 and the Fig. 5.5.

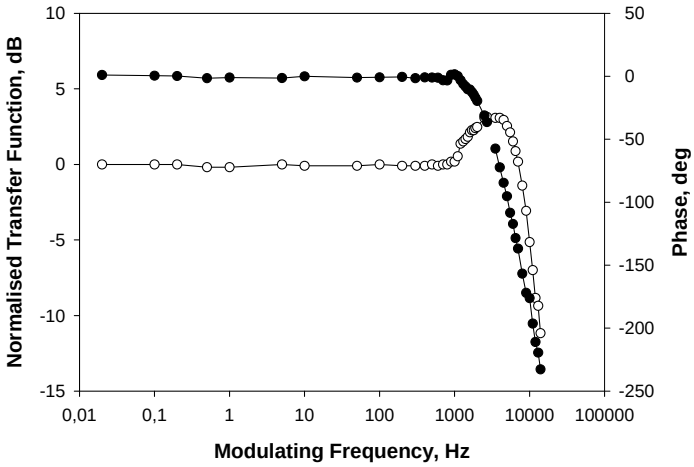

Fig. 5.4. System Frequency Response, ○— Normalised Transfer Function, ●— Phase Response. Adapted from [Torres06-2].

Fig. 5.4 shows the *normalised transfer function*, NTF (f_m), and the *phase response* of the PLL designed. The normalised transfer function is obtained as the ratio between the peak amplitude of the demodulated signal (ΔV_o) and the peak amplitude of the modulating signal (ΔV_i) normalised to the value of this quotient for the lowest frequency modulating signal (f_{mo}):

$$NTF(f_m) = \frac{\left[(\Delta V_o / \Delta V_i) \mid f_m\right]}{\left[(\Delta V_o / \Delta V_i) \mid f_{mo}\right]} \tag{5.1}$$

As it can be observed the transfer function and the phase response of the PLL are flat in the desired frequency range, until modulating frequencies as high as 1 KHz as it was predicted by the script simulation.

Fig. 5.5. Preliminary step response of the system,—Modulating Signal, ▬ Step Response. Adapted from [Torres06-2].

Fig. 5.5 shows the experimental response of the system to a *frequency step* in the EQCM output signal. This response was obtained using a 500 Hz square wave modulating signal, similar to the signal introduced in Fig. 5.1d. In general, this sharp frequency step does not occur in AC Electrogravimetry real experiments and this result is included to describe the dynamic behaviour of the system designed against very sharp frequency changes. The system has been designed almost critically dumped as it was shown before to have the best trade-off between a quick response and a short settling time. As it can be observed the rise time is less than 200 µs and the settling time is around 400 µs, again, as it was predicted by the script simulation. Thus, the system provides a reliable F-V conversion for frequency shifts which occur up to rates as high as 1000 times per second.

In order to obtain a complete static and dynamic characterization several experiments were conducted after the preliminary characterization. The results achieved are shown next.

5.2.2 Static Characterisation

According to the measurement method stated in section 4.4.1 the aim of the *static characterisation* is to obtain the *sensitivity* of the system designed and the *dynamic range* in which the system's behaviour is linear.

Fig. 5.6 shows the *static characterisation response* with the data obtained as it was stated above.

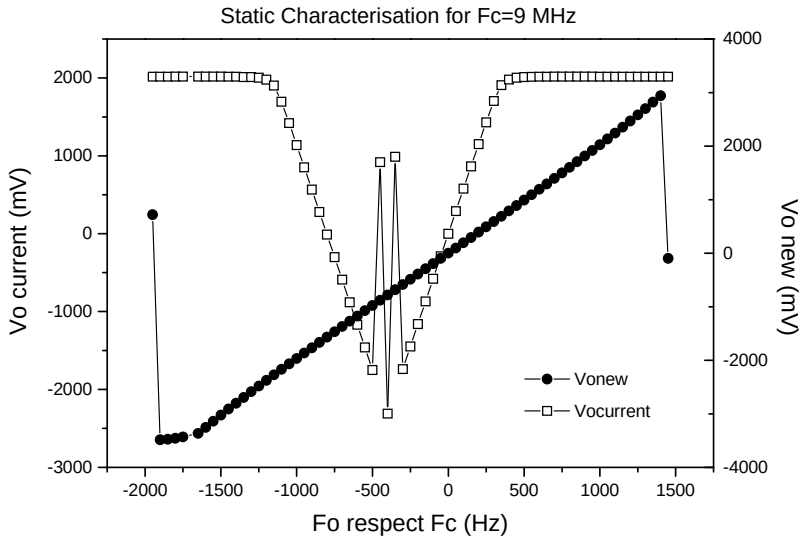

Fig. 5.6. Static characterisation responses for: ●— New system, □— Current system.

In the previous figure the responses of both current and new systems under the static characterisation are displayed. F_o represents the manual frequency shifts (with regard to the central frequency of the oscillator, F_c) introduced in the reference signal and V_o for each plot is the output system response.

The first interesting result observed in Fig. 5.6 is the *linear shape* of both responses in the range of frequencies analysed, but taking into account that the *linear range* covered by the new system is broader than the current's one. It can be noticed that for the current system the linear range goes from $F_o \approx$ -1000 Hz until $F_o \approx$ +500 Hz with its central point around -400 Hz whose value coincides with the difference frequency introduced by the auxiliary synthesiser in Fig. 4.21. The linear range of the current system for positive values of F_o (Adding the 400 Hz difference introduced by the auxiliary synthesiser) is around 750 Hz. Equally, for the negative values of F_o this range is around 750 Hz.

Both for positive and negative values of F_o once the current's system response reach the 750 Hz frequency limit the output system's response becomes saturated and the linear response is no longer present. Another important aspect of the current system's response is the instability noted around -400 Hz which is due to the *auxiliary synthesiser*, i.e., the current system needs a permanent 400 Hz frequency difference for a good operation. This limitation introduces the necessity of the additional synthesiser which constitutes the first drawback of the current system regarding the new one.

On the other hand the response obtained for the new systems exhibits a complete linear response from $F_o \approx$ -1500 Hz until $F_o \approx$ +1500 Hz for a total covered frequency range of 3000 Hz. After this point instead of having saturation the system reveals an abrupt change in its response, but this is due to the *feedforward* correction introduced by the secondary loop as it was planned in the design stage (see section 3.2.2.2).

Another interesting point of the new system's response is its symmetrical plot around $F_o = 0$ Hz; this is because the new system does not need to maintain a permanent minimum frequency difference; finally after the ±1500 frequency limit the system's output response starts again a linear shape.

After the linear dynamic frequency range investigation the next step is to conduct an analysis about the *sensitivity* of both systems.

A *fitting procedure* with *linear regression* was performed in order to obtain the sensitivity of the system which is directly obtained from the *slope* of each curve using the data of Fig. 5.6.

For the current system the linear regression was performed in each sub region of the plot in which the shape is linear. The equation obtained for this system leads to:

$$V_o = 5.76 \cdot F_o - 5.15 \tag{5.2}$$

where V_o is given in mV and F_o is given in Hz.

And for the new system the regression was performed in the whole frequency range and the fitting procedure leads to:

$$V_o = 1.99 \cdot F_o - 25.93 \tag{5.3}$$

Equations (5.2) and (5.3) indicate that under certain special configuration parameters like amplifier gain, K_a, low pass filters, etc., the sensitivity of the system is 5.55 mV/Hz and 1.99 mV/Hz for the current and new system respectively.

It is important to notice that this characterisation was performed putting the mentioned parameters at their lowest possible limits, i.e., the output

signal of each system can be amplified to obtain a better sensitivity according to the necessity of any particular AC Electrogravimetry experiment. These low level restrictions where needed due to the huge frequency shifts (until ±1000 Hz) introduced in the oscillator carrier frequency to investigate the dynamic range, otherwise with these huge values the system's outputs become saturated; under normal circumstances these high frequency shifts are not present in the AC Electrogravimetry technique (see 1.4.3.1).

Finally the sensitivity obtained for both the current and for the new system can be increased even more by applying an amplifier or any conditioning system similar to the DC level canceller implemented for the new system and shown in Fig. 3.10 whose output sensitivity level can be configured with the gain potentiometer (*R38* in the figure).

In the next section a first dynamic characterisation was performed at these low level restrictions to test the correspondence with the static characterisation, and then the parameters were modified to conduct the experimental section exposed in the subsequent section.

5.2.3 Dynamic Characterisation

The first step in the *dynamic characterisation* is to find the *frequency response* for both systems under the minimum gain conditions as it was conducted in the previous static characterisation achieved.

The results obtained for the current system using the system configuration shown in Fig. 4.22 are shown in Fig. 5.7.

Fig. 5.7 shows the frequency response of the current system under the conditions established for the characterisation setup in Fig. 4.22. The frequency of the carrier signal was programmed to be 9 MHz and its *frequency deviation*, introduced by the modulating low voltage (100 mV) sine wave signal, was 10 Hz. It was performed a *frequency sweep* on the modulating signal from 1 mHz until 10 KHz approximately. In Fig. 5.7 both the *magnitude and the phase response* are shown.

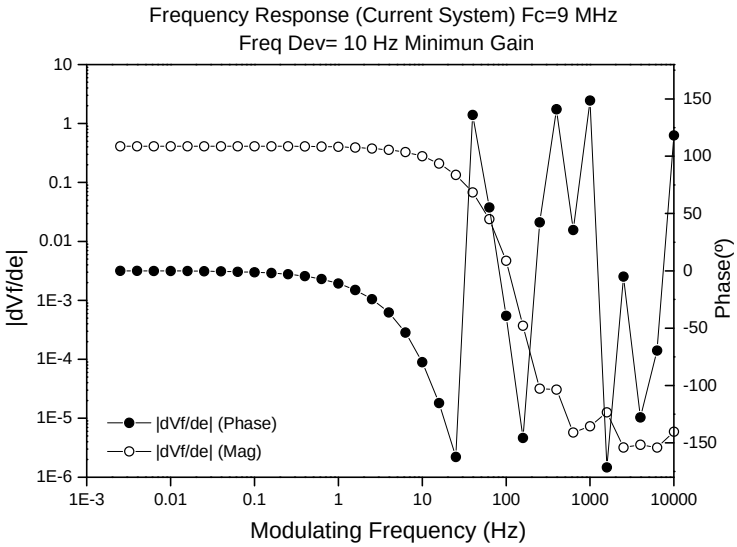

Fig. 5.7. Frequency response of the current system in the dynamic characterization. —●— Phase response. —○— Magnitude response.

The results obtained for the new system using the system configuration shown in Fig. 4.23 are shown in the next figure.

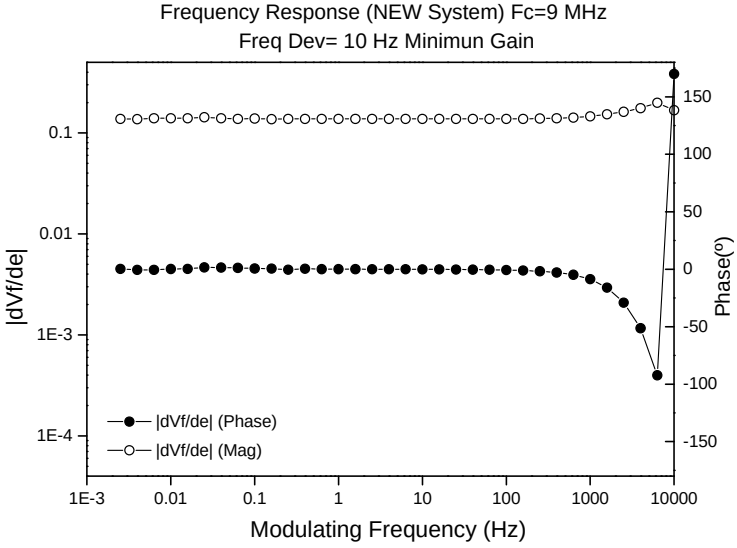

Fig. 5.8. Frequency response of the new system in the dynamic characterization. —●— Phase response. —○— Magnitude response.

In order to establish a comparison between the responses of the two systems the magnitude response on each figure were taken into a single plot and the same for the phase responses. The plots for comparing the systems are shown in the Fig. 5.9a for the magnitude and Fig. 5.9b for the phase.

As it can be noticed in the Fig. 5.9 the new system enhances the frequency response for the AC Electrogravimetry system regarding the current one; in the *magnitude response* of the current system the response does not go beyond 10 Hz without distortion whereas the new systems goes until 1 KHz approximately as it was anticipated by the preliminary characterisation (see Fig. 5.4). In addition, the *phase response* of the current system presents an oscillation beyond 10 Hz; so that when a polymer with a "fast" response is analysed, as it will be shown later on, the old system will distort the polymer response. For the new system the phase response is approximately constant and small until 1 KHz.

Regarding the *Nyquist response*, as it was introduced in section 1.4.3.3 and elsewhere [Torres06-1], the dynamic characterisation for both the old and new systems give the responses shown in the Fig. 5.10. The open circles represent the *complex response* (magnitude and phase shift of the demodulated signal) at different modulating frequencies. Each open circle corresponds to a specific modulating frequency. The response of an ideal system would maintain a constant amplitude and null phase shift and then the plot would be reduced to a dot on the real axis for all the modulating frequencies. Some *modulating frequencies* have been represented with solid circles in the figures.

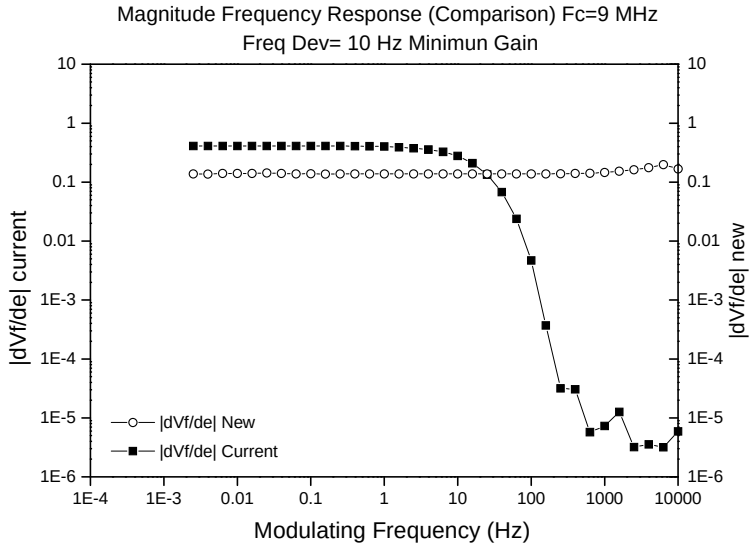

a.

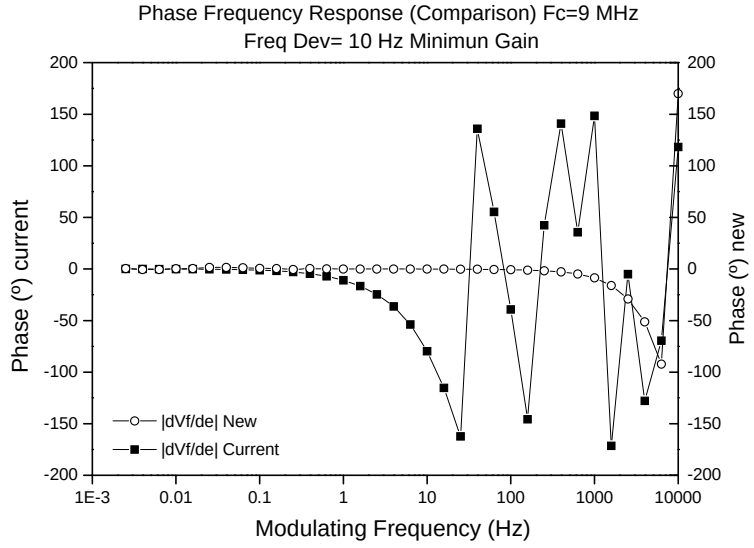

b.

Fig. 5.9. Frequency response comparison between the current and new systems. a) Magnitude response, b) Phase response.─○─ New system response ─■─ Current system response.

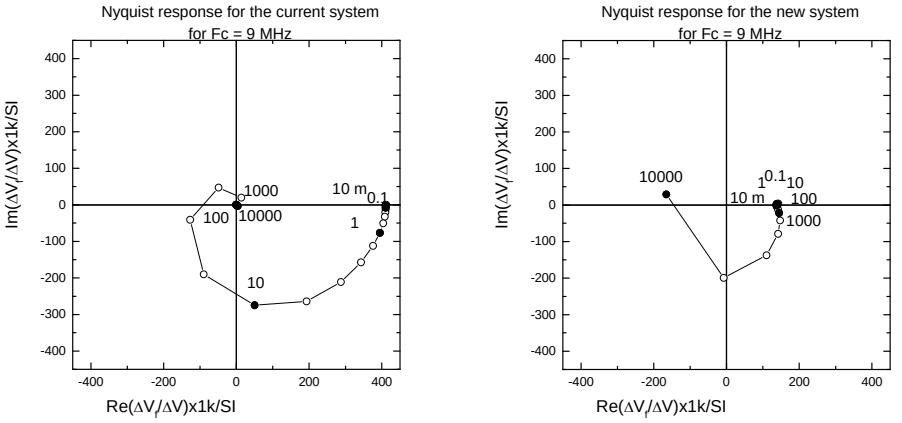

a. b.

Fig. 5.10. Nyquist Response for the systems compared, a. Old system response and b. New system response. ─○─Nyquist response, ● Some modulating frequencies.

As it can be noticed in the figure when the *modulating frequency* increases, the distortion can be appreciated in the *Nyquist diagram* as a separation from the real axis and a decrease of the amplitude in the response. For the current system it can be observed that a significant distortion can be found for 1 Hz modulating signal while it is necessary to increase the frequency of the modulating signal until 1 KHz for obtaining the same distortion with the new system.

The second purpose of the dynamic characterisation is to perform a verification of the *sensitivity* obtained in the static characterisation.

For each one of the frequency response figures shown above the sensitivity is given by:

$$\frac{\Delta V_o}{\Delta f_m} = \frac{\Delta V_o}{\Delta e} \times \frac{\Delta e}{\Delta f_m} \tag{5.4}$$

where $\Delta V_o / \Delta f_m$ is the sensitivity of the system given in mV/Hz. $\Delta e / \Delta f_m$ is a variable related to the variation in the voltage provided by the potentiostat to the cell according to the *modulation depth* given by the modulating signal in mV/Hz, this variable is calculated by the following expression:

$$\frac{\Delta e}{\Delta f_m} = \frac{V_{eff}(1254) \times \sqrt{2}}{\max imum \ \mathrm{mod} ulation \ depth} = \frac{Vpeak(1254)}{\max imum \ \mathrm{mod} ulation \ depth} \tag{5.5}$$

and $\Delta V_o / \Delta e$ is a dimensionless quantity obtained from the value of the magnitude response in the flat zone.

According to this the sensitivity of the current system can be calculated as follows:

From Eq. (5.5):

$$\frac{\Delta e}{\Delta f_m} = \frac{0.1V \times \sqrt{2}}{10Hz} = \frac{0.14142V}{10Hz} = 14.142\frac{mV}{Hz} \tag{5.6}$$

where V_{eff} =0.1V is the amplitude of the sine wave signal configured according to the characterisation setup introduced in Fig. 4.22, and 10 Hz of the modulation depth is the maximum frequency deviation the carrier signal.

From the data obtained to plot the magnitude response in Fig. 5.7 the dimensionless quantity is given:

$$\frac{\Delta V_o}{\Delta e} = 0.411 \tag{5.7}$$

Replacing Eq. (5.6) and Eq. (5.7) in the Eq. (5.4) leads to:

$$\frac{\Delta V_o}{\Delta f_m} = 0.411 \times 14.142\frac{mV}{Hz} = 5.81\frac{mV}{Hz} \tag{5.8}$$

Similarly for the new system the sensitivity is calculated as follows:

$$\frac{\Delta e}{\Delta f_m} = \frac{0.1V \times \sqrt{2}}{10Hz} = \frac{0.14142V}{10Hz} = 14.142\frac{mV}{Hz} \tag{5.9}$$

From the magnitude response of the Fig. 5.8:

$$\frac{\Delta V_o}{\Delta e} = 0.139 \tag{5.10}$$

And the sensitivity is:

$$\frac{\Delta V_o}{\Delta f_m} = 0.139 \times 14.142\frac{mV}{Hz} = 1.97\frac{mV}{Hz} \tag{5.11}$$

As it can be noticed the sensitivity values calculated by the dynamic characterisation correspond in a very approximately way with those calculated by the static characterisation. The result of the validation regards the sensitivity of each system is summarised in the next table.

Table 5.3. Results of the validation of the static and dynamic characterization for the sensitivity values.

Characterisation	**Current system sensitivity (mV/Hz)**	**New system sensitivity (mV/Hz)**
Static	5.76	1.99
Dynamic	5.81	1.97

Once this dynamic characterisation was achieved the general gain of both systems was calibrated to obtain a better working conditions for the AC Electrogravimetry experimentation in which three different polymers were studied.

The graphic result of the dynamic characterisation for the new system recalibrated is shown in Fig. 5.11.

Using Eq. (5.4), Eq. (5.5) and the value in the flat zone of the magnitude response the new sensitivity is given by:

$$\frac{\Delta V_o}{\Delta f_m} = 1.06 \times 14.142 \frac{mV}{Hz} = 14.99 \frac{mV}{Hz} \tag{5.12}$$

With this calibration conditions it was performed the experimental section.

Next section describes the experimentation process conducted to each polymer and the different comparisons established between the current and the new systems.

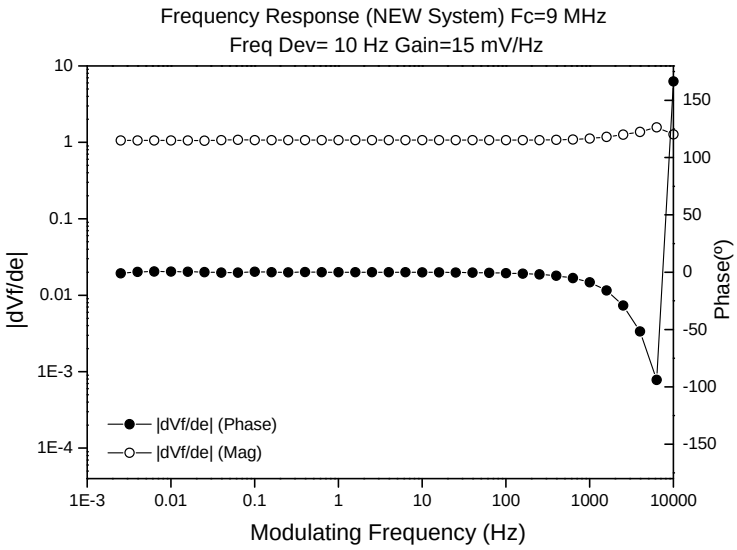

Fig. 5.11. Frequency response of the new system recalibrated in the dynamic characterization. —●— Phase response. —○— Magnitude response.

5.3 Experimentation Results

The results for the three *polymer experimentation process* in the arrangements shown in Fig. 4.24 and Fig. 4.25 which corresponds to the current and the new system, respectively, are introduced in this section. In order to discriminate the process followed for each polymer the results will be introduced in different and subsequent subsections. For each polymer both the results in frequency response and the result in the Nyquist plot will be introduced separately.

5.3.1 Experimentation with Polypirrole

For testing the systems with *Polypirrole*, PPy, polymer, experiments with the current system and the new system were conducted, and then two more experiments with the new system were developed in different time in order to check its repeatability.
The parameters introduced into the experimental setups for PPy [Gabrielli01, Gabrielli02-2], shown in Fig. 4.24 for the current system and in Fig. 4.25 for the new system, are summarised next:

- Carrier Frequency: 9 MHz.
- Auxiliary synthesiser frequency (only for the current system): 8.999600 MHz
- Deviation voltage (at TFA file setup): 80 mV rms.
- Carrier voltage (from the home made oscillator at LISE):1V
- Modulator frequency sweep: (1 mHz- 63 KHz).
- Polymer used: Polypirrole deposited with 2 mA during 2 s.
- Electrolyte used: KCl 0.1 M.
- Potentiostat voltage reference: +0.100 V.

5.3.1.1 Frequency response results

The frequency response results obtained for the current system under the experimental arrangement shown in Fig. 4.24 is shown in Fig. 5.12 and for the new system with the experimental arrangement shown in Fig. 4.25 is shown in Fig. 5.13.

Similarly to the procedure followed for the dynamic characterisation, in order to establish a comparison between the responses of the two systems the magnitude response on each figure were taken into a single plot and the same for the phase responses. The plots for comparing the systems are shown in Fig. 5.14a for the magnitude and in Fig. 5.14b for the phase.

As it can be noticed practically until a little bit more than 1 Hz the results for both systems are the same both in magnitude and in phase, but when the *modulating frequency* goes beyond this limit the current system introduce a distortion in the signal which is more evident in the phase response where some extra oscillations appear in the plot. This behaviour was anticipated by the frequency response in the dynamic characterisation. Because the new system does not introduce any additional loop or distortion in the figures according to Fig. 5.8 and Fig. 5.10 it can be said that the part of the new system's plot that does not appear in the current's one belongs effectively to the *Polypirrole response*.

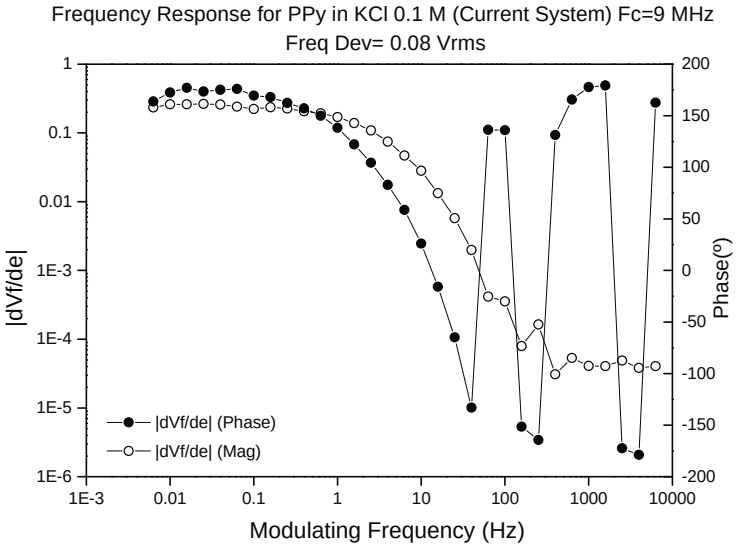

Fig. 5.12. Result of the frequency response of the current system for Polypirrole experimentation. ─○─Magnitude response, ─●─ Phase response.

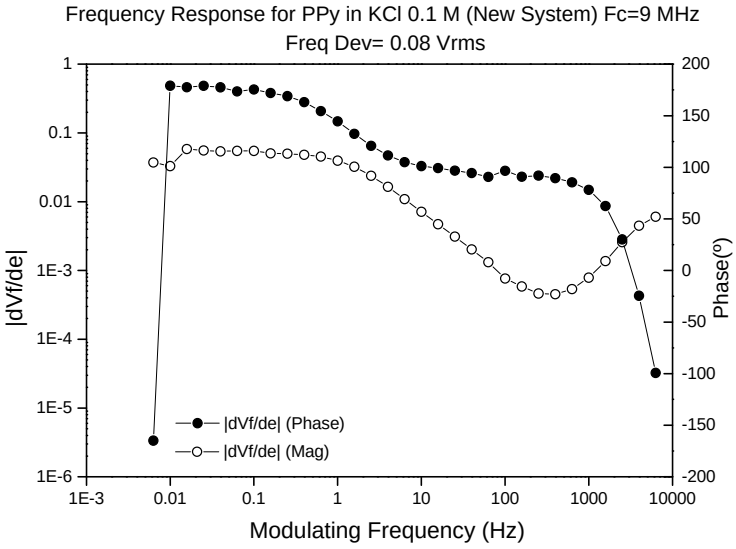

Fig. 5.13. Result of the frequency response of the new system for Polypirrole experimentation. ─○─Magnitude response, ─●─ Phase response.

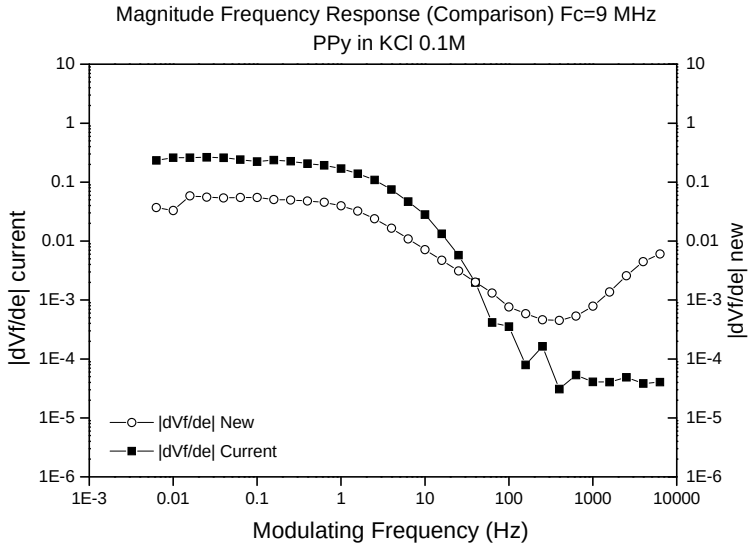

a.

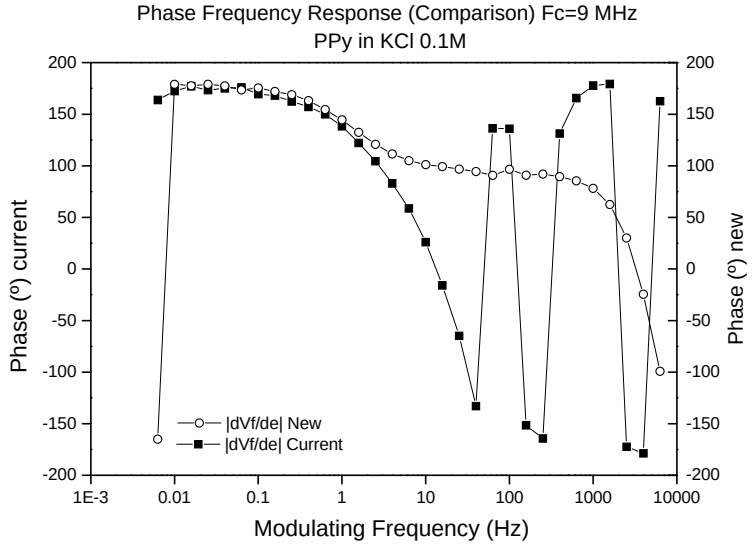

b.

Fig. 5.14. Frequency response comparison between the current and new systems for Polypirrole experimentation. a) Magnitude response, b) Phase response.─○─ New system response ─■─ Current system response.

Regarding the magnitude response in Fig. 5.14a the amplitudes of both signals are not exactly the same, but this not constitutes a disadvantage for the new system because its gain can be modified depending of the requirements of the measurement.

With reference to the phase response in Fig. 5.14b. it could be said that the new system's responses exhibits a low frequency distortion, but this is not real indeed, because this abrupt change in the phase values follows a tendency in the Nyquist response just as it will be shown next.

According to the previous frequency responses it can be inferred the new system extend the possibility of the AC Electrogravimetry technique to characterise the Polypirrole polymer regarding the frequency of the modulating signal applied to the EQCM.

Before showing the Nyquist response results the responses obtained for two more experiments performed with the new system in order to see its *repeatability* are illustrated. The three responses acquired are presented in Fig. 5.15.

In Fig. 5.15a. the *magnitude response* for the three experiments is shown, whereas the *phase response* is shown in Fig. 5.15b.

As it can be noticed in the figure the correspondence achieved between the three experiments conducted is very good and then under certain circumstances the new system has a good behaviour concerning the repeatability.

5.3.1.2 Nyquist response results

Maybe the most interesting response obtained in the experimentation with each polymer is the *Nyquist response* because, as it was explained in the section 1.4.3.3, it mixes the magnitude and phase plots in the frequency response into a single plot. In addition, the Nyquist response is a way broadly accepted to show the transfer functions in the AC Electrogravimetry technique.

The following figure shows the Nyquist responses obtained for the current system and one of the responses quoted above for the new system. It is important to say that these curves have been normalised in order to establish a better comparison between them and correspond to the raw $\Delta V_f / \Delta V(\omega)$ transfer function. in order to find the final EGTF, $\Delta m / \Delta E(\omega)$, a fitting procedure must be followed [Gabrielli07]

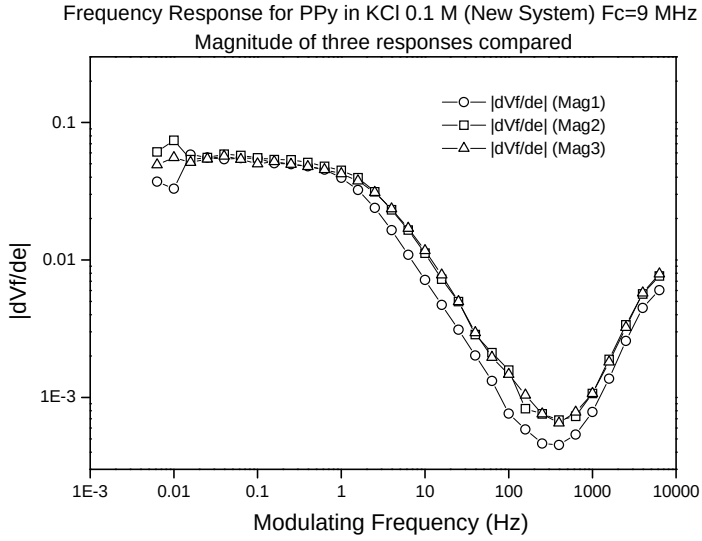

a.

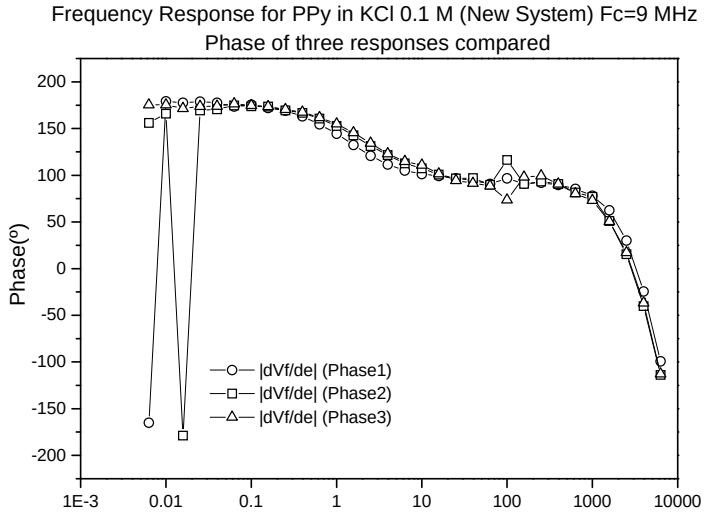

b.

Fig. 5.15. Comparison of the frequency response for the results of three different experiments with the new system. ─○─ Experiment 1, ─□─ Experiment 2 and ─Δ─ Experiment 3.

Fig. 5.16a shows the *normalised Nyquist response* for the current system and Fig. 5.16b for the new system. Again, the open circles represent the *complex response* at different modulating frequencies. Each open circle corresponds to a specific modulating frequency and some *modulating frequencies* have been represented with solid circles in the figures.

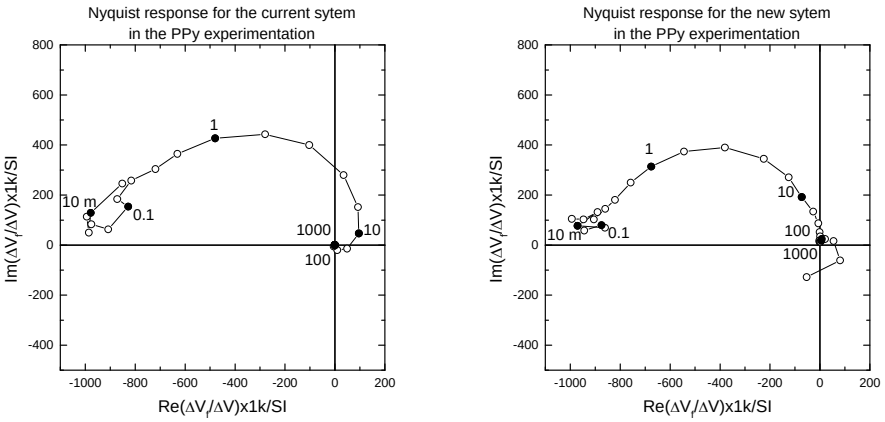

a. b.

Fig. 5.16. Normalised Nyquist Response for the systems compared for PPy experimentation, a. Old system response and b. New system response. ─○─Nyquist response, ● Some modulating frequencies.

According to the Nyquist responses obtained during the dynamic characterisation the current system introduces an *additional loop* to the polymer response which can be noticed in the loop that crosses the imaginary axes in the Fig. 5.16a after 1 Hz frequency; practically until this point both responses are similar, but after 1 Hz the current system crosses the axis whereas the new one has an *asymptotically approaching* to the imaginary axis. This extra loop in the current system must be corrected by an algorithm in order to provide the real polymer response [Gabrielli07]

In the following figure appears a direct contrast of the results obtained from the two systems.

The Fig. 5.17a. shows the complete Nyquist responses of the two systems analysed whereas the Fig. 5.17b shows the details of the high frequency region. It must be remembered that the filled dots represent some frequency points plotted.

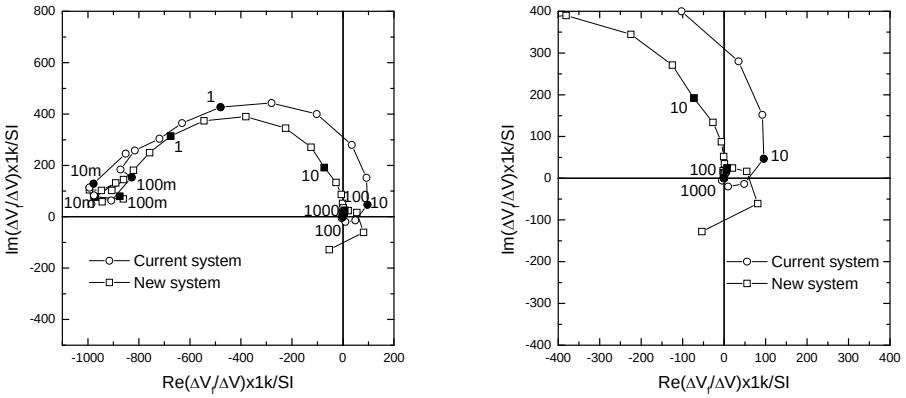

Fig. 5.17. Comparison of the normalised Nyquist responses of ─○─ Current system and ─□─ New system for Polypirrole characterisation; a) complete Nyquist response and b) high frequency detail.

As it can be noticed in the figures the current system introduces an additional loop that cross the imaginary axis for a frequency lower than 10 Hz; this additional loop must be removed from the plot in order to obtain an acceptable response of the current system [Gabrielli07]. On the other hand the response of the new system does not cross the imaginary axis on the contrary in this curve the approaching of the Nyquist response, when the frequency is increased, is asymptotic as it was previously anticipated. The Fig. 5.17b shows clearly the asymptotic approaching of the new system and the distortion introduced by the current one.

The results obtained from this contrast are convincing to validate the improvement introduced by the new system with regards the current one in the acquisition of data for the AC Electrogravimetry setup because they reveal the good performance of the new system in the high frequency zone and the results are conclusive to assure that the response obtained with the new system is only due to the polymer behaviour with minimum intervention of the electronics, contrary to what happens in the current system where some fitting procedures to obtain the real polymer response is required.

5.3.2 Experimentation with Prussian Blue

Similarly as in the PPy experimentation, for testing the systems with the *Prussian Blue*, PB, polymer, experiments with the current system and the new one were conducted, but instead of conducting a repeatability a study to see the *influence of the polarisation voltage* mainly in the Nyquist diagram for both the old system and the new one was performed. Then two more experiments for each system were conducted employing different *polarisation voltage*.

The parameters introduced into the experimental setups for PB [Gabrielli02-1, García-Jareño03], shown in Fig. 4.24 for the current system and in Fig. 4.25 for the new system, are summarised next:

- Carrier frequency: 9 MHz.
- Auxiliary synthesiser frequency (only for the current system): 8.999600 MHz
- Deviation voltage (at TFA file setup): 50 mV rms.
- Carrier voltage (from the home made oscillator at LISE):1V
- Modulator frequency sweep: (1 mHz- 63 KHz).
- Polymer used: Prussian Blue deposited with 2 μA during 150s.
- Electrolyte used: KCl 1 M.
- Potentiostat voltage reference: +0.000 V, +0.200 V and +0.300 V.

5.3.2.1 Frequency response results

Among the different experiments performed for PB, the +0.002 V polarisation voltage to be shown in this *frequency response analysis* was selected.

The frequency response results obtained for the current system are shown in Fig. 5.18 and for the new system in Fig. 5.19.

To establish a comparison between the responses of the two systems the magnitude response on each figure were taken into a single plot and the same for the phase responses. The plots for comparing the systems are shown in the Fig. 5.20a for the magnitude and in Fig. 5.20b for the phase.

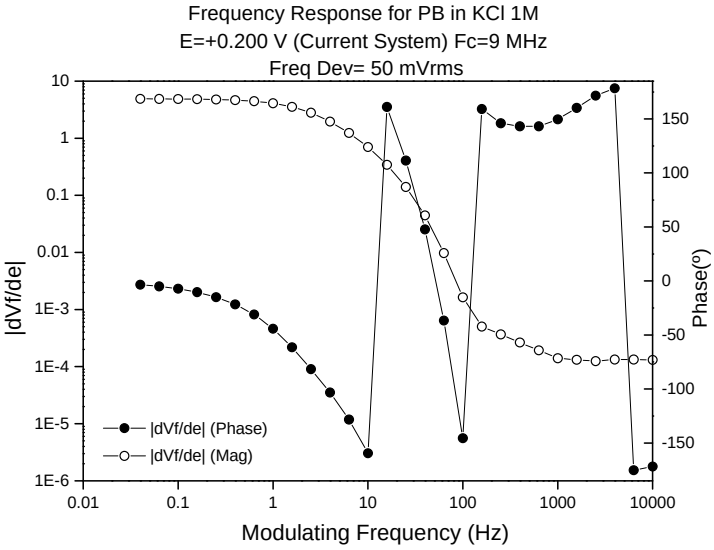

Fig. 5.18. Result of the frequency response of the current system for Prussian Blue experimentation. ─○─Magnitude response, ─●─ Phase response.

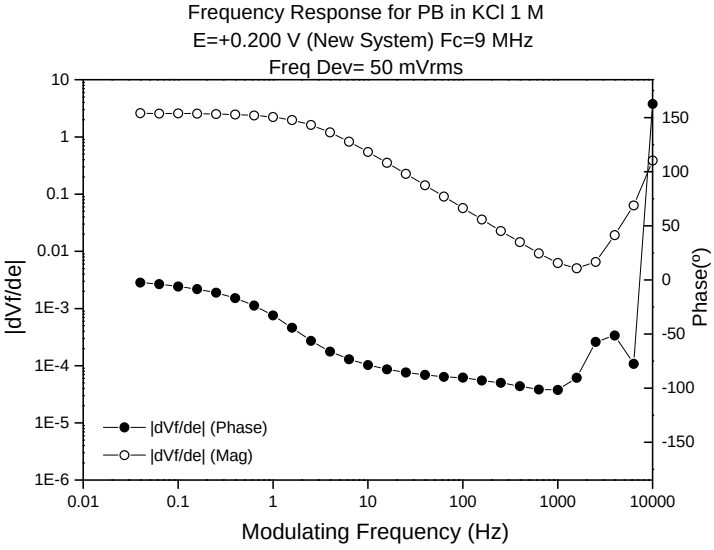

Fig. 5.19. Result of the frequency response of the new system for Prussian Blue experimentation. ─○─Magnitude response, ─●─ Phase response.

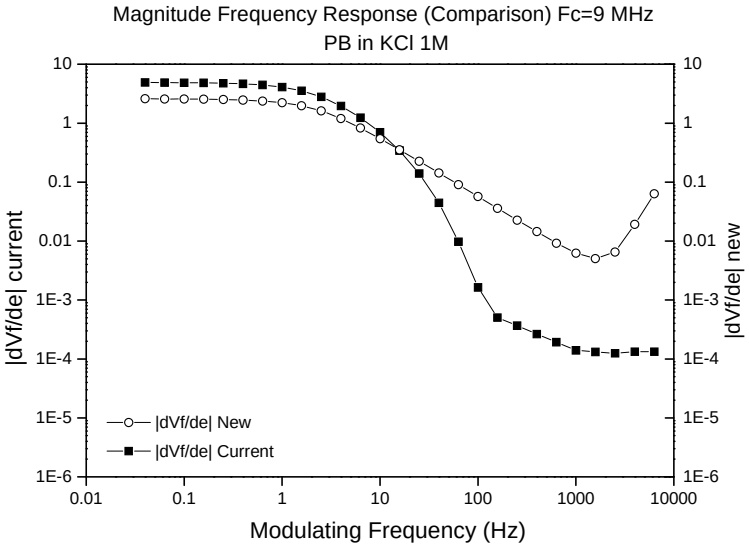

a.

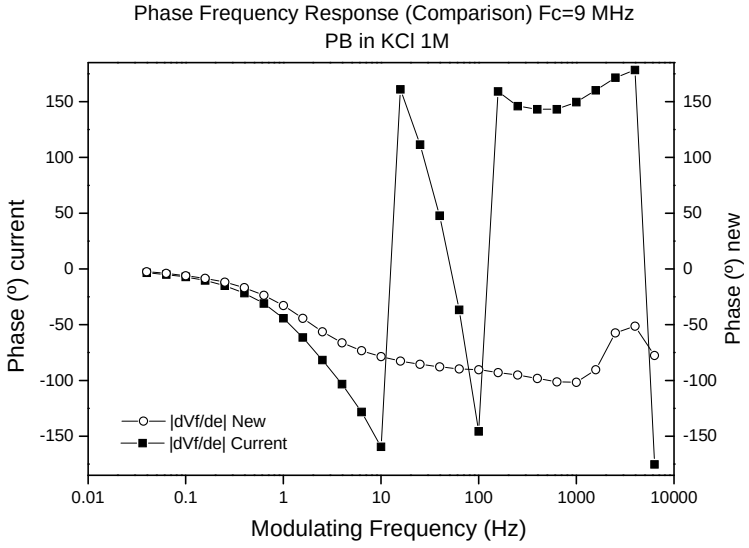

b.

Fig. 5.20. Frequency response comparison between the current and new systems for Polypirrole experimentation. a) Magnitude response, b) Phase response.─○─ New system response ─■─ Current system response.

Similarly to the frequency responses obtained for PPy, the curves shown in Fig. 5.18 and Fig. 5.19 the comparison established in Fig. 5.20 demonstrates the current system distorts the *polymer response* beyond 1 Hz more or less, because until this point the responses are practically the same.

It can be noticed how the shape and the tendency of both system responses are equal until 1 Hz, but after this point the current system exhibits a noticeable and progressive decrease in the magnitude response (Fig. 5.20a) whereas the new system continues with the polymer response until 1 KHz approximately. In the case of the phase after 1 Hz the current system reveals an erratic behaviour that is proved by the abrupt changes in the phase plot.

The *Nyquist analysis* introduced in the next section provides more information about the better behaviour of the new system regarding to the current one to determine the Electrogravimetry transfer function in the PB polymer characterisation.

In addition, the analysis of the influence of the polarisation voltage in the Nyquist diagram will be introduced in this section too.

5.3.2.2 Nyquist response results

Firstly, the *Nyquist response* for the experiment introduced in the previous frequency response analysis, i.e., the experiment with +0.200 V as a polarisation voltage is illustrated here. Afterwards an analysis concerning the influence of that polarisation voltage is conducted for both the current and the new systems.

The following figure shows the Nyquist responses obtained for the current system and the new one. In this case, again the curves have been normalised in order to establish a better comparison between them and correspond to the raw $\Delta V_f / \Delta V(\omega)$ transfer function..

One more time the hypothesis of the improvement achieved by the new system developed is validated by the Nyquist responses in Fig. 5.21 when it can be noticed how the current system introduces an additional loop in the polymer response. The crossing of the imaginary axis is confirmed by the data obtained for a modulating frequency of 10 Hz in Fig. 5.21a. whereas for this frequency the response of the new system is just having an *asymptotically approaching* to this axis.

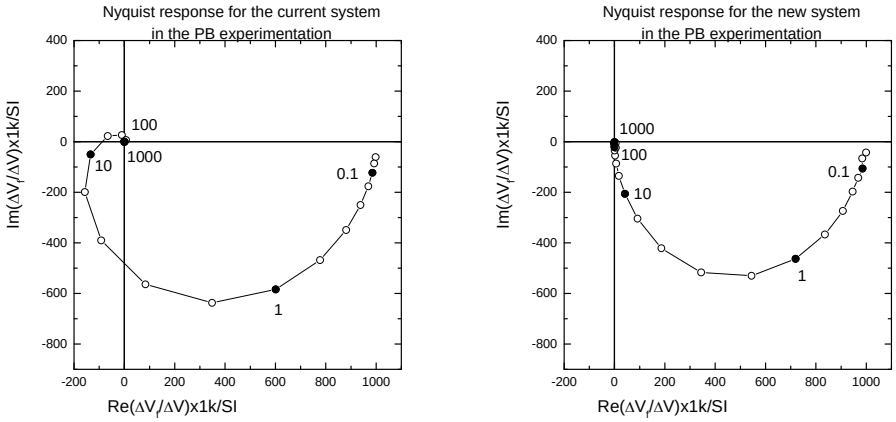

a. b.

Fig. 5.21. Normalised Nyquist Response for the systems compared for PB experimentation, a. Old system response and b. New system response. ─○─Nyquist response, ● Some modulating frequencies.

The response obtained in this simple analysis means that the response for the current system is already distorted for that frequency whereas the new system gives the real response for the PB characterisation.

In order to conduct a better contrast to corroborate the improvement introduced for the new system the following experimental strategy was performed. From the direct results given by the TFA measurements, two methods of correction [Gabrielli07] were used:

a. Basic correction: by considering a linear factor for each system. In this case the sensitivity of each system is considered as constant and the value for the current system and the new one are respectively, 28 mV/Hz and 15 mV/Hz. In other words, the phase shift is neglected for this correction. The responses obtained are presented in Fig. 5.22a.
b. Complete correction: by considering all the calibration procedure followed in [Gabrielli07]. The responses obtained are shown in Fig. 5.22b.

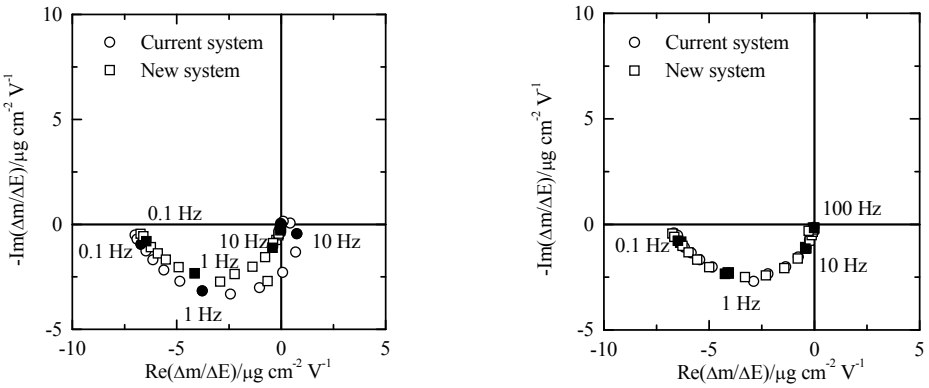

Fig. 5.22. Comparison of the normalised Nyquist responses of the ○ Current system and the □ New system for Prussian Blue characterisation; a) basic correction response and b) complete correction response.

In Fig. 5.22a, the two responses are completely different, in terms of shape and also frequency distribution. With the current system, the electronic contribution is clearly shown at high frequencies which can explain the loops given in the third and fourth quadrants. These loops are related to the electronic part of the experiment and are not related to the electrochemical response. With the new system, only one loop is obtained localised only in the third quadrant. The most important difference is presented in the frequency distribution after 1 Hz. Then, after corrections with the complete procedure, two equivalent responses are obtained as it is presented in the Fig. 5.22b; the diameter of the two loops is equivalent and the frequency distribution is perfectly the same. These results show the improvement achieved with the new system.

Finally, the results of the influence of the *polarisation voltage* for both the current system and the new one are illustrated in Fig. 5.23 and in Fig. 5.24 respectively.

As it can be noticed the responses of both systems are similar in shape, but the additional loop introduced by the current system appears again in the plots. Fig. 5.23 shows the crossing of the imaginary axis at 10 Hz for the current system whereas the new system has the *asymptotically approaching* mentioned above and showed again in Fig. 5.24. In both figures the influence of the polarisation voltage in the radio of each Nyquist response is shown, as it was demonstrated elsewhere [García-Jareño03].

Practically, both systems have the same behaviour in the PB polymer characterisation, but the current system has the disadvantage of the high frequency distortion introduced.

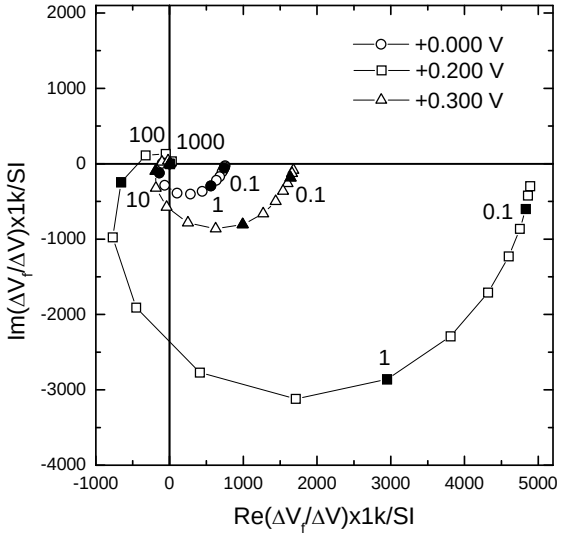

Fig. 5.23. Nyquist responses for three polarisation voltages in the PB experimental characterization in the current system. —○— +0.000 V, —□— +0.200 V, —Δ— +0.300 V.

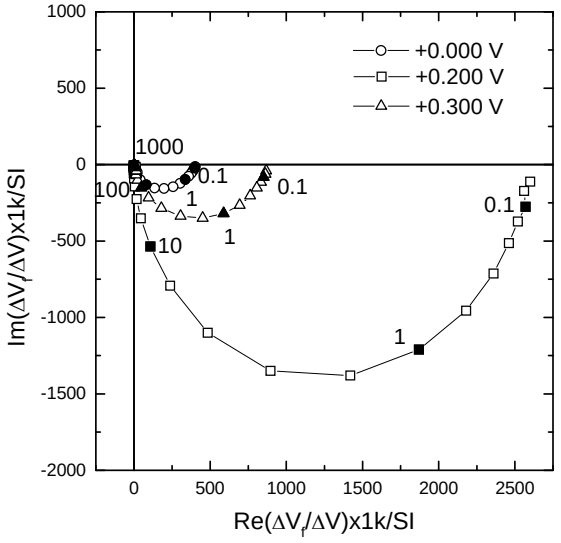

Fig. 5.24. Nyquist responses for three polarisation voltages in the PB experimental characterization in the new system. —○— +0.000 V, —□— +0.200 V, —Δ— +0.300 V.

5.3.3 Experimentation with Polyaniline

The last polymer studied with both systems in this experimental validation of the behaviour of the system designed is the *Polyaniline, PANI.*

The first experiment conducted with PANI was the comparison of both systems as it was performed with the two previous polymers, and then a study to see the *influence of the ion* involved in the redox process in the *Nyquist diagram* for both the old system and the new one. Then two more experiments for each system were conducted using different media in which the EQCM is immersed, i.e., two additional electrolytes.

The parameters introduced into the experimental setups for PANI [Gabrielli99], shown in Fig. 4.24 for the current system and in Fig. 4.25 for the new system, are summarised next:

- Carrier frequency: 9 MHz.
- Auxiliary synthesiser frequency (only for the current system): 8.999600 MHz
- Deviation voltage (at TFA file setup): 50 mV rms.
- Carrier voltage (from the home made oscillator at LISE):1V
- Modulator frequency sweep: (1 mHz- 63 KHz).
- Polymer used: Polyaniline deposited with 10 μA during 150s.
- Electrolyte used: KCl 1 M, $HClO_4$ 1M, and HNO_3 1M.
- Potentiostat voltage reference: +0.200 V.

5.3.3.1 Frequency response results

The experiment with $HClO_4$ media was selected to show the results of the *frequency response* of both systems.

The result obtained for the current system is shown in Fig. 5.25 and for the new system in Fig. 5.26.

To establish the comparison between the responses of the two systems the magnitude response on each figure were taken into a single plot and the same for the phase responses as it was performed in the two previous polymers. The plots for comparing the systems are shown in Fig. 5.27a for the magnitude and in Fig. 5.27b for the phase.

As in the previous cases studied the results found are almost similar until few hertz just as it is illustrated in the Fig. 5.27, but when the frequency of the modulating signal is near 10 Hz the responses of both systems differ notably presenting an oscillatory behaviour for the current system. In the phase response of the new system appears an abrupt variation of phase which could be interpreted as an error, but indeed this

change is completely normal and it is related to a small loop at low frequency that can be seen in the Nyquist response presented below.

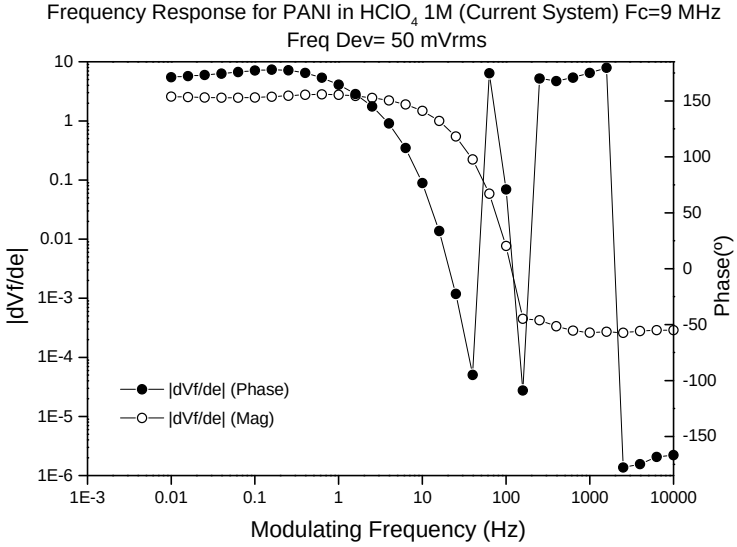

Fig. 5.25. Result of the frequency response of the current system for Polyaniline experimentation. —○—Magnitude response, —●— Phase response.

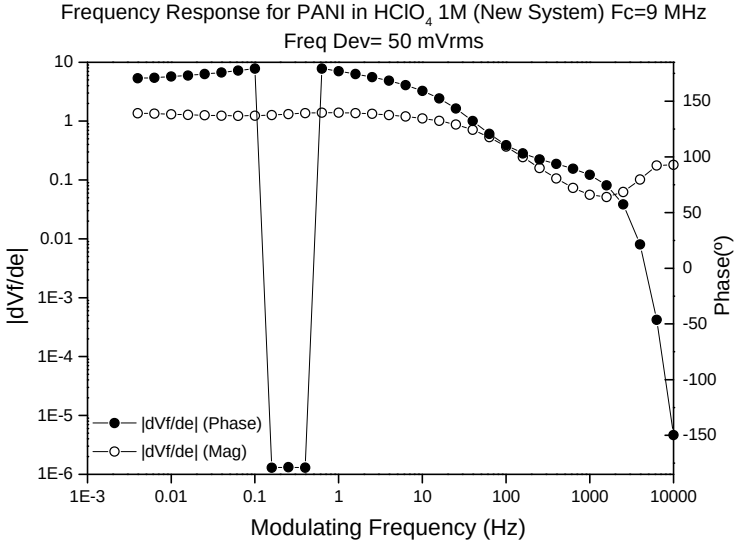

Fig. 5.26. Result of the frequency response of the new system for Polyaniline experimentation. —○—Magnitude response, —●— Phase response.

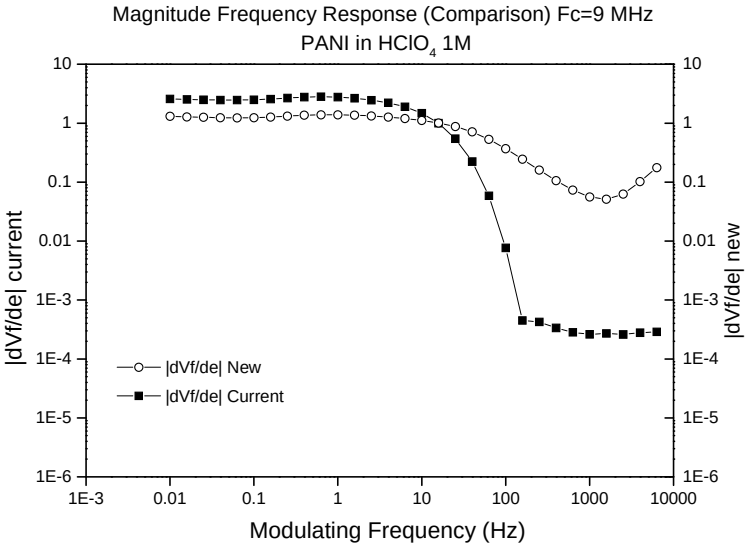

a.

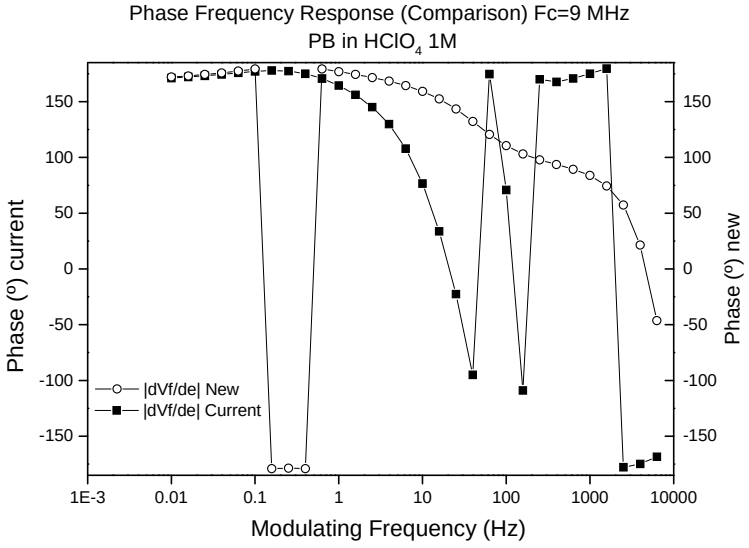

b.

Fig. 5.27. Frequency response comparison between the current and new systems for Polyaniline experimentation. a) Magnitude response, b) Phase response.─○─ New system response ─■─ Current system response.

5.3.3.2 Nyquist response results

Firstly, the *Nyquist response* for the experiment introduced in the previous frequency response analysis, i.e., the experiment with $HClO_4$ medium as electrolyte is illustrated here. Afterwards an analysis concerning the *influence of different media* is conducted for both the current and the new systems.

The following figure shows the Nyquist responses obtained. The curves have been normalised and correspond as in the previous polymers to the raw $\Delta V_f / \Delta V(\omega)$ transfer function.

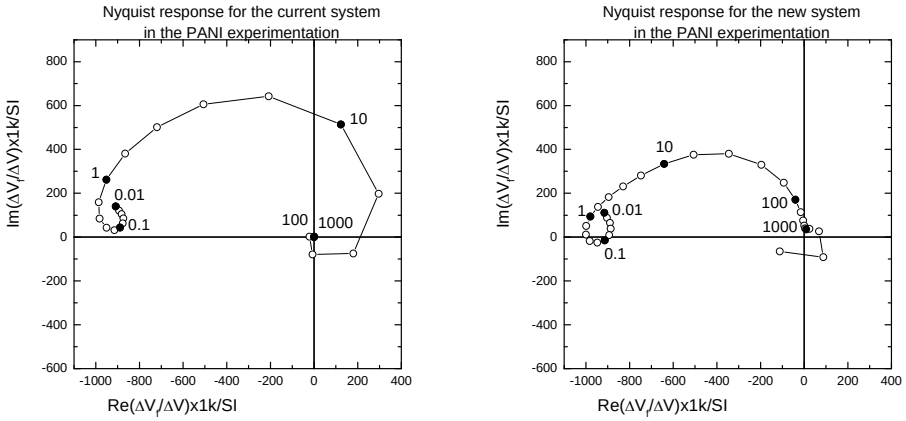

a. b.

Fig. 5.28. Normalised Nyquist Response for the systems compared for PANI experimentation in $HClO_4$, a. Old system response and b. New system response. ─○─Nyquist response, ● Some modulating frequencies.

The first feature observed in the previous figure is the additional loop in high frequency introduced by the current system as it happened with the other two polymer responses exposed, but there is an additional feature that can be useful to explain the apparent abrupt behaviour at low frequency of the new system: there is an additional loop at low frequency that appears in the response of the both systems.

This additional loop is related to the specific polymer behaviour because neither current system nor new one have problems in the low frequency range. Particularly for the new system this low frequency loop crosses the real axis from the second quadrant to the third quadrant which implies a change of 180º in the imaginary component of the Nyquist response then

in the phase response; this is the reason for the apparent abrupt or erratic response that appears in the Fig. 5.26. This low frequency loop for the current system is not large enough to cross the real axis, but it is present in the Nyquist response.

Next, the study of the influence of the different media in the Nyquist response will be presented both for the current system and the new one. Fig. 5.29 and Fig. 5.30 show the responses obtained for the current and the new systems respectively.

The influence of the media in the Nyquist response is observed by the modification of the radio of the plot according to the molar mass of the ion involved in the reaction according with some results presented elsewhere [Gabrielli00-3].

Regarding the electronic behaviour of both systems it can be observed one more time the distortion introduced by the current system with the extra loop since 10 Hz approximately whereas this loop is absent in the response of the new system. Concerning the shape of the responses obtained with both systems it can be noticed that they are similar especially for low frequencies when the current system does not introduce the mentioned distortion.

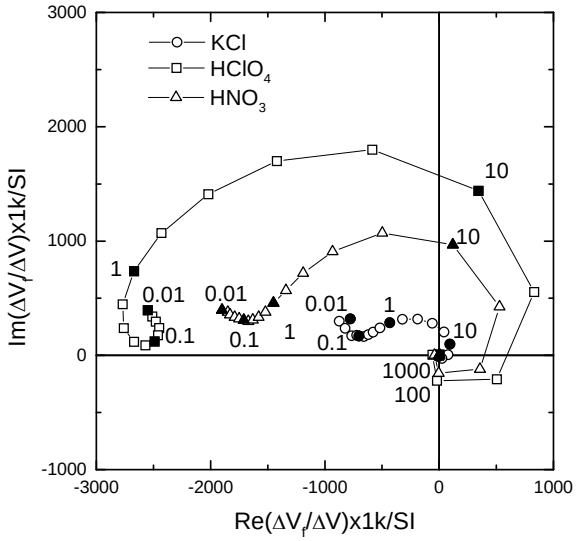

Fig. 5.29. Nyquist responses for three media voltages in the PANI experimental characterization in the current system. —○— KCL, —□— $HClO_4$, —Δ— HNO_3.

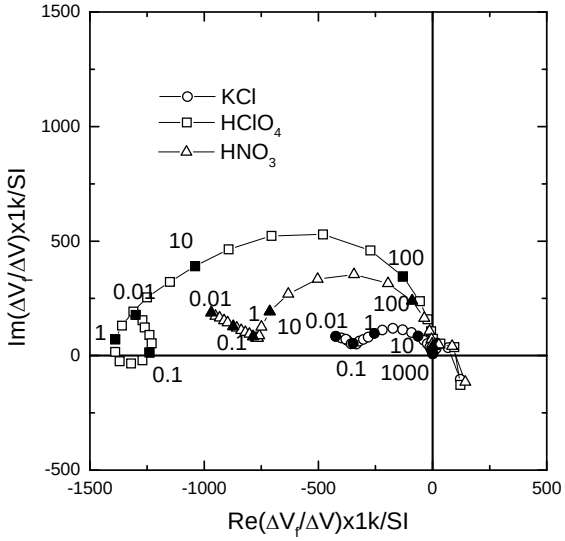

Fig. 5.30. Nyquist responses for three media voltages in the PANI experimental characterization in the new system. —○— KCL, —□— $HClO_4$, —Δ— HNO_3.

Finally, a similar analysis concerning the correction of the raw transfer function given by the TFA, as conducted for Prussian Blues, was established for PANI.

The contrast result of the two systems is shown in the following figure.

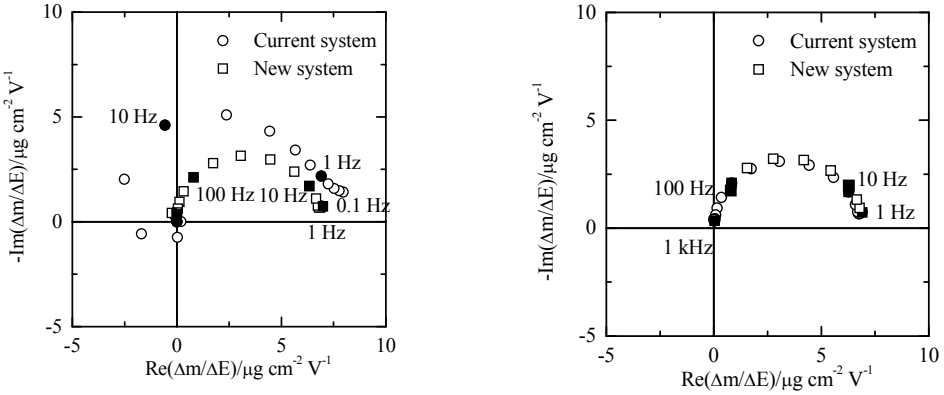

a. b.

Fig. 5.31. Comparison of the normalised Nyquist responses of the ○ Current system and the □ New system for Polyaniline characterisation in HNO_3 at 0.2 V/SCE; a) basic correction response and b) complete.

The results found for the contrast established for the PANI experimentation plotted in Fig. 5.31 are, maybe, the most conclusive regarding the validation of the improvement introduced by the new system to the measurements in the AC Electrogravimetric technique, because PANI has an effective high frequency response up to 1 kHz as it is shown in Fig. 5.31b.
Similarly to the results obtained for Prussian Blue, in Fig. 5.31a the two responses are completely different. The current system introduces additional loops in the two and third quadrants. Again, these loops are related to the electronic part of the experiment and are not related to the electrochemical response. With the new system, only one loop is obtained localised only in the first quadrant. The most important difference becomes from the frequency distribution. Indeed, at low frequencies, the repartition is different: the point measured at 10 Hz with the new system is equivalent to the point measured at 1 Hz with the current one. Subsequently, after corrections with the complete procedure, two equivalent responses are obtained as it is presented in Fig. 5.31b; the diameter of the two loops is equivalent and the frequency distribution is the same. Nevertheless, with the current system, the points measured after 100 Hz are not seen as it is impossible to do a correction of inexistent data, even with the complete correction. Clearly, the improvement of the new system is demonstrated: On one hand, the high frequency responses are reached without any problem up to 1 kHz and on the other hand, only a linear correction is necessary.

Now a comparison of the new system with the electrochemical model, presented in the first chapter, is introduced. For this comparison the data of the experimentation developed in the HNO_3 were taken and corrected according to the procedure indicated elsewhere [Gabrielli07].

The result of the comparison is shown in Fig. 5.32. As it can be noticed in the figure two ionic species are involved in this experiment, one anion and one cation. As it can be noticed in the figure three loops are observed: the first one located at high frequencies, in the one hundred Hz range, related to the anion. It should be noted that the high frequency range is necessary to reach the complete response of the PANI polymer. With the current system the anion response is masked by the electronic response as it was demonstrated above. The intermediate loop, very small, depends on the cation. This loop has a characteristic frequency between 10 Hz and 1 Hz, and the low frequency loop is related to the solvent.

It can be noticed the good correspondence between the theoretical electrochemical model and the experimental data obtained with the new

system developed; this corroborate the improvement obtained in the measurements of AC Electrogravimetry with this thesis work.

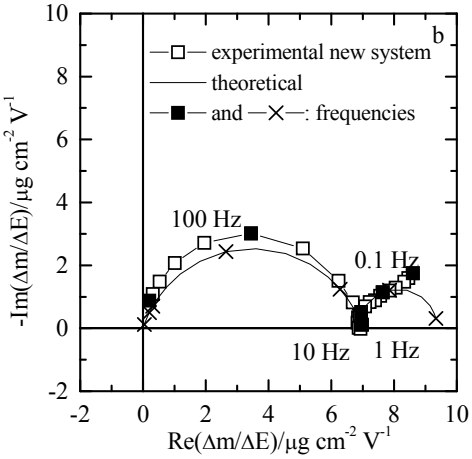

Fig. 5.32. Comparison of the normalised Nyquist responses of the ─ Theoretical model and the □ New system for Polyaniline characterisation in HNO_3 1M at 0.2 V/SCE.

5.4 Summary

In this chapter the total experimental processes developed with both systems were introduced in order to conduct a complete characterisation of the A-D PLL designed. This has also permitted to establish some contrast to compare the new system with the current system employed in the LISE to extract the Electrogravimetry transfer function in the AC Electrogravimetry experimental setups.

After the realisation of all these experiments some ideas have appeared to be proposed for some future improvements of the system. These new ideas constitute the future research lines of the project developed and are included in this thesis. These future research lines will be introduced in the next chapter.

Finally, all the results obtained during this experimentation process were presented and discussed and the main conclusions derived from these will be presented below in a separately chapter.

6 Future Research Lines

The present doctoral thesis provides continuity in the *research line* of piezoelectric system and sensors opened in the Electronic Engineering Department of the Polytechnic University of Valencia with the doctoral thesis “El cristal de cuarzo como sensor microgravimétirico en medios amortiguados” by Dr. Antonio Arnau Vives and followed by two more doctoral thesis in topics related to piezoelectric sensor characterisation and modelling and its electronic instrumentation interfaces.

As a direct continuity of the *future research line* in electrochemical applications proposed by the doctoral thesis: “Caracterización y desarrollo de un dispositivo electrónico para la monitorización continua de la frecuencia de resonancia serie y resistencia dinámica de una microbalanza de cristal cuarzo como sensor de procesos superficiales en medios fluidos” by Dr. Tomás Sogorb Devesa the project exposed in the previous chapters was proposed.

This doctoral thesis tackle a specific application of quartz crystal microbalance in an electrochemical application, the AC Electrogravimetry; to investigate the current electronic instrumentation employed to conduct polymer characterisations and proposes a new strategy and an electronic instrument to solve some drawbacks in these current systems to determine the Electrogravimetry transfer function.

Nevertheless the research line is not closed because some future research lines to the present project can be proposed in two complementary frames. On one hand, the improvement of the electronic instrumentation for piezoelectric sensors and systems and on the other hand the application of the electronic instrumentation to different specific fields. Some of these future research lines are introduced next.

6.1 Electronic System including a QCM Sensor

As it was exposed in this doctoral thesis the A-D PLL proposed is an electronic instrumentation system designed to measure the small mass changes performed in a polymer under study which is deposited over the surface of a quartz crystal microbalance. For achieving this, the system

provides a voltage whose value is proportional to the variation in the central frequency of an electrochemical quartz crystal controlled oscillator. Under these circumstances the EQCM controlled oscillator does not strictly take part in the system designed, because the A-D PLL takes the signal provided by the oscillator and starts the measurement process.

Instead of taking the modulated signal provided by the EQCM controlled oscillator it can be proposed a new system which can include the *QCM sensor inserted in the instrument* in such a way that it is not required a separate sensor controlled oscillator, i.e., a system that includes the EQCM as an integral and active part of the measurement system. The Fig. 6.1 shows a block diagram of the new system proposed.

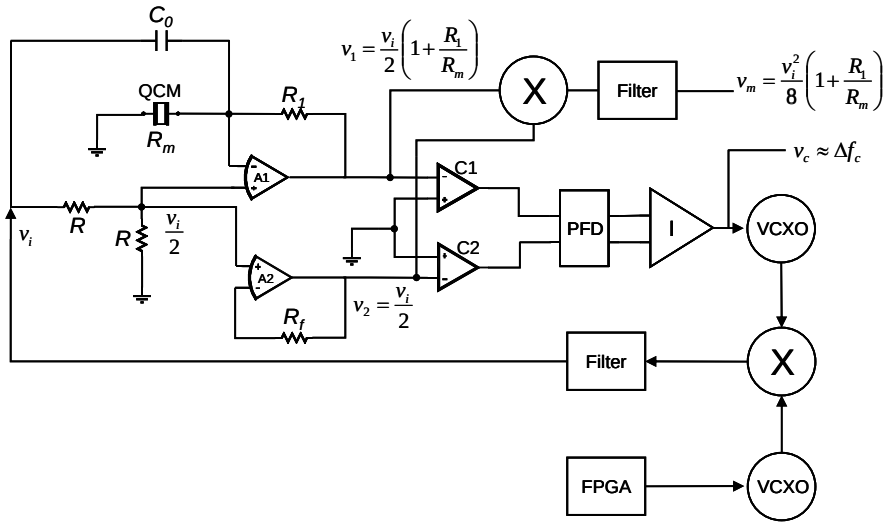

Fig. 6.1. Autonomous QCM sensor system proposed as one future research line of the A-D PLL system designed.

The system proposed in the previous figure is a kind of PLL, but modified according to some features explored in the project developed in the present doctoral thesis. The main important aspect is that the system includes the QCM inside the loop of the PLL. The system is formed by two amplifiers, A1 and A2; the first one takes the feedback signal modified by the QCM characteristics and the second, A2, acts as a follower. The phases of the output signals of the amplifiers are monitored by a phase-frequency detector (PFD), previously conditioned by the two comparators.. The output of the PFD is carried to an integrator, I, which provides a property voltage level to control the voltage controlled crystal oscillator, VCXO; this control signal is proportional to the frequency shift

experienced by the QCM according to the modification of the conditions on its surface. The set-up provides a locking frequency which corresponds to the zero-phase frequency of the sensor. When a C_0 capacitance similar to that of the QCM sensor is included, as indicated in Fig. 6.1, in the circuit, the locking frequency corresponds to the motional series resonant frequency; and then the circuit can be used to monitor the changes of the motional resistance of the QCM by taking the mixing of the input signals of the comparators. In fact the capacitor C_0 is used to compensate the parallel capacitance of the QCM.

The amplitudes of the signals at the outputs of the amplifiers are given, at the locking condition, by:

$$v_1 = \frac{v_i}{2}\left(1+\frac{R_1}{R_m}\right) \tag{6.1}$$

and

$$v_2 = \frac{v_i}{2} \tag{6.2}$$

for the first and the second amplifier respectively. In Eq. (6.1) the resistor R_m is the unknown motional resistance of the QCM.

It is important to say that the composite of NCO-FPGA should introduced a property frequency signal to put the mixing with the VXCO around the central frequency of the QCM employed, because if some big variations happen in this central frequency, the VCXO would be unable to follow these big changes and the system becomes unlocked; then any "feedforward" is necessary to be present in the system to provide the FPGA with information about the system's conditions, in terms of frequency or voltage, all the time.

The development of this interesting system could contribute to improve not only the AC Electrogravimetry measurements, but many instrumentation systems and applications in which the QCM is employed and then it is an important future research line that needs to be considered.

6.2 Autonomous QCM sensor system

As a possible following step in the design of these instrumentation systems with QCM, an *autonomous QCM sensor system* could be proposed which would include all the previous developments achieved in the previous and the present doctoral thesis presented in this research line.

This autonomous sensor system could be composed by a QCM inserted in the sensor system as it was presented in the previous section, an automatic parallel capacitance compensation schema as it was propose before [Arnau02] and the inclusion of some other features which can do the experimentation and acquiring data processes easier, like an automatic gain control subsystem, an automatic DC level control subsystem, an kindly input interface in which by a touch screen the experimenter can introduce the particular setup parameters for the experiment, date, temperature, etc; a communication interface with the computer to send the data acquired and even a software interface to present the data for their posterior fitting and analysis; among others.

6.3 Electrochemical characterisation systems

The most imminent future research line derived from the doctoral thesis presented here is the development of robust and accuracy instrumentation systems to characterise different electrochemical process and applications.

These instruments can be tailored according to the specific conditions of the applications which can be provided by the different electrochemical research groups to have excellent instrumentation systems to acquire better experimental data helping the analysis processes and the conclusions obtained from that experimentation.

6.4 Opening a research line in biosensors investigated by QCM techniques

From a practical application point of view and because of this doctoral thesis contributed to the research formation of the author in a non common topic in his own country, a clear future research line derived from the realisation of the project is the opening of a research line in Colombia in the area of the electronic instrumentation systems using quartz crystal microbalances applied fundamentally to biological or biomedical areas.

Some of the possible applications in biological or biomedical areas are:

- Due to Colombia is an agriculture oriented country it is important to development QCM instrumentation systems based in immunosensors to detect pesticides present in the products cultivates.

- It could be proposed the design and implementation of QCM sensor based systems to detect some biomedical variables like glucose, haemoglobin, proteins, hormones, etc, to investigate novel methods of medical diagnosis.
- Explore the possibility to create some devices that emulate certain corporal senses function like smell [Beeley04] to be used in these inhospitable conditions for human beings in which some measurement is required.
- Many other applications in biomedical areas that can appear once the research line had been created.

The research conducted in this doctoral thesis has allowed the publication of the following papers and the presentation in one international congress:

1. R. Torres, A. Arnau, H. Perrot. “Electronic System for experimentation in AC Electrogravimetry I: Technique Fundamentals”. Revista EIA, Volumen 5, p. 9-21, junio 2006.
2. R. Torres, A. Arnau, H. Perrot, J. García, C. Gabrielli. “Analog-Digital Phase Locked Loop for Alternating Current Quartz Electrogravimetry”. Electronics Letters. October 2006.
3. R. Torres, A. Arnau, H. Perrot. “Electronic System for experimentation in AC Electrogravimetry II: Implemented design”. Revista EIA, in press, junio 2007.
4. R. Torres, A. Arnau, H. Perrot. “Fast, Continuous and Accurate Frequency Shift Measurement in the AC Electrogravimetry Technique”. Poster presentation in the Joint Meeting of the European Frequency and Time Forum and the IEEE International Frequency Control Symposium. Geneva, Switzerland, May 2007.

7 Conclusions

As a result of the development of the entire project both from the design and implementation point of view and from the experimental stage it can be stated the following conclusions:

1. A detailed exploration and study of the *quartz crystal microbalances, QCM*, application to the *AC Electrogravimetry technique* was developed in order to identify the main challenges involved in the measurement process and the appropriate monitoring of very small and high rate frequency changes that appear in it, i.e., monitoring frequency shifts in the order of tens of cycles around 10 MHz at high rates (until 1 KHz), moreover, in a broad range of carrier frequencies (from 6 to 12 MHz). All the information gathered was useful to define the specific features of an *electronic instrumentation system* that pretended to fulfil with those challenges imposed.
2. In order to determine the *Electrogravimetry transfer function, EGTF*, in an AC Electrogravimetry experimental setup the continuous monitoring of the resonance frequency shifts of the QCM must be done accurately, with a good resolution and covering a broad frequency range. All these conditions imposed a non trivial problem to be solved to any measurement system.
3. An electronic instrumentation system based on a mixture of analogical and digital subsystems configured as a phase locked loop, *A-D PLL*, was proposed as a better trade-off between accuracy, resolution and bandwidth to solved the specific challenge proposed by the EGTF measurement in the AC Electrogravimetric technique.
4. The solution achieved by the system proposed is based on a *double frequency tuning*. On one hand, the first tuning is performed by the inclusion of a *voltage controlled crystal oscillator, VCXO*, which allows the improvement in the resolution (15mV/Hz was measured, but it can be increased even more); and on the other hand a second coarse tuning to compensate the decrease in the dynamic range due to the inclusion of the VCXO. This double

tuning is performed by the inclusion of a *feedforward subsystem* composed by the combination of an algorithm programmed into a FPGA and a numerically controlled oscillator, NCO.

5. After the system was designed and implemented a complete *electronic characterisation processes* both in static conditions and dynamic one, were conducted to evaluate the system performance under controlled situations and the experimental data obtained validate the system proposed and warrant that the data to be obtained in real experimentation process are indeed due to the responses of the polymers studied by the AC Electrogravimetry experimental technique without any intervention of the electronic instrumentation.
6. In the electronic characterisation a comparison with the current experimental setups used was developed to determine the EGTF with the new system proposed, and the results obtained proof that the new system performs an important improvement in the measurement regarding the current one.
7. In conjunction to the electronic characterisation a complete *experimental validation* was developed employing real polymer studies for both the current and the proposed systems. All data obtained validated the preliminary responses obtained in the electronic characterisation; i.e., the new system proposed improves the measurement process in terms of accuracy, resolution and bandwidth regarding the current system employed.
8. From a specific point of view the current system exhibits a poor high frequency behaviour, which is no higher than few hertz, that is evidenced in the introduction of additional loops in the *Nyquist responses* of the polymers studied; whereas the new system does not introduced these loops, but provides the real polymer high frequency response because its frequency responses goes until even more 1 KHz.

9. Due to the presence of the extra loops contributed by the current system a software procedure is required to process the data obtained in order to extract the real polymer response. With the new system the polymer response is obtained directly from the experiments without using posterior software processing.
10. The way in which the system proposed was designed allows certain automation and turns the experimentation process more versatile and easier. The designed system simplifies the equipment involved in the measurement process while the current system

employs some additional equipment, like the auxiliary synthesiser, to work properly.

11. The responses of the systems were contrasted with the results of a *mathematical model* of the AC Electrogravimetric response for each polymer investigated. The results of the contrast validate the hypothesis that the new system exhibits a general improvement of the EGTF measurement regarding the current system in terms of frequency response and resolution.

Appendix I: Electronic Interface Systems for AT-cut QCM Sensors

The most general model which includes almost all quartz crystal applications is the model presented in Fig. 1.1, due from this it is possible obtain the rest of limit cases.

Both the electrical impedance (admittance) expression deduced for this model and the expressions for elements that constitute the equivalent circuits depends on sensor characteristics and physical an d geometrical properties of the media deposited on it, i.e., h_1, G_1', G_1'', ρ_1, G_2', G_2'' and ρ_2. In that sense, for any quartz crystal and some media with known characteristics, for obtaining electrical impedance (admittance) or elements for equivalent circuit is immediate.

Nevertheless, when a quartz crystal is employed as a sensor the challenge is on the contrary, i.e., it is required the extraction of the physical and geometrical properties for the media deposited on the crystal from some electrical measurements taken from the resonator. The main difficulty to obtain for this reverse process consists in the obtaining information enough, from electrical measurements to obtain a unique solution for multiple parameters extraction problem. Then, it is fundamental to describe the kind of information given by the current characterisation electronics systems.

Prior to discuss about different characterisation system it is necessary first to define the parameters to be measured for an appropriate evaluation of the sensor response. These parameters have to be measured in two steps:

STEP 1: Determination of the elements C_o^*, R_m^q, L_m^q and C_m^q for an evaluation of the unperturbed device response.

Generally, values of C_o^*, R_m^q, L_m^q and C_m^q are provided by the manufacturer, but sometimes they are not accurate enough and must be obtained prior to the experiment. Normally, they can be determined with impedance or network analysers by measuring the electrical response of the unperturbed resonator over a range of frequencies near resonance and fitting the equivalent-circuit model to these data. If an impedance analyzer is not available, the corresponding standard [IEC302, IEC444], or an alternative method described elsewhere [Arnau00-1], can be used. A more

accurate determination of C_o^* can be made at a frequency twice as high as the resonant frequency [Cady64, SanEmeterio92]. From these values, the following parameters of interest can be extracted:

f_s: motional series resonant frequency (MSRF). It is defined as the frequency at which the motional reactance vanishes. It can be determined directly by frequency measurements or by Eq.(1.9).

In practice, the frequency corresponding to the maximum conductance typically monitored in impedance analysis is very close in most practical cases to the MSRF [Arnau00-2].

h_q: quartz thickness. It can be determined from Eq.(1.8):

$$h_q \approx \frac{1}{\omega_s}\sqrt{\frac{\bar{c}_{66}}{\rho_q}}\sqrt{(n\pi)^2 - 8K^2} \tag{I.1}$$

C_o: static capacitance (Fig. 1.2 a). This capacitance arises from electrodes located on opposite sides of the dielectric quartz resonator. This capacitance does not include parasitic capacitances external to the resonator (C_p) which do not influence the motional parameters [Martin91]. The static capacitance can be determined from the values of C_m^q or L_m^q applying one of the expressions in Eq.(1.7).

A_S: effective electrode surface area. It can be determined from C_o and h_q along with the quartz permittivity from:

$$A_S = \frac{h_q}{\varepsilon_{22}} C_0 \tag{I.2}$$

its value is necessary in applications involving film thickness.

C_p: parasitic parallel capacitance, external to the resonator. $C_p = C_o^* - C_o$. Its value is useful in applications where the influence of the dielectric properties of the load have to be accounted for.

These parameters have to be measured as reference and must be taken into account for an appropriate load characterisation.

STEP 2: Measuring of those parameters of the loaded thickness shear mode (TSM) resonator which can more appropriately characterise the physical or geometrical properties of the load on the basis of current models.

From Fig. 1.2 a) it is shown that the load contribution is characterised by the elements R_m^L, L_m^L and C_m^L of the motional branch. A change in both

L_m^L and C_m^L produces a change in the MSRF. On the other hand, changes in the loading properties are also reflected on changes in the motional resistance R_m^L, which does not produce MSRF changes. Thus, both MSRF and motional resistance are useful and necessary parameters for a complete sensor characterisation.

In addition, it is important to state that the majority of the simpler models derived from the most comprehensive TLM, such as the Lumped Element Model (LEM) [Cernosek98], or the extended BVD model [Martin91, Arnau04], assume that the resonator operates around the MSRF. Furthermore, it is important to mention that most of simpler equations used to relate frequency and resistance shifts to the properties of the load have been derived assuming that the resonator is oscillating at its true MSRF. Thus, measurements of loading-induced frequency changes made with the resonator operating at a frequency different from the true MSRF could not agree with the models derived for QCMS. This discrepancy is specially pronounced when the resonator is loaded with heavy damping media.

Another characteristic which makes the MSRF more interesting than other frequencies is that its value is independent of parallel capacitance changes.

For all that mentioned, the MSRF and the motional resistance are the parameters of the loaded resonator to be measured. Then, the problem associated with the measuring system will be discussed in relation to the accuracy in the determination of these parameters of interest.

Now, the discussion will be focused on the interface circuits currently used for sensor characterization which are based on five principles: network or impedance analysis, impulse excitation or decay method, oscillators, parallel capacitance compensation techniques and the Transfer Function Method. Type of information provided by each one is summarized in Table I.1.

Table I.1. Information provide by current characterisation systems [Jimenez04]

System Type	Y(f) ó Z(f)	MSRF y R_m	R_m, L_m, C_m, C_0^*
Impedance or network analyser	Yes	Yes[a)]	Yes[a)]
Decay and Impulse Excitation Methods	No	Yes[a)]	No
Oscillators	No	Yes[a)]	No
Parallel Capacitance Compensation	No	Yes	No
Transfer Function Method	No	Yes[a)]	Yes[a)]

[a)] Measurements become wrong for great loads.

I.1 Impedance or Network Analysis

Impedance or network analysers measure the electrical impedance or admittance of the quartz sensor over a range of frequencies near resonance for a complete characterisation of the device response. As a test instrument, an impedance analyser has the following advantages in evaluating the sensor response:

1. The device is measured in isolation and no external circuitry influences the electrical behaviour of the sensor.
2. Parasitic influences can be excluded by calibration due to passive operation of the sensor.
3. Differentiated information in relation to diverse contributions of the load can be obtained by measuring both the conductance and the susceptance of the sensor over a range of frequencies around resonance.

However, several inconveniences remain when using this technique for sensor applications [Eichelbaum99]:

1. Its high cost and large dimensions of the associated equipment prevent its use for *in situ* or remote measurements.
2. The connection between the sensor and the equipment is sometimes difficult to accomplish such as in electrochemical or biological applications where it is convenient to ground one of the quartz electrodes.
3. It is not suitable for simultaneous multiple sensor characterisation. Sometimes a multiplexing interface is used for a sequential connection of different sensors to the same analyzer, but it can perturb the device response.

On the other hand, the impedance analyser can determine with high accuracy the MSRF and motional resistance of the unperturbed quartz sensors as reference values. The MSRF is obtained by measuring the frequency corresponding to the conductance peak around resonance. The motional resistance is determined as the reciprocal of the conductance peak value. The evaluation of the MSRF and the motional resistance in this way is based on the suitability of the BVD model for characterising the sensor response. In BVD circuits the relationships between MSRF and maximum conductance frequency and between the motional resistance and the reciprocal of the conductance peak value are exact [Arnau04]. For an unperturbed resonator, the BVD circuit can very accurately represent the device response. Additionally, the range of frequencies in which the resonance happens is very narrow and therefore the frequency resolution of the instrument is very high. However, for heavy damping loads the quality factor of the device is considerably reduced which expands the resonance range and reduces the frequency resolution and the suitability of the BVD circuit for representing the sensor response.

The determination of the MSRF and motional resistance by using the mentioned relationships is not as accurate as for the unperturbed situation, but remains accurate enough for these applications in which the sensor can be used [Arnau00-2]. On the contrary, the determination of BVD parameters for high damping loads does not give additional information apart from the parallel capacitance, which can be measured more appropriately at double of the resonant frequency. Furthermore, the MSRF determination from the motional components in Eq. (1.9) can produce great errors depending on the algorithm used for the motional parameters extraction.

Thus, an impedance analyser can be used for an accurate determination of the magnitudes considered of interest. The accuracy in the determination of the MSRF is reduced for high damping loads. However, this loss in frequency resolution does not affect the relative accuracy in the motional resistance determination due to the flatness of the conductance peak for high damping loads.

I.2 Decay and Impulse Excitation Methods

Impulse excitation and decay methods are based on the same principles. To illustrate the principle let it considers the electrical circuit in Fig. I.1. At

$t = 0$ the switch connects a voltage source (E) with a very low output resistance (r) to the sensor modeled in the figure as a BVD circuit. From this moment the current *i(t)* changes according to the following expression (assuming $r << R_m$):

$$i(t) = i_{C_o^*}(t) + i_m(t) \approx \frac{E}{r} e^{-\frac{t}{rC_o^*}} + \frac{E}{L_m} \frac{1}{\sqrt{\frac{1}{L_m C_m} - \left(\frac{R_m}{2L_m}\right)^2}} e^{-\frac{R_m}{2L_m}t} \sin \sqrt{\frac{1}{L_m C_m} - \left(\frac{R_m}{2L_m}\right)^2}\, t \qquad \text{(I.3)}$$

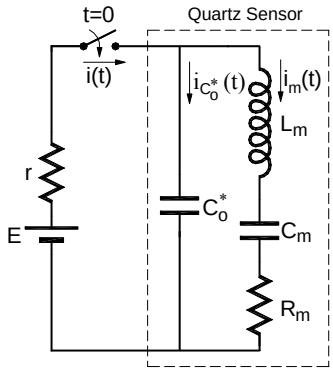

Fig. I.1. Impulse Excitation Method Principle [Arnau04].

The first term associated to the current through the parallel capacitance, $i_{C_0^*}(t)$, has a time constant $\tau_{C_0^*} = rC_o^*$ while the time constant for second term associated with current through the motional branch of the sensor, $i_m(t)$, is $\tau_m = 2L_m / R_m$. Assuming typical values for a 10 MHz loaded AT cut quartz resonator ($R_m{}^q$= 10Ω, $L_m{}^q$= 7.5 mH, $C_m{}^q$= 33.774 *f*F, C_0= 7pF, $C_0{}^*$= 10pF) and r = 2Ω, the decay time constant $\tau_{C_0^*}$ is about 10^6 times smaller than τ_m. Then, total current *i(t)*, is dominated by the second term in Eq. (I.3) once the first instant has passed. With a proper interface circuit, the damped oscillation can be recorded on a digitizing oscilloscope and subsequently transferred, e.g., via GPIB, to a computer. A numerical fitting of the recorded curve permits to obtain the time constant τ_m and the frequency of the damped oscillation given by:

$$f_m = \frac{1}{2\pi}\sqrt{\frac{1}{L_m C_m} - \left(\frac{R_m}{2L_m}\right)^2} \tag{I.4}$$

The time constant τ_m can be related to the quality factor Q by using the approximate expression: $Q \approx 2\pi f_s L_m / R_m = \pi \tau_m f_s$, where f_s is the MSRF of the loaded QCR. Then, the frequency of the damped oscillations can be written as a function of f_s and Q as follows:

$$f_m \approx f_s\sqrt{1 - \frac{1}{4Q^2}} \tag{I.5}$$

Thus, by measuring the time constant and frequency for the damped oscillations, quality factor and MSRF can be determined. It can be considered, without incurring a significant error, that the reduction in quality factor is proportional to an increase in the motional resistance. In such a way a measurement of this magnitude can be obtained.

In practice, the impulse excitation method is difficult to apply for two reasons:

1. Ideal pulse front slopes are difficult to achieve.
2. Other harmonics different from that desired can be excited. Thus, in order to avoid them, additional circuitry which perturbs the sensor response is necessary.

Instead of the impulse method, the decay method is used in practice [Rodahl96-1, Rodahl96-2]. The measuring principle is very similar to the described one just above. A piezoelectric resonator is excited with a signal generator approximately tuned to the frequency of the desired harmonic. Then, at $t = 0$ the signal excitation is eliminated by opening the appropriate relay (Fig. I.2 and Fig. I.3). At this moment, the voltage or current (depending on whether the parallel or series resonant frequency is excited according to the electrical setup) [Rodahl96-3] decays as an exponentially damped sinusoidal signal, mathematically expressed by:

$$A(t) \approx A_0 e^{-\frac{t}{\tau_m}} \sin(2\pi f t + \varphi), \qquad t \geq 0 \tag{I.6}$$

Where A_o is the amplitude of the magnitude at $t = 0$; φ is the phase and f is the frequency given by:

$$f \approx f_i \sqrt{1 - \frac{1}{4Q_L^2}} \tag{I.7}$$

Where f_i is the MSRF of the loaded QCR, f_s, or the parallel resonant frequency, f_p, given by:

$$f_p = f_s \sqrt{1 + \frac{C_m}{C_0^*}} \tag{I.8}$$

In Eq. (I.7), it has been implicitly assumed that the quality factor is the same for both series and parallel mode, and is given by:

$$Q_L = \frac{L_m \omega_s}{R_m} \approx \frac{L_m \omega_p}{R_m} \tag{I.9}$$

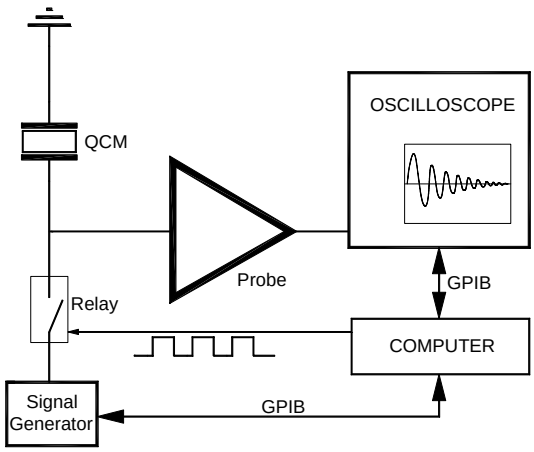

Fig. I.2. Experimental setup to measure parallel resonant frequency and parallel dissipation factor [Arnau04].

In the series excitation mode (Fig. I.3), the parallel capacitance effect is eliminated by short-circuiting and the frequency of the damping oscillations is very close to the true MSRF. This is one of the principal advantages of the method. The accuracy of the decay method is high, provided that the measurement of the frequency and the envelope are obtained with high accuracy, which becomes complicated for strongly damping loads. This technique reduces the cost of the instrumentation in comparison with network analysis; however, the quality and dimensions of the required equipment still remain high, mainly if an accurate determination of the frequency and the envelope of the exponentially damped sinusoidal is necessary. Therefore, this method is more

appropriate for laboratory environment than for sensor applications and becomes more sophisticated when simultaneous multiple sensor characterization at high sampling rates have to be performed.

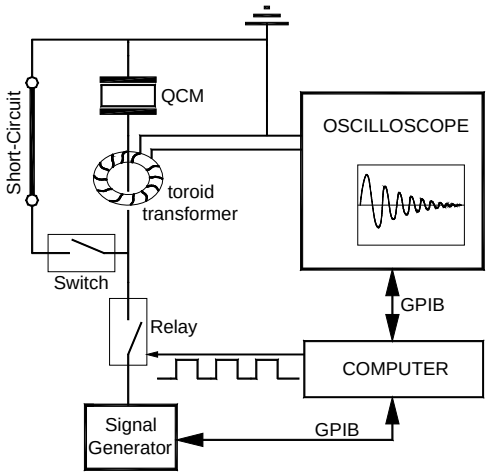

Fig. I.3. Experimental setup to measure series resonant frequency and series dissipation factor [Arnau04].

I.3 Oscillators

The systems described before passively interrogate the quartz resonator and, with an appropriate interface circuit, the desired characteristic parameters of the sensor are measured in isolation, i.e., the external circuitry does not interfere with the sensor response. This is the greatest advantage of the methods described. However, in oscillators the sensor takes part of the feedback path and the oscillating frequency is characterised by a certain phase of the quartz impedance, which depends on both the quartz resonator and the external circuitry to the sensor. When real characteristics of the amplifier and the rest of the components in the oscillator must be taken into account, it is difficult to know precisely the phase of the circuitry external to the sensor as a function of the frequency. Therefore, in general, the phase of the sensor for oscillating condition can not be accurately known, which makes the problem associated to oscillators more critical.

When the phase shift provided by the external circuitry in the range of frequencies around resonance can be considered constant, the phase provided by the quartz impedance at which the oscillation takes place can be considered constant as well. Thus, when the resonator properties are

altered due to loading effects, the phase of the resonator changes and the oscillating frequency shifts to find the new frequency at which the phase of the sensor fits the oscillating condition. Therefore, due to the operation principle of the oscillator, the true MSRF can not be tracked continuously when an oscillator is used for monitoring load–induced frequency changes, at least in an oscillator in which the phase of the quartz impedance for oscillating condition is maintained constant. This can be easily illustrated using the BVD circuit as sensor–model (Fig. 1.2 c). It can be understood that the MSRF only depends on L and C components of the motional branch, but the phase of the complete resonator also depends on the specific values of the motional resistance R and on the parallel capacitance C_o^*. Thus, if the motional resistance changes while remaining constant L and C, the MSRF does not change but the quartz phase changes. Then the oscillating frequency has to change in order to find the quartz phase corresponding to the oscillating condition and this frequency shift supposes a frequency error, which can be significant when the MSRF is taken as a parameter of interest. Fig. I.4 shows how the oscillating frequency and the frequency shift regarding the frequency of the resonator in the unperturbed state depend on the oscillating phase condition in an oscillator. Sometimes the oscillation ceases because the oscillation phase condition can not be reached.

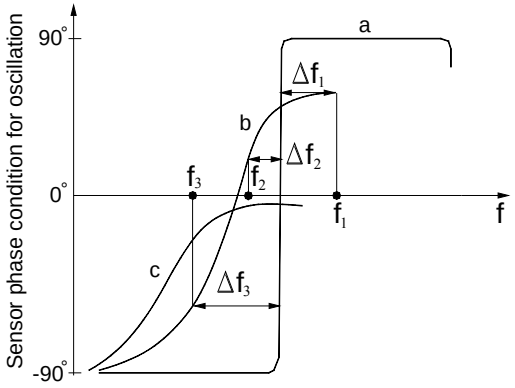

Fig. I.4. Plot for illustrating different frequency shifts regards to resonant frequency of the resonator in unperturbed state, associated with different sensor phase conditions for oscillation in an oscillator [Arnau04].

Another consideration which makes clear the selection of MSRF as a parameter of interest is its independence of the parasitic capacitances in parallel with the sensor. However, due to the operation principle of the oscillator, the stray capacitances in parallel with the sensor always have

important effects on the oscillating frequency. This is because an oscillator looks for a certain phase and not for a certain frequency of the sensor. Thus, although a change in the parallel capacitance due to parasitic effects does not change the MSRF, the phase of the sensor changes and, consequently, a shift in the oscillating frequency takes place.

As described, the oscillator frequency is dependent not only on "mass loading" (motional inductance) but on "dissipation" (motional resistance). This must be taken into account and carefully considered when using an oscillator in a specific application, in which the physical properties of the load can change producing changes in both the mass loading and dissipation.

On the other hand, in a great deal of applications in which the quartz resonator is used as a sensor, an additional magnitude to the MSRF shift is necessary in order to discriminate different physical contributions [Martin91]. Regarding to oscillators, many designs incorporate an automatic gain control (AGC) system for the measurement of the activity of the quartz sensor at resonance [Bottom82]. The AGC system tries to maintain the level of the signal constant in a selected point of the oscillator. With this purpose, it provides a voltage (AGC voltage) that modifies the gain of the amplifier so as to maintain the signal level in the selected point constant in relation to a reference voltage. In many of these designs proportionality between the change in the AGC voltage and the change in the motional resistance is claimed [Wessendorf93, Chagnard96, Auge95]. In some of these AGC systems the proportionality is justified only from a physical point of view [Chagnard96]. In others, mathematical expressions in which some simplifications were made show this proportionality [Wessendorf93], although it is also shown that this proportionality is lost in some cases [Martin97].

It can be shown that even in the most ideal situation it is very difficult to ensure that the voltage shift provided by an AGC system included in an oscillator is proportional to the change in the motional resistance; unless the parallel capacitance of the sensor is suppressed or compensated. This demonstration can be found elsewhere [Arnau02].

The most important aspects concerning the problem associated with oscillators as electronic drivers for QCMS have been treated. It has been shown that although the simplicity of an oscillator makes this device very attractive for sensor applications, some limitations remain. These limitations have to be taken into account in the interest of accuracy and they should be kept in mind in any new work that looks for the simplicity and autonomy of oscillators for sensor applications.

There is a great number of published circuits using oscillators for QCM sensor applications, some of them provide the sensor's resonance frequency [Thompson87], others in addition provide the motional resistance [Wassendorf93, Eichelbaum99]. Results provide by these systems are acceptable when sensor work without load or small loads, but it could be made considerable errors when these condition are no kept. There is a deep study about all problematic concerning this kind of systems elsewhere [Sogorb03].

I.4 Parallel Capacitance Compensation Techniques

These techniques aim at the simplicity of oscillators while overcoming their limitations. From the previous analysis on oscillators, it can be seen that their limitations come from the existence of the parallel capacitance. It can be deduced that, if the parallel capacitance of a QCM sensor were eliminated, an ideal quartz resonator controlled oscillator with 0º oscillation phase condition would provide continuously the MSRF. Additionally, changes in the motional resistance do not produce changes in the oscillation frequency.

The parallel capacitance can be compensated by the circuit shown in Fig. I.5 [Geelhood01, Behrends01] which can be incorporated in an oscillator. The main problem of this technique is the lack of ideality of the transformers and the selection of the capacitance C_v for compensating the parallel capacitance, i.e., the calibration of the parallel capacitance compensation.

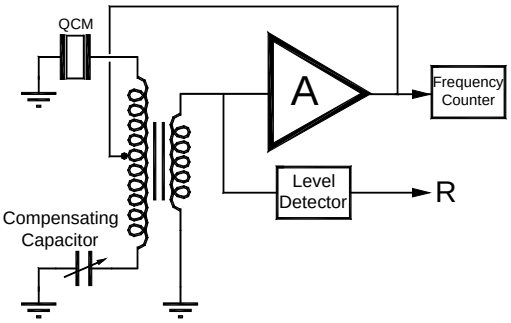

Fig. I.5. Schematic circuit for parallel capacitance compensation based on a three winding transformer [Arnau04].

An additional problem associated with oscillators is the typical loop gain dependence and its relation to the appropriate oscillating phase condition. Phase Locked Loop, PLL, techniques permit the system to lock automatically to the appropriate MSRF while maintaining the isolation between the sensor and the electronic interface thanks to a passive interrogation of the resonator [Arnau02, Ferrari00, Ferrari01]. Additionally, these techniques make the calibration procedures of the system and its automation easier, which is also important. A circuit implementing a phase locked loop technique for parallel capacitance compensation is shown in Fig. I.6 [Arnau02].

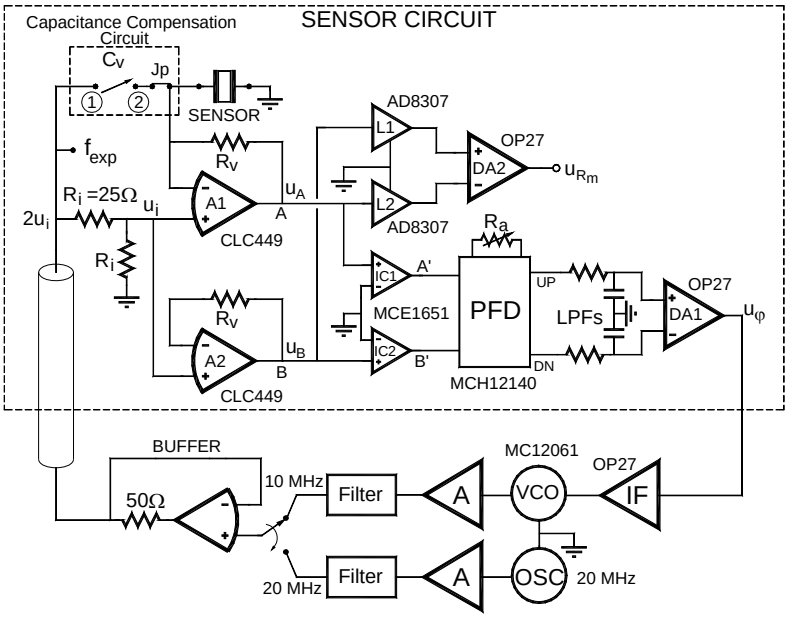

Fig. I.6. Circuit for parallel capacitance compensation based on a Phase-Locked Loop (PLL) Technique.

I.5 Transfer Function Method

This technique was introduced by Calvo and Etchenique in 1997 [Calvo97] and it is based on the voltage divider shown in Fig. I.7 a) which can be represented by Fig. I.7 b), if is it is assume that the resonant compound can be modelled by BVD circuit.

A sinusoidal signal applied at the input sweeps a range of frequencies around the resonant frequency of the sensor; the average values of the

input and output voltages are measured and acquired with an analog-digital converter and captured with a computer. Thus, an experimental measure of the absolute value of the voltage transfer function is obtained in the range of frequencies considered. The theoretical transfer function is used to find the set of parameters that best fit to the experimental data. It is assumed that the motional capacitance remains constant, the rest of parameters C_o, L_m and R_m are obtained by a non-linear fitting.

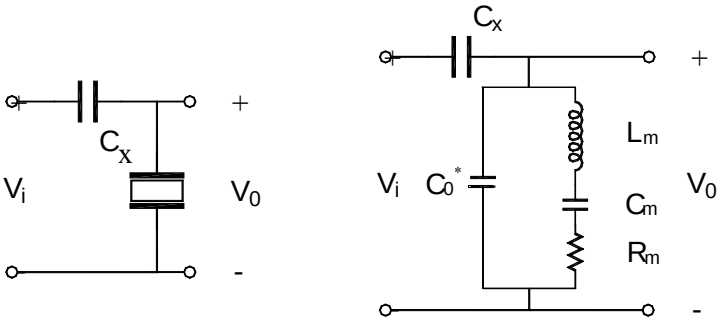

Fig. I.7. Measurement Circuit used by Calvo et al. [Calvo97]. a) Voltage divider, b) Substitution of the crystal by its BVD model.

Finally the authors of this technique noticed the advantage of using a capacitor C_x instead of a resistor as the other branch of the voltage divider, as shown in Fig. I.7. In this context the theoretical transfer function is:

$$\left|\frac{V_o}{V_i}\right| = \frac{\sqrt{\left(\omega L_m - \frac{1}{\omega C_m}\right)^2 + R_m^2}}{\sqrt{\left(\omega L_m - \frac{1}{\omega C_m} + \frac{\omega L_m C_o}{C_x} - \frac{C_o}{\omega C_m C_x} - \frac{1}{\omega C_x}\right)^2 + \left(R + \frac{RC_o}{C_x}\right)^2}} \qquad \text{(I.10)}$$

In spite of the fact this technique is simple and non-expensive its applicability is conditioned to the BVD model effectiveness for characterising the resonant compound; in addition, this technique does not allow the sensor characterisation in the whole frequency spectrum [Jimenez04].

I.6 Summary

Problems associated with QCRS interface circuits reveals that an optimal device for sensor characterization does not exist at present. The systems that better characterize the sensor are those which passively interrogate the quartz resonator so that the sensor is measured in isolation. However, these systems based on impedance analysers or decay/impulse excitation methods include expensive equipment and do not fulfil the autonomy normally required for sensor applications. On the other hand, those systems which fulfil the simplicity, autonomy and low price requirements appropriate for sensor applications have less accuracy in the determination of sensor parameters; mainly, because the external circuitry influences the sensor response which is not measured in isolation. This problem becomes more critical due to the difficulty of calibrating the response of the external circuitry in typical oscillators. Thus, the monitored parameters can not be accurately associated to a certain phase of the sensor.

Consequently, when using an oscillator to measure the frequency shift, it is necessary to consider the change in the motional resistance as well. If the motional resistance changes during experiment, the frequency shift monitored with the oscillator can not be considered equal to the MSRF shift. Thus the associated physical parameters extracted from the monitored frequency shift will include an error which can be significant.

For the purposes of the thesis work presented here, as it was mentioned before in the chapter 1, the specific characteristics of the AC Electrogravimetry make impossible the use of the impedance analyser for an appropriate monitoring of the interesting parameters. The reason is that an impedance analyser can not follow the very quick changes of the parameters of interest that are induced in this technique, then the best but not the ideal way is to monitor the parameters of interest by an oscillator-like circuit which permits the continuous monitoring of these parameters of interest [Torres06-1].

Appendix II: VHDL code programmed in the FPGA

The code in the FPGA is structured by the following modules: main.vhd, count_aux.vhd, contador1.vhd, contador2.vhd, maq_estado.vhd, medicion.vhd and multiplexor.vhd. These modules correspond to the hardware architecture designed for the FPGA and shown in the Fig. 3.19. The programmed code for each one of these modules is shown below.

```
----------------------------------------------------------------------
--  main.vhd --Sistema de control del NCO AD9851 para PLL an-dig v2.0 --
----------------------------------------------------------------------
-- Autor:  Róbinson Torres                                    --
--        Copyright 2005 Universidad Politécnica de Valencia                    --
--                                    Laboratorio integrado de Bioelectrónica     --
----------------------------------------------------------------------
-- Este programa sirve para controlar la frecuencia de oscilación de   --
-- de un oscilador controlado numéricamente NCO, por medio de una FPGA --

                                    --
-- Spartan II E, dentro del lazo de realimentación de un PLL que sirve --
-- para un sistema de Electrogravimetría AC                                                --
-- Entradas:
                                                --
--                        REF:                    Señal de referencia del PLL
                         --
--                        CLK_in:    Reloj externo del sistema (50 MHz)          --
--                        Reset_gen: Reset externo de todo el sistema (pulsador)          --
-- Salidas:
                                 --
--                        W_CLK:   Pulsos para cargar cada uno de lo WX                   --
--                        FQ_UD:   Pulso necesario ara cargar todos los W al        --
--                                                Registro de configuración del NCO          --
--                        Reset_nco:Reset general del NCO                    --
--                        Data_nco: W0 hasta W4, bits de programación del NCO       --
--                        led_nco:   Indica cuando se programó el NCO
--
--                        led_pll:    Indica cuando está "desenganchado" el PLL     --
--                        CLK_out: Mapeo del reloj interno hacia el exterior          --
--                        LDG:                    Hailita led de la placa DIO4
                         --
------        LEDS:     Leds de prueba de la palabra digital de salida          --
----------------------------------------------------------------------
-- Historial:
                                --
```

```
--            11/10/2005(RT): Creación
                        --
--            21/03/2006(RT): Depuración y pruebas
--            10/02/2007(RT): Ajustes finales                    --
----------------------------------------------------------------------------

library IEEE;
use IEEE.STD_LOGIC_1164.ALL;
use IEEE.STD_LOGIC_ARITH.ALL;
use IEEE.STD_LOGIC_UNSIGNED.ALL;

--  Uncomment the following lines to use the declarations that are
--  provided for instantiating Xilinx primitive components.
--library UNISIM;
--use UNISIM.VComponents.all;

entity main is
   Port ( REF : in std_logic;
          CLK_in : in std_logic;
          Reset_gen : in std_logic;
          W_CLK : out std_logic;
          FQ_UD : out std_logic;
          Reset_nco : out std_logic;
          Data_nco : out std_logic_vector(7 downto 0);
          led_nco : out std_logic;
          led_pll : out std_logic;
          CLK_out : out std_logic;
                    LDG : out std_logic;
                    LEDS : out std_logic_vector(7 downto 0));
end main;

architecture Behavioral of main is

----------------------------------------------------------------------------
--                                                  Declaración de componentes
                    --
----------------------------------------------------------------------------

----------------------------------------------------------------------------
-- maq_estado : Se define una máquina de estados para controlar las    --
-- transiciones de todo el sistema, es decir, la medición de la                --
-- frecuencia de la señal de REF y la carga de los registros W0 hasta  --
-- W4 en el NCO, con el fin de programarlo a una determinada                   --
-- frecuencia.
                                                --
-- Entradas:
                                                --
--                    CLK:              Reloj de salida del DCM (50 o 100 MHz.)          --
--                    RESETGEN:         Reset externo de todo el sistema (pulsador)      --
--                    QCA:              Salida del contador auxiliar
          --
--                    status_MED:Indica cuando MEDICIÓN actualizó la Frec de salida--
--                    c_frec:     Indica si se debe cambiar la frec del NCO          --
--                    mux_out:    Salida del multiplexor
                     --
-- Salidas:
```

```
                                --
--                      clkenable_contaux:  Habilita contador auxiliar                  --
--                      inic_contaux:       Inicialización en cero del contador auxiliar  --
--                      clkenable_mux:      Habilita el multiplexor
                         --
--                      SEL:                Bits de selección de salida del multiplexor    --
--                      h_MED:              Habilita MEDICIÓN
                         --
------  i_SAR:                  Inicializa el SAR
            --
--                      W_CLK:              Pulsos para cargar cada uno de los WX           --
--                      FQ_UD:              Pulso necesario ara cargar todos los W al     --
--                                                  Registro de configuración del NCO       --
--                      RESET:              Reset general del NCO                 --
--                      led_nco:            Indica cuando se programó el NCO
            --
--                      led_pll:            Indica cuando está "desenganchado" el PLL     --
--                      LEDS:               Leds de prueba dela palabra digital de salida --
-------------------------------------------------------------------------
component maq_estado
            Port ( CLK : in std_logic;
        RESETGEN : in std_logic;
        QCA : in std_logic_vector(3 downto 0);
        status_MED : in std_logic;
                        c_frec :  in std_logic;
                        mux_out : in std_logic_vector(7 downto 0);
        clkenable_contaux : out std_logic;
        inic_contaux : out std_logic;
        clkenable_mux : out std_logic;
        SEL : out std_logic_vector(2 downto 0);
        h_MED : out std_logic;
        W_CLK : out std_logic;
        FQ_UD : out std_logic;
        RESET : out std_logic;
        led_nco : out std_logic;
        led_pll : out std_logic;
                        LEDS : out std_logic_vector(7 downto 0));

end component;

-------------------------------------------------------------------------
-- medicion : Sirve para buscar la frecuencia a programar en el NCO a  --
-- partir de la medición de la frecuecia de referencia y comparándola          --
-- con una frecuencia almacenada, que corresponde a la frecuencia              --
-- central del PLL la última vez que esuvo enganchado. Como valor              --
-- se porgramará en 10 MHz.
                         --
-- Entradas:
                                        --
--                      CLK:                        Reloj de salida del DCM (50 o 100 MHz.)
            --
--                      RESET:              Reset externo de todo el sistema (pulsador)   --
--                      h_MED:              Habilita la medición
            --
--                      Q_REF:              Valor de frecuencia de la señal de REF          --
--                      fin_con1:           Marca el final del contador 1       (Base de Tpo.)          --
```

```
--                      fin_mult:  Bandera que indica fin de multiplicación          --
-- Salidas:
                                --
--                      WX:                         Salida de frecuencia para programar NCO
            --
--                      status_MED:Indica cuando MEDICIÓN actualizó la Frec de salida--
--                      inic_cont1:         Inicializa el contador 1      (Base de tiempo)    --
--                      start_cont1:        Habilita el contador 1
            --
--                      inic_cont2:         Inicializa el contador 2      (Conteo de REF)     --
--                      start_cont2:        Habilita    el contador 2
                         --
--                      c_frec:    Indica si se debe cambiar la frec del NCO          --
--                      e_mult:    Habilitación del multiplicador                     --
----------------------------------------------------------------------------
component medicion
Port ( CLK : in std_logic;
       RESET : in std_logic;
       h_MED : in std_logic;
              Q_REF : in std_logic_vector(19 downto 0);
       fin_con1 : in std_logic;
       WX : out std_logic_vector(31 downto 0);
       status_MED : out std_logic;
       inic_cont1 : out std_logic;
       start_cont1 : out std_logic;
       inic_cont2 : out std_logic;
       start_cont2 : out std_logic;
                      c_frec :  out std_logic);
end component;

----------------------------------------------------------------------------
-- contador1:Sirve para contar 50 pulsos de reloj principal(50o100 MHz)--
-- con lo cual se tendrá una resolución de 1 MHz para la medición de          --
-- la frecuencia central de la señal de referencia.                           --
                                                                              --
-- Entradas:
                                        --
--                      CLK:                Reloj de entrada al contador (CLK_dcm)      --
--                      CE:                 Habilitación del contador
                         --
--                      INIT:      Pulso de inicialización del contador con valor      --
--                                          predefinido de cero
                                                --
-- Salidas:
                                --
--                      fin_con1:  Marca el final del contador1(Base de Tpo.50 pulsos)--
----------------------------------------------------------------------------
component contador1
Port ( CLK : in std_logic;
       CE : in std_logic;
                      INIT : in std_logic;
       fin_con1 : out std_logic);
end component;

----------------------------------------------------------------------------
-- contador2:Sirve para contar el número de pulsos de la señal de REF  --
```

```
-- como máximo serán 10 pulsos dado que la resolición del sistema es   --
-- 1 MHz para la medición de la frecuencia central                      --
                                                                        --
-- Entradas:
                                                --
--                      CLK:            Reloj de entrada al contador (REF)
                --
--                      CE:             Habilitación del contador
                 --
--                      INIT:       Pulso de inicialización del contador con valor      --
--                                  predefinido de cero
                                --
-- Salidas:
                                --
--                      Q:              Salida del contador (Número de pulsos Q_REF)
--
----------------------------------------------------------------------
component contador2
Port ( CLK : in std_logic;
       CE : in std_logic;
       INIT : in std_logic;
       Q : inout std_logic_vector(19 downto 0));
end component;

----------------------------------------------------------------------
-- cont_aux : Sirve para contar algunos pulso de reloj necesarios para --
-- el reset del NCO. Entrega una señal cuando van 5 pulsos del reloj    --
-- del reloj principal y otra cuando van once.                          --

--
-- Los cinco ciclos sirven para controlar el tiempo que el reset del   --
-- NCO y los once ciclos controlan el tiempo de latencia total del NCO --
-- tras el reset. A partir de esos once ciclos se puede empezar a       --
-- programar cada uno de los WX.
-- Entradas:
                                                --
--                      CLK:            Reloj de entrada al contador (CLK_dcm)      --
--                      CE:             Habilitación del contador
                 --
--                      INIT:       Pulso de inicialización del contador con valor      --
--                                  predefinido de cero
                                                        --
-- Salidas:
                                --
--                      Q:              Salida del contador auxiliar
                --
----------------------------------------------------------------------
component cont_aux
Port ( CLK : in std_logic;
                        RESET: in std_logic;
       CE : in std_logic;
       INIT : in std_logic;
       Q : inout std_logic_vector(3 downto 0));
end component;
----------------------------------------------------------------------
-- multiplexor : Se define un multiplexor de buses de datos de ocho    --
```

```
-- bits para determinar cuál de las palabras WX se cargará en un       --
-- momento dado al bus de datos del NCO. Este mux es controlado por la --
-- máquina de estados.
                                        --
-- Entradas:
                                                --
--                      MA:                Entrada W0
                                                --
--                      MB:                Entrada W1, se conecta a los 8 bits MSB WX        --
--                      MC:                Entrada W2, se conecta a los bits 23 a 16 de WX   --
--                      MD:                Entrada W3, se conecta a los bits 15 a 8 de WX    --
--                      ME:                Entrada W4, se conecta a los bits 7 a 0 de WX     --
--                      SEL:               Bits de selección de salida, se conectan a la maq --
--                      CLK:               Reloj de salida del DCM (50 o 100 MHz.)                  --
-- Salidas:
                                        --
--                      DATA:    Salida de ocho bits para el bus de datos del NCO  --
--------------------------------------------------------------------------------
component multiplexor
   Port ( CLK : in std_logic;
                        RESET : in std_logic;
                        CE : in std_logic;
                        W0 : in std_logic_vector(7 downto 0);
        W1 : in std_logic_vector(7 downto 0);
        W2 : in std_logic_vector(7 downto 0);
        W3 : in std_logic_vector(7 downto 0);
        W4 : in std_logic_vector(7 downto 0);
        SEL : in std_logic_vector(2 downto 0);
        DATA : out std_logic_vector(7 downto 0));
end component;


--------------------------------------------------------------------------------
--                                                      Declaración de señales
                        --
--------------------------------------------------------------------------------

signal QCA : std_logic_vector (3 downto 0);--Salida contador auxiliar  --
signal status_MED : std_logic;   -- Indica el estado de medicion     --
signal clkenable_contaux : std_logic;                   -- Habilita contaux                  --
signal inic_contaux : std_logic;                        -- Inicializa cont_aux  --
signal clkenable_mux: std_logic;-- Activa el mux con un alto                  --
signal SEL_mux : std_logic_vector(2 downto 0);-- sel de bus a salir    --
signal h_MED : std_logic;                       -- Habilita medicion                         --
signal Q_REF : std_logic_vector (19 downto 0);-- Salida contador 2      --
signal fin_con1 : std_logic;                    -- final del contador 1 (50 pulsos) --
signal WX : std_logic_vector (31 downto 0); -- Salida medicion Freq              --
signal inic_cont1 : std_logic;                          -- Inicializa contador 1             --
signal start_cont1 : std_logic;                         -- Habilita contador 1  --
signal inic_cont2 : std_logic;                          -- Inicializa contador 2             --
signal start_cont2 : std_logic;                         -- Habilita contador 2  --
signal w0 : std_logic_vector(7 downto 0):= "00000001";-- config el 6X  --
signal mux_out: std_logic_vector(7 downto 0);           -- auxiliar de DATA  --
signal c_frec :  std_logic;             -- Indica si se cambia la frec     --

--------------------------------------------------------------------------------
```

```
--                                                      Implementación del programa
                        --
-------------------------------------------------------------------------

begin
-------------------------------------------------------------------------
--                                                      Instancias de componentes
                        --
-------------------------------------------------------------------------
maquina_de_estados: maq_estado
                        port map (
                                        CLK => CLK_in,
                                        RESETGEN => Reset_gen,
                                        QCA => QCA,
                                        status_MED => status_MED,
                                        c_frec => c_frec,
                                        mux_out => mux_out,
                                        clkenable_contaux => clkenable_contaux,
                                        inic_contaux => inic_contaux,
                                        clkenable_mux => clkenable_mux,
                SEL => SEL_mux,
                                        h_MED => h_MED,
                                        W_CLK => W_CLK,
                FQ_UD => FQ_UD,
                RESET => Reset_nco,
                                        led_nco => led_nco,
                                        led_pll => led_pll,
                                        LEDS => LEDS);
medicion_frec: medicion
                        port map (
                                        CLK => CLK_in,
                                        RESET => Reset_gen,
                                        h_MED => h_MED,
                                        Q_REF => Q_REF,
                                        fin_con1 => fin_con1,
                                        WX => WX,
                                        status_MED => status_MED,
                                        inic_cont1 => inic_cont1,
                                        start_cont1 => start_cont1,
                                        inic_cont2 => inic_cont2,
                                        start_cont2 => start_cont2,
                                        c_frec => c_frec);

contador_base: contador1
                        port map (
                                        CLK => CLK_in,
                                        CE => start_cont1,
                                        INIT => inic_cont1,
                                        fin_con1 => fin_con1);

contador_referencia: contador2
                        port map (
                                        CLK => REF,
                                        CE => start_cont2,
                                        INIT        => inic_cont2,
                                        Q => Q_REF);
```

```
contador_auxiliar: cont_aux
                        port map (
                                CLK => CLK_in,
                                RESET => Reset_gen,
                                CE => clkenable_contaux,
                                INIT => inic_contaux,
                                Q => QCA);

mux : multiplexor
                        port map (
                                CLK => CLK_in,
                                RESET => Reset_gen,
                                CE  => clkenable_mux,
                                W0 => w0,
                                W1 => WX(31 downto 24),
                                W2 => WX(23 downto 16),
                                W3 => WX(15 downto 8),
                                W4 => WX(7 downto 0),
                                SEL => SEL_mux,
                                DATA => mux_out);


Data_nco <= mux_out;            -- Salida de datos para el NCO
----CLK_out <= CLK_in; -- Saca el reloj interno
CLK_out <= REF; -- Saca el reloj externo
LDG <= '1';             -- Sirve para habilitar los buffer de leds en la DIO4   --


end Behavioral;

----------------------------------------------------------------------------------------------
-- count_aux.vhd   --

library IEEE;
use IEEE.STD_LOGIC_1164.ALL;
use IEEE.STD_LOGIC_ARITH.ALL;
use IEEE.STD_LOGIC_UNSIGNED.ALL;

--  Uncomment the following lines to use the declarations that are
--  provided for instantiating Xilinx primitive components.
--library UNISIM;
--use UNISIM.VComponents.all;

entity cont_aux is
   Port ( CLK : in std_logic;
                        RESET: in std_logic;
          CE : in std_logic;
          INIT : in std_logic;
          Q : inout std_logic_vector(3 downto 0));
end cont_aux;

architecture Behavioral of cont_aux is

begin
             process (CLK, RESET, CE, INIT)
```

```
            begin
              if (INIT='1' or RESET='1') then
                Q <= "0000";
              elsif CLK='1' and CLK'event then
                if CE='1' then
                                Q <= Q + 1;
                end if;
              end if;
            end process;
end Behavioral;

----------------------------------------------------------------------------------------------
-- contador1.vhd --

library IEEE;
use IEEE.STD_LOGIC_1164.ALL;
use IEEE.STD_LOGIC_ARITH.ALL;
use IEEE.STD_LOGIC_UNSIGNED.ALL;

--  Uncomment the following lines to use the declarations that are
--  provided for instantiating Xilinx primitive components.
--library UNISIM;
--use UNISIM.VComponents.all;

entity contador1 is
   Port ( CLK : in std_logic;
          CE : in std_logic;
                        INIT : in std_logic;
          fin_con1 : out std_logic);
end contador1;

architecture Behavioral of contador1 is
-----signal Q : std_logic_vector(5 downto 0) := "000000";
signal Q : std_logic_vector(19 downto 0) := x"00000";

begin
            process (CLK, CE, INIT,Q)
            begin
                        -----if (Q = "110001") then
                        if (Q = x"7A11F") then              --499999 pulsos
                                    fin_con1 <= '1';
                    else
                                    fin_con1 <= '0';
                        end if;
                        if INIT='1' then
                        -----Q <= "000000";
                                    Q <= x"00000";
                    elsif CLK='1' and CLK'event then
                        if CE='1' then
                                                Q <= Q + 1;
                        end if;
                        end if;
            end process;

end Behavioral;
```

```
----------------------------------------------------------------------------
-- contador2-vhd --

library IEEE;
use IEEE.STD_LOGIC_1164.ALL;
use IEEE.STD_LOGIC_ARITH.ALL;
use IEEE.STD_LOGIC_UNSIGNED.ALL;

--  Uncomment the following lines to use the declarations that are
--  provided for instantiating Xilinx primitive components.
--library UNISIM;
--use UNISIM.VComponents.all;

entity contador2 is
   Port ( CLK : in std_logic;
          CE : in std_logic;
          INIT : in std_logic;
          Q : inout std_logic_vector(19 downto 0));
end contador2;

architecture Behavioral of contador2 is

begin
                process (CLK, CE, INIT)
                begin
                  if INIT='1' then
                    Q <= x"00000";
                  elsif CLK='1' and CLK'event then
                    if CE='1' then
                                        Q <= Q + 1;
                    end if;
                  end if;
                end process;

end Behavioral;

----------------------------------------------------------------------------------------------------
-- maq_estado.vhd --

library IEEE;
use IEEE.STD_LOGIC_1164.ALL;
use IEEE.STD_LOGIC_ARITH.ALL;
use IEEE.STD_LOGIC_UNSIGNED.ALL;

--  Uncomment the following lines to use the declarations that are
--  provided for instantiating Xilinx primitive components.
--library UNISIM;
--use UNISIM.VComponents.all;

entity maq_estado is
   Port ( CLK : in std_logic;
          RESETGEN : in std_logic;
          QCA : in std_logic_vector(3 downto 0);
          status_MED : in std_logic;
                        c_frec :  in std_logic;
                        mux_out : in std_logic_vector(7 downto 0);
```

```
        clkenable_contaux : out std_logic;
        inic_contaux : out std_logic;
        clkenable_mux : out std_logic;
        SEL : out std_logic_vector(2 downto 0);
        h_MED : out std_logic;
        W_CLK : out std_logic;
        FQ_UD : out std_logic;
        RESET  : out std_logic;
        led_nco : out std_logic;
        led_pll : out std_logic;
                        LEDS : out std_logic_vector(7 downto 0));
end maq_estado;

architecture Behavioral of maq_estado is

signal estado : std_logic_vector (4 downto 0);          -- estado actual     --
signal est_sig : std_logic_vector (4 downto 0);         -- estado siguiente  --
signal W_CLK_aux : std_logic; -- W_CLK registrado                                    --
signal FQ_UD_aux : std_logic; -- FQ_UD registrado                                    --
signal RESET_aux : std_logic; -- RESET registrado                                    --
signal h_MED_aux : std_logic; -- h_MED registrado                                    --
signal clkenable_contaux_aux : std_logic;-- clkenable_contaux registrado-
signal inic_contaux_aux : std_logic; -- inic_contaux registrado                --
signal clkenable_mux_aux : std_logic; -- clkenable_mux registrado              --
signal led_pll_aux: std_logic; -- led_pll registrado                                      --
signal led_pll_aux2: std_logic; -- led_pll registrado                                     --

constant S0 : std_logic_vector (4 downto 0) := "00000";
constant S1 : std_logic_vector (4 downto 0) := "00001";
constant S2 : std_logic_vector (4 downto 0) := "00010";
constant S3 : std_logic_vector (4 downto 0) := "00011";
constant S4 : std_logic_vector (4 downto 0) := "00100";
constant S5 : std_logic_vector (4 downto 0) := "00101";
constant S6 : std_logic_vector (4 downto 0) := "00110";
constant S7 : std_logic_vector (4 downto 0) := "00111";
constant S8 : std_logic_vector (4 downto 0) := "01000";
constant S9 : std_logic_vector (4 downto 0) := "01001";
constant S10 : std_logic_vector (4 downto 0) := "01010";
constant S11 : std_logic_vector (4 downto 0) := "01011";
constant S12 : std_logic_vector (4 downto 0) := "01100";
constant S13 : std_logic_vector (4 downto 0) := "01101";
constant S14 : std_logic_vector (4 downto 0) := "01110";
constant S15 : std_logic_vector (4 downto 0) := "01111";


begin
        process (CLK,RESETGEN,est_sig)
        begin
                if (RESETGEN = '1') then
                        estado <= S0;
                        W_CLK <= '0';           -- No envía pulsos al NCO
                        FQ_UD <= '0';
                        RESET <= '1';           -- Envía Reset al NCO
                        h_MED <= '0';           -- Deshabilita medición de frec
                        clkenable_contaux <= '1';   -- Habilita contador auxiliar
                        inic_contaux <= '0'; -- Inicializa contador auxiliar
```

```
                                clkenable_mux <= '0'; -- Deshabilita salida del mux
----                            SEL <= "000";           -- Preselecciona entrada de W0
                                led_pll <= '0';
                                led_pll_aux <= '0';
                        elsif (CLK ='1' and CLK'event)then
                                estado <= est_sig;
                                W_CLK <= W_CLK_aux;
                                FQ_UD <= FQ_UD_aux;
                                RESET <= RESET_aux;
                                h_MED <= h_MED_aux;
                                clkenable_contaux <= clkenable_contaux_aux;
                                inic_contaux <= inic_contaux_aux;
                                clkenable_mux <= clkenable_mux_aux;
----                            SEL <= SEL_aux;
                                led_pll <= led_pll_aux;
                                led_pll_aux <= led_pll_aux2;

                        end if;
                end process;
process (estado,QCA,status_MED,c_frec,mux_out,led_pll_aux)

                begin

                        est_sig <= estado;      -- Toma como valor predefinido el actual --

                        case    estado is
                                when S0 =>              -- Entra en estado de reset para el NCO  --
                                        clkenable_contaux_aux <= '0';
                                        inic_contaux_aux <= '1';
                                        h_MED_aux <= '0';
                                        W_CLK_aux <= '0';
                                        FQ_UD_aux <= '0';
                                        RESET_aux <= '1';
                                        led_nco <= '1'; -- Enciendo sólo para ver estado de reset
                                        led_pll_aux2 <= '1'; -- Indica PLL desenganchado
                                        clkenable_mux_aux <= '0';
                                        LEDS <= "00000000";
                                        SEL <= "000";
                                        est_sig <= S1;
                                when S1 =>              -- Reset del NCO por 11 ciclos de 50 MHz --
                                        if (QCA > "0101")then  -- 5 ciclos en alto y 6 en bajo
                                                RESET_aux <= '0';-- Cambia el estado a bajo -
-
                                                led_nco <= '0';         -- Apago el reset
                --
                                        else
                                                RESET_aux <= '1';-- Deja el reset como está --
                                                led_nco <= '1';
                                        end if;
                                        clkenable_contaux_aux <='1';
                                        inic_contaux_aux <='0';
                                        h_MED_aux <= '0';
                                        W_CLK_aux <= '0';
                                        FQ_UD_aux <= '0';
                                        led_pll_aux2 <= '0'; -- Indica PLL enganchado
                                        clkenable_mux_aux <= '1';
```

```
                    LEDS <= "00000000";
                    SEL <= "000";
                    if (QCA >= "1011")then
                              est_sig <= S2;
                    else
                              est_sig <= S1;
                    end if;
          when S2 =>          -- Carga W0 en el reg. de conf del NCO   --
                    clkenable_contaux_aux <='0';
                    inic_contaux_aux <='1';
                    h_MED_aux <= '0';
                    W_CLK_aux <= '1';
                    FQ_UD_aux <= '0';
                    RESET_aux <= '0';
                    led_nco <= '1'; -- Muestra pulso de W_CLK
                    led_pll_aux2 <= '1'; -- Indica PLL desenganchado
                    clkenable_mux_aux <= '1';
                    SEL <= "000";
                    LEDS <= "00000001";
                    est_sig <=S3;
          when S3 =>
                    clkenable_contaux_aux <='0';
                    inic_contaux_aux <='0';
                    h_MED_aux <= '0';
                    W_CLK_aux <= '0';
                    FQ_UD_aux <= '0';
                    RESET_aux <= '0';
                    led_nco <= '0';
                    led_pll_aux2 <= '1'; -- Indica PLL desenganchado
                    clkenable_mux_aux <= '1';
                    SEL <= "001";
                    LEDS <= "00000000";
                    est_sig <= S4;
          when S4 =>          -- Carga W1 en el reg. de conf del NCO   --
                    clkenable_contaux_aux <='0';
                    inic_contaux_aux <='0';
                    h_MED_aux <= '0';
                    W_CLK_aux <= '1';
                    FQ_UD_aux <= '0';
                    RESET_aux <= '0';
                    led_nco <= '1';
                    led_pll_aux2 <= '1'; -- Indica PLL desenganchado
                    clkenable_mux_aux <= '1';
                    SEL <= "001";
                    LEDS <= mux_out;
                    est_sig <= S5;
          when S5 =>
                    clkenable_contaux_aux <='0';
                    inic_contaux_aux <='0';
                    h_MED_aux <= '0';
                    W_CLK_aux <= '0';
                    FQ_UD_aux <= '0';
                    RESET_aux <= '0';
                    Led_nco <= '0';
                    led_pll_aux2 <= '1';
                    clkenable_mux_aux <= '1';
```

```
                SEL <= "010";
                LEDS <= "00000000";
                est_sig <= S6;
        when S6 =>              -- Carga W2 en el reg. de conf del NCO   --
                clkenable_contaux_aux <='0';
                inic_contaux_aux <='0';
                h_MED_aux <= '0';
                W_CLK_aux <= '1';
                FQ_UD_aux <= '0';
                RESET_aux <= '0';
                led_nco <= '1';
                led_pll_aux2 <= '1';
                clkenable_mux_aux <= '1';
                SEL <= "010";
                LEDS <= mux_out;
                est_sig <= S7;
        when S7 =>
                clkenable_contaux_aux <='0';
                inic_contaux_aux <='0';
                h_MED_aux <= '0';
                W_CLK_aux <= '0';
                FQ_UD_aux <= '0';
                RESET_aux <= '0';
                led_nco <= '0';
                led_pll_aux2 <= '1';
                clkenable_mux_aux <= '1';
                SEL <= "011";
                LEDS <= "00000000";
                est_sig <= S8;
        when S8 =>              -- Carga W3 en el reg. de conf del NCO   --
                clkenable_contaux_aux <='0';
                inic_contaux_aux <='0';
                h_MED_aux <= '0';
                W_CLK_aux <= '1';
                FQ_UD_aux <= '0';
                RESET_aux <= '0';
                led_nco <= '1';
                led_pll_aux2 <= '1';
                clkenable_mux_aux <= '1';
                SEL <= "011";
                LEDS <= mux_out;
                est_sig <= S9;
        when S9 =>
                clkenable_contaux_aux <='0';
                inic_contaux_aux <='0';
                h_MED_aux <= '0';
                W_CLK_aux <= '0';
                FQ_UD_aux <= '0';
                RESET_aux <= '0';
                led_nco <= '0';
                led_pll_aux2 <= '1';
                clkenable_mux_aux <= '1';
                SEL <= "100";
                LEDS <= "00000000";
                est_sig <= S10;
        when S10 =>             -- Carga W4 en el reg. de conf del NCO   --
```

```
                clkenable_contaux_aux <='0';
                inic_contaux_aux <='0';
                h_MED_aux <= '0';
                W_CLK_aux <= '1';
                FQ_UD_aux <= '0';
                RESET_aux <= '0';
                led_nco <= '1';
                led_pll_aux2 <= '1';
                clkenable_mux_aux <= '1';
                SEL <= "100";
                LEDS <= mux_out;
                est_sig <= S11;
        when S11 =>
                clkenable_contaux_aux <='0';
                inic_contaux_aux <='0';
                h_MED_aux <= '0';
                W_CLK_aux <= '0';
                FQ_UD_aux <= '0';
                RESET_aux <= '0';
                led_nco <= '0';
                led_pll_aux2 <= '1';
                clkenable_mux_aux <= '1';
                SEL <= "000";
                LEDS <= "00000000";
                est_sig <= S12;
        when S12 =>             -- Pulso FQ_UD para actualizar reg compl --
                clkenable_contaux_aux <='0';
                inic_contaux_aux <='0';
                h_MED_aux <= '0';
                W_CLK_aux <= '0';
                FQ_UD_aux <= '1';
                RESET_aux <= '0';
                led_nco <= '1';
                led_pll_aux2 <= '1';
                clkenable_mux_aux <= '0';
                SEL <= "000";
                LEDS <= "00000000";
                est_sig <= S13;
        when S13 =>
                clkenable_contaux_aux <='0';
                inic_contaux_aux <='0';
                h_MED_aux <= '0';
                W_CLK_aux <= '0';
                FQ_UD_aux <= '0';
                RESET_aux <= '0';
                led_nco <= '1';         -- Indica NCO programado
                led_pll_aux2 <= '1';
                clkenable_mux_aux <= '0';
                SEL <= "000" ;
                LEDS <= "00000000";
                est_sig <= S14;
        when S14 =>             -- Aquí se habilita medicion
                clkenable_contaux_aux <='0';
                inic_contaux_aux <='0';
                h_MED_aux <= '1'; -- Habilita el medicion para procesar
--
```

```
                                        W_CLK_aux <= '0';
                                        FQ_UD_aux <= '0';
                                        RESET_aux <= '0';
                                        led_nco <= '1';
                                        led_pll_aux2 <= led_pll_aux;
                                        clkenable_mux_aux <= '1';
                                        SEL <= "000" ;
                                        LEDS <= "10000001";             -- Espera inicio de
medicion
                                        if (status_MED  = '0')then -- Espera inicio de medicion
                                                est_sig <= S14;
                                        else
                                                est_sig <= S15;
                                        end if;
                                when S15 =>
                                        clkenable_contaux_aux <='0';
                                        inic_contaux_aux <='0';
                                        h_MED_aux <= '0';
                                        W_CLK_aux <= '0';
                                        FQ_UD_aux <= '0';
                                        RESET_aux <= '0';
                                        led_nco <= '0';
                                        clkenable_mux_aux <= '1';
                                        SEL <= "000" ;
                                        LEDS <= "11111111";             -- Espera final de
medicion
                                        if (status_MED  = '1')then --Espera final de medicion--
                                                est_sig <= S15;
                                                led_pll_aux2 <= led_pll_aux;
                                        elsif (status_MED  = '0' and c_frec = '1')then -- Espera
orden de cambio de frec
                                                est_sig <= S2;
                                                led_pll_aux2 <= '1';
                                        elsif (status_MED  = '0' and c_frec = '0')then
                                                est_sig <= S14;
                                                led_pll_aux2 <=         '0';
                                        else                                            -- si es un
estado ambiguo, reset
                                                est_sig <= S0;
                                                led_pll_aux2 <= '0';
                                        end if;

                                when others =>
                                        clkenable_contaux_aux <= '0';
                                        inic_contaux_aux <= '0';
                                        SEL <= "000";
                                        h_MED_aux <= '0';
                                        W_CLK_aux <= '0';
                                        FQ_UD_aux <= '0';
                                        RESET_aux <= '0';
                                        led_nco <= '0';
                                        led_pll_aux2 <= '1';
                                        clkenable_mux_aux <= '0';
                                        LEDS <= "00000000";
                                        est_sig <= S0;
                        end case;
```

```
            end process;
end Behavioral;

----------------------------------------------------------------------------------------------------------------
-- medicion.vhd --

library IEEE;
use IEEE.STD_LOGIC_1164.ALL;
use IEEE.STD_LOGIC_ARITH.ALL;
use IEEE.STD_LOGIC_SIGNED.ALL;

--  Uncomment the following lines to use the declarations that are
--  provided for instantiating Xilinx primitive components.
--library UNISIM;
--use UNISIM.VComponents.all;

entity medicion is
   Port ( CLK : in std_logic;
        RESET : in std_logic;
        h_MED : in std_logic;
                Q_REF : in std_logic_vector(19 downto 0);
        fin_con1 : in std_logic;
        WX : out std_logic_vector(31 downto 0);
        status_MED : out std_logic;
        inic_cont1 : out std_logic;
        start_cont1 : out std_logic;
        inic_cont2 : out std_logic;
        start_cont2 : out std_logic;
                        c_frec :  out std_logic);

end medicion;

architecture Behavioral of medicion is

signal estados : std_logic_vector (2 downto 0);             -- estado actual     --
signal pro_est : std_logic_vector (2 downto 0);             -- estado siguiente  --
--signal frec_out: std_logic_vector (31 downto 0):=x"26666666";--aux de WX--
signal frec_out: std_logic_vector (31 downto 0):=x"2EEEEEEE";  --11MHz
signal frec_out_aux: std_logic_vector (31 downto 0):=x"2EEEEEEE"; -- 11MHz
signal status_MED_aux: std_logic;               -- Salida status_MED registrada  --
signal inic_cont1_aux: std_logic;               -- Salida inic_cont1 registrada      --
signal start_cont1_aux: std_logic;              -- Salida start_cont1 registrada     --
signal inic_cont2_aux: std_logic;               -- Salida inic_cont2 registrada      --
signal start_cont2_aux: std_logic;              -- Salida start_cont2 registrada     --
signal c_frec_aux: std_logic;       -- Salida c_frec registrada                                     --
signal c_frec_aux2: std_logic;     -- Salida c_frec registrada          2              --
signal resta: std_logic_vector (31 downto 0):=x"00000000";--dif de frec--
signal resta_aux: std_logic_vector (31 downto 0):=x"00000000";--resta reg--
signal multi: std_logic_vector (35 downto 0):= x"000000000";--aux multi--
signal multi_aux: std_logic_vector (35 downto 0):= x"000000000";--aux multi--


constant S0 : std_logic_vector (2 downto 0) := "000";
constant S1 : std_logic_vector (2 downto 0) := "001";
constant S2 : std_logic_vector (2 downto 0) := "010";
constant S3 : std_logic_vector (2 downto 0) := "011";
```

```
constant S4 : std_logic_vector (2 downto 0) := "100";
constant S5 : std_logic_vector (2 downto 0) := "101";
constant S6 : std_logic_vector (2 downto 0) := "110";
constant S7 : std_logic_vector (2 downto 0) := "111";



begin

        process (CLK,RESET,pro_est)
        begin
                if (RESET = '1') then           --Inicialización de variables      --

                        estados <= S0;
--                      frec_out <= x"26666666";            --Frec inicial de 9 MHz
aprox--
                        frec_out <= x"2EEEEEEE";            --Frec inicial de 11 MHz
aprox--
                        status_MED <= '0';
                        inic_cont1 <= '1';
                        start_cont1 <= '0';
                        inic_cont2 <= '1';
                        start_cont2 <= '0';
                        -----c_frec <= '0';
                        c_frec_aux <= '0';
                        resta <= x"00000000";
                        multi <= x"000000000";

                elsif (CLK ='1' and CLK'event)then       -- Registro de variables --
                        estados <= pro_est;
                        frec_out <= frec_out_aux;
                        status_MED <= status_MED_aux;
                        inic_cont1 <= inic_cont1_aux;
                        start_cont1 <= start_cont1_aux;
                        inic_cont2 <= inic_cont2_aux;
                        start_cont2 <= start_cont2_aux;
                -----   c_frec <= c_frec_aux;
                        c_frec_aux <= c_frec_aux2;
                        resta <= resta_aux;
                        multi <= multi_aux;
                end if;
        end process;
process (estados,h_MED,fin_con1,Q_REF,multi,frec_out,resta,c_frec_aux)
        begin
                pro_est <= estados;    -- Toma como valor predefinido el actual --

                case estados is
                        when S0 =>
--                              frec_out_aux <= x"26666666"; --Frec inicial a programar
9MHz      --
                                frec_out_aux <= x"2EEEEEEE"; --Frec inicial a
programar 11MHz     --
                                status_MED_aux <= '0';
                                inic_cont1_aux <= '1';
                                start_cont1_aux <= '0';
                                inic_cont2_aux <= '1';
```

```
                                        start_cont2_aux <= '0';
                                        -----c_frec_aux <= '0';
                                        c_frec_aux2 <= '0';
                                        resta_aux <= x"00000000";
                                        multi_aux <= multi;
                                        pro_est <= S1;
                                when S1 =>-- Aquí espera la autorización desde MEF ppal--
                                        frec_out_aux <= frec_out;
                                        status_MED_aux <= '0';
                                        inic_cont1_aux <= '1';
                                        start_cont1_aux <= '0';
                                        inic_cont2_aux <= '1';
                                        start_cont2_aux <= '0';
                                        -----c_frec_aux <= '0';
                                        c_frec_aux2 <= '0';
                                        resta_aux <= resta;
                                        multi_aux <= multi;
                                        if (h_MED = '1') then --Espera habilitación desde MEF--
                                                pro_est <= S2;
                                        else
                                                pro_est <= S1;
                                        end if;
                                when S2 =>              -- Habilito contadores
        --
                                        frec_out_aux <= frec_out;
                                        status_MED_aux <= '0';
                                        inic_cont1_aux <= '0';
                                        start_cont1_aux <= '1';
                                        inic_cont2_aux <= '0';
                                        start_cont2_aux <= '1';
                                        -----c_frec_aux <= '0';
                                        c_frec_aux2 <= '0';
                                        resta_aux <= resta;
                                        multi_aux <= multi;
                                        if (fin_con1 = '1') then--Espera fin del contador 1--
                                                pro_est <= S3;
                                        else
                                                pro_est <= S2;
                                        end if;

                                when S3 => --Deshabilito contadores y calculo nueva resta--
                                        frec_out_aux <= frec_out;
                                        status_MED_aux <= '0';
                                        inic_cont1_aux <= '0';
                                        start_cont1_aux <= '0';
                                        inic_cont2_aux <= '0';
                                        start_cont2_aux <= '0';
                                        ------c_frec_aux <= '0';
                                        c_frec_aux2 <= '0';
                                        --multi_aux <= "-"(x"45E7B272","*"(Q_REF,x"1BF6"));
--16,384 MHz-Q_REF*100Hz--
                                        multi_aux <= "*"(Q_REF,x"1BF6"); --16,384 MHz-
Q_REF*100Hz--
                                        resta_aux <= resta;
                                        pro_est <= S4;
```

```
                        when S4 => --Deshabilito contadores y calculo nueva resta--
                                frec_out_aux <= frec_out;
                                status_MED_aux <= '0';
                                inic_cont1_aux <= '0';
                                start_cont1_aux <= '0';
                                inic_cont2_aux <= '0';
                                start_cont2_aux <= '0';
                                ------c_frec_aux <= '0';
                                c_frec_aux2 <= '0';
                        --              multi_aux  <=  "-"(x"45E7B272",multi);  --16,384  MHz-
Q_REF*100Hz--
                                multi_aux  <=  "-"(x"45E77A86",multi);  --16,3838  MHz-
Q_REF*100Hz--
                                resta_aux <= resta;
                                pro_est <= S5;
                        when S5 =>--
                                frec_out_aux <= frec_out;
                                status_MED_aux <= '0';
                                inic_cont1_aux <= '0';
                                start_cont1_aux <= '0';
                                inic_cont2_aux <= '0';
                                start_cont2_aux <= '0';
                                -----c_frec_aux <= '0';
                                c_frec_aux2 <= '0';
                                multi_aux <= multi;
                                --if (frec_out >= multi(31 Downto 0)) then
                                if (">="(frec_out,multi(31 Downto 0))) then
                                        --resta_aux <= frec_out-multi(31 Downto 0);
                                        resta_aux  <=  "-"(frec_out,multi(31  Downto
0));
                                else
                                        --resta_aux <= multi(31 Downto 0)-frec_out;
                                        resta_aux      <=      "-"(multi(31      Downto
0),frec_out);
                                end if;
                                pro_est <= S6;
                        when S6 =>-- Decide si se programa una nueva frec o no          --
                        --if (resta >= x"00006FD9") then -- si dif > 400Hz       --
                        --if (">="(resta,x"0001179E")) then -- si dif > 1000Hz
                        --if (resta >= x"04444444") then -- si dif > 1MHz        --
                        --if (resta >= x"1BF64") then -- si dif > 1.6 KHz        --
                        if (">="(resta,x"22F3D")) then -- si dif > 2 KHz        --
                                        frec_out_aux <= multi(31 Downto 0);
                                        c_frec_aux2 <= '1';
                                else
                                        frec_out_aux <= frec_out;
                                        c_frec_aux2 <= '0';
                                end if;
                                inic_cont1_aux <= '0';
                                start_cont1_aux <= '0';
                                inic_cont2_aux <= '0';
                                start_cont2_aux <= '0';
                                status_MED_aux <= '1';
                                multi_aux <= multi;
                                resta_aux <= resta;
                                pro_est <= S7;
```

```
                                when S7 =>
                                        frec_out_aux <= frec_out;
                                        inic_cont1_aux <= '0';
                                        start_cont1_aux <= '0';
                                        inic_cont2_aux <= '0';
                                        start_cont2_aux <= '0';
                                        status_MED_aux <= '0';
                                        multi_aux <= multi;
                                        c_frec_aux2 <= c_frec_aux;
                                        resta_aux <= resta;
                                        if (h_MED = '1') then --Espera habilitación desde MEF--
                                                pro_est <= S7;
                                        else
                                                pro_est <= S1;
                                        end if;
                                when others =>
--                                      frec_out_aux <= x"26666666"; --Frec inicial a programar
9MHz
                                   frec_out_aux <= x"2EEEEEEE"; --Frec inicial a programar
11MHz      --
                                        --frec_out_aux <= frec_out;
                                        status_MED_aux <= '0';
                                        inic_cont1_aux <= '1';
                                        start_cont1_aux <= '0';
                                        inic_cont2_aux <= '1';
                                        start_cont2_aux <= '0';

            multi_aux <= x"000000000";-----             c_frec_aux <= '0';
                                        multi_aux <= x"000000000";
                                        c_frec_aux2 <= '0';
                                        resta_aux <= x"00000000";
                                        pro_est <= S0;
                        end case;
            end process;
            WX <= frec_out;
            c_frec <= c_frec_aux;
end Behavioral;

----------------------------------------------------------------------------------------------------------------
-- multilexor.vhd --

library IEEE;
use IEEE.STD_LOGIC_1164.ALL;
use IEEE.STD_LOGIC_ARITH.ALL;
use IEEE.STD_LOGIC_UNSIGNED.ALL;

--  Uncomment the following lines to use the declarations that are
--  provided for instantiating Xilinx primitive components.
--library UNISIM;
--use UNISIM.VComponents.all;

entity multiplexor is
   Port ( CLK : in std_logic;
                        RESET : in std_logic;
                        CE : in std_logic;
                        W0 : in std_logic_vector(7 downto 0);
```

```
        W1 : in std_logic_vector(7 downto 0);
        W2 : in std_logic_vector(7 downto 0);
        W3 : in std_logic_vector(7 downto 0);
        W4 : in std_logic_vector(7 downto 0);
        SEL : in std_logic_vector(2 downto 0);
        DATA : out std_logic_vector(7 downto 0));
end multiplexor;

architecture Behavioral of multiplexor is
----signal DATA_aux: std_logic_vector (7 downto 0);
begin
            process (CLK, RESET)
            begin
                        if RESET ='1' then
                                    DATA <= "ZZZZZZZZ";
                        elsif CLK'event and CLK ='1' then
                                    if CE ='1' then

                                                case SEL is
                                                            when "000" => DATA <= W0;
                                                when "001" => DATA <= W1;
                                                   when "010" => DATA <= W2;
                                                   when "011" => DATA <= W3;
                                                            when "100" => DATA <= W4;
                                                            when others => NULL;
                                      end case;
                                    elsif CE = '0' then
                                                DATA <= "ZZZZZZZZ";
                                    end if;
                        end if;
            end process;
----DATA <= DATA_aux;
end Behavioral;
-------------------------------------------------------------------------------------------------------------
```

References

[Agilent97] Agilent, T.: "Fundamentals of the Electronic Counters", *Electronic Counter Series.* AN 200, pp. 44, US. 1997.

[AlSana03] Al Sana, S., Gabrielli, C. Perrot, H.: "Influence of antibody insertion on the Electrochemical Behaviour of Polypyrrole Films by Using Fast QCM Measurements", *Journal of Electrochemical Society*, vol. 150, No. 9, pp. E444-E449, 2003.

[AlSana04] Al Sana, S., Gabrielli, C. Perrot, H.: "Rate Limitating steps of Charge Transfer at Conducting Polymers", *Russian Journal of Electrochemistry*, vol. 40, No. 3, pp. 267-272, 2004.

[Analog04] Analog, D.: "CMOS 180 MHz DDS/DAC synthesizer. AD9851", *Datasheet*. Rev. D, available online at www.analog.com. US, 2004.

[Arnau99] Arnau, A.: "El Cristal de Cuarzo como Sensor Microgravimétrico en Medios Amortiguados (TOMOS 1 y 2)", *Tesis Doctoral*, 1999.

[Arnau00-1] Arnau, A., Sogorb, T., Jiménez, Y.: "A Continuous Motional Series Resonant Frequency Monitoring Circuit and a New Method of Determining Butterworth-Van Dyke Parameters of a Crystal Microbalance in Fluid Media", *Rev. Sci. Instrum.*, vol. 71, nº 6, pp. 2563-2571, 2000.

[Arnau00-2] Arnau, A., Jiménez, Y., Sogorb, T.: "Thickness-Shear Mode Quartz Crystal Resonators in Viscoelastic Fluid Media", *J. Appl. Phys.*, vol. 88, nº 8, pp. 4498-4506, 2000.

[Arnau00-3] Arnau, A., Ferrero, J., Jiménez, Y., Sogorb, T.: "Sistemas electrónicos de comunicaciones II", *Ed. UPV*, Valencia, 2000. Cap 8-9.

[Arnau01-1] Arnau, A., Sogorb, T., Jiménez, Y.: "A New Method for Continuous Monitoring of Series Resonance Frequency and Simple Determination of Motional Impedance Parameters for

Loaded Quartz-Crystal Resonators", *IEEE Trans. Ultrason., Ferroelect. Freq. Contr*., vol. 48, nº 2, pp. 617-623, 2001.

[Arnau01-2] Arnau, A., Jiménez, Y., Sogorb, T.: "An Extended Butterworth-Van Dyke Model for Quartz Crystal Microbalance Applications in Viscoelastic Fluid Media", *IEEE Trans. Ultrason., Ferroelect. Freq. Contr*., vol. 48, nº 5, pp. 1367-1382, 2001.

[Arnau02] Arnau, A., Sogorb, T., Jiménez, Y.: "Circuit for Continuous Motional Series Resonant Frequency and Motional Resistance Monitoring of Quartz Crystal Resonators by Parallel Capacitance Compesation", *Rev. Sci. Instrum.*, vol. 73, nº 7, pp. 2724-2737, 2002.

[Arnau04] Arnau, A. Editors: "Piezoelectric Transducers and Applications", *Springer-Verlag, (Berlin). 1ª Ed 2004 (Cap. 1, 4, 12, 13, 11, 16, and appendix B).*

[Auge94] Auge, J., Hauptmann, P.: "Quartz-Crystal Microbalance Sensor in Liquids", *Sensors and Actuators B-Chemical*, vol. 19, nº 1-3, pp. 518-522, 1994.

[Auge95] Auge, J., Hauptmann, P.: "New Design for QCM Sensors in Liquids", *Sensors and Actuators B-Chemical*, vol. 24, nº 1-3, pp. 43-48, 1995.

[Bandey97] Bandey, H.L., Hillmann, A.R., Brown, M.J., Martin, S.J.: "Viscoelastic Characterization of Electroactive Polymer Films at Electrode/Solution Interface", *Faraday Discuss*, vol. 107, pp. 105-121, 1997.

[Beeley04] Beeley, J. M., Mills, C., Hammond, P.A., Glidle, J., Cooper, M., Wang, L., Cumming, D. R. S.: "All-digital interface ASIC for a QCM-based electronic nose", *Sensors and actuators B: Chemical*, vol. 103, issue 1-2, pp. 31-36, 2004.

[Behrends01] Behrends, R., Kaatze, U.: "A high frequency shear wave impedance spectrometer for low viscosity liquids", *Measurement Science and Technology*, vol. 12, pp. 519-524, 2001.

[Benito02] Benito, C., Gabrielli, C., García-Jareño, J.J., Keddam, M., Perrot, H., Vicente, F.: "Fast Three-Step Method for Shear Moduli Calculation from Quartz Crystal Resonator Measurements", *Electrochemistry Communications*, vol. 4, issue 8, pp. 613-619, 2002.

[Benje86] Benje, M., Eiermann, M., Pittermann, U., Weil, K.G.: "An Improved Quartz Microbalance. Applications to the

Electrocrystallization and Dissolution of Nickel", *Ber. Bunsenges. Phys. Chem.*, vol. 90, issue 5, pp. 435-439, 1986.

[Best05] Best, R.: "Phase-locked Loops, design and applications", *McGraw Hill (New York) 2005.*

[Bottom82] Bottom, V.E.: "Introduction to Quartz Crystal Unit Design", *Van Nostrand Reinhold Company (New York) 1982.*

[Bourkane88] Bourkane, S., Gabrielli, C., Keddam, M.: "Kinetic study of electrode processes by ac quartz electrogravimetry", *Electroanalytical Chemistry,* vol. 256, issue 2, pp. 471-475, December 1988.

[Bourkane89] Bourkane, S., Gabrielli, C., Keddam, M.: "Study of Electrochemical Phase Formation and Dissolution by ac Quartz Electrogravimetry", *Electrochimica Acta*, vol. 34, issue 8, pp. 1081-1092, 1989.

[Bruckenstein85] Bruckenstein, S., Shay, M.: "Experimental aspects of use of the quartz crystal microbalance in solution", *Electrochimica Acta*, vol. 30, issue 10, pp. 1295-1300, 1985.

[Buckin01] Buckin V., Kudryashov E.: "Ultrasonic Shear Wave Rheology of Weak Particle Gels", *Advances in Colloid and Interface Science*, vol. 89, nº 90, pp. 401-422, 2001.

[Buttry91] Buttry, D.A.: "The Quartz Crystal Microbalance as in situ tool in electrochemistry", In: Abruña, II.D. (ed.), Electrochemical interfaces: modern technique for in-situ interface characterization, VCII, 1991.

[Calvo97] Calvo, E.J., Etchenique, R., Barlett, P.N., Singhal, K., Santamaria, C.: "Quartz Crystal Impedance Studies at 10MHz of Viscoelastic Liquids and Films", *Faraday Discuss.*, vol. 107, pp. 141-157, 1997.

[Cady64] Cady, W.G.: "Piezoelectricity (An Introduction To The Theory And Applications Of Electromechanical Phenomena In Cristals)", *Dover Publication, Inc. (New York). 1ª Ed 1946, 2ª Ed 1964 (II Vols).*

[Cernosek98] Cernosek, R.W., Martin, S.J., Hillman, A.R., Bandey, H.L.: "Comparison of Lumped-Element and Transmision-Line Models for Thickness-Shear-Mode Quartz Resoantor Sensors", *IEEE Trans. Ultrason., Ferroelect., Freq. Contr.*, vol. 45, nº 5, pp. 1399-1407, 1998.

[Chagnard96] Charganrd, C., Gilbert, P., Watkins, A.N., Beeler, T., Paul, D.W.: "An electronic oscillator with automatic gain control:

EQCM applications", *Sensors and Actuators B*, vol. 32, issue 2, pp. 129-136, 1996.

[Coombs00] Coombs, C: "Electronic Instrument Handbook", *McGraw Hill Handbooks, USA. 1ª Ed 1972, 2ª Ed 1995, 3ª Ed 2000.*

[Coughlin93] Coughlin, R., Driscoll, F.: "Amplificadores operacionales y circuitos integrados lineales", *Prentice-Hall, México* 1993.

[Daikhin96] Daikhin, L., Urbakh, M.: "Effect of Surface Film Structure on the Quartz Crystal Microbalance Response in Liquids", *Langmuir*, vol. 12, pp. 6354-6360, 1996.

[Daikhin97] Daikhin, L., Urbakh, M.: "Influence of Surface Roughness on the Quartz Crystal Microbalance Response in a Solution", *Faraday Discuss*, vol. 107, pp. 27-38, 1997.

[Daikhin02] Daikhin, L., Gileadi, E., Katz, G., Tsionsky, V., Urbakh, M., Zagidulin, D.: "Influence of Roughness on the Admittance of the Quartz Crystal Microbalance Immersed in Liquids", *Anal. Chem.*, vol. 74, pp. 554-561, 2002.

[Digilent03] Digilent: "Digilent D2SB system board", *Reference manual datasheet*, available online at www.digilentinc.com. US, 2003.

[DiNatale00] Dinatale, C. et al.: "Electronic Nose and Electronic Tongue Integration for Improved Classification of Clinical and Food Samples", *Sens. Actuators B.*, vol. 64, 1-3, pp. 15-22, 2000.

[Edmonds80] Edmonds, T.E., West, T.S.: "A Quartz Crystal Piezoelectric Device for Monitoring Organic Gaseous Pollutants", *Analytica Chimica Acta*, vol. 117, pp 147-157, 1980.

[Edwards94] Edwards, V., Martin, S.: "Characterization of a thickness-shear mode quartz resonator with multiple nonpiezoelectric layers", *Journal od applied physics*, vol. 75, issue 3. pp 1319-1329, February 1994.

[Eichelbaum99] Eichelbaum, F., Borngräber, R., Schröder, J., Lucklum, R., Hauptmann, P.: "Interface Circuits for Quartz-Crystal-Microbalance Sensors", *Rev. Sci. Instrum.*, vol. 70, pp. 2537, 1999.

[Etchenique00] Etchenique, R., Brudny, V.L.: "Characterization of Porous Thin Films Using Quartz Crystal Shear Resonators", *Langmuir*, vol. 16, pp. 5064-5071, 2000.

[Ferrante94] Ferrante, F., Kipling, A.L., Thompson, M.: "Molecular Slip at the Solid-Liquid Interface of an Acoustic-Wave Sensor", *J. Appl. Phys.*, vol. 76, nº 6, pp 3448-3462, 1994.

[Ferrari00] Ferrari, V., Marioli, D., Taroni, A.: "Oscillator Circuit Configuration for Quartz-Crystal-Resonator Sensors Subject to Heavy Acoustic Load", *Electronics Letters*, vol. 36, nº 7, pp 601-612, 2000.

[Ferrari01] Ferrari, V., Marioli, D., Taroni, A.: "improving the accuracy and operating range of quartz microbalance sensors by a purposely designed oscillator circuit", *IEEE Transcactions on instrumentation and measurement,* vol. 50, issue 5 , pp 1119-1122, 2001.

[Fruböse93] Fruböse, C., Soares, D.M., Doblhofer, K.: "Impedance Analysis of the Quartz Micro-Balance Signal", *Berichte De Bunsen Gesellschaft Fur Physikalische Chemie,* vol. 97, nº 4, pp 475-478, 1993.

[Gabrielli99-1] Gabrielli, C., Keddam, M., Nadi, N., Perrot, H.: "a.c. Electrogravimetry on conductive polymers. Application to polyanilina", *Electrochimica Acta,* vol. 44, issue 12, pp. 2095-2103, January 1999.

[Gabrielli99-2] Gabrielli, C., Keddam, M., Perrot, H., Pham, M.C., Torresi, R.: "Separation of ionic and solvent transport during charge compensation processes in electroactive polymers by a.c. electrogravimetry", *Electrochimica Acta,* vol. 44, issue 24, pp. 4217-4225, July 1999.

[Gabrielli00-1] Gabrielli, C., Garcia-Jareño, J., Keddam, M., Perrot, H.: "Ion and solvent exchange between the electroactive polymer film and the solution investigated by ac electrogravimetry", *NATO Advance Research Workshop on Electrochemistry of Electroactive Polymer Films WEEPF,* 2000.

[Gabrielli00-2] Gabrielli, C., Garcia-Jareño, J.J., Perrot, H.: "Investigation of Ions and Solvent Insertion in Conducting Polymers by ac-Electrogravimetry", *U.S. ARMY ASIAN RESEARCH OFFICE (ARO-FE),* Simposium speech, 200th meeting.

[Gabrielli00-3] Gabrielli, C., Keddam, M., Nadi, H., Perrot, H.: "Ions and solvent transport across conducting polymers investigated by ac electrogravimetry. Application to polyaniline", *Journal of Electroanalytical Chemistry,* vol. 485, pp. 101-113, 2000.

[Gabrielli01] Gabrielli, C., Garcia-Jareño, J.J., Perrot, H.: "charge compensation process in polypyrrole studied by ac electrogravimetry", *Electrochimica Acta,* vol. 46, issues 26-27, pp. 4095-4103, August 2001.

[Gabrielli02-1] Gabrielli, C., Garcia-Jareño, J.J., Keddam, M., Perrot, H., Vicente, F.: "Ac-Electrogravimetry Study of Electroactive

Thin Films I. Application to Prussian Blue", *Journal of Physical Chemistry B*, vol. 106, issue 12, pp. 3182-3191, March 2002.

[Gabrielli02-2] Gabrielli, C., Garcia-Jareño, J.J., Keddam, M., Perrot, H., Vicente, F.: "Ac-Electrogravimetry Study of Electroactive Thin Films II. Application to Polypyrrole", *Journal of Physical Chemistry B*, vol. 106, issue 12, pp. 3192-3201, March 2002.

[Gabrielli07] Gabrielli, C., Perrot, H., Rose, D., Rubin, A., Toqué, J.P., Pham, M.C. and Piro, B.: "New frequency/voltage converters for ac-Electrogravimetric measurements based on fast QCM", *Rev. Sci. Instrum.*, in press, 2007.

[García-Jareño00-1] García-Jareño, J.J., Gabrielli, C., Perrot, H.: "Validation of the mass response of a quartz crystal microbalance coated with Prussian Blue film for ac electrogravimetry", *Electrocemistry Communications*, vol. 2, issue 3, pp. 195-200, March 2000.

[García-Jareño00-2] García-Jareño, J.J., Sanmatías, A., Vicente, F., Gabrielli, C., Keddam, M., Perrot, H.: "Study of Prussian Blue (PB) films by ac-electrogravimetry: influence of PB morphology on ions movement", *Electrochimica Acta*, vol. 45, issues 22-23, pp. 3765-3776, July 2000.

[García-Jareño03] García-Jareño, J.J., Jimenez-Romero, D., Keddam, M., Perrot, H., Vicente, F.: "Study of Prussian Blue (PB) films by ac-electrogravimetry: influence of PB morphology on ions movement", *Journal of Physical Chemistry B*, vol. 107, pp. 11321-11330, 2003.

[Geelhood01] Geelhood, S., Frank, C.W., Kanazawa, K.: "", *Acoustic Wave Sensor Workshop 3*, Taos, New Mexico, 2003.

[Granstaff94] Granstaff, V.E., Martin, S.J.: "Characterization of a Thickness Mode Quartz Resonator with Multiple Nonpiezoelectric Layers", *J. Appl. Phys.*, vol. 75, nº 3, pp. 1319-1329, 1994.

[Guilbault81] Guilbault, G.G., Affolter, J.: "Piezoelectric Crystal Coating for Detection of Organophosphorus Compounds", *Analytical Chemistry*, vol. 53, pp. 2057-2060, 1981.

[Guilbault83] Guilbault, G.G.: "Determination of Formaldehyde with an Enzyme-Coated Piezoelectric Crystal Detector", *Analytical Chemistry*, vol. 55, nº 11, pp. 1662-1684, 1983.

[Guilbault85] Guilbault, G.G., Kristoff,J.: “Detection of Organo-phosphorus Compounds with a Coated Piezoelectric Crystal”, *Analytical Chemistry*, vol. 57, pp. 1754-1756, 1985.

[Hager86] Hager, H. E., Ruedisueli, R. D., Buehler, M. E.: “The Use of Piezoelectric Crystals as Electrode Substrates in Iron Corrosion Studies: the Real-Time, In Situ Determination of Dissolution and Film Formation Reaction Rates”, *Corrosion (NACE)*, vol. 42, issue 6, pp. 345-351, 1986.

[Hengerer99] Hengerer, A., Decker, J., Prohaska, E., Hauck, S., Köβlinger, C., Wolf, H.: “Quartz crystal Microbalance (QCM) as a Device for the Screening of Phage Libraries”, *Biosens. Bioelectron.*, vol. 14, pp. 139-144, 1999.

[Hillman01] Hillman, A.R., Jackson, A., Martin, S.J.: “The Problem of Uniqueness of Fit for Viscoelastic Films on Thickness-Shear Mode Resonator Surfaces”, *Anal. Chem.*, vol. 73, nº 3, pp. 540-549, 2001.

[IEC302] IEC: “Standart definitions and methods of measurement for piezoelectric vibrators operating over the frequency range up to 30 MHz”, *International Electrotecnical Commision- IEC Standart*, Publication 302, 1969.

[IEC444] IEC: “Measurement of Quartz Crystal Unit Parameters By Zero Phase Tecnique In a Pi-Network (Part 1)”, *International Electrotecnical Commision- IEC Standart*, Publication 444-1, 1986.

[Jiménez04] Jiménez, Y.: “Contribución a la resolución de la problemática asociada a la medida de las propiedades físicas de recubrimientos viscoelásticos en sensores de cuarzo”. *Tesis doctoral*, 2004.

[Jones91] Jones, L., Foster, A.: “Electronic Instruments and Measurements”. *Prentice-Hall, USA, 2nd Ed*, 1991.

[Kanazawa85-1] Kanazawa, K.K., Gordon II, J.G.: “Frequency of a Quartz Crystal Microbalance in Contact with a Liquid”, *Analytical Chemistry*, vol. 57, pp. 1770-1771, 1985.

[Kanazawa85-2] Kanazawa, K.K., Gordon II, J.G.: “The Oscillation Frequency of a Quartz Resonator in Contact with a Liquid”, *Analytica Chimica Acta*, vol. 175, pp. 99-105, 1985.

[Kanazawa93] Kanazawa, K.K., Melroy, O.R.: “The Quartz Resonator: Electrochemical applications”, *IBM J. Res. Dev.*, vol. 37, nº 2, pp. 157-171, 1993.

[King64] King, W.H.:*Analytical Chemistry*, vol. 36, pp.1735, 1964.

[Konash80] Konash, P.L., Bastiaans, G.J.: “Piezoelectric Crystals as Detectors for Liquid Chromatography”, *Analytical Chemistry*, vol. 52, pp. 1929-1931, 1980.

[Lu72] Lu, C., Lewis, O.: *Appl. Phys.*, vol. 43, pp. 4385, 1972.

[Lu84] Lu, C., Czaderna, A..: “Applications of the piezoelectric Quartz Crystal Microbalance. Methods and Phenomena”, *Elsevier*, vol. 7, Amsterdam, 1984.

[Lucklum97-1] Lucklum, R., Behling, C., Cernosek, R.W., Martin, S.J.: "Determination of Complex Shear Modulus with Thickness Shear Mode Resonators", *J. Phys. D. Appl. Phys.*, vol. 30, pp. 346-356, 1997.

[Lucklum97-2] Lucklum, R., Behling, C., Cernosek, R.W., Martin, S.J.: "Determination of Complex Shear Modulus with Thickness Shear Mode Resonators", *J. Phys. D. Appl. Phys.*, vol. 30, pp. 346-356, 1997.

[Martin91] Martin, S.J., Granstaff, V.E., Frye, G.C.: "Characterization of Quartz Crystal Microbalance with Simultaneous Mass and Liquid Loading", *Anal. Chem.*, vol. 63, nº 20, pp. 2272-2281, 1991.

[Martin97] Martin, S.J., Spates J.J., Wessendorf, K. O., Schneider, T.W., Huber, R.J.: "Resonator/Oscillator Response to Liquid Loading", *Anal. Chem.*, vol. 69, issue 11, pp. 2050-2054281, 1997.

[Mecea89] Mecea, V.M.: “A New Method of Measuring the Mass Sensitive Area of Quartz Crystal Resonators”, *Journal Of Physics. E*, vol. 22, pp. 59-61, 1989.

[Mecea96] Mecea, V.M., Carlsson, J.O.: “Extensions of The Quartz-Crystal-Microbalance Technique”, *Sensors And Actuators A-Physical*, vol. 53, pp. 371-378, 1996.

[Melroy86] Melroy, O., Kanazawa, K., Gordon, J.G., Buttry, D.: “Direct determination of the mas of an underpotentially deposited monolayer of lead on gold”, *Langmuir*, vol. 2, issue 6, pp. 697-700, 1986.

[Miller68] Miller, J.G., Bolef, D.I.: *Appl. Phys.*, vol. 39, pp. 4589, 1968.

[Nwankwo98] Nwankwo, E., Durning, C.J.: “Mechanical Response of Thickness-Shear Mode Quartz-Crystal Resonators to Linear Viscoelastic Fluids”, *Sensors and Actuators A.*, vol. 64, pp. 119-124, 1998.

[Oyama95] Oyama, N., Ohsaka, T.: *Prog. Polym. Sci.*, vol. 20, pp. 761-818, 1995.

[Pertence94] Pertence, A.: “Amplificadores operacionales y filtros activos: Teoría, proyectos y aplicaciones prácticas”, *McGraw-Hill Madrid*, 1994.

[Philips88] Philips, S.: “An overview of the phase-locked loop (PLL)”, *Integrated Circuits.* AN 177, Dec 1988.

[Rayleigh45] Rayleigh, J.W.S.: “The Theory of Sound”, *Dover Publications New York*, 1945.

[Reed90] Reed, C.E., Kanazawa, K.K., Kaufman, J.H.: “Physical Description of a Viscoelastically Loaded AT-Cut Quartz Resonator”, *Journal of Applied Physics*, vol. 68, 5, pp. 1993-2001, 1990.

[Rodahl96-1] Rodahl, M., Kasemo, B.: “A Simple Setup to Simultaneously Measure the Resonant Frecuency and the Absolute Dissipation Factor of a Quartz Crystal Microbalance”, *Rev. Sci. Instrum.*, vol. 67, pp. 3238, 1996.

[Rodahl96-2] Rodahl, M., Kasemo, B.: “Frequency and Dissipation-Factor Responses to Localized Liquids Deposits on a QCM Electrode”, *Sensors And Actuators B-Chemical*, vol. 37, pp. 111-116, 1996.

[Rodahl96-3] Rodahl, M., Höök, F., Kasemo, B.: “QCM Operation in Liquids: An Explanation of Measured Variations in Frequency and *Q* Factor with Liquid Conductivity”, *Analytical Chemistry*, vol. 68, pp.2219-2227, 1996.

[Rosenbaum88] Rosenbaum. J.F.: Bulk Acoustic Wave Theory and Devices, *Artech House, Inc. Boston*, 1988.

[SanEmeterio92] San Emeterio, J.L., Montero, F., Pardo, L., Mendiola, J.: “An Alternative Method for Measurement of Clamped Capacitance of Disk Shaped Piezoelectric Ceramics”, *Ferroelectrics*, vol. 109, pp. 83-88, 1992.

[Sauerbrey59] Sauerbrey G.: "Verwendung von Schwingquarzen sur Wägung Dünner Schichten und zur Mikrowägung", *Z. Physik*, vol. 155, pp. 206-222, 1959.

[Sakti00] Sakti, S.P., Hauptmann, P., Zimmermann, B., Bühling, F., Ansorge, S.: “Disposable QCM-Immunosensor for Practical Qualitative and Quantitative Diagnosis”, *Eurosensors XIV. Gopenhagen*, pp. 475-476, 2000.

[SanEmeterio92] San Emeterio, J.L., Montero, F., Pardo, L., Mendiola, J.: “An Alternative Method for Measurement of Clamped Capacitance of Disk Shaped Piezoelectric Ceramics”, *Ferroelectrics*, vol. 109, pp. 83-88, 1992.

[Skoog94] Skoog, D., Leary, J.: "Análisis instrumental", *McGraw Hill/Interamericana de España 4ª Ed.*, Madrid 1994.

[Skoog97] Skoog, D., West, D., Holler, J.: "Funadamentos de química analítica", *Reverté, D.L. 4ª Ed.*, Barcelona, 1997.

[Sogorb03] Sogorb T.: "Caracterización y Desarrollo de un Dispositivo Electrónico para la Monitorización Continua de la Frecuencia de Resonancia Serie y Resistencia Dinámica de una Microbalanza de Cristal de Cuarzo como Sensor de Procesos Superficiales en Medios Fluidos", *Tesis Doctoral*, 2003.

[Stockbridge62] Stockbridge, C.D., Warner, A.W.: "A Vacuum System for Mass and Thermal Measurement with Resonating Crystaline Quartz", *Vacuum Microbalance Techniques (Plenum Press 1962)*, vol. 2, pp. 93-114, 1962.

[Thompson87] Thompson, M., Dhaliwal, G.K., Turner, C.L., Clabrese, G.S.: "The Potential of the Bulk Wave Device as a Liquid Phase Immunosensor", *IEEE Trans. Ultrason. Ferroelectr. Freq. Control, UFFC-34*, pp. 131-135, 1987.

[Tomita79] Tomita, Y., Guilbault, G.G.: "Detection of Explosives with a Coated Piezoelectric Quartz Crystal", *Analytical Chemistry*, vol. 51, nº 9, pp. 1475-1478, 1979.

[Torres05] Torres, R.: "Electronic system for an AC Electrogravimetry experimental set-up", Seminar. *PETRA II Project second meeting*, Brazil, November 2005.

[Torres06-1] Torres, R., Arnau, A., Perrot, H.: "Electronic system for experimentation in AC Electrogravimetry I: technique fundamentals", *Revista EIA*, vol. 5, pp. 9-21, Junio 2006.

[Torres06-2] Torres, R., Arnau, A., Perrot, H., García, J., Gabrielli, C.: "Analog-Digital Phase Locked Loop for Alternating Current Quartz Electrogravimetry", *Electronics Letters*, vol. 42, issue 22, pp. 1272-1273, October 2006.

[Torres07-1] Torres, R., Arnau, A., Perrot, H.: "Electronic system for experimentation in AC Electrogravimetry II: implemented design", *Revista EIA*, vol. 7, submitted.

[Torres07-2] Torres, R., Arnau, A., Perrot, H.: "Fast, Continous and Accurate Frequency Shift Measurement in the AC Electrogravimetry Technique". *Joint meeting of the European Frequency and Time Forum and IEEE international Frequency Control Symposium*. Geneva, Switzerland, May, 2007.

[Varela00] Varela, H., Malta, M., Torresi, R.: "Técnicas in situ de baixo custom em electroquímica: A microbalança a cristal de quartzo", *Química Nova,* vol. 23, issue 5, pp. 664-679, 2000.

[Villar97] Villar, E., Terés, Ll., Olcoz, S., Torroja, Y.: "VHDL. Lenguaje estándar de diseño electrónico", *McGraw-Hill, Madrid*, 1997.

[Wolaver91] Wolaver, D., Cliffs, E.:"Phase-locked Loop circuit design", *Prentice-Hall (New Jersey), 1991*.

[Wessendorf93] Wessendorf, K.O.: "The Lever Oscillator for Use in High Resistance Resonator Applications", *IEEE International Frequency Control Symposium*, pp. 711-717, 1993.

[Williams95] Williams, A., Taylor, F.: "Electronic filter design handbook", *McGraw-Hill 3rd ed., New York*, 1995.

[Wolff00] Wolff, O., Johannsmann, D.: "Shear Moduli of Polystyrene Thin Films Determined with Quartz Crystal Resonators in the Sandwich Configuration", *J. Appl. Phys.*, vol. 87, nº 9, pp. 4182-4188, 2000.